

SS-24.2 MAIN  
COPY 1

Copy 19  
Copy 1

NASA PROJECT MERCURY WORKING PAPER NO. 107

PROJECT MERCURY  
PRELIMINARY FLIGHT TEST RESULTS OF THE  
"BIG JOE", MERCURY R AND D CAPSULE

Classification changed  
to UNCLASSIFIED

per authority of NASA  
Sec. Class Officer Mainis  
5-29-75 ✓

CLASSIFIED DOCUMENT

This material contains information affecting the national defense of the United States within the meaning of the espionage laws, Title 18, U.S.C., Secs. 793 and 794, the transmission or revelation of which in any manner to an unauthorized person is prohibited by law.

Distribution and Referencing  
This paper is not suitable for general distribution or referencing. It may be referenced only in other working correspondence and documents on Project Mercury by participating organizations.

I.N. 59-1344  
NOV 3 1959

NATIONAL AERONAUTICS AND SPACE ADMINISTRATION  
SPACE TASK GROUP  
Langley Field, Va.

OCTOBER 12, 1959



(NASA-TM-X-73017) PROJECT MERCURY  
PRELIMINARY FLIGHT TEST RESULTS OF THE BIG  
JOE, MERCURY R AND D CAPSULE (NASA) 143 P

N76-72326 20811

198

Unclas  
00/98 20811

NASA PROJECT MERCURY WORKING PAPER NO. 107

PROJECT MERCURY  
PRELIMINARY FLIGHT TEST RESULTS OF THE  
"BIG JOE", MERCURY R AND D CAPSULE

Prepared By Performance Branch

Approved: Alex C. Bond  
A. C. Bond  
Head, Performance Branch

Approved: M. A. Faget  
M. A. Faget  
Head, Flight Systems Division

NATIONAL AERONAUTICS AND SPACE ADMINISTRATION  
SPACE TASK GROUP  
LANGLEY FIELD, VA.

OCTOBER 12, 1959

*1.N. 59-1344*

NOV 3 1959

TABLE OF CONTENTS

INTRODUCTION . . . . .	1
CAPSULE DESCRIPTION . . . . .	4
Configuration . . . . .	4
Structure . . . . .	4
Systems . . . . .	7
Instrumentation . . . . .	7
Recovery System . . . . .	9
Control System . . . . .	11
Cooling System . . . . .	13
BOOSTER DESCRIPTION . . . . .	14
RESULTS AND DISCUSSION . . . . .	15
Flight Test and Trajectory . . . . .	15
Motions and Accelerations . . . . .	17
Aerodynamic Heating . . . . .	19
Description of Recovered Capsule . . . . .	19
Afterbody Temperature Histories . . . . .	21
Heat Shield Performance . . . . .	24
Sound Measurements . . . . .	26
Vibration Measurements . . . . .	28
Recovery System Performance . . . . .	28
CONCLUDING REMARKS . . . . .	30

## TABLES

- Table I - Afterbody Instrumentation
- Table II - Heat shield instrumentation
- Table III - Weights and moments of inertia
- Table IV - Events

## LIST OF FIGURES

- Figure 1 - Sketch of "Big Joe" Configuration
- Figure 2 - Photograph of assembled "Big Joe" capsule
- Figure 3 - Schematic of heat shield
- Figure 4 - Inside view of heat shield
- Figure 5 - Structural details of the pressurized instrument compartment
- Figure 6 - View at top of parachute container (cylindrical section)
- Figure 7 - Sketch of afterbody thermocouple locations
- Figure 8 - Arrangement of instrumentation in pressurized compartment
- Figure 9 - Aft canister showing drogue chute attachments.
- Figure 10 - View of top of cylindrical portion
- Figure 11 - View upward on pressure bulkhead
- Figure 12 - Mercury "Big Joe" capsule mounted on Atlas 10-D booster on launch stand
- Figure 13 - Big Joe trajectory
  - (a) Exit
  - (b) Reentry
- Figure 14 - Atmospheric pressure
- Figure 15 - Positive accelerations and angular rates
- Figure 16 - Partial time history of on-board recorded data
- Figure 17 - Time history of altitude and velocity showing events
- Figure 18 - Comparison of Atlas and Big Joe angular rates as a function of time
- Figure 19 - Cross-plots of pitch rate against yaw rate
  - (a) Time = 310 - 431 seconds
  - (b) Time = 431 - 494 seconds

- (c) Time = 494 - 520 seconds
- (d) Time = 520 - 530 seconds
- (e) Time = 530 - 537 seconds
- (f) Time = 537 - 542 seconds

- Figure 20 - Control supply tank pressure as a function of time
- Figure 21 - Reaction control nozzle pressures
- Figure 22 - Longitudinal accelerations as a function of time
- Figure 23 - Trim accelerations as a function of time
- Figure 24 - Frequency of oscillation from pitch and yaw rate
- Figure 25 - Maximum oscillatory amplitude about trim as a function of time
- Figure 26 - Recovered heat shield
- Figure 27 - Heat shield before test flight
- Figure 28 - Recovered heat shield showing typical ring cracking
- Figure 29 - Close-up of recovered heat shield showing delamination and center plug area
- Figure 30 - Ring separation at center plug of heat shield
- Figure 31 - Comparison of measured heat shield profile before and after flight
- Figure 32 - Close-up of roll and pitch jet areas
- Figure 33 - Recovered afterbody
  - (a) Quad I and IV
  - (b) Quad II and III
- Figure 34 - Close-up of localized heating near recovery hooks
  - (a) Hook located in pitch plane
  - (b) Hook located in quad II
- Figure 35 - Recovery hook in quad III
- Figure 36 - View of internal damage near recovery hook (Quad II)
- Figure 37 - Recovered afterbody interior
- Figure 38 - Sample telemeter record
- Figure 39 - Exit heating on afterbody
  - (a) Pressure vessel sidewalls
  - (b) Top canister, cylinder and cone sidewall
  - (c) Antenna skin, drogue chute and main chute

- (d) Internal temperatures (pressure vessel and dome)
- Figure 40 - Exit heating for sections A-A and B-B  
(a) Section A-A  
(b) Section B-B
- Figure 41 - Temperature distribution along afterbody during exit  
(a) Time = 100 seconds  
(b) Time = 140 seconds  
(c) Time = 180 seconds
- Figure 42 - Afterbody temperatures during reentry heating  
(a) Top canister  
(b) Cylinder  
(c) Cone sidewall  
(d) Pressure vessel sidewalls  
(e) Pressure vessel internal temperatures  
(f) Antenna skin, drogue chute and main chute
- Figure 43 - Temperature distribution along afterbody after peak heating  
(a) Time = 592 seconds  
(b) Time = 620 seconds  
(c) Time = 660 seconds
- Figure 44 - Temperature at section A-A and B-B during reentry heating  
(a) Section A-A  
(b) Section B-B
- Figure 45 - Probable maximum temperature reached on afterbody as indicated by thermocolor paint
- Figure 46 - Temperature time history in heat shield  
(a) through (m) - Sensors 1 through 13
- Figure 47 - Temperature distribution in heat shield at sensor locations for times of 580, 620 and 660 seconds  
(a) Sensors 1 and 2  
(b) Sensors 3 and 4  
(c) Sensors 5 and 6  
(d) Sensors 7 and 8  
(e) Sensors 9 and 10  
(f) Sensors 11 and 12  
(g) Sensor 13
- Figure 48 - Depth of temperature penetration in heat shield

- Figure 49 - Comparison of temperature distribution through heat shield at selected time intervals
- (a) Time 580 seconds (sensors 1 through 9)
  - (b) Time 580 seconds (sensors 5, 9, 13, 10, 11 and 12)
  - (c) Time 620 seconds (sensors 1 through 9)
  - (d) Time 620 seconds (sensors 5, 9, 13, 10, 11 and 12)
  - (e) Time 660 seconds (sensors 1 through 9)
  - (f) Time 660 seconds (sensors 5, 9, 13, 10, 11 and 12)
- Figure 50 - Time history of apparent thermal penetration of heat shield as obtained from sensors
- Figure 51 - Comparison of sensor data and measured char and material discoloration
- (a) Yaw plane
  - (b) Pitch plane
- Figure 52 - Core samples obtained from recovered heat shield
- Figure 53 - Typical core sample (plug number 10)
- Figure 54 - Char and discoloration measurements on Big Joe heat shield
- (a) Radial distribution
  - (b) Edge effect
- Figure 55 - Comparison of Big Joe and nominal stagnation point heating rates.
- Figure 56 - Acoustic analyzer record
- Figure 57 - Harmonic sound analysis at 59 seconds

PRELIMINARY FLIGHT TEST RESULTS OF THE  
"BIG JOE", MERCURY R AND D CAPSULE

INTRODUCTION

During the early conceptual stages of Project Mercury it was deemed very necessary to include in the planned research and development program an early capsule flight test to investigate some of the many problems associated with satellite reentry from orbit, as well as to check some of the basic concepts being employed in the Mercury capsule design. It was felt that none other than a full-scale capsule test would be satisfactory and thus it was readily apparent that the Atlas booster should be used to achieve the desired reentry conditions. The Atlas guidance system was to be used to properly match conditions of reentry from orbit at a high enough altitude to encounter all important heating effects.

The capsule for this flight test was code-named "Big Joe". It had the same general lines or external configuration as the Mercury capsule, with the exception that it was not equipped with the Mercury escape tower. The structural and detailed design were governed by the particular requirements of the test and hence differs quite markedly from that of the more sophisticated Mercury capsule. The "Big Joe" employed an ablation heat shield on the blunt reentry face and the afterbody was constructed of inconel sheet. Four primary systems were incorporated in the "Big Joe" capsule, namely, instrumentation, recovery, controls and internal cooling.

The primary test objectives as set forth for the Big Joe flight test were as follows:

- a. recover capsule
- b. determine the performance of the ablation shield and measure afterbody heating.

- c. determine the flight dynamic characteristics of the capsule during reentry
- d. establish the adequacy of the capsule recovery system and procedures.
- e. establish the adequacy of recovery aids in assisting the recovery of the capsule
- f. conduct familiarization of NASA operating personnel with Atlas launch procedures

Secondary objectives of the test included the following:

- a. evaluate the loads on the capsule during the actual flight environment
- b. evaluate operation of the capsule control system

The detailed design, instrumentation and development of the recovery system for the Big Joe was done "in-house" by various members of the Space Task Group. The design and development of the capsule control system was accomplished by members of the Lewis Research Center. Construction of the capsule was done by both the Langley and Lewis Research Center shops. Many items including the ablation heat shield, instrumentation components and recovery system components were procured from outside vendors to meet the particular design requirements and specifications as set forth by the Space Task Group.

Some of the primary components along with the supplying vendor are given below:

- a. Ablation Heat Shield - General Electric Company and B. F. Goodrich Company
- b. Antenna components - General Electric Company
- c. Control System Components - Minneapolis-Honeywell Regulator Company
- d. On-board tape recorders - Cook Electric Company and Ampex Corporation
- e. Telemetry system - Electro-Mechanical Research, Inc.
- f. Radar Tracking Beacons - Aero-Geo-Astro Corporation

- g. Recovery beacons - Ultra-Electric, Ltd.
- h. Parachutes - Radioplane Division of Northrup Corporation
- i. Booster Adapter - McDonnell Aircraft Corporation

The initial work on the "Big Joe" was started during the latter part of November 1958. The flight test was conducted at 2:19 AM EST on September 9, 1959, from the Air Force Missile Test Center Cape Canaveral Florida. The purpose of this paper is to present the preliminary results of this flight test and to provide early availability of these data.

## CAPSULE DESCRIPTION

### Configuration

The geometrical configuration of the Big Joe capsule is shown in figure 1. The over-all external dimensions were for all practical purposes identical to those of the full-scale Mercury capsule although the external makeup was different. A photograph of the assembled capsule is shown in figure 2.

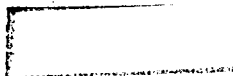
The capsule was mounted on the Atlas booster through the use of an adapter or intermediate structural section attached to the forward mating flange on the booster. The capsule was mounted with the blunt face or ablation shield toward the booster and was held fast to the adapter by means of a Marmon type clamping band. Explosive bolts were incorporated in the band which allowed the release of the capsule from the adapter at the prescribed separation time. Three small retro motors, mounted on the adapter, were employed to separate the capsule from the sustainer after disengagement of the Marman band.

### Structure

The capsule structure consisted of four major assemblies. Starting from the bottom they were:

1. the heat shield
2. the pressurized instrument compartment
3. the conical and cylindrical afterbody
4. the aft canister

The heat shield consisted of a 74.5 inch maximum diameter spherical segment whose radius of curvature was 80 inches. A sketch of the heat shield is presented as figure 3.



~~SECRET~~

- 5 -

The shield consisted of an outer ablation laminate and an inner structural laminate. The outer laminate was oriented so the individual layers of cloth were at a 20 degree angle with the outer surface. The structural laminate was fabricated of parallel layers. Both laminates were constructed from a 181 weave, Volan A finish fiberglass cloth with a 91LD resin. Resin content of the outer laminate was 40 percent whereas the inner laminate had a 30 percent resin content. To the inner surface of the shield was attached a ring three inches high, made of the same material as the shield, which served to bolt the shield to the pressurized compartment. (See figure 4).

The pressurized compartment consisted of a frustum of a cone extending from the heat shield up about two feet capped by a detachable pressure dome. (See figure 5). Its sidewalls were pure monocoque .062 inch sheet inconel. About 5 inches above the outer edge of the shield and inside the shell was attached a flat sheet inconel disc which formed the lower pressure bulkhead. Attached to the bulkhead and running radially from the center were six inconel webs which spanned the gap between the disc and the heat shield. Flanges were attached to the lower edges of the webs and served to support the heat shield when loaded in an upward direction, as in a water landing. The volume between the heat shield and the lower pressure bulkhead was vented to the outside so that it flooded after impact thereby increasing the water stability, and allowing the dye marker and shark repellent to escape. It also served to house accessory equipment. The instrumentation housed in the pressurized section, was bolted to the lower bulkhead.

A flange was welded at the top of the pressurized compartment which served to attach the pressure dome and afterbody. The dome was a 4-1/2 foot diameter spherical segment with a 33-inch radius of curvature, constructed of sheet inconel.

~~SECRET~~

The inside of the dome and the sidewalls of the pressurized section were lined with two inches of 7 lb/ft<sup>3</sup> thermoflex insulation. There was no insulation between the lower bulkhead and the heat shield. Instrumentation leads and devices in the rest of the capsule were locally insulated.

The conical and cylindrical afterbody was vented to the outside by holes just above its junction with the pressurized compartment. The conical part consisted of .050 inch and the cylindrical of .032 inch sheets of corrugated inconel stiffened by internal rings, rivetted together.

The cylindrical part housing the main parachute contained in its top ring, a three legged spider beam made of fiberglass (to minimize heat conduction) (See figure 6). Near the central junction of the three beams was the attachment point of the main parachute. Three steel supporting rods attached at the juncture and at the base of the cylindrical section formed a tripod which took out the main chute loads. Hooks for raising the capsule protruded out the top of the cylindrical section and were supported internally by the three-legged spider.

The aft canister was a bucket shaped structure made out of corrugated inconel and contained the drogue parachute. It was attached to the cylindrical afterbody at the center of the three-legged spider by a single connector separable by an explosive device. This connector could take shear normal to the capsule centerline and tension. The single connector was attached to the canister by a tripod of steel rods which ran to three points at the upper corner of the canister where they were securely attached. On top of the canister the drogue risers attached to these three points. Bending moment in the canister produced by drogue chute load eccentricity was reacted by tension in the single connector and compression in a sidewall of the canister. A fiberglass lid was used to cover the canister for heat protection during exit.

~~SECRET~~

- 7 -

### Systems

Instrumentation - The Big Joe capsule was instrumented with three FM/FM, 20 watt RF links which transmitted data measurements from the capsule to ground receiving stations. One telemetry link transmitted primary data and a second link was used for transmittal of secondary data. The third telemetry link provided for complete redundancy in the transmittal of primary data and was also employed to re-broadcast primary link data which was on-board recorded (by a magnetic tape play-back recorder) during the period of ionization blackout of the signal. A 28-volt battery was used as the telemetry power supply.

A total of 139 measurements were made including 52 ablation shield temperatures, 52 afterbody temperatures, 13 ablation shield char rates, pitch, yaw and roll rates (coarse and fine measurements for each rate) and pitch, yaw and roll positions, normal, transverse and longitudinal accelerations (coarse and fine for each direction), 4 control system nozzle pressures, 2 afterbody static pressures and control system supply pressure. Only the shield char rate and temperature data were commutated; all other data were transmitted continuously.

Each group of 52 thermocouples was commutated on a single telemeter channel by means of a 60-point switch. The rate of commutation was such that each given thermocouple was sampled about once every 0.62 seconds. In addition to the data measurements, the resulting wave trains included master identification pulses as well as calibrate signals corresponding to the low, medium and high value of the preselected ranges for each thermocouple group. These provided continuous in-flight calibration of the thermocouples. The 13 ablation shield char rate sensors were also commutated on a single telemetry channel, however, in this case a 30 point switch was employed and the sampling rate was approximately once every 0.40 seconds. Calibrate signals corresponding to minimum and maximum voltage outputs were also provided in wave trains from the char rate sensors.

~~SECRET~~

~~SECRET~~

- 8 -

A detailed list of the afterbody thermocouple instrumentation with tabulated values of wall thickness and locations is given in Table I. A sketch showing the relative locations of these thermocouples is presented in figure 7. Details of the heat shield instrumentation are given in Table II. Each of 13 sensors were instrumented to determine temperature distribution as well as char depth. These sensors were developed by the Missile and Space Vehicle Department of General Electric in Philadelphia, Pennsylvania. Each of 13 sensors consisted of 6 thermocouples and 20 pairs of make wires spaced in depth through the shield. The 20 pairs of make wires were connected to give a single signal corresponding to the char depth. They were designed to sense changes in electrical resistance of the heat shield material. As heat penetrated the shield, the resistance variations were indicated by changes in voltage output to a sub-carrier oscillator. Calibrated variations in sub-carrier frequency indicated char penetrations of the shield.

Although each sensor was instrumented with 6 thermocouples a total of 52 available commutator segments reduced the number of thermocouples, for which data was actually recorded. As a result 3 thermocouples were recorded for each of the following sensors: 3, 4, 6, 8, 9, 10, 11, 12, 13. The sensors which recorded all 6 available thermocouples were 1, 2, 5, and 7.

A total of four magnetic tape recorders were included in the capsule instrumentation. One of these recorders was a single track recorder used, as previously mentioned, to record and playback primary data obtained during the telemetry blackout period. This recorder had a recording duration of four minutes and was programmed to playback after the expected period of blackout had been encountered. The other three recorders were triple track and had a tape capacity which provided approximately 16 minutes of running time. Two of these recorders were used to record all the primary link data and were programmed such as to

~~SECRET~~

~~SECRET~~

- 9 -

cover the entire time period of flight. The other triple track recorder was employed to record noise data from three highly sensitive microphone pickups. Two pickups were located to provide data on the noise levels within the instrument compartment and another was installed to pick up aerodynamic noise at the skin of the instrument compartment.

The capsule was equipped with both S-band and C-band radar beacons (AN/DPN-48, Model 1) to aid in the tracking of the capsule during reentry.

Figure 8 shows the arrangement of the instrumentation within the instrument compartment.

The antenna elements for both the telemetry system and radar beacons were located on the conical afterbody. (See figure 2.) Each beacon utilized three of the smaller elements while each telemetry link was allotted two of the larger elements. All elements were of the tuned slot or cavity type antenna elements with fused quartz flush covers.

Recovery System - The Big Joe recovery system included both a landing system, for safely depositing the capsule on the water after reentry, and a series of recovery aids to assist in the locating of the capsule after landing. The landing system consisted of a drogue parachute, a main parachute, three pairs of baroswitches and an inertia switch.

A six-foot diameter fist ribbon, conical parachute was used as the drogue parachute. It was ejected from a mortar, located in the aft canister, figure 9, which was energized by the closing of either of a pair of baroswitches set for a pressure altitude of approximately 45,000 feet. The drogue was used to stabilize the capsule and also act as a pilot chute for the main parachute.

The second pair of baroswitches was set for a pressure altitude of approximately 10,000 feet and was used to fire an explosive disconnect which released the aft canister. The main parachute deployment bag

~~SECRET~~

~~SECRET~~

- 10 -

was connected to the canister by a 3-foot nylon strap, and hence the release of the canister served to deploy the main parachute. This parachute was a 63-foot diameter, nylon, ring-sail parachute which was preset for 10 percent reefing for a period of 4 seconds. See figure 10.

The inertia switch was employed to fire an explosive bolt which was to release the main parachute when a longitudinal acceleration greater than about 9 "g" was experienced. This switch was to be armed by either one of a pair of baroswitches set for a pressure altitude of 3,000 feet.

The baroswitches sensed the pressure obtained in a manifold ring, which was made integral with the pressurized compartment structure and was located just ahead of the juncture between the pressure compartment and conical afterbody. Twelve equally spaced 3/32-inch diameter orifices were located in the exterior skin of the manifold.

Redundancy was obtained in the landing system by incorporating duplicate circuitry and pairs of baroswitches as mentioned above. The landing system was locked out during the boosted portion of flight by means of a pair of separation switches which armed the landing circuits upon release of the Marman band.

The recovery aids incorporated in the capsule included underwater sound, radio signal and visual locating devices. Two Sofar bombs set to detonate at 3,000 feet below sea level were carried on-board. One bomb was to be ejected with the deployment of the main parachute and the other was stored on board to indicate the futility of further search in the event the capsule sank.

Two types of radio signal transmitters were employed, Sarah beacons and free running telemetry. Two lightweight Sarah distress radio beacons with peak power of 15 watts transmitted 210 double pulses per second at 235 megacycles and were set to operate for approximately 24 hours. (figure 10.) As a back-up for the Sarah beacons, one telemetry

~~SECRET~~

~~SECRET~~

- 11 -

RF link was designed to switch to its unmodulated carrier, 225.7 megacycles, after impact and to transmit one minute on and two off for an expected period of about 24 hours.

The visual aids consisted of a flashing light, a smoke generator and combination dye marker and shark repellent. The light which was activated by deployment of the aft canister was designed to emit 2-million lumens for 2 milliseconds 30 times per minute. The smoke generator was to provide dense yellow smoke for a period of 10 minutes. It was to be fired one hour after impact by a timer which was started at impact. Two water-soluble containers of dye marker and shark repellent were stored in the vented compartment below the pressure bulkhead, and were to be dispersed upon contact with the water.

Control System - The "Big Joe" control system was comprised of an autopilot, a system programmer and a jet reaction system made up of a high pressure nitrogen supply and associated control valves and nozzles. Figure 8 shows the control system assembly mounted in the pressure compartment of the capsule. The location of the nozzles is shown in the sketch of figure 1. The autopilot employed three rate gyroscopes and two attitude gyroscopes (one for sensing pitch attitude and the other for sensing both yaw and roll attitudes). The system was designed such that the jet control valves would be energized when the attitude error was 3 degrees at zero rate, or when the angular rate was 1 degree per second at zero attitude error.

The control system was programmed for two modes of operation, an attitude holding mode and a damping mode. The gyros were uncaged just prior to launch, however, the signals from the gyros were prevented from activating the control valves by means of electrical lockouts until the jettisoning of the Marman band. At Marman band release the control system was programmed to hold the capsule at a predetermined attitude, close to the predicted attitude of the booster, for a period of 15 seconds.

~~SECRET~~

~~SECRET~~

- 12 -

After this period, the programmer was to initiate a pitch-over maneuver to bring the heat shield forward and approximately align the capsule along the flight path. Upon completion of the pitch-over maneuver, which was estimated to require approximately 18 seconds, the flight attitude was to be held until a longitudinal deceleration of .05 g was experienced. At this time, the programmer was to effect a lock-out of the attitude holding mode, leaving only the rate damping mode in both the pitch and yaw planes and further initiate a programmed steady roll rate of 1 rpm. The programmer was set to continue this mode of control until a prescribed period of time after the predicted impact time.

Nitrogen for the control jets was stored at an initial pressure of 3100 psi in the four fiberglass containers located below the pressure bulkhead of the instrument compartment. (Figure 11.) The four containers which were manifolded had a total volume of 2000 cubic inches. One of the four containers was isolated by means of a check valve which permitted flow only from the container to the manifold. A take-off was provided at the isolated bottle for providing gas for auxiliary functions such as instrument compartment pressurization and refrigerant expulsion. The supply line for the control jets passed through the pressure bulkhead to the distribution manifold. As a safety feature, an explosive shut-off valve provided isolation of the high pressure storage from the pressure compartment until after launch.

The control valves supplying the jets were normally closed and were activated directly by solenoids; pressure forces on the valves were pressure balanced. Opening and closing time was approximately 0.02 seconds.

The nozzles for pitch and yaw produced 10 pounds of thrust while the roll nozzles produced a thrust of 2 pounds at a supply pressure of 3000 psi. The actual chamber pressure of the pitch and yaw nozzles was reduced to one half the supply pressure by an orifice just upstream of the nozzle chamber. The roll nozzles were identical with the pitch and yaw nozzles, however, the chamber pressure was reduced to one-tenth

~~SECRET~~

~~SECRET~~

- 13 -

the supply pressure by a series of two orifices ahead of the chamber.

Cooling System - The capsule was equipped with a simple ammonia cooling system for the purpose of preventing internal temperatures in the instrument compartment from exceeding allowable limits. The system was designed to handle a total heat load of 150 BTU/minute and had an approximate running time of 23 minutes. Cooling was accomplished by expanding liquid ammonia through a fixed orifice into a heat exchanger located in the instrument compartment. (See figure 8.) The ammonia vapor was exhausted overboard through two fixed back pressure orifices located in the sides of the capsule. A high velocity fan was utilized to circulate the compartment air past the heat exchanger coils and over the instruments.

Approximately 7.5 pounds of ammonia was stored in an aircraft hydraulic accumulator bottle located in the area between the heat shield and instrument deck. (See figure 11.) The accumulator was equipped with a diaphragm and one side of the bottle was pressurized by nitrogen (reduced to 150 psi) from one of the control system nitrogen storage bottles. The cooling system was activated at missile lift-off by means of an explosive Conax valve in the ammonia system.

~~SECRET~~

~~SECRET~~

- 14 -

BOOSTER DESCRIPTION

The booster employed for the Big Joe flight test was the Atlas-10D missile, designed and constructed by the Convair Astronautics Division of General Dynamics Corporation. This was the sixth series D missile to be flight tested and the first Atlas missile designated to support the NASA Project Mercury. Subsequent Mercury-Atlas flight tests are also to be conducted with the Series D missile. Further details regarding the booster may be found in references 1 and 2. Figure 12 shows a photograph of the capsule booster combination on the launch stand.

~~SECRET~~

~~SECRET~~

- 15 -

RESULTS AND DISCUSSION

The reader is reminded that the results presented herein should be treated as preliminary since they were obtained by quick reading of only a minimum number of points from the various telemeter and on-board tape records. Faired curves are presented based on data as originally read without following the usual data reduction cross-checking procedures. In the interest of expediency, the data are presented without analysis at this writing.

Flight Test and Trajectory

The flight test of the capsule herein reported was conducted at the AFMTC, Cape Canaveral, Florida at 2:19 AM September 9, 1959. The approximate intended insertion conditions were altitude 459,450 feet, airspeed 23,890 ft/sec and path angle -1.50 degrees which were to simulate reentry from a shallow earth orbit. The desired reentry altitude, velocity and path angle were not achieved due to the failure of the Atlas booster engine to separate. Burnout conditions achieved were altitude 491,320 feet, airspeed 20,628 ft/sec and path angle -0.92 degrees.

Other problems arose as a result of the additional weight of the booster engines being carried throughout the flight. No discrete engine cutoff signal was sent due to the failure to obtain the desired insertion conditions, thus the sustainer and vernier engines operated until all fuel was expended from the tank. Because there was no valve closure there was expulsion of residual fuel and/or oxygen, either liquid or gaseous form, from the sustainer and vernier engines which produced a low level of thrust. This thrust continued for a considerable period of time. Separation of the Marman band was effected and the retro-rockets on the Atlas adapter were ignited. Due to the thrust being produced by the Atlas engines and the additional weight of the booster engines,

~~SECRET~~

~~SECRET~~

- 16 -

the retro-rockets could not impart enough differential acceleration to effect a clean separation. There is evidence the capsule was moving within the adapter at times but it is conclusively established the capsule did not separate for considerable time after the intended separation. The flight test evaluation of the Atlas booster is reported in reference 2.

Upon sustainer engine burnout, the Atlas and capsule went into a slow rolling motion. The capsule control system was functioning trying to control the motions and affect the proper turn over but the high inertia of the combination precluded any effect on the motion. The control system depleted its gas supply such that at actual separation the controls were inadequate to perform their intended duty. The pitch and yaw rate data at this time represent the type of motion expected from a variable applied moment. This indicates aerodynamic control rather than reaction jet control which produces constant torque.

Successful reentry was accomplished without aid of the rate damping control mode through maximum dynamic pressure to drogue chute deployment. Although the range fell short by 500 nautical miles of its intended range of 1800 nautical miles, the capsule was recovered approximately 7 hours after launch in excellent condition.

The exit trajectory presented in figure 13(a) was obtained from reference 2. The reentry trajectory presented in figure 13(b) was calculated using the conditions of altitude, velocity and path angle obtained from the General Electric Burroughs tracking data. No downrange tracking data were available at the time of this reporting. The atmospheric conditions used in the trajectory calculations are presented in figure 14. Rawinsonde data was available to 100,000 feet altitude. The extrapolation of the data for altitudes above 100,000 feet was done so that event times (.05 g, max. g's, drogue deployment, etc.) would closely correspond with the event times established from telemetered data.

~~SECRET~~

~~SECRET~~

- 17 -

### Motions and Accelerations

The sources of data presented in this section are (1) telemetered data received at Station 1, (Cape Canaveral), (2) telemetered data received at Station 9.1, (Antiqua), and (3) on-board tape recorded data. These sources are so noted on the figures of this section.

The positive directions of accelerations and angular rates are presented in figure 15 along with measured capsule center of gravity location. The capsule weights and moments of inertia are given in Table III.

Presented in figure 16 are sample records from one of the on-board tape recorders which show partial time histories of some of the measured quantities throughout the important phases of flight. The on-board timer produced a time pulse that lagged real time by approximately 6 percent. Corrections were made to the on-board data for this discrepancy. The events pointed out are defined in Table IV. Figure 17 shows the altitude and velocity when the events occurred.

Figure 18 gives a comparison of the angular rates as measured from the capsule and Atlas instrumentation. The signs have been deleted to avoid confusion due to sign differences occurring from the different axes systems used on the booster and on the capsule. For the time period between 310 seconds (Marman band release) to 390 seconds (loss of signal from Station 1) the angular rates are approximately the same. The fact that the capsule rates were hand read and represent only ten percent of the full-scale instrument range may indicate the origin of the small differences that occur. The high frequency oscillation on the capsule rates indicate the capsule was rocking within the adapter. The phase and magnitude relationship of the comparison over the time period between 310 and 390 seconds is anything but coincidental. The control system, which was on continuously is sufficiently strong to produce an angular acceleration of greater than

~~SECRET~~

~~SECRET~~

- 18 -

3 deg/sec<sup>2</sup> in one plane. No such rate of change is noted except possibly in the high frequency oscillation. On the basis of this comparison it was concluded the capsule and Atlas were together at 390 seconds.

Presented in figure 19 are plots of pitch rate versus yaw rate which represent the capsule motion from 310 seconds to 542 seconds. From figure 19(b) it is apparent that shortly after 448 seconds the capsule is a free body under some rate control. From the roll rate time history it appears some control is in effect possible before 448 seconds. From the time histories of these channels over this time period an abrupt change in all three rates is noted at 448 seconds. This change could result from the decrease in inertia of the system by capsule separation from the Atlas. The control tank supply pressure, figure 20, and nozzle pressure, figure 21, indicate any control produced by the reaction jets would be small. The angular rate traces (figure 16) are indicative of aerodynamic forces instead of constant torque control as supplied by the reaction jets. From the above data it was concluded that the capsule became a free body from shortly after 448 seconds and was prevented from tumbling, strictly by aerodynamic action.

A partial time history of the longitudinal acceleration, figure 22; shows higher values than that anticipated during the intended flight. This is easily explained by the difference between intended and achieved insertion conditions.

The maximum normal and transverse accelerations never exceeded one g as evidenced in the time history presented in figure 16. The trim normal, transverse and resultant accelerations are presented as partial time histories in figure 23. From estimates of the dynamic pressure, a resultant force coefficient was obtained and from wind tunnel estimates of coefficient versus angle, a trim angle was calculated. This was in close agreement with the trim angle expected from the measured center of gravity offset shown in figure 15. The center of gravity offset is

~~SECRET~~

~~SECRET~~

- 19 -

largest in the yaw plane and the effect is shown in figure 23.

The frequency of oscillation is given as a function of time in figure 24 over the reentry range until nearly drogue deployment. The frequency was obtained from the pitch and yaw rate traces.

The approximate maximum oscillatory amplitude about trim is shown in figure 25 as a function of time from apparent separation to drogue deployment. The data were determined by two approximate methods as shown on the figure. At the time of apparent separation the indicated angle was  $123^\circ$  converging to  $10^\circ$  at maximum dynamic pressure and diverging to  $35^\circ$  at drogue chute deployment. This divergence is on the order of  $1/2$  that calculated from trajectory studies based on questionable values of the rotary damping derivative

$$C_{m_q} + C_{m_{\dot{\alpha}}}$$

### Aerodynamic Heating

Description of Recovered Capsule - A photograph of the recovered heat shield is presented as figure 26. The large pie shaped discolored area in quadrant II was caused by the dye marker recovery aid and not by reentry heating. Local scuff marks caused by handling during the recovery operation are also clearly visible. For comparison purposes the heat shield prior to flight is shown in figure 27. A closeup of the recovered shield is shown in figure 28. The speckled appearance is caused by droplets of fused glass which covered the entire surface of the shield. Local hairline cracks which form circular rings throughout the shield are clearly visible in figure 28. These cracks were surface cracks and were not deep enough to structurally damage the shield. The only significant damage occurred in quadrant III near the center. A 3-inch de-lamination occurred which is shown in figure 29. It is significant

~~SECRET~~

~~SECRET~~

- 20 -

that the de-lamination did not penetrate the heat shield further than the char depth. The center plug edge cracks and the ring separation at the stagnation point sensor are also shown in figure 29. Neither of these apparent damages should be considered as problem areas in heat shield design. All physical damage was limited to the surface. Figure 30 clearly shows the ring separation has penetrated only as far as the char line. An indication of the performance of the heat shield is given in figure 31. A comparison is made of the shield profile which shows that the contour remained unchanged as a result of the reentry heat pulse. Measurements of the surface profile indicated maximum deviation of only .015 inches as a result of the flight. The thermal performance of the shield will be discussed in a later section.

Visual inspection of the recovered capsule afterbody showed very little thermal damage had taken place. Figure 32 shows a close-up view of the pressure vessel sidewall. The damage was minor and even the painted letters spelling UNITED STATES were still clearly visible. No damage is visible near the reaction control jet openings. Also shown in figure 32 is the afterbody heat shield joint. This joint was uneven and a waviness of the surface was apparent prior to the test flight. However, no indications of localized heating were observed around the entire periphery of the joint.

Photographs of the conical skin and cylindrical afterbody are shown in figure 33. Again there are no indications of thermal damage. Local hot spots were non-existent around areas such as:

- a. protruding rivet heads
- b. antenna and skin joints
- c. structure corrugation

The cylindrical section, however, showed evidence of high local temperatures and local buckling was evident as shown in figure 33.

~~SECRET~~

~~SECRET~~

- 21 -

The area of intense localized heating is clearly shown in figure 34. Two of the recovery hooks were highly eroded and small skin areas near the hooks were destroyed. The third recovery hook (figure 35) remained relatively undamaged. This unsymmetrical afterbody heating is due to an out of trim condition caused by the center of gravity offset discussed earlier. Figure 36 shows internal areas damaged by the hot gases issuing through the burned out skins in the vicinity of the recovery hooks. The internal damage was slight, but serves to emphasize the possible danger to internal hardware as a result of large external skin proturbances. The lack of any extensive internal damage is shown in figure 37. Examination of the internal structure shown in figure 37 gave evidence of fine powder or dust deposits. The coatings had apparently been blown into the structure by the hot jets of air coming through the holes near the recovery hooks. Chemical analysis of these deposits proved them to be very fine particles of  $\text{SiO}_2$  or glass.

Weighing the heat shield before and after the test flight showed that only 6 pounds of material had been lost. This number is not precise due to the absorption of moisture in the heat shield. However, the amount of heat shield material lost is considered to be insignificant.

Afterbody Temperature Histories - Time histories of the temperatures and distributions at specific times are shown in figures 38 through 45. The measured temperatures are assumed to be within  $\pm 50$  degrees on the heat shield and  $\pm 30$  degrees on the afterbody. Temperatures were ranged from  $-30^\circ \text{F}$  to  $2600^\circ \text{F}$  and  $-30^\circ \text{F}$  to  $1500^\circ \text{F}$  on the heat shield and afterbody respectively. The normal radio transmission was affected by signal blackout for a period of approximately 100 seconds (480 to 580) during reentry. The data, during this time interval, were recorded on on-board tapes but had not been processed at this writing. A sample of the recorded data which has been hand read is shown in figure 38.

~~SECRET~~

~~SECRET~~

- 22 -

The afterbody temperature time histories during the exit phase of the flight trajectory are shown in figure 39. Significant heating began near 60 seconds, maximum heating rates occurred near 90 seconds and peak temperatures were recorded about 130 seconds. The free stream conditions at these times are summarized as follows:

Time Seconds	Free Stream Dynamic Pressure lb/sq ft	Free Stream Mach number	Altitude ft	Comments
60	900	1.5	35,000	Max. dynamic pressure
90	410	3.5	85,000	Max. heating rates
130	30	8.5	195,000	Max. temperatures

Sidewall temperatures along the pressure vessel (figure 39(a)) were reasonably uniform with peak temperatures generally at 380° F. The cone sidewall, cylinder, and top canister shown in figure 39(b) were slightly warmer. The different temperature levels can be attributed to differences in wall thickness, heating rates and surface emissivity. The preliminary nature of this report precludes further analysis at this time. Time histories of the wall temperatures near the antenna are given in figure 39(c). The temperatures reached peak values of 600° F. Drogue and main chute temperatures are also shown in figure 39(c). No temperature rise was recorded by these thermocouples. Additional time histories of internal temperatures are shown in figure 39(d). Very slight temperature rise was noted during exit heating for these locations. Figure 40 presents temperature time histories of all thermocouples at sections A-A and B-B during exit heating. Additional data showing temperature distributions along the afterbody at times of 100, 140 and 180 seconds are shown in figure 41. The temperature distributions are consistent with increasing time and show excellent agreement between rows A, B, and C on the pressure vessel sidewalls and the conical afterbody.

~~SECRET~~

~~SECRET~~

- 23 -

The afterbody temperature time histories for the reentry phase of the flight trajectory are shown in figure 42. A summary of the maximum recorded temperatures are as follows:

Approximate Time, Second	Location	Temperature °F
580	Top Canister	1470
580	Cylinder	1760
580	Cone-Sidewall	1090
580	Pressure Vessel Sidewall	
580	Row A	870
580	Row B	600
580	Row C	670

The temperature distribution shown in the above table should be representative of the distribution at peak heating. The top canister of course was not recovered but figure 33 indicates that peak temperatures were considerably higher on the cylinder than on other portions of the recovered afterbody. Typical temperature distributions along the body are presented in figure 43 at selected time intervals. Figure 43(a) shows that maximum temperature differentials along row A were as much as 800 degrees at 592 seconds. The cooling rates were such that the maximum temperature difference at 660 seconds (figure 43(c)) was only 220 degrees. An indication of the temperature distribution circumferentially at Sections A-A and B-B are given in figure 44. Maximum temperature differences were:

~~SECRET~~

~~SECRET~~

- 24 -

Time	Maximum Temperature Differences	
	Sec. A-A	Sec. B-B
580	280	250
670	200	90

The afterbody interior was coated with a temperature sensitive paint. Inspection of the recovered afterbody indicated that the maximum temperature varied from 1200° F to 2000° F. These temperatures are presented in figure 45.

Heat Shield Performance - Time history of the heat shield temperatures are presented in figure 46. The data are grouped according to sensor number and a typical plot is shown in figure 46(a). Cross-plots of the data in figure 46 are shown in figure 47. The curves have been faired through six points for sensors 1, 2, 5, and 7 but only 3 temperatures were available at the other sensor locations. Consequently, caution should be used in interpreting the thermal gradients shown in figure 28. Although the data at peak heating is not available the shield temperature at later times do present useful results. For example, the temperature distribution shown in figure 47(a) indicates the large temperature gradients that can occur as late as 580 seconds. This is approximately 40 seconds later than the estimated time of peak heating rate. Although outer edge temperatures decrease with increasing time, it is apparent that a large time lag exists within the heat shield. At the time of drogue chute deployment (660 seconds), the internal shield temperatures have not increased appreciably.

~~SECRET~~

~~SECRET~~

- 25 -

The temperature cross-plots of figure 47 have been checked to determine the maximum depths of penetration that occurred for temperatures between 200 and 800 degrees Fahrenheit. Each of the 13 sensors of figure 47 has been checked and a numerical average of the results are presented in figure 48. Temperatures of 800° F penetrated only 0.21 inches into the heat shield whereas temperatures of 200° F were noted at 0.56 inches.

Additional cross-plots of temperature versus depth in inches are presented in figure 49 at selected time intervals. Figure 49(a) compares the temperature distribution at 580 seconds for the effects of radial distribution. Sensors 1 through 5 along one radius are compared as well as sensors 1, 6, 7, 8, and 9 along the other radius. The data are in good agreement and no significant effects due to radial distribution are apparent. Figures 49(b) through (f) present the same type of comparison at later times. From the available data, the heat shield seems to have undergone a uniform heating.

The char indications provided by the sensors are presented as time histories in figure 50. These data are subject to interpretation, but considered at face value give very conservative estimates of char depth. The data presented herein are estimated from calibration curves obtained from an arbitrary definition of char temperature. A re-appraisal of this definition would probably give better agreement between char indications from the sensors and the measured values from the recovered heat shield. A comparison of the measured values and the maximum char depths indicated by the sensors is shown in figure 51. The arrows indicate both measured char depth and material discoloration. Measured char depths were approximately 0.15 inches less than the sensor data. However, the sensor data generally agreed with the depths for which material discoloration was observed. The maximum sensor reading was at sensor number 9. This indicated char to 0.41 inches, but the measured char was only 0.2 inches.

Core samples of the heat shield were taken in order to accurately determine the heat shield performance. A total of 17 samples were

~~SECRET~~

~~SECRET~~

- 26 -

removed from the shield and a photograph of all 17 is presented as figure 52. An individual test sample is shown in figure 53. The char depth and material discoloration areas are clearly visible. A summary of all the measured char and discoloration depths as obtained from the core samples is given in figure 54. The radial distribution is shown in figure 54(a). The char depth was uniform throughout the shield and measured 0.2 inches. A slight variation in the depth of material discoloration was observed. Values of 0.35 inches of discoloration are typical. The data of figure 54(b) shows that the distribution of char and material discoloration near the edge is uniform around the heat shield. Depths of 0.19 and 0.34 inches of char and discoloration respectively were observed.

The nature of the heat pulse to which the heat shield has been subjected must be considered in determining the significance of the char measurements. Uncertainties in the trajectory insertion conditions make it difficult to determine precisely what the heat pulse was. However, a trajectory has been determined which gives the heat pulse labeled  $3032 \text{ BTU/ft}^2$  in figure 55. The nominal heat pulse which was desired was  $6550 \text{ BTU/ft}^2$ . An effective heat of char may be computed to be  $1624 \text{ BTU/lb}$ . (Based on 0.2 inch of char and  $3032 \text{ BTU/ft}^2$ ).

#### Sound Measurements

The capsule was equipped with three condensor microphones. Two were mounted inside the pressure vessel and one was mounted in the skin of the pressure vessel. The ranges were such that all information was obtained with the internal low-level microphone and the information cited in the following paragraphs refers only to this instrument. The internal noise was recorded on an on-board tape recorder running at a speed of 15 inches per second.

~~SECRET~~

~~SECRET~~

- 27 -

The data presented has not yet been corrected for the frequency response of the various components involved in the measurement, but the responses of all systems involved are essentially flat within  $\pm 2$  db from 100 to 10,000 cps.

Figure 56 is a reproduction of a record made on an acoustic analyzer and indicates the over-all noise level recorded during exit and reentry. In addition to flight times, various events are indicated on the record. It is interesting to note that the maximum level encountered is not at lift-off as was originally expected, but occurred slightly before maximum dynamic pressure was encountered on exit from the atmosphere at a Mach number of about 1.4. The level of external noise at the skin of the capsule was determined to be 150 db at lift-off.

Sometime after sustainer burnout (about 516 seconds) a recurrent regular sound similar to that produced by a drummer's wood blocks occurred. These sounds are indicated by the peaks on the figure from 516 to 610 seconds. The source of this sound has not been definitely established, but it is believed, from an inspection of other records, to be produced by some component in the control system. Immediately after this, a sound similar to sawing wood is evident (615 to 660 seconds) and is attributed to aerodynamic noise that builds up and decays as the capsule yaws or pitches from side to side. At 660 seconds, the sawing sound disappears and the wood blocks sound again becomes more evident, but random. In addition, there is noise similar to that made by a bowling ball rumbling down an alley. Practically all noise stops after about 751 seconds with the exception of the wood block sound which gradually decreases in frequency from then until the tape runs out.

Figure 57 is a plot of a harmonic analysis of the sound at the time of peak value (59 seconds). The response of the system is down several db below 100 cps and the spectrum has not been corrected.

~~SECRET~~

The points plotted indicate sound content in 1/3 octave bands. The frequency is the center frequency of the band. The high points at 100, 200, and 400 cps are believed to be caused by resonances in the capsule structure.

### Vibration Measurements

Vibration data was obtained with five seismic accelerometers. The nominal ranges were: longitudinal + 12 to -3 g, transverse  $\pm$  10 g and  $\pm$  1 g, normal  $\pm$  10 g and  $\pm$  1 g. The vibration levels encountered were such that the data was obtained from the low-range normal and transverse instruments. The natural frequency of these instruments was approximately 50 cps and they were damped to about two-thirds critical damping so that the response would be flat to about 40 cps.

The maximum values of vibration were encountered at and shortly after ignition. They were as follows:

Direction	Vibratory Load, g's	Frequency Cycles/Second
Normal	$\pm$ .85	15.8
Transverse	$\pm$ .75	11.75
Longitudinal	$\pm$ .15	5.1

The degree of vibration encountered at times other than at the maximum already cited was in the range of 0.25 g at a frequency of 5 to 6.25 cps. These occurred at various times during the boosted portion of the flight, and are attributed to the first body bending of the Atlas - Big Joe missile.

### Recovery System Performance

All elements of the landing system functioned satisfactorily. The deployment action of both the drogue and main parachutes was

~~SECRET~~

- 29 -

indicated on the on-board records and it was noted that these actions essentially occurred at the preselected altitudes. Figure 16 shows the character of the trace of longitudinal acceleration at the time of main chute deployment, 751 seconds. The two peaks in the trace indicate the reefed and full open conditions of the chute. The second peak registers approximately 3 g's for the full open condition.

Although essentially all the recovery aids functioned properly, not all were necessary in this case to accomplish the recovery. The report from the Sofar bomb jettisoned at main chute deployment was received by the Navy Missile Impact Landing System and fixed the general impact area. This area coincided with that estimated by the recovery forces on the basis of several reported headings determined from visual sightings. After the search area was established a search aircraft was dispatched to the area and picked up the Sarah beacons signals from a distance of approximately 50 miles. Shortly thereafter a large area of fluorescent dye (described as one block wide and three blocks long) was sighted and then the capsule. The flashing light was functioning, however, the smoke had expended itself at the time of sighting. It was reported that the pulsed telemetry signal was not received by the recovery forces. The visual sighting occurred approximately 3-1/2 hours after launch and the capsule was recovered by a destroyer approximately 7 hours after launch.

~~SECRET~~

~~SECRET~~

- 30 -

CONCLUDING REMARKS

The majority of the test objectives were accomplished by the flight of the "Big Joe" Atlas boosted test vehicle. Although the desired trajectory insertion conditions were not attained, the actual insertion conditions were such as to provide extremely valuable design data for application to Project Mercury as well as to reentry satellites in general.

The ability of the test capsule to survive the severe test of reentry from near-orbital velocities in spite of its unprecedented release conditions, is certainly worthy of note. The heat shield performance was excellent and no special problem areas were uncovered as a result of the flight. The capsule performance as a free-body reentry vehicle was exceptional. It was demonstrated that the capsule could reenter the atmosphere at high angles of attack and maintain its position with the heat shield forward without the aid of a control system.

~~SECRET~~

~~SECRET~~

- 31 -

REFERENCES

1. Anon - "Flight Test Directive, Series"D", Missile No. 10, Convair Astronautics Report No. ZC-7-134A-28, August 1959. Secret
  
2. Anon - Flight Test Evaluation Report, Missile 10D, Convair Astronautics Report No. AZC-27-077-23 September, 1959. Secret

~~SECRET~~

~~CONFIDENTIAL~~

TABLE I

AFTERBODY INSTRUMENTATION

T.C. Number	Material	Wall Thickness, In.	Wetted distance from Shoulder, in.	Station in.
1	inconel	0.0625	7.78	7.31
2	inconel		11.78	11.08
3	inconel		15.78	14.81
4	inconel		19.78	18.60
5	inconel		23.78	22.30
6	inconel	.050	31.78	29.92
7	inconel		39.78	37.30
8	inconel		47.78	45.00
9	inconel		55.78	52.50
10	inconel		63.08	59.40
11	inconel	.03125	67.04	63.14
12	inconel		74.04	70.14
13	inconel		81.04	77.14
14	inconel		90.04	86.12
15	inconel		104.04	100.07
16	fiberglass	.125	109.04 (9 in. radius on pitch plane)	105.14
17	inconel	.03125	97.04	93.07
18	inconel		77.54	73.14
19	inconel		70.54	66.14
20	inconel	.050	55.78	52.50
21	inconel	.0625	23.78	22.30
22	inconel		15.78	14.81
23	inconel	.0625	7.78	7.31
24	inconel		15.78	14.81
28	inconel	.050	47.78	45.00
29	inconel	.03125	74.04	70.14
30	inconel		97.04	93.07
31	stainless steel	.038	(32 in. radius at 45°)	30.58

~~CONFIDENTIAL~~

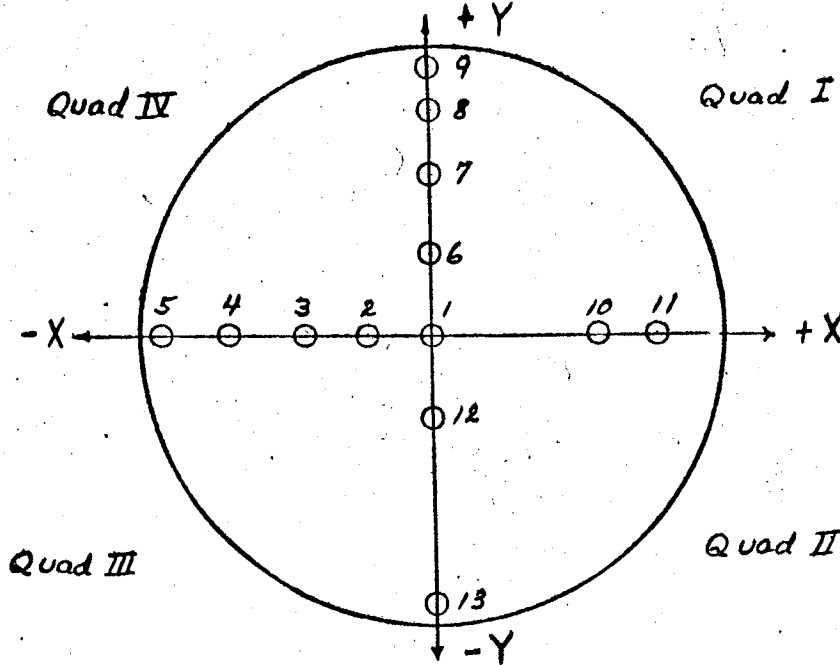
T.C. Number	Material	Wall Thickness, In.	Wetted distance from Shoulder, in.	Station in.
32	insulation (2 in. thermo-flex)	(2 in. insulation)	(30 in. radius at 45°)	29.
33	insulation (2 in. thermo-flex)	(2 in. insulation)	11.78	1 08
34	inconel	.0625	15.78	14.81
35	inconel		15.78	14.81
36	inconel		15.78	14.81
37	instrument deck	.125	6.28	5.90
38	instrument deck		6.28	5.90
39	stainless steel	.038	(32 in. radius at 30°)	35.58
40	insulation (2 in. thermo-flex)	(2 in. insulation)	19.78	18.60
41	insulation (2 in. thermo-flex)	(2 in. insulation)	11.78	11.08
42	inconel	.0625	23.78	22.30
43	inconel		19.78	18.60
44	inconel		11.78	11.08
45	inconel		7.78	7.31
46	fiberglas	6.25 (on parachute canister)	(12.5 in. radius)	54.78
47	inconel	.050	62.08	58.40
48	inconel		37.78	35.60
49	inconel	.050	47.78	45.00
50	inconel		47.78	45.00
51	inconel		47.78	45.00
52	inconel		47.78	45.00
53	fiberglas	.125	109.04 (9 in. radius, 60° from pitch plane)	105.14

T.C. Number	Material	Wall Thickness, In.	Wetted distance from Shoulder, in.	Station in.
54	fiberglas	.03125	89.64	85.72
55	fiberglas		89.64	85.72

Note: All T.C. were chromel-alumel.

~~CONFIDENTIAL~~

TABLE II  
HEAT SHIELD INSTRUMENTATION



Sensor Number	Location		T. C. Number	Depth from surface, inches
	X	Y		
1	0	0	1	0.067
			2	.187
			3	.347
			4	.677
			5	1.067
			6	1.607
2	-7.4	0	34	.071
			35	.191
			36	.351
			37	.681
			38	1.071
			39	1.611
3	-14.8	0	7	.085
			8	.365
			9	1.085
4	-26.6	0	40	0.092

~~CONFIDENTIAL~~

Sensor Number	Location		T. C. Number	Depth from surface Inches
	X	Y		
5	-35.8	0	41	.372
			42	1.092
			43	.096
			44	.216
			45	.376
			46	.706
			47	1.096
			48	1.636
6	0	11.2	10	.099
			11	.379
			12	1.099
			13	.086
7	0	21.6	49	.086
			50	.206
			51	.366
			52	.696
			53	1.086
			54	1.626
			13	.080
			14	.360
8	0	29.2	15	1.080
			16	.098
			17	.378
			18	1.098
9	0	35.8	55	1.098
			19	.092
			20	.372
			21	1.092
10	21.6	0	22	.099
			23	.379
			24	1.099
			21	1.092
11	29.2	0	22	.099
			23	.379
			24	1.099
			21	1.092

Sensor Number	Location		T. C. Number	Depth from surface, Inches
	X	Y		
12	0	-11.2	28	.095
			29	.375
			30	1.095
13	0	-35.8	31	.103
			32	.383
			33	1.103

Note: All T.C. were chromel-alumel.

~~CONFIDENTIAL~~

TABLE III

<u>Component</u>	<u>Weight, lbs</u>	<u>Moment of inertia, slugs/ft<sup>2</sup></u>		
		X	Y	Z
Capsule (empty)	2555	320.26	498.70	525.82
NH <sub>4</sub>	7	.26	.32	.69
N <sub>2</sub>	17	<u>.69</u>	<u>3.23</u>	<u>2.62</u>
Total (launch)	2579	321.21	502.25	529.13

CONFIDENTIAL

~~CONFIDENTIAL~~

TABLE IV

<u>Event</u>	<u>Description</u>	<u>Approximate time, sec</u>
1	T = 0 2" lift-off	0
2	Booster Engine Cut-off	137
3	Sustainer Engine Cut-off	296
4	Marman Band Release	310
5	Retromotor Firing	312
6	Apparent Separation	448
7	0.05 g's	503
8	Max Longitudinal g's	560
9	Drogue Chute Deployment	661
10	Main Chute Deployment	751
11	Water Impact	1055

CONFIDENTIAL

CONFIDENTIAL

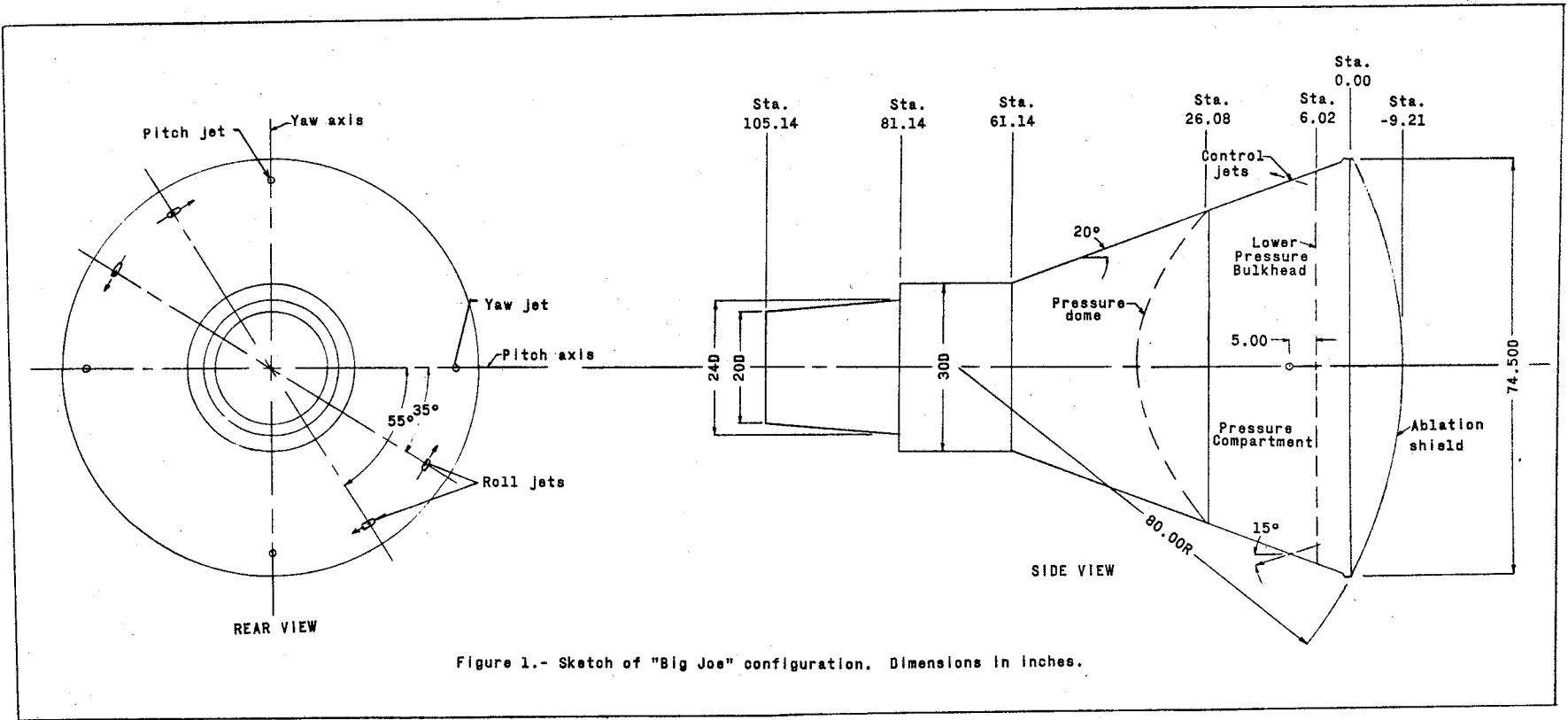


Figure 1.- Sketch of "Big Joe" configuration. Dimensions in inches.

CONFIDENTIAL

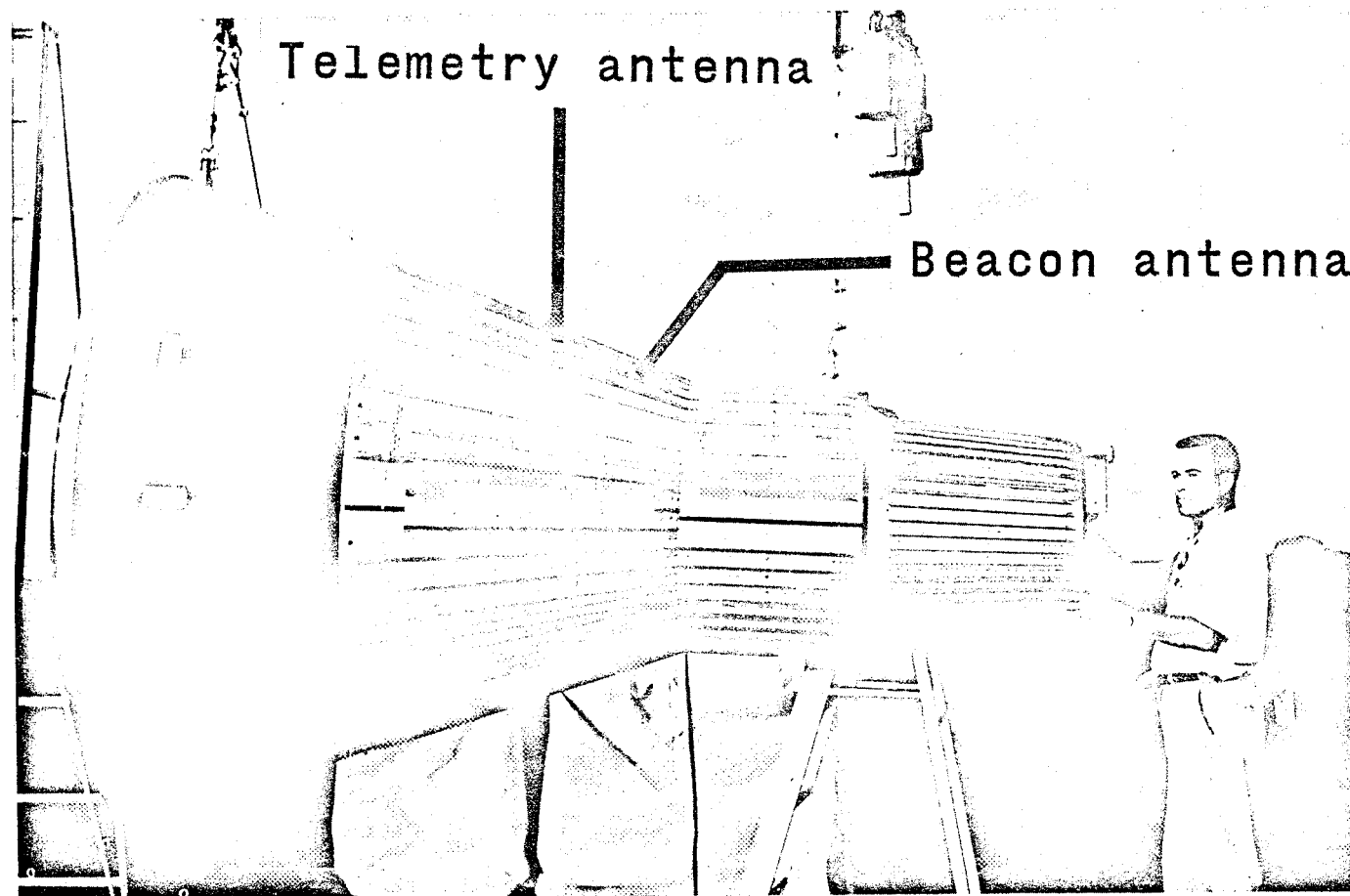


Figure 2.- Photograph of assembled "Big Joe" capsule.

~~CONFIDENTIAL~~

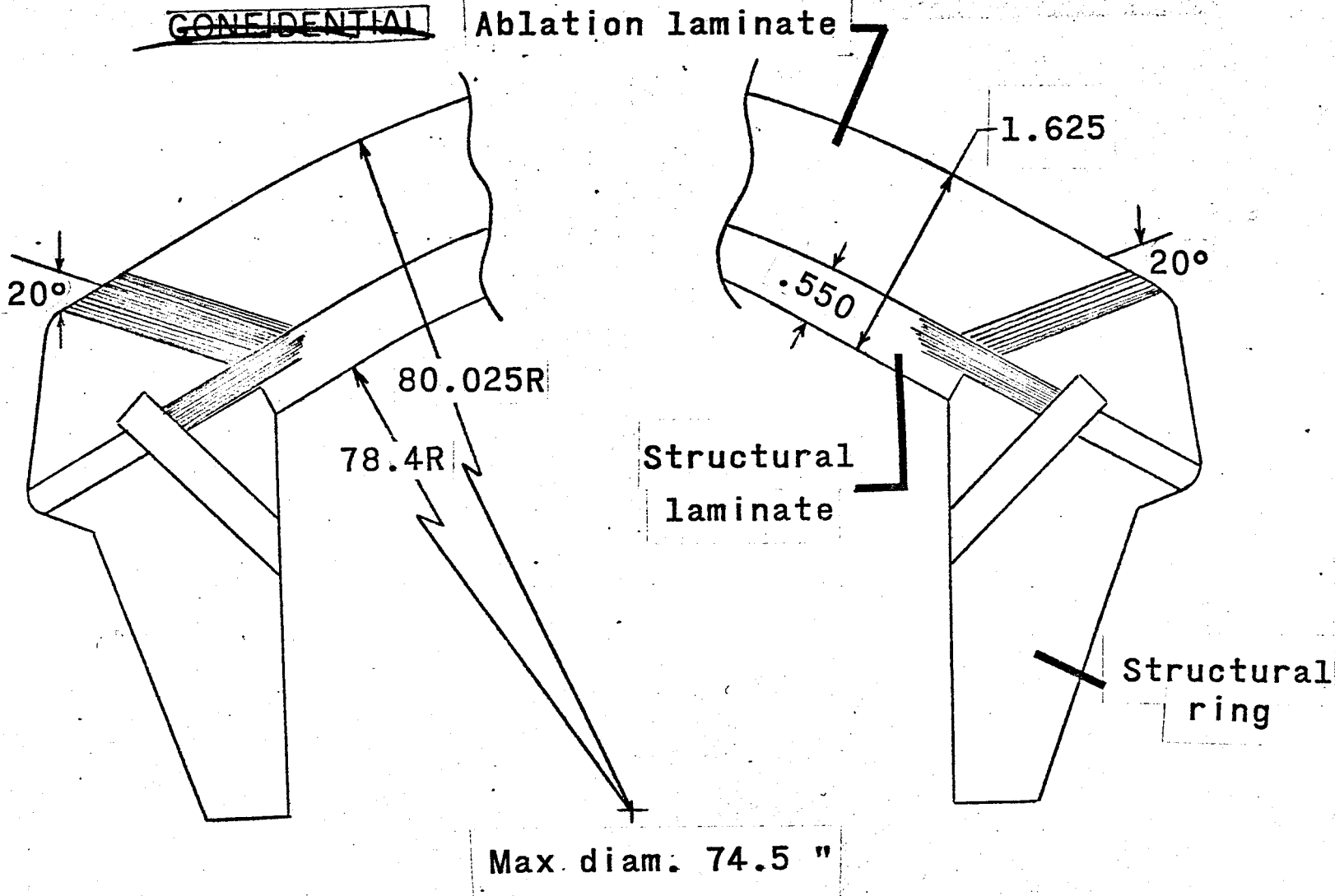


Figure 3.- Schematic of heat shield. Dimensions in inches.

~~CONFIDENTIAL~~

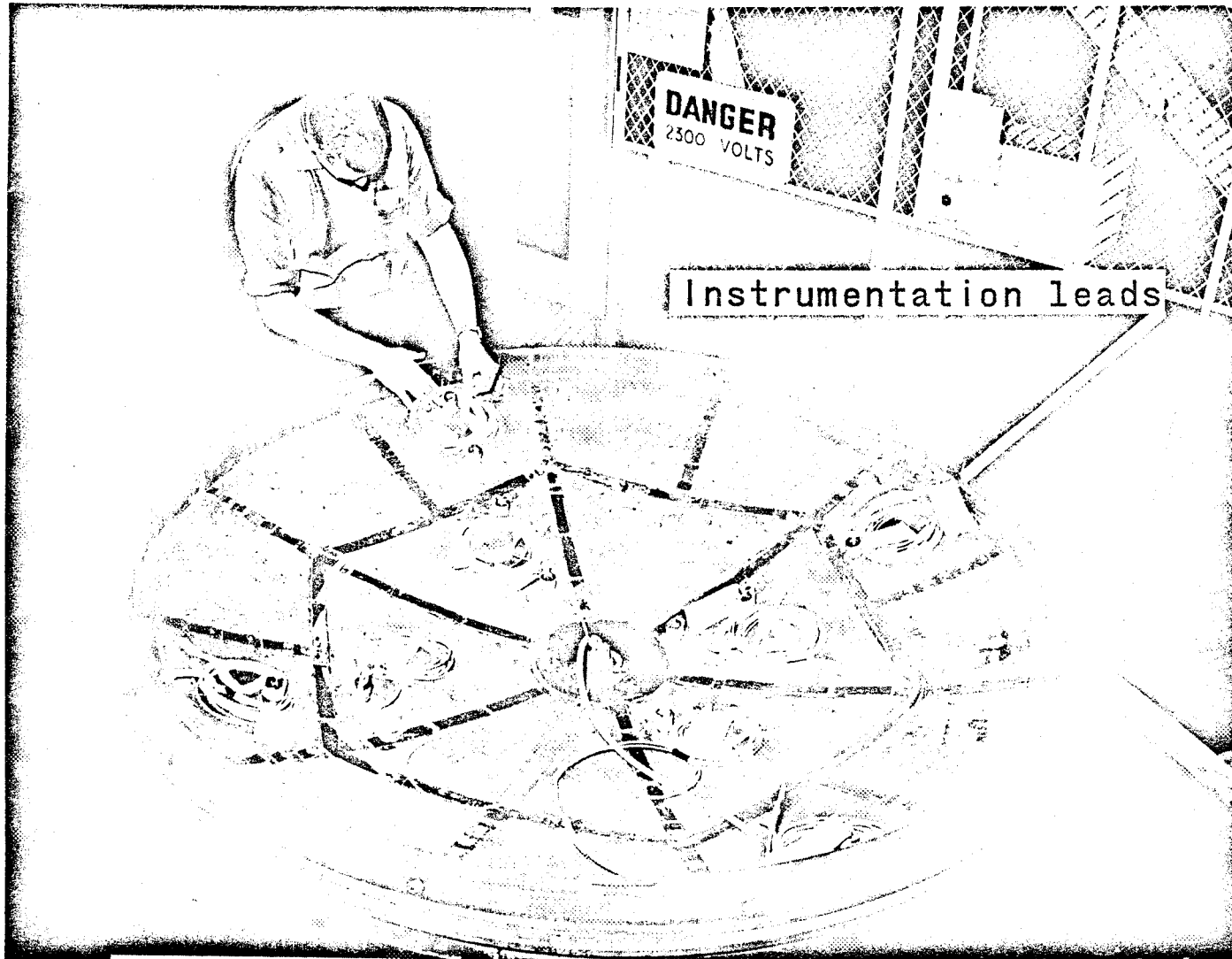
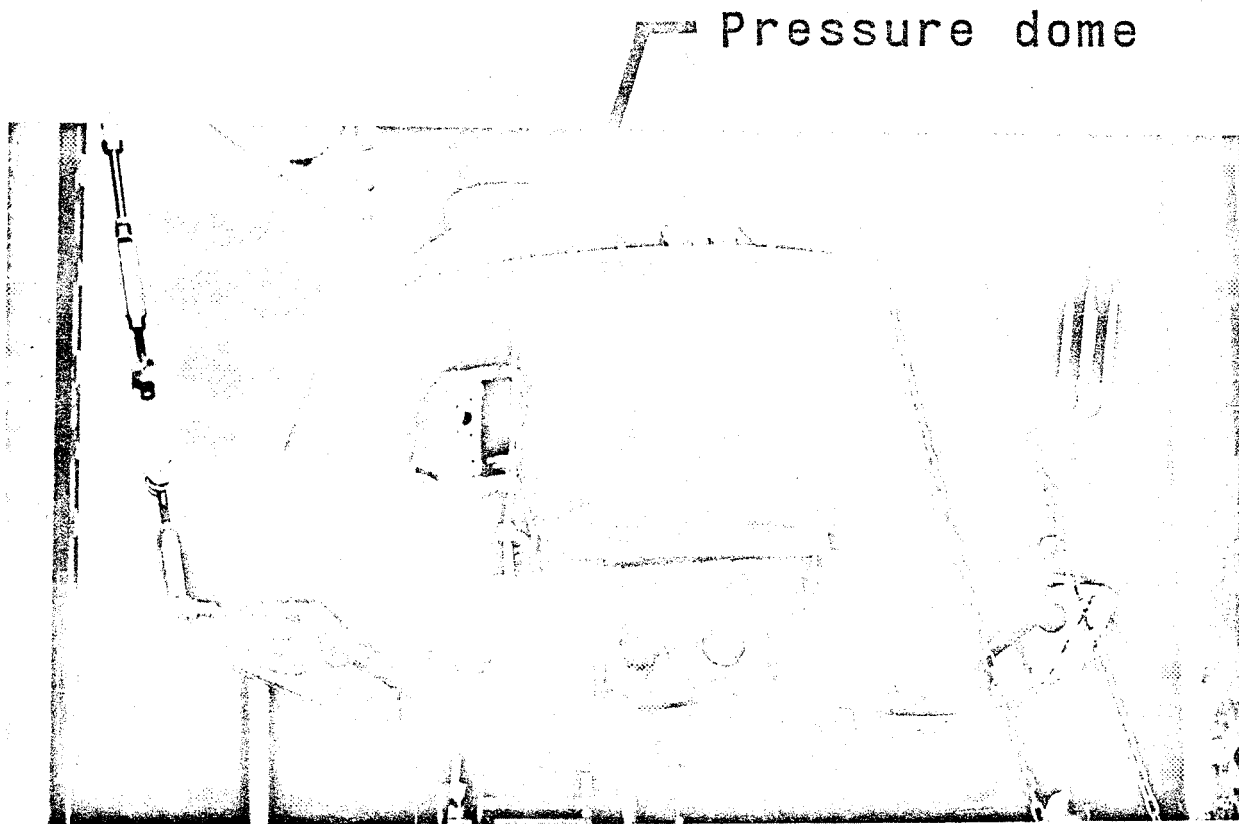


Figure 4.- Inside view of heat shield



Pressure dome

Lower pressure bulkhead

Figure 5.- Structural details of the pressurized instrument compartment.

Three legged spider beams

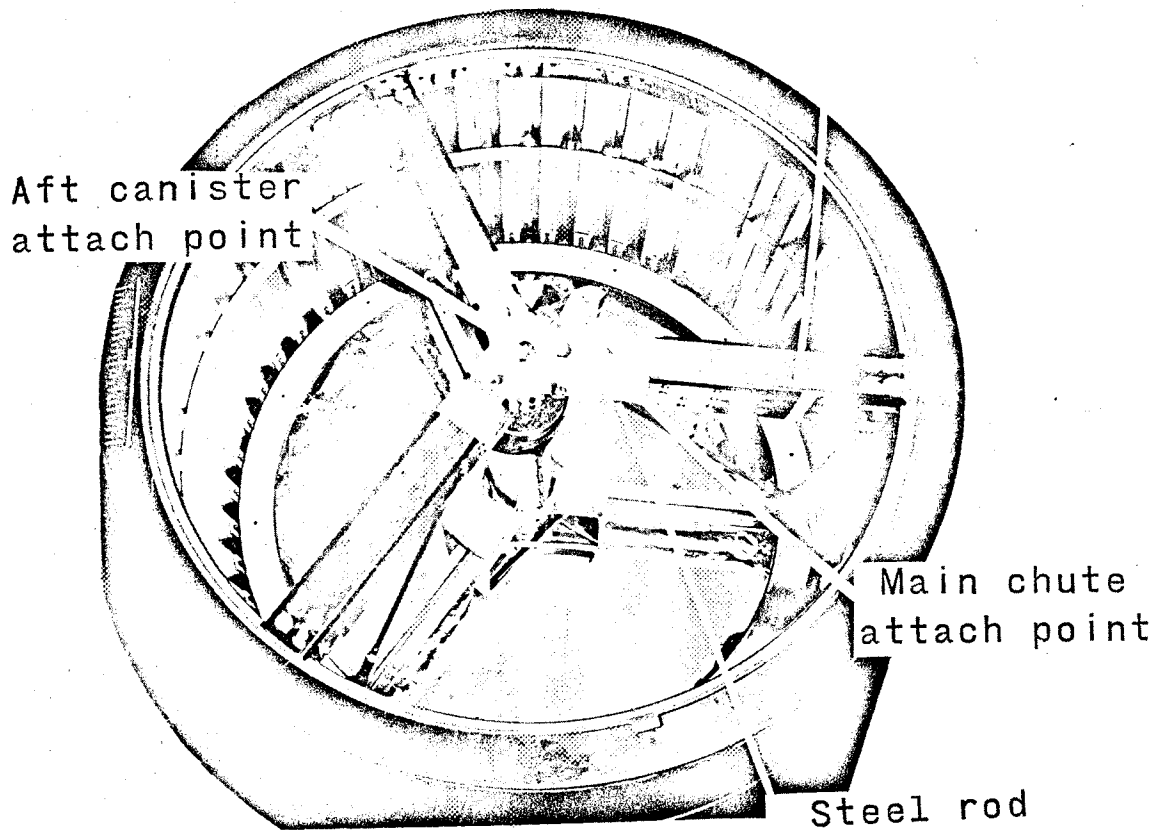
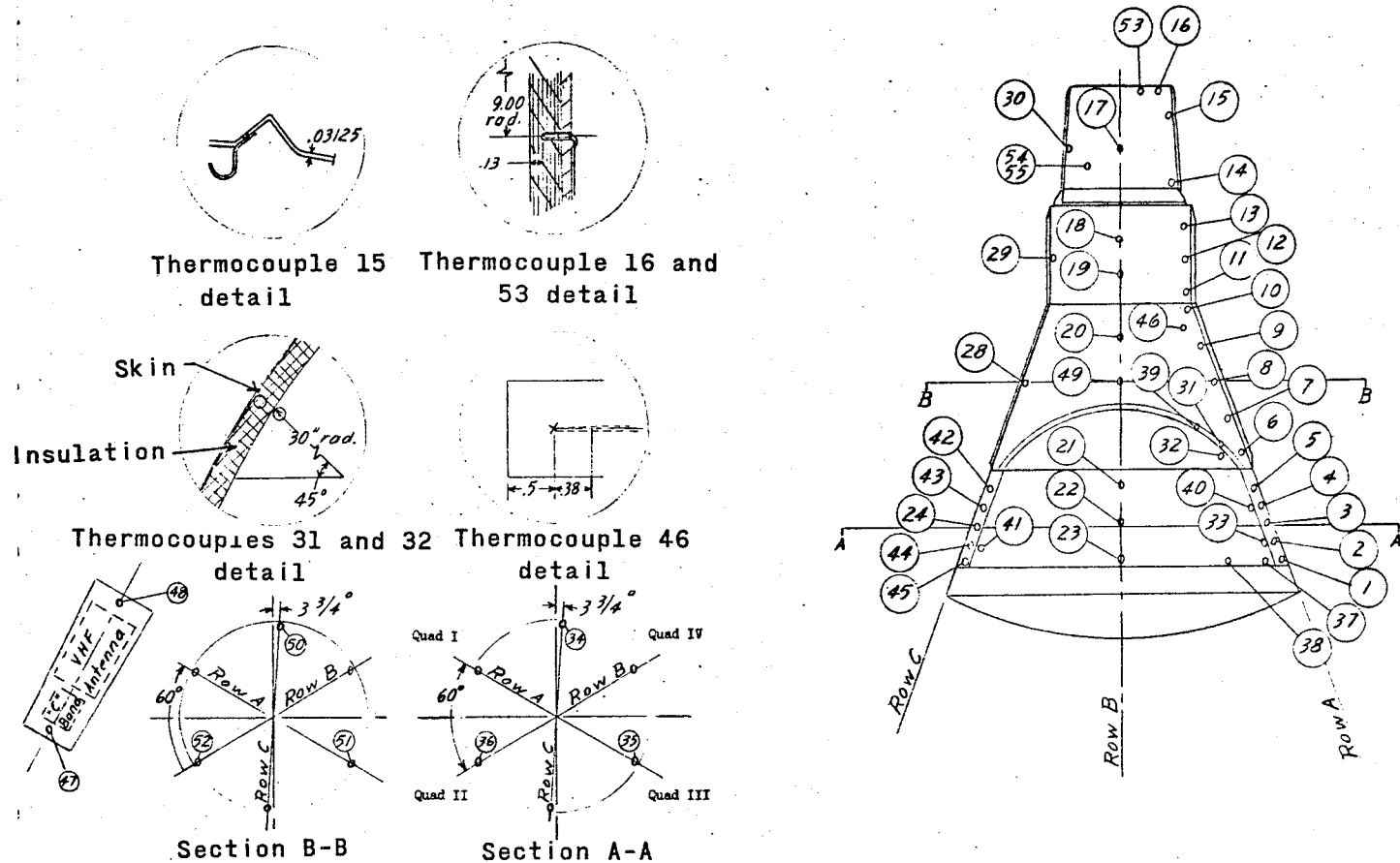


Figure 6. - View at top of parachute container  
(cylindrical section)

~~CONFIDENTIAL~~



Note: The 6 T.C.'s in A-A and B-B are equally spaced.

Figure 7 .- Sketch of afterbody thermocouple locations. **CONFIDENTIAL**

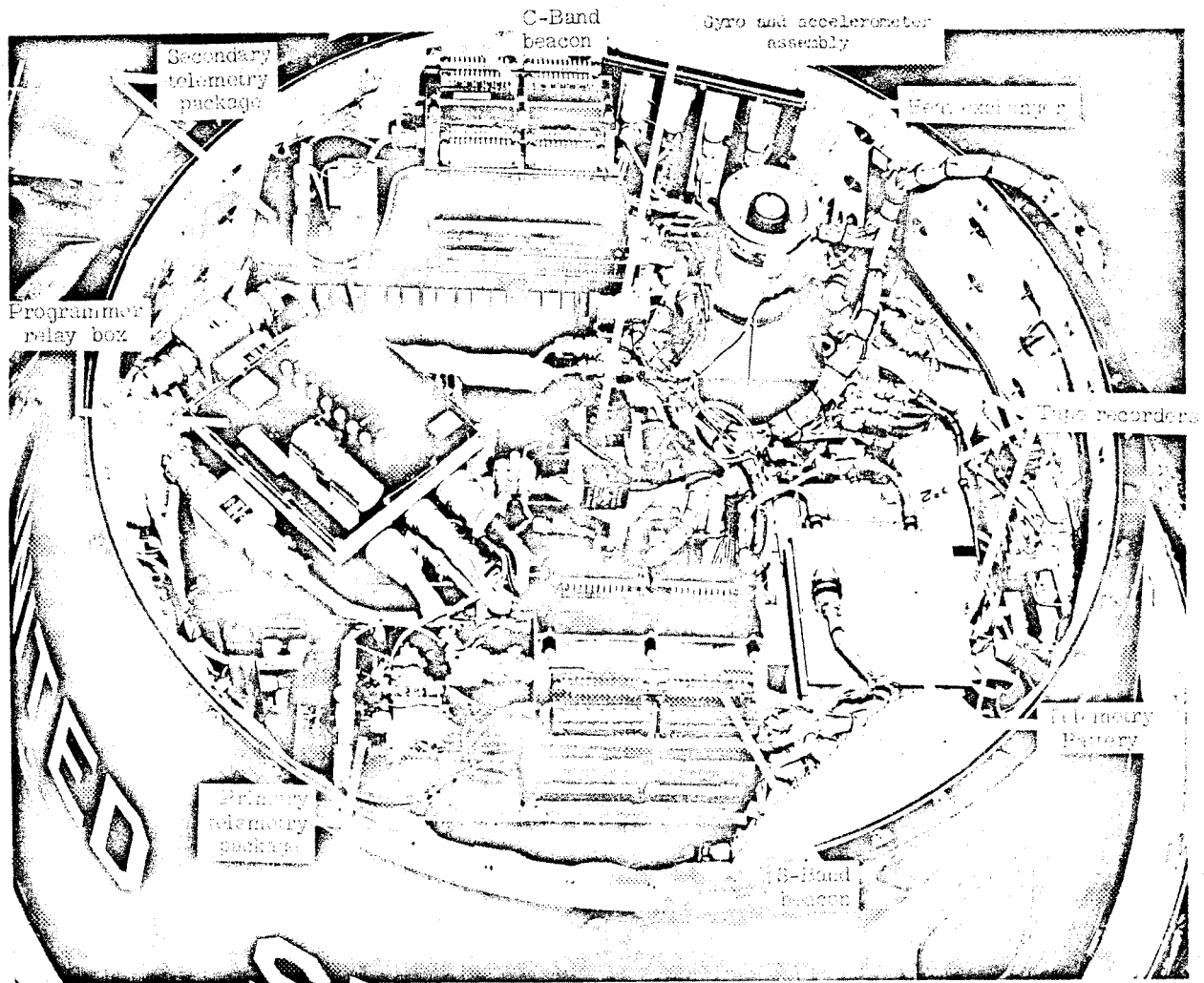


Figure 8.- Arrangement of instrumentation in pressurized compartment.

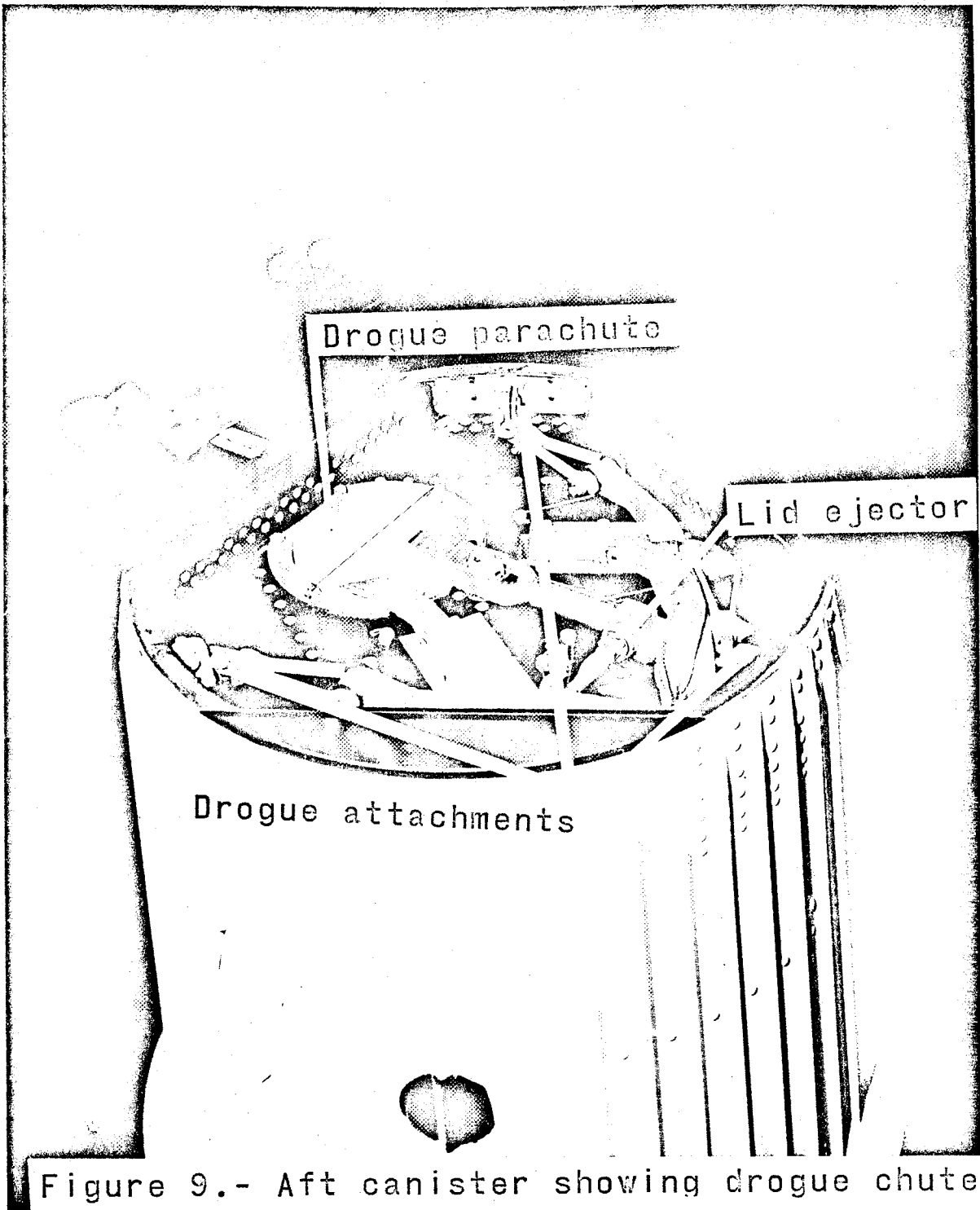


Figure 9.- Aft canister showing drogue chute attachments.

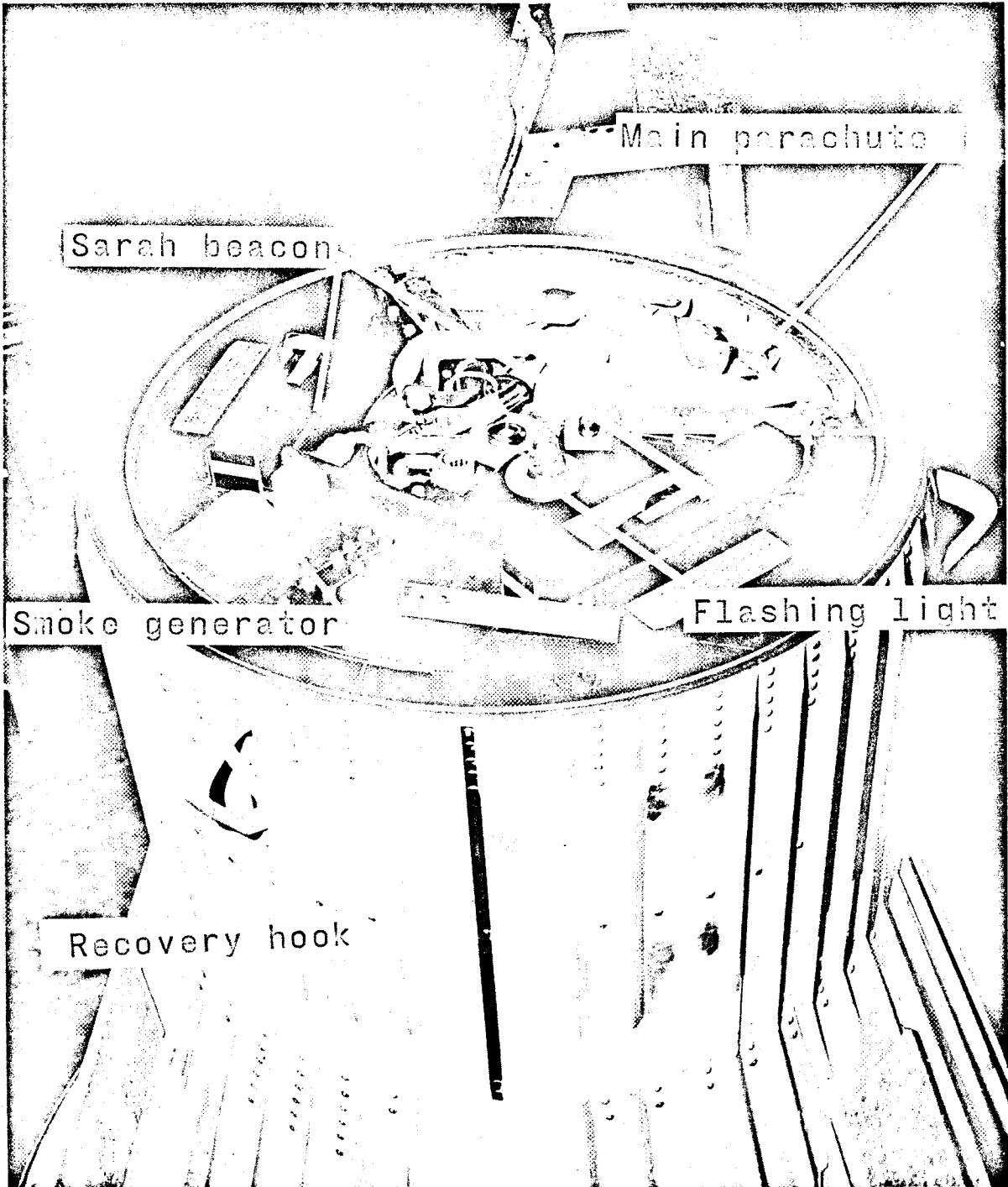


Figure 10.- View of top of cylindrical portion.

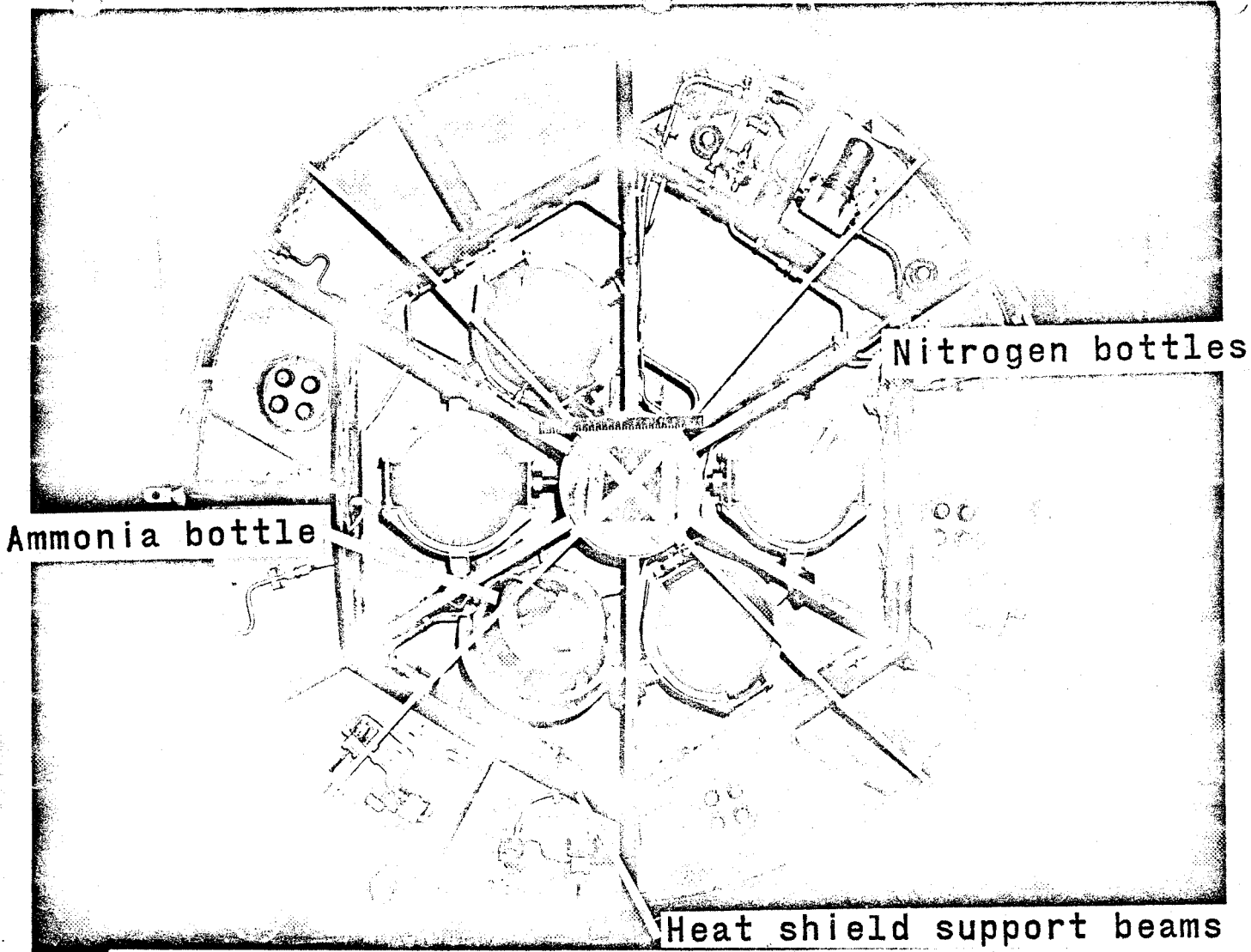


Figure 11.- View upward on pressure bulkhead.

CONFIDENTIAL

CONFIDENTIAL

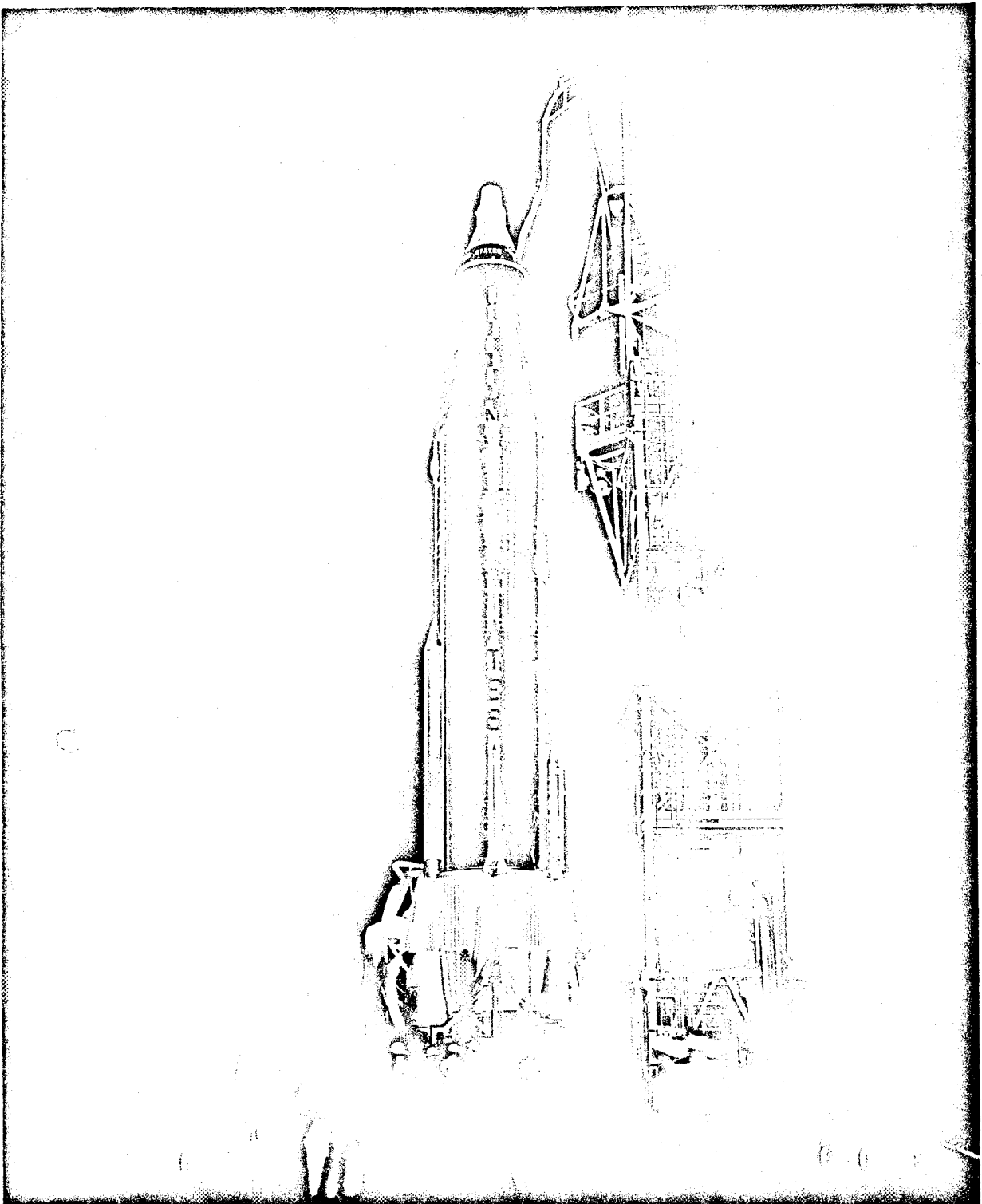
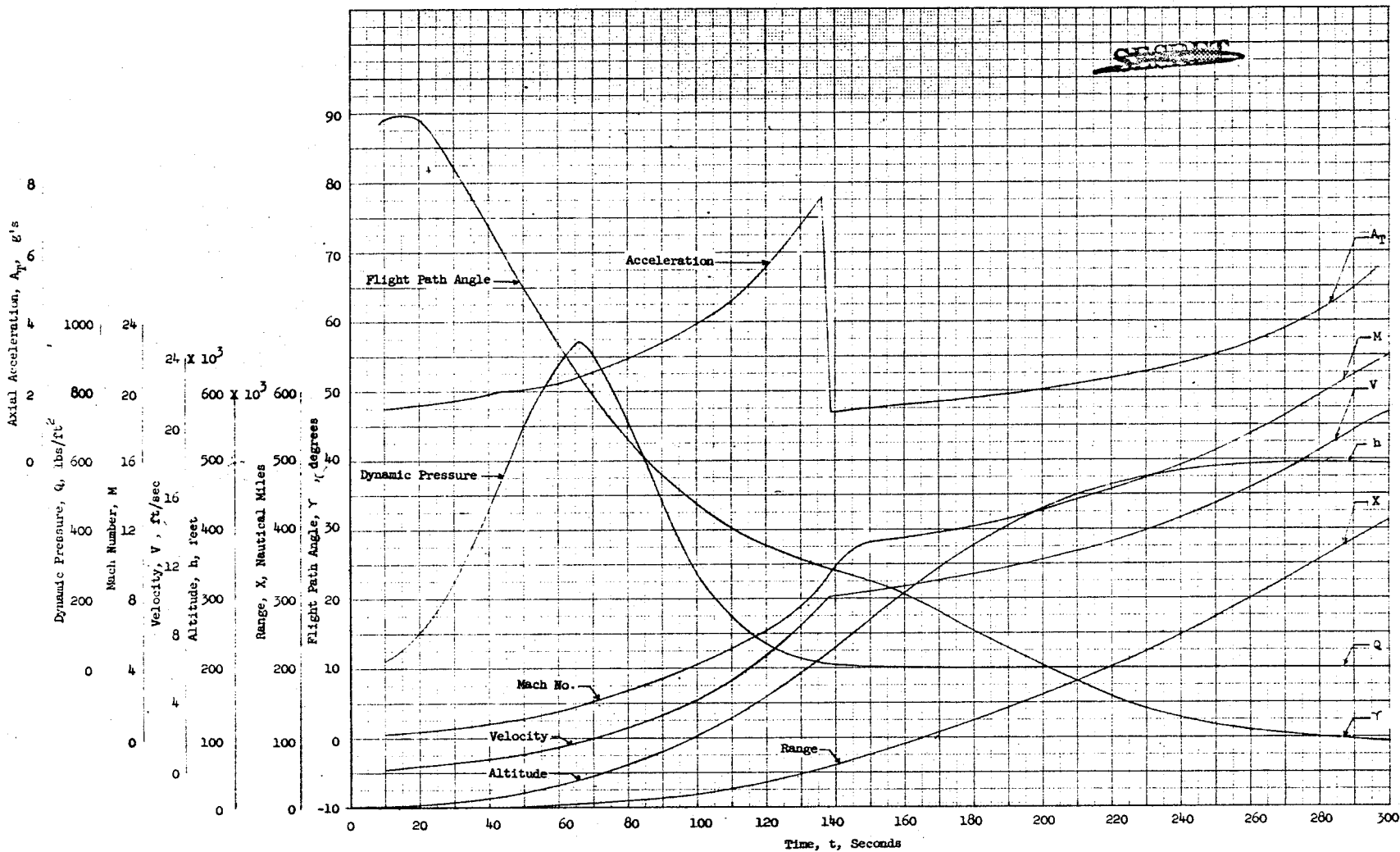


Figure 12.- Mercury "Big Joe" capsule mounted on Atlas 10-D booster on launch stand.



NASA SPACE TASK GROUP

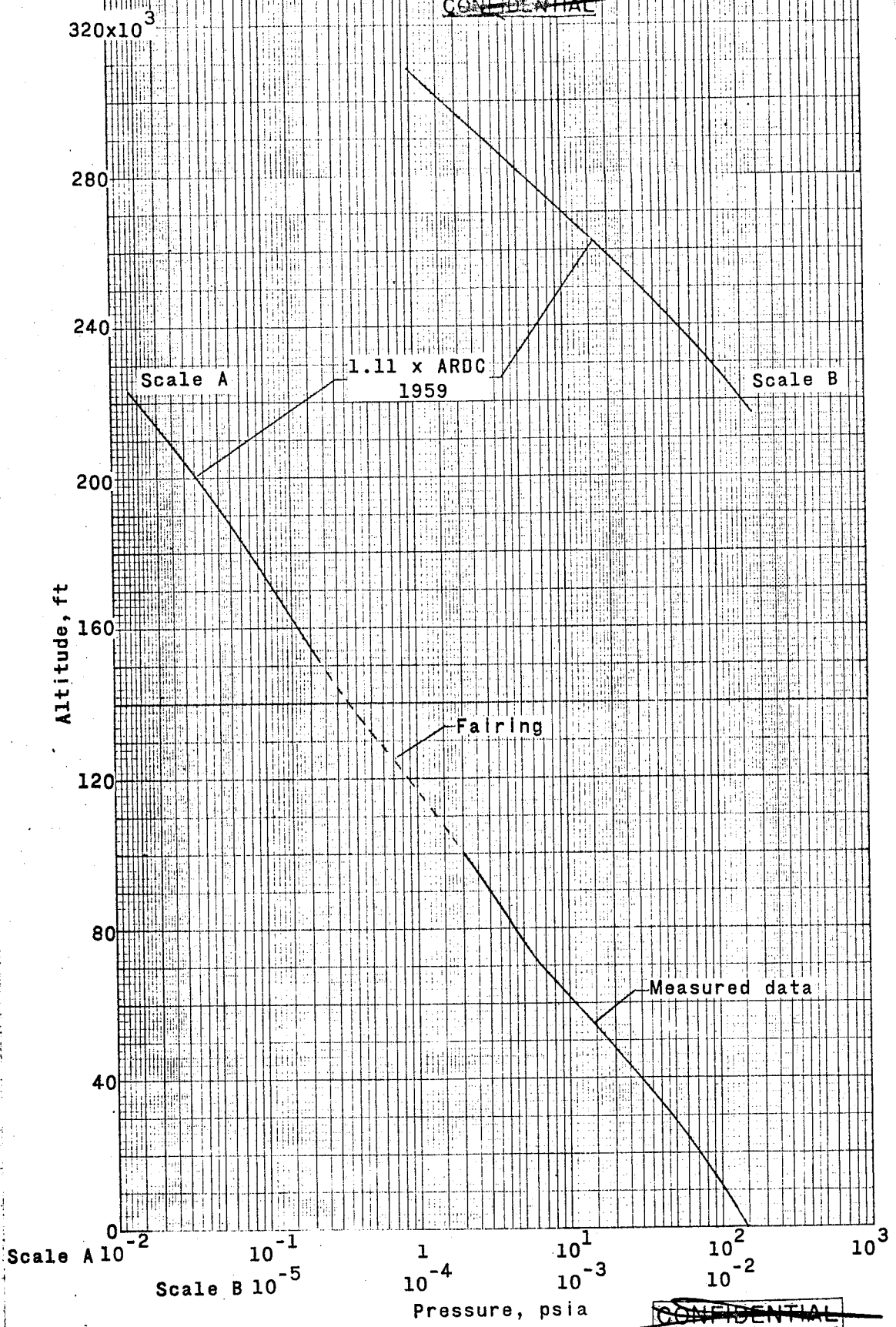
(a) Exit.

Figure 13.- "Big Joe" trajectory.

~~SECRET~~



~~CONFIDENTIAL~~

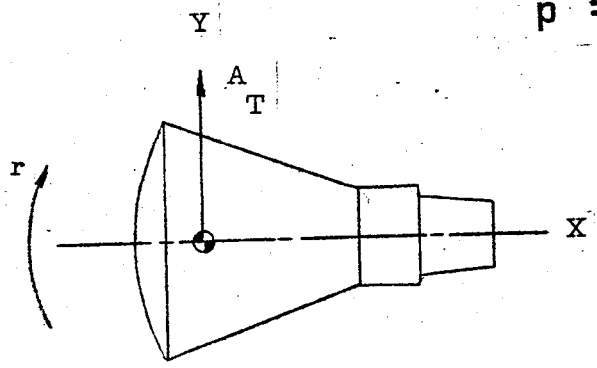


~~CONFIDENTIAL~~

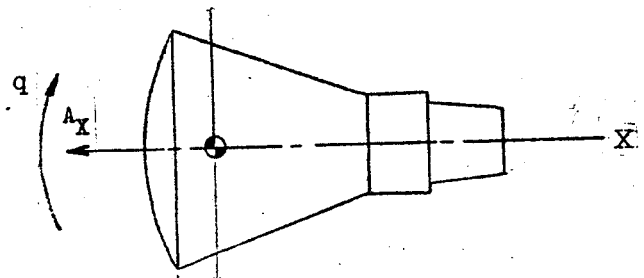
Figure 14.- Atmospheric Pressure vs. Altitude.

**CONFIDENTIAL**

$r$  = Yaw rate  
 $q$  = Pitch rate  
 $p$  = Roll rate

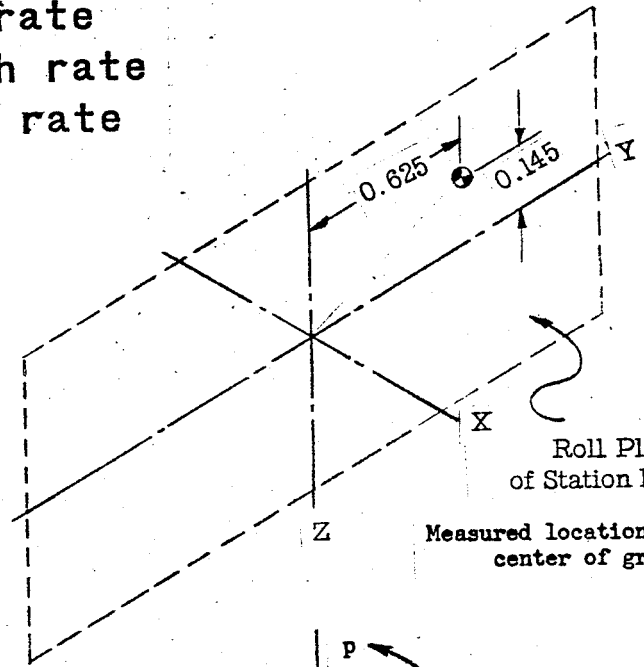


Yaw Plane (Top View)



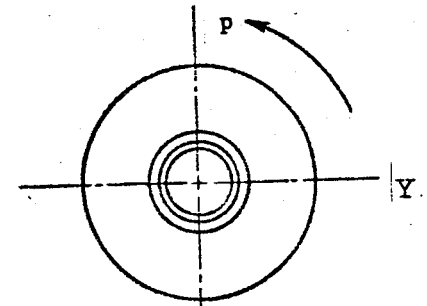
Pitch Plane (Left Side View)

Sta. 0  
Sta. 17.63  
Z



Roll Plane of Station 17.63

Measured location of capsule center of gravity



Roll Plane (Rear View)

Locations and angular rates.

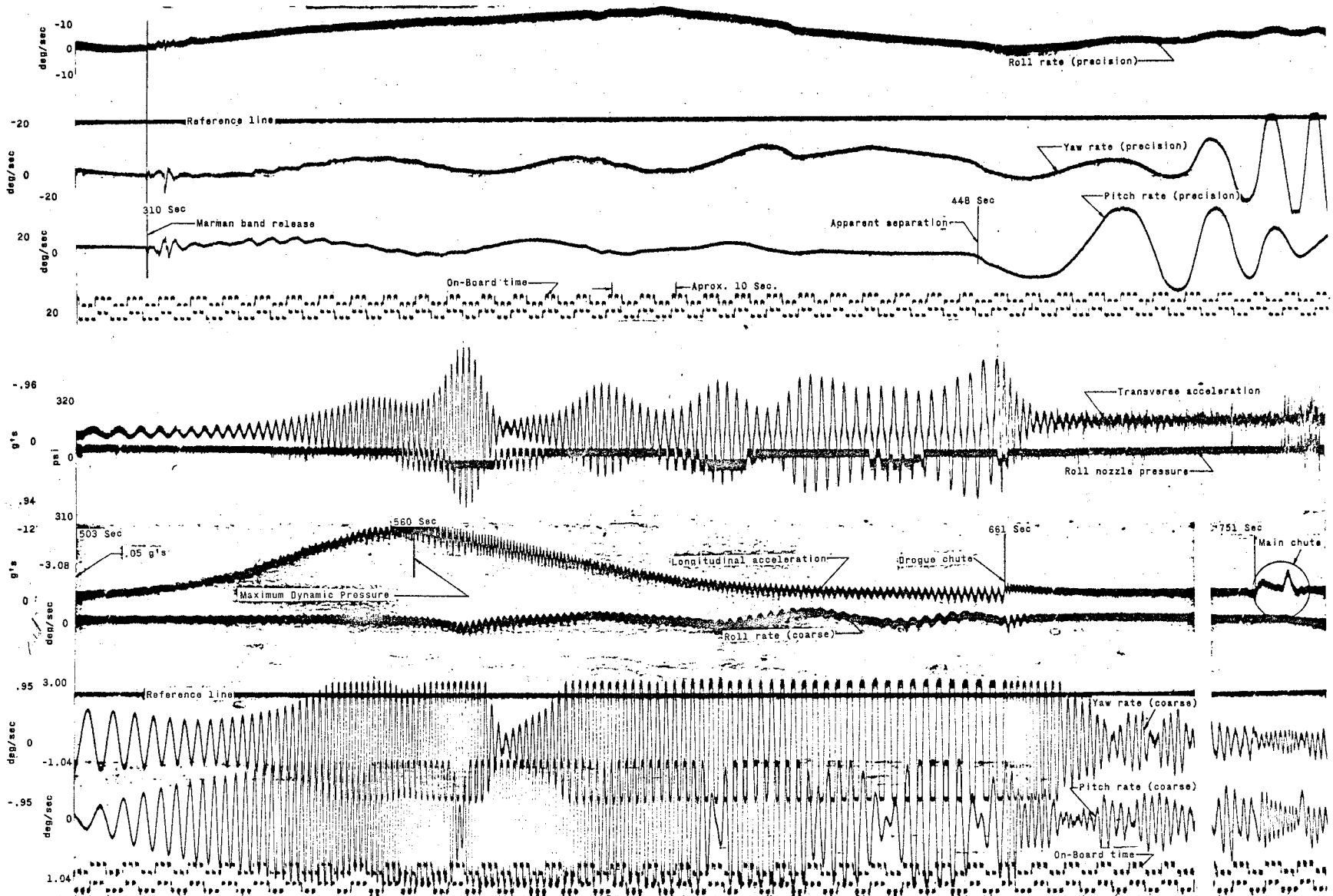


Figure 16 - Partial time history of on-board recorded data.

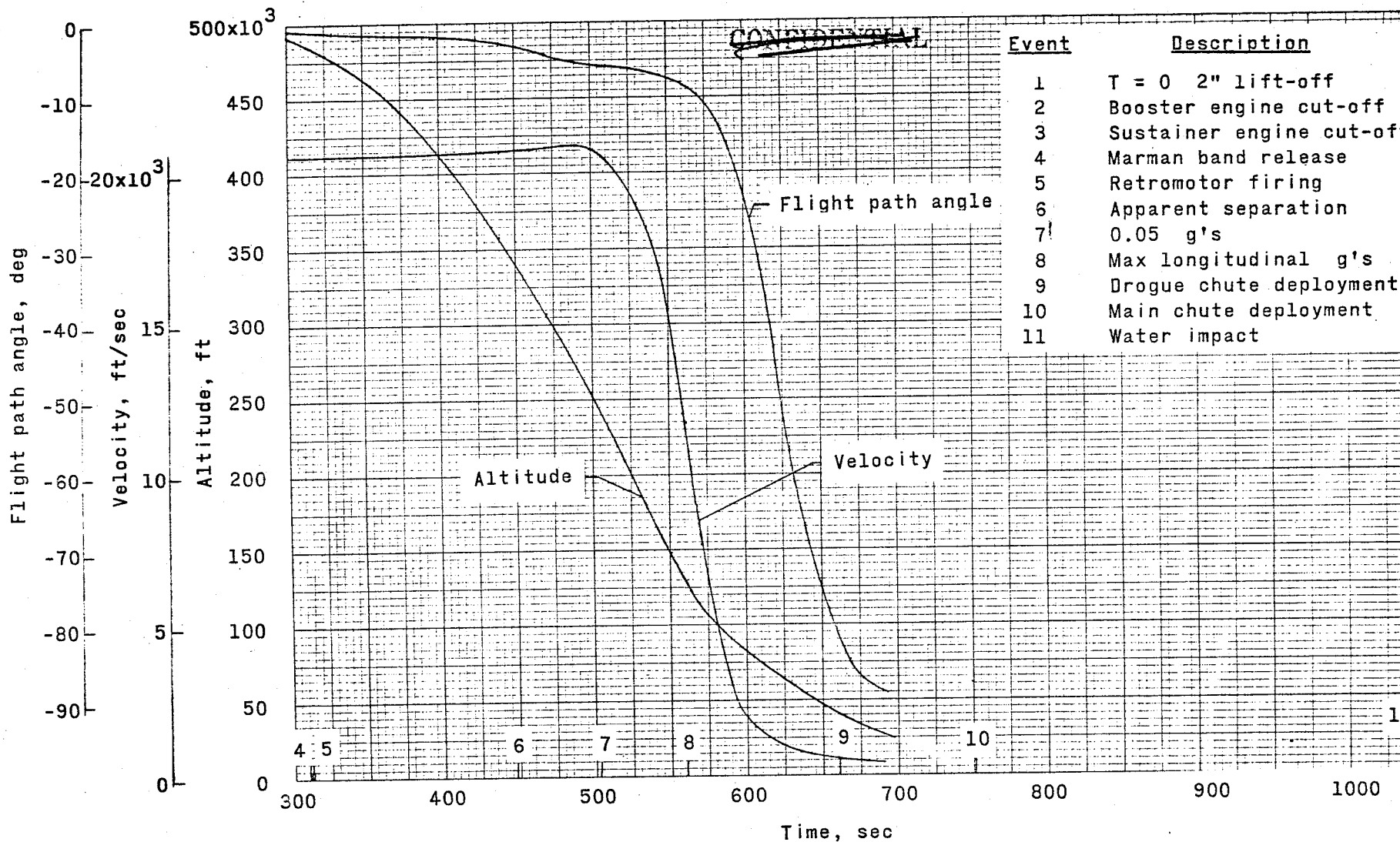


Figure 17.- Time history of altitude and velocity showing events.

~~CONFIDENTIAL~~

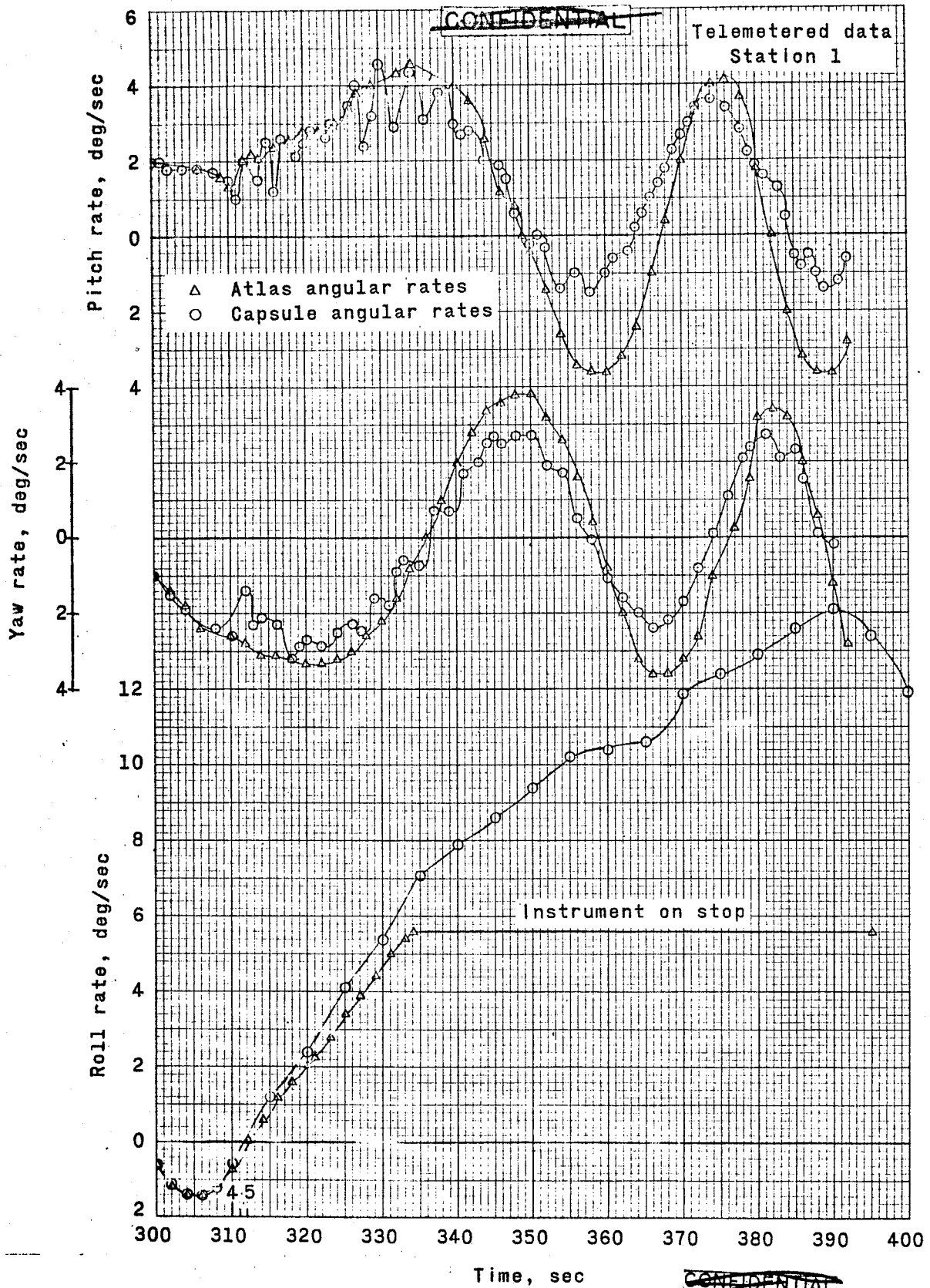


Figure 18.- Comparison of Atlas and Big Joe angular rates as a function of time.

~~CONFIDENTIAL~~

On-board recorded data

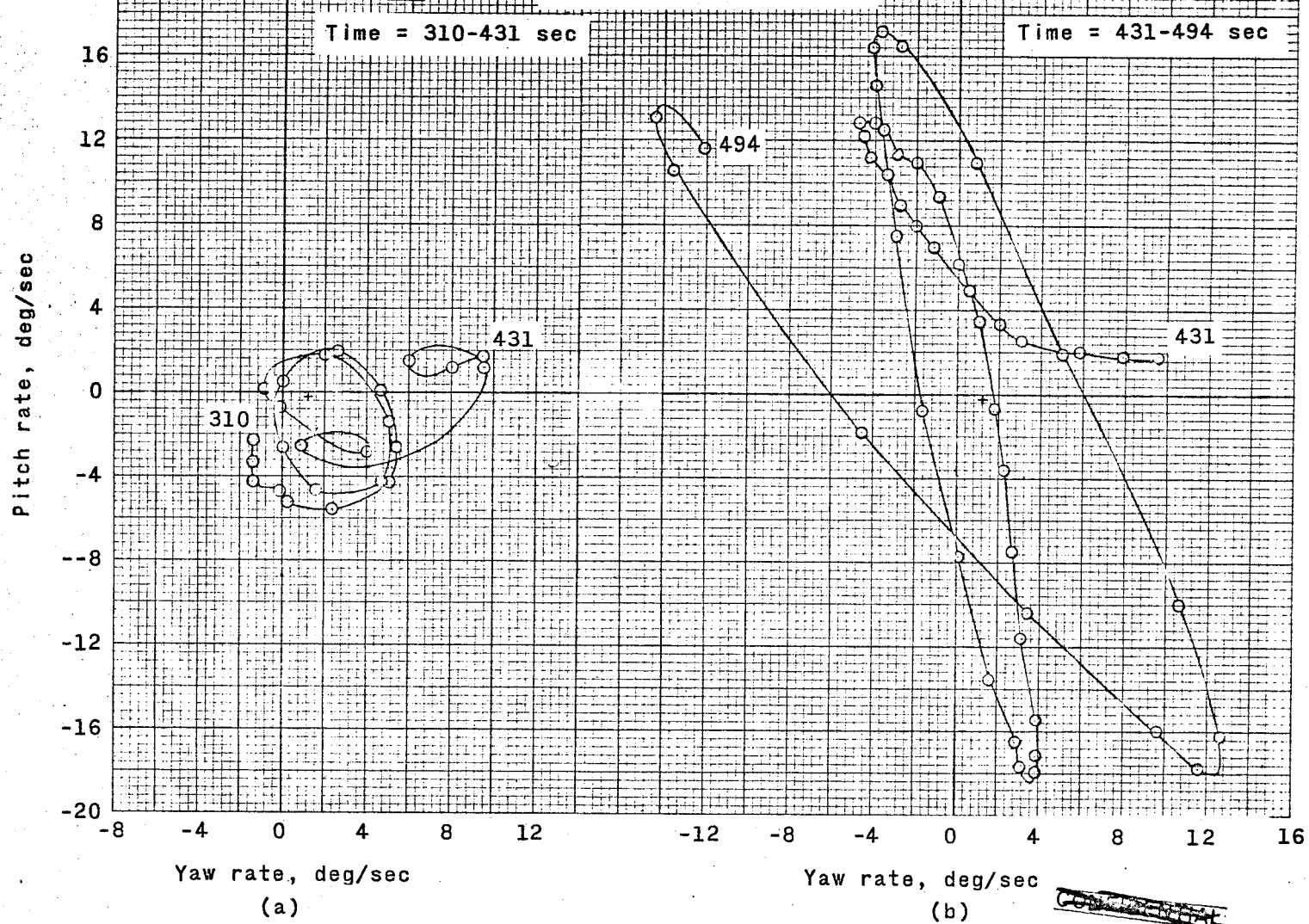


Figure 19.- Crossplots of pitch rate against yaw rate.

~~CONFIDENTIAL~~

~~CONFIDENTIAL~~

On-board recorded data

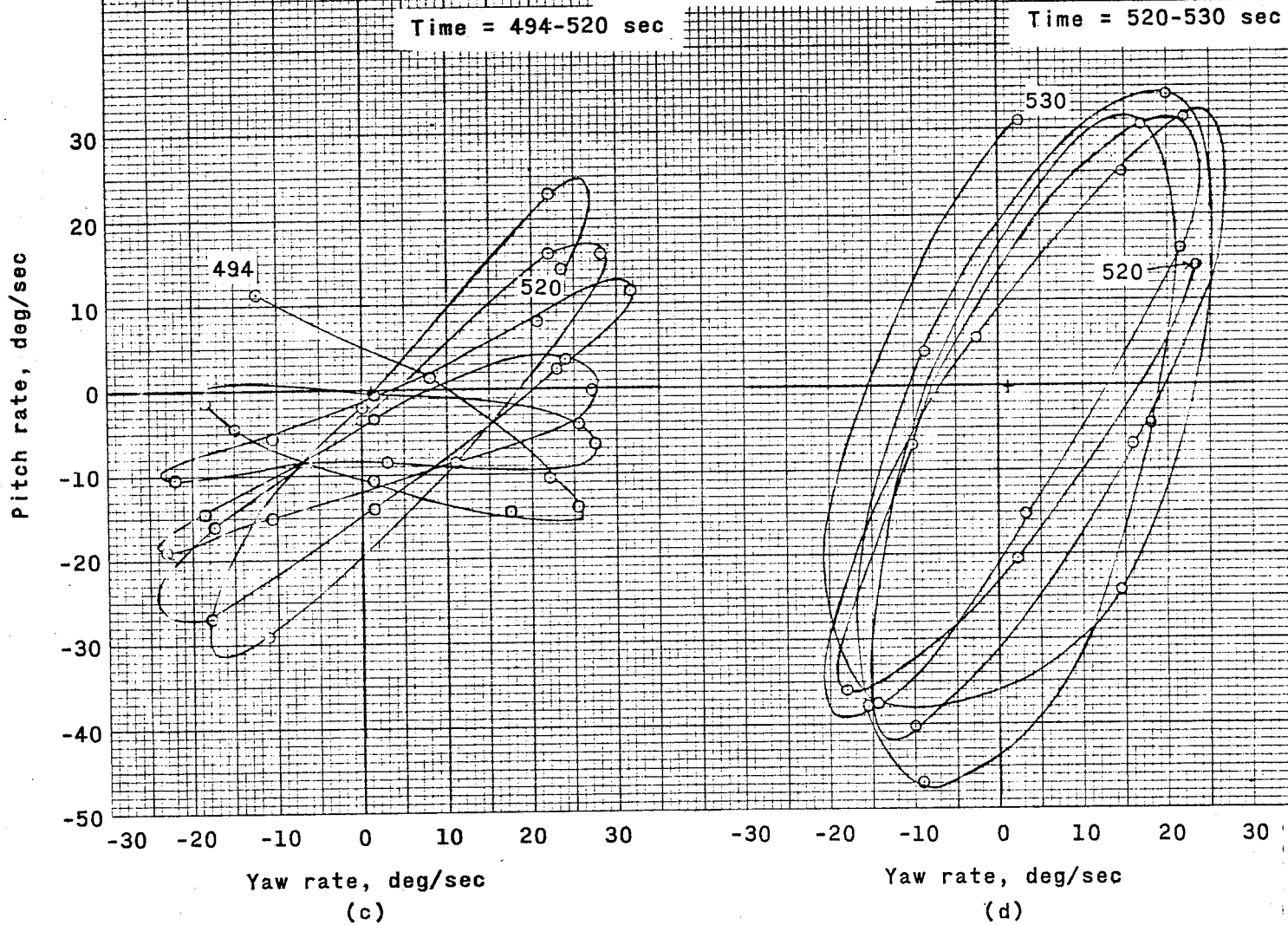


Figure 19.- Continued.

~~CONFIDENTIAL~~

~~CONFIDENTIAL~~

On-board recorded data

Time = 530-537 sec

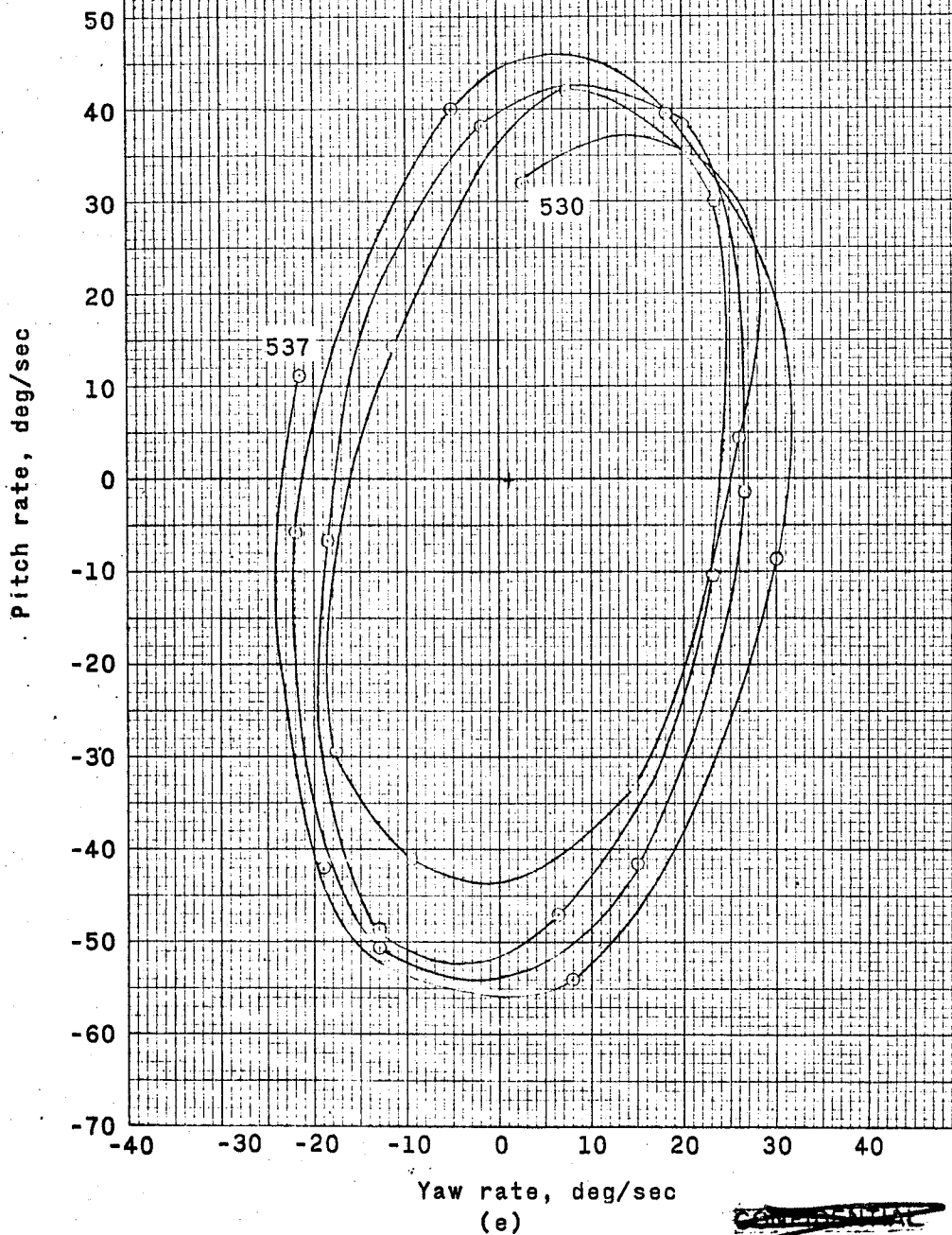


Figure 19.- Continued.

~~CONFIDENTIAL~~

~~CONFIDENTIAL~~

On-board recorded data

Time = 537-542 sec

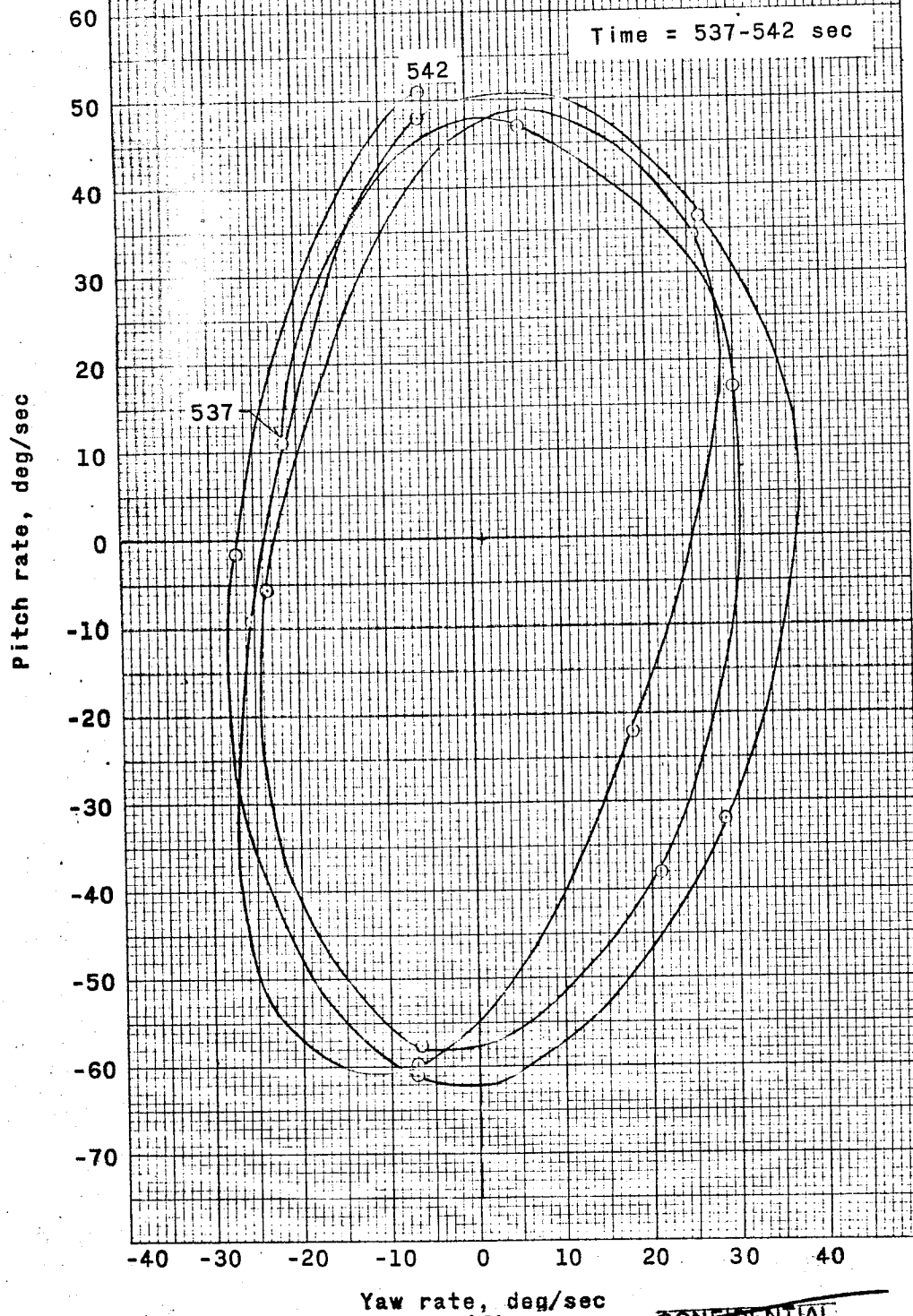


Figure 19.- Concluded.

~~CONFIDENTIAL~~

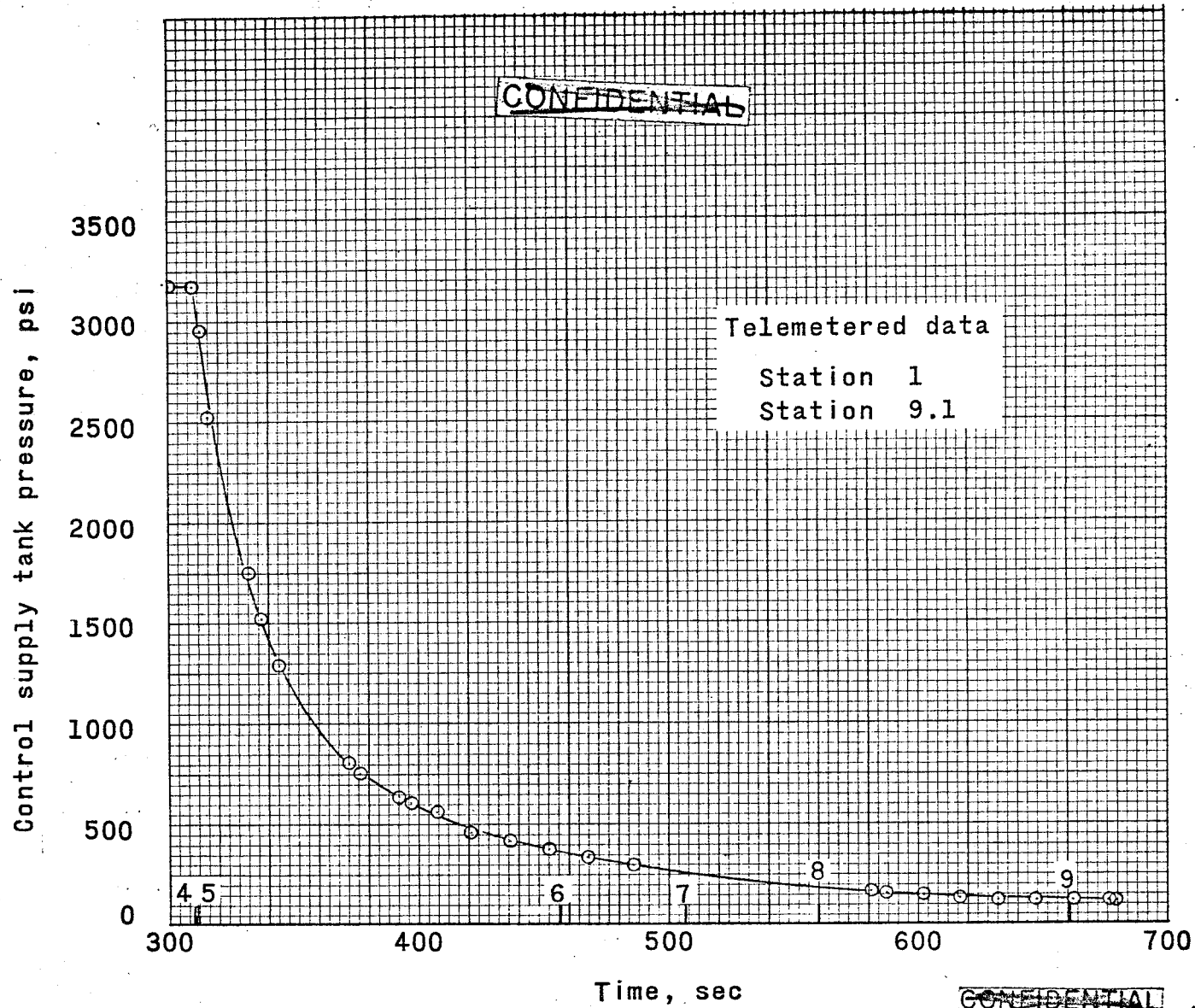


Figure 20.- Control supply tank pressure as a function of time.

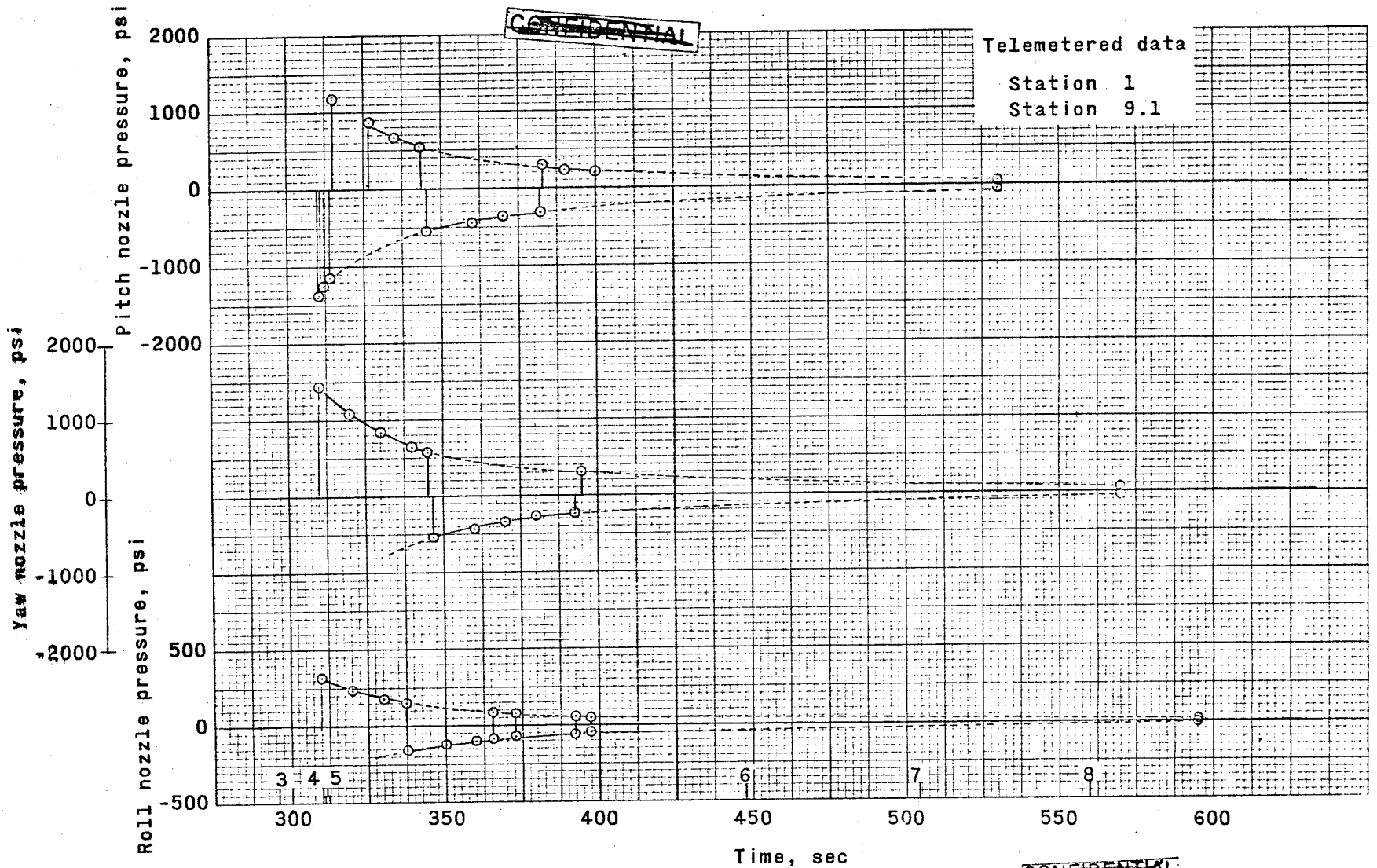


Figure 21.- Reaction control nozzle pressures.

Longitudinal acceleration,  $A_L$ , g's

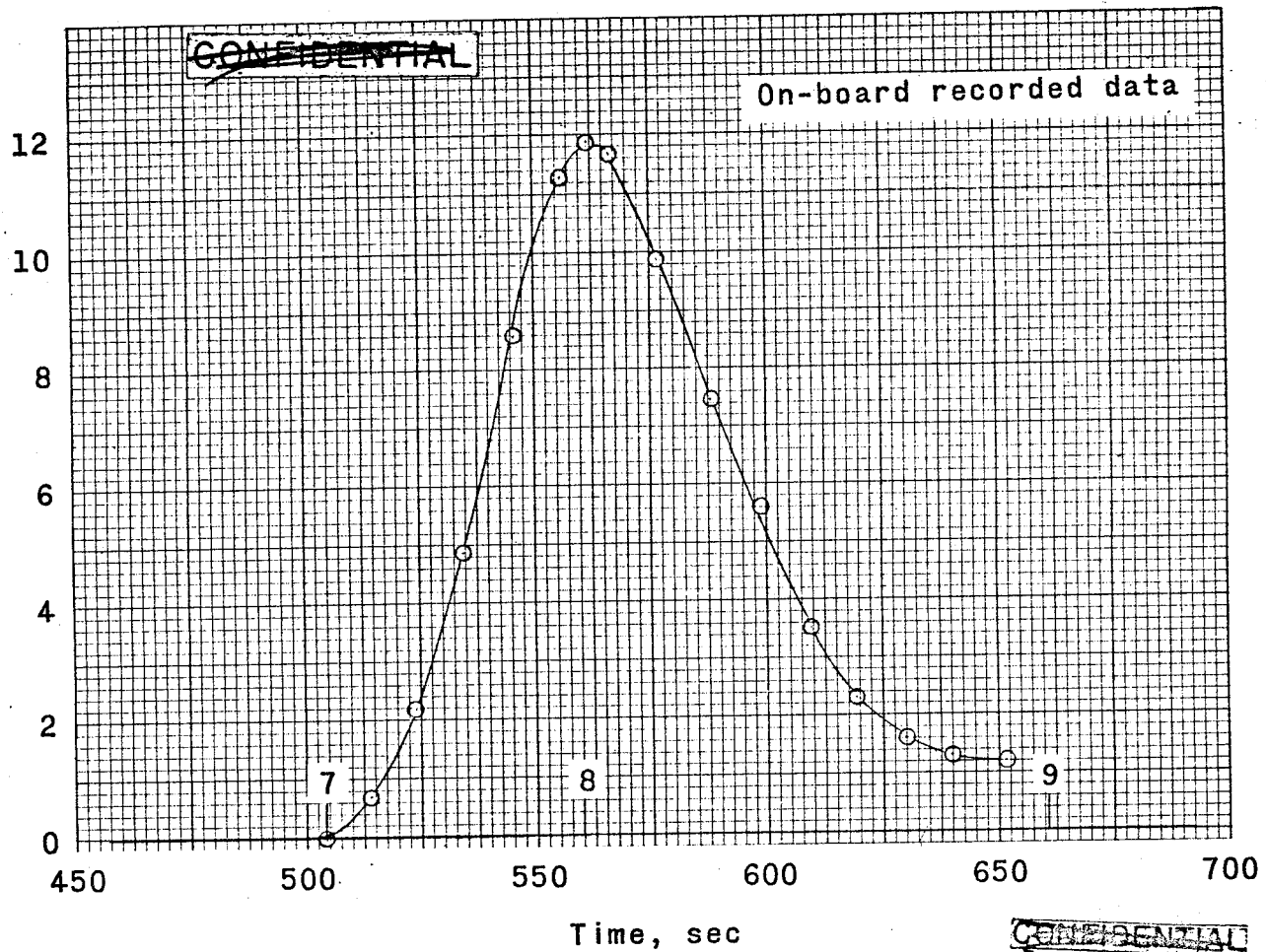


Figure 22.- Longitudinal accelerations as a function of time.

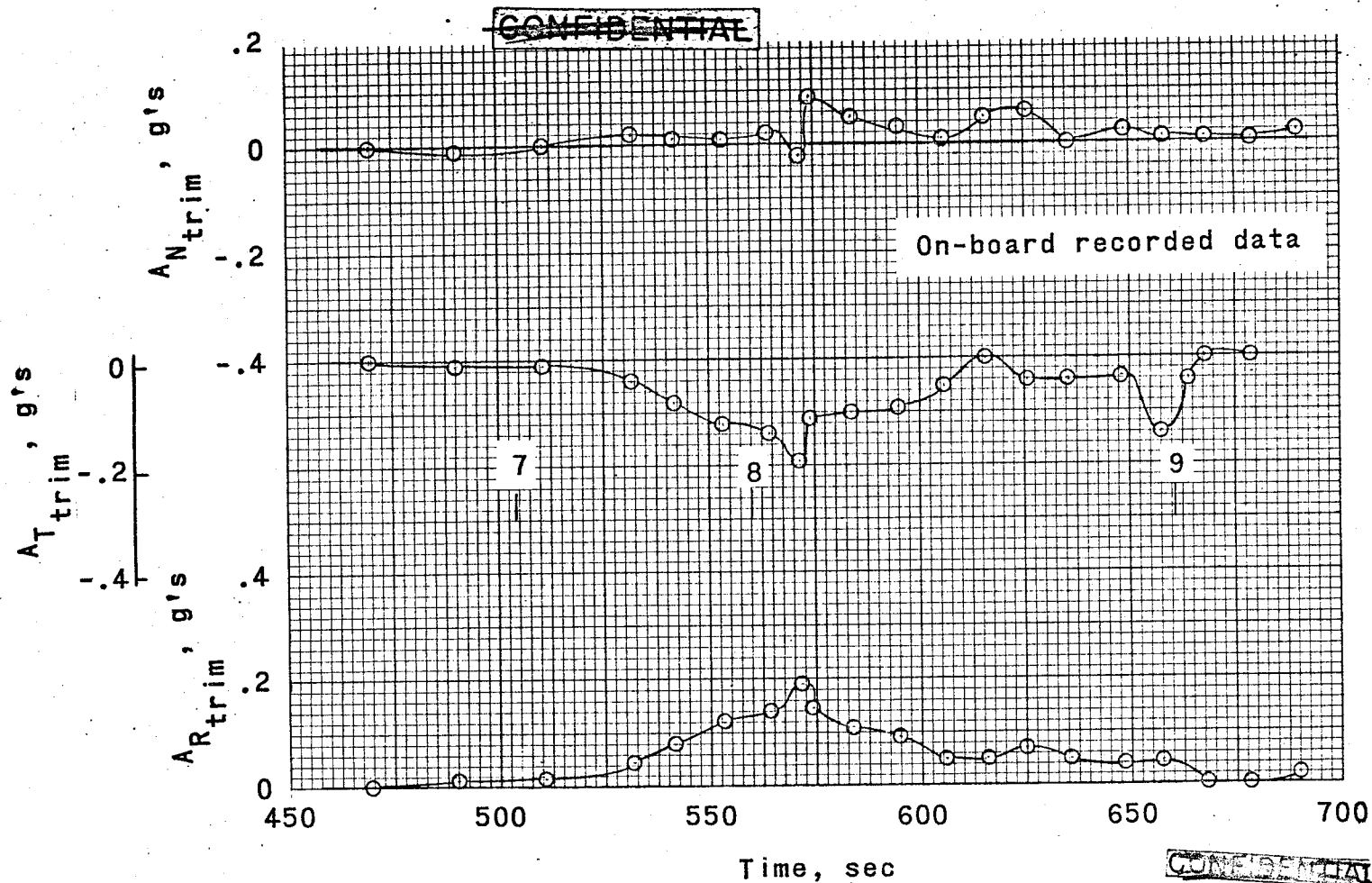


Figure 23.- Trim accelerations as a function of time.

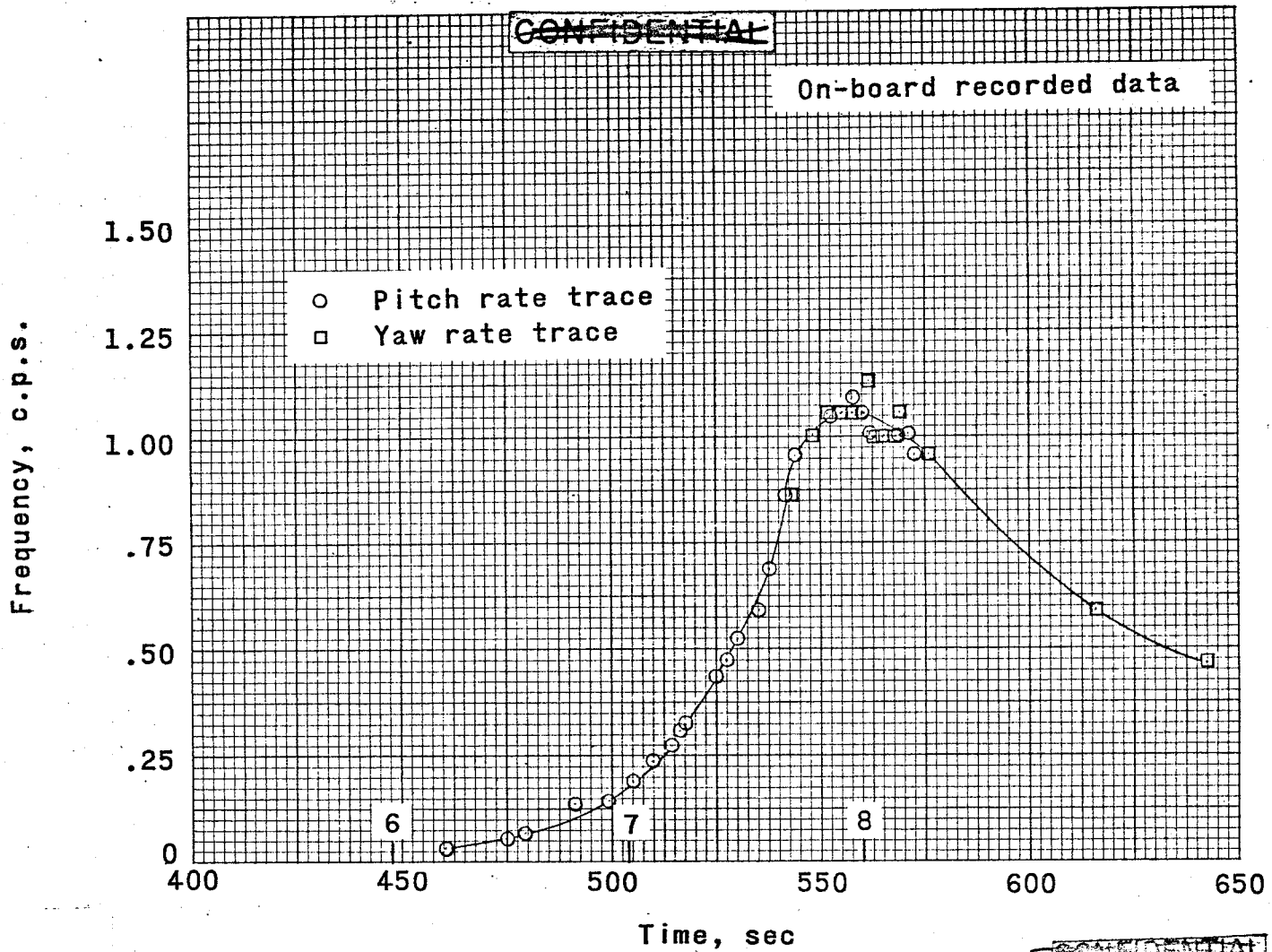


Figure 24.- Frequency of oscillation from pitch and yaw rate.

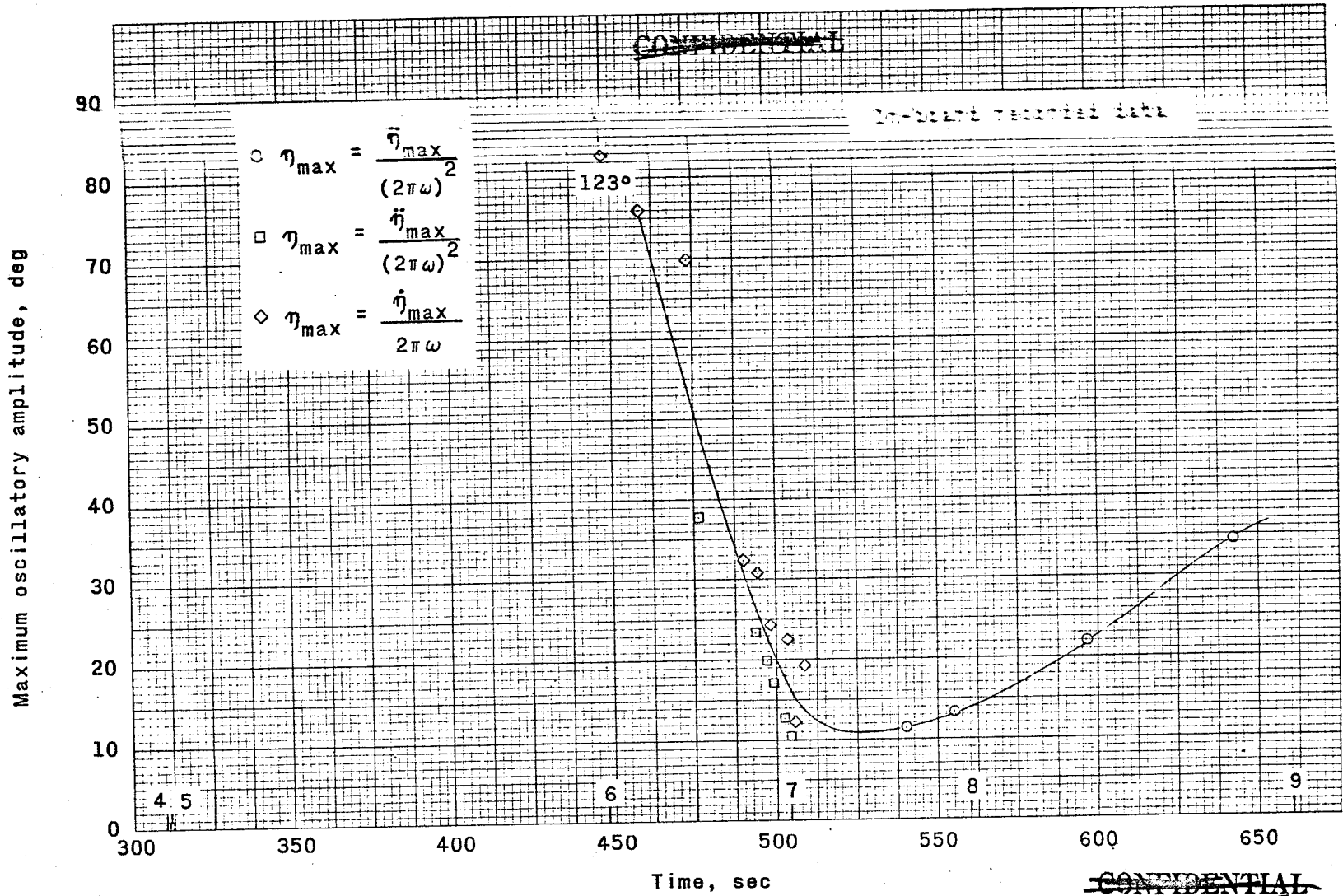
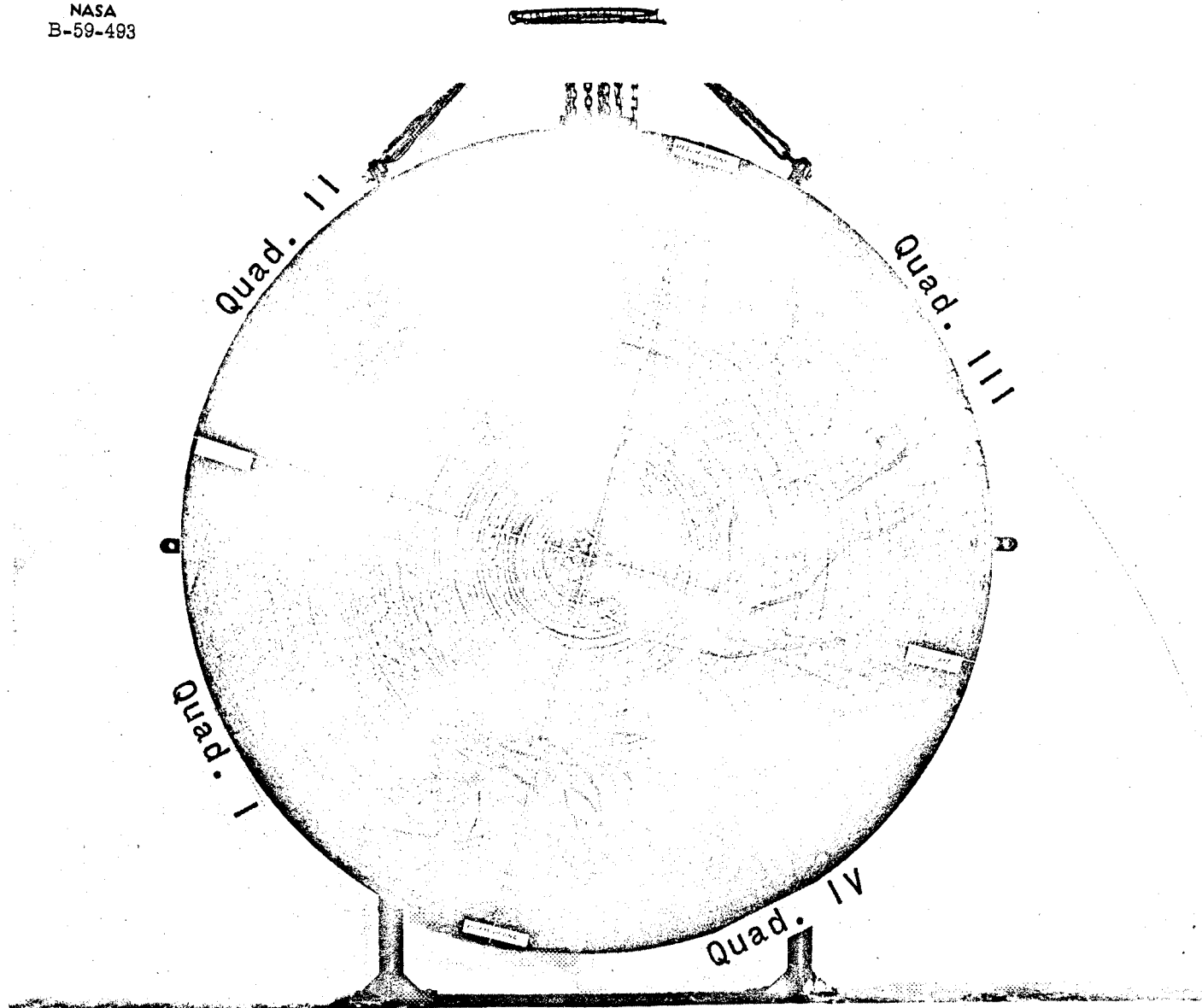


Figure 25.- Maximum oscillatory amplitude about trim as a function of time.



CONFIDENTIAL

Figure 26.- Recovered heat shield.

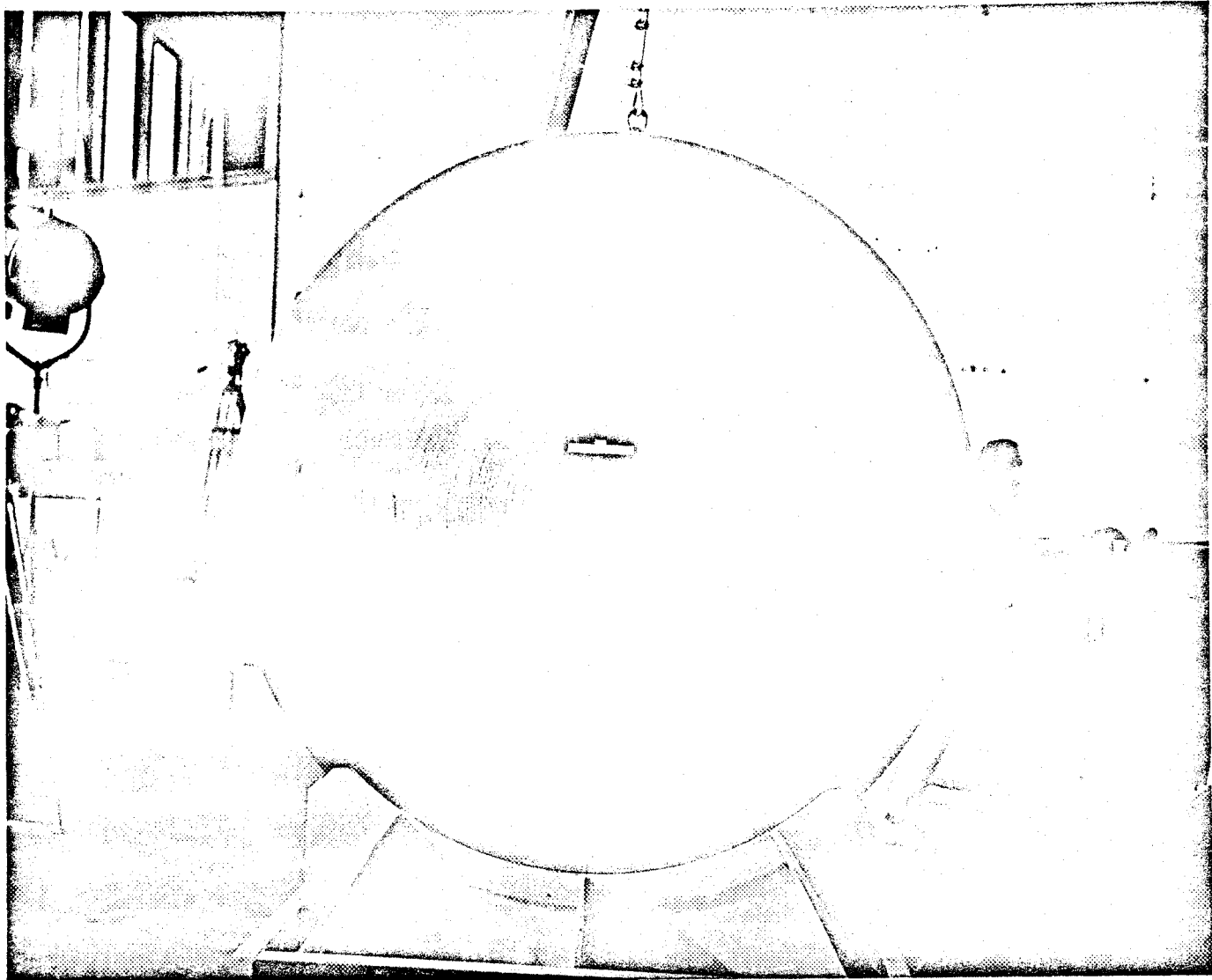


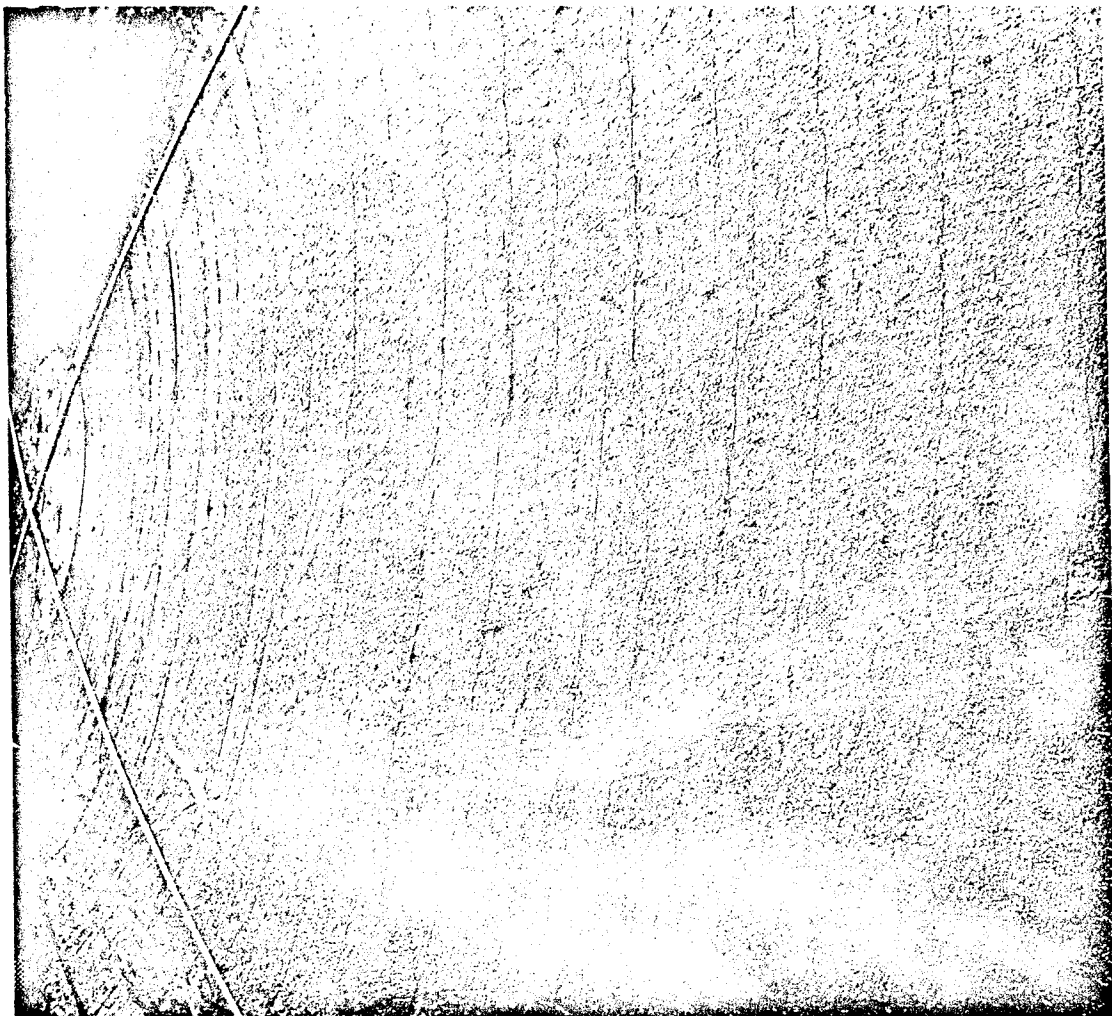
Figure 27 .- Heat shield before test flight.

~~CONFIDENTIAL~~

~~CONFIDENTIAL~~

NASA  
B-59-504

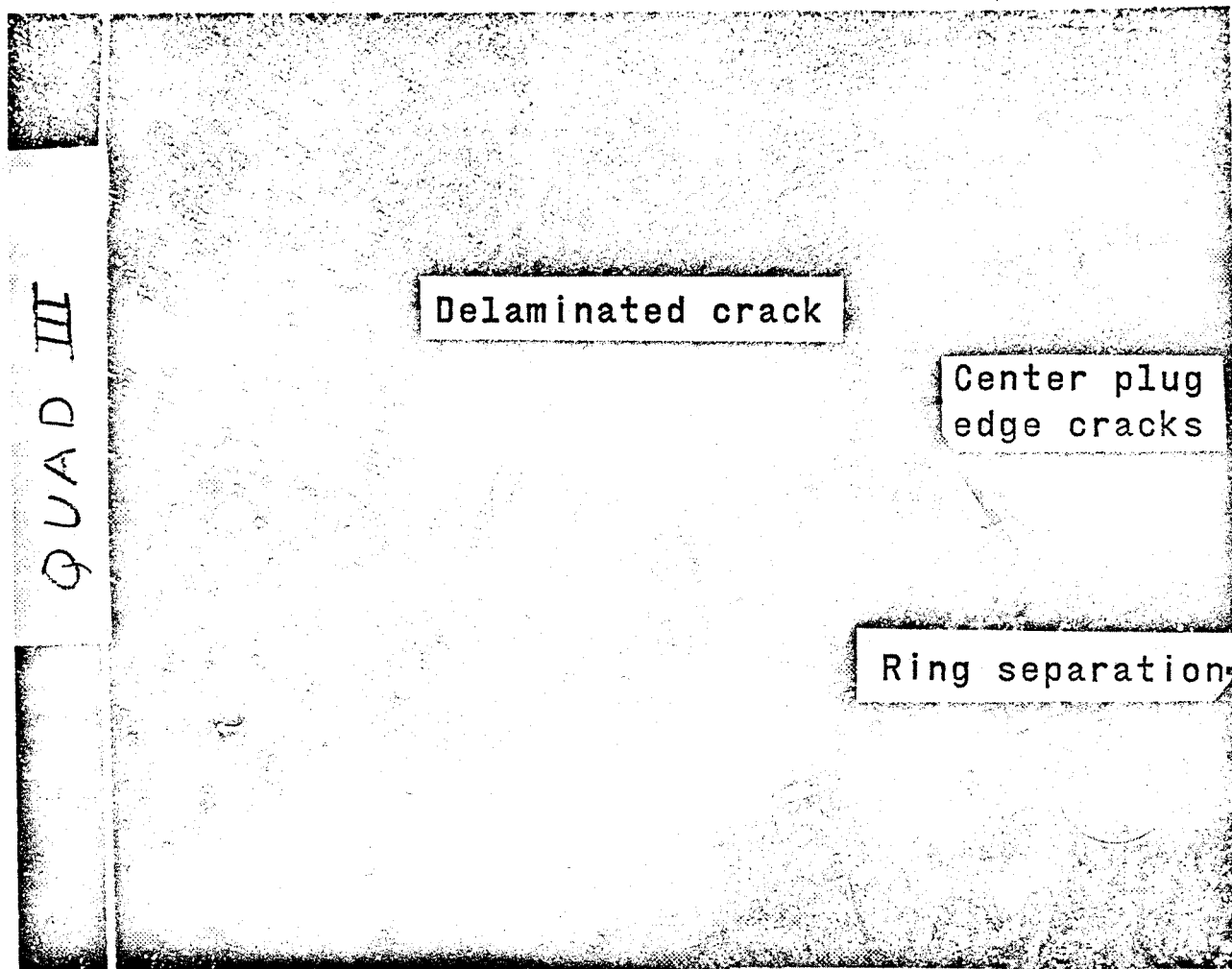
~~CONFIDENTIAL~~



~~CONFIDENTIAL~~

Figure 28 .- Recovered heat shield showing  
typical ring cracking.

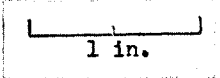
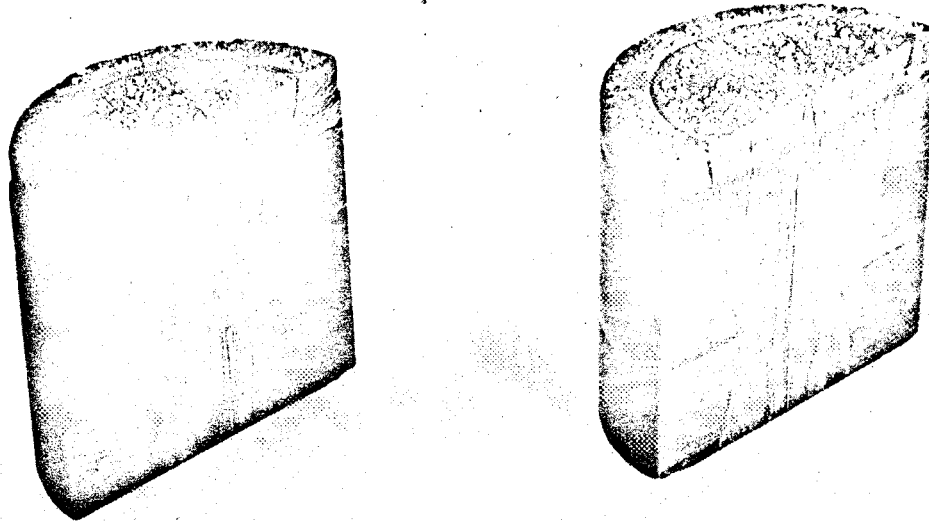
~~CONFIDENTIAL~~



~~CONFIDENTIAL~~

Figure 29.- Close-up of recovered heat shield showing delamination and center plug area.

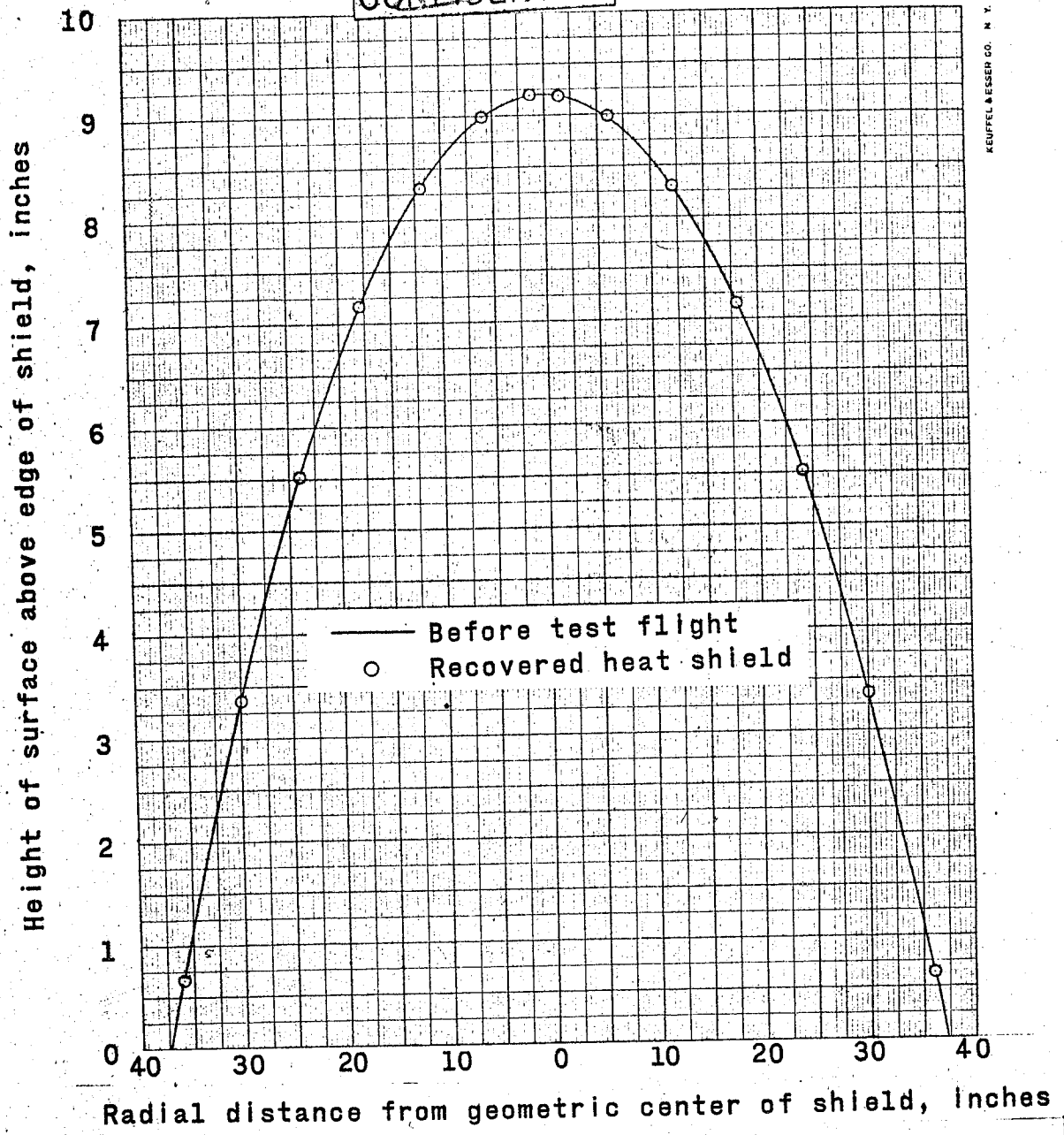
~~CONFIDENTIAL~~



~~CONFIDENTIAL~~

Figure 30.- Ring separation at center plug of heat shield.

~~CONFIDENTIAL~~



KEUFFEL & ESSER CO. N. Y.

Figure 31.- Comparison of measured heat shield profile before and after flight.

~~CONFIDENTIAL~~

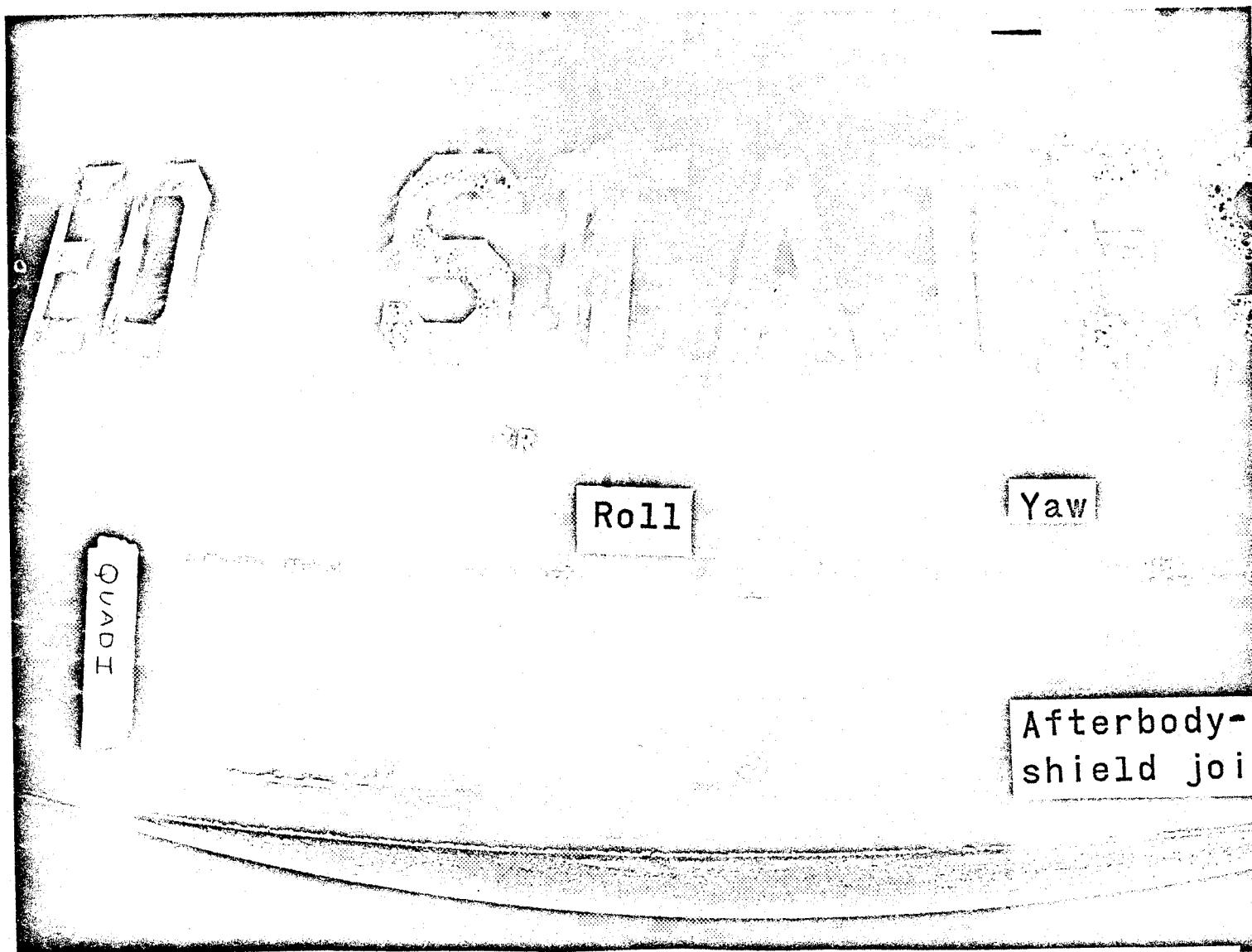
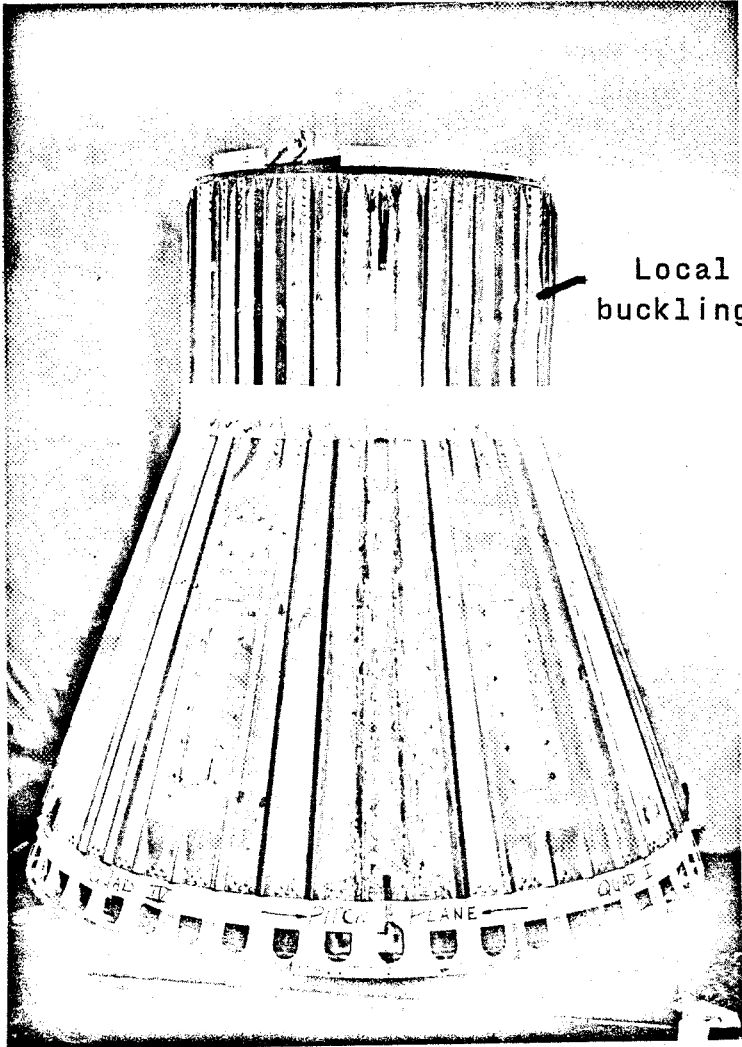


Figure 32.- Close-up of roll and pitch jet areas.

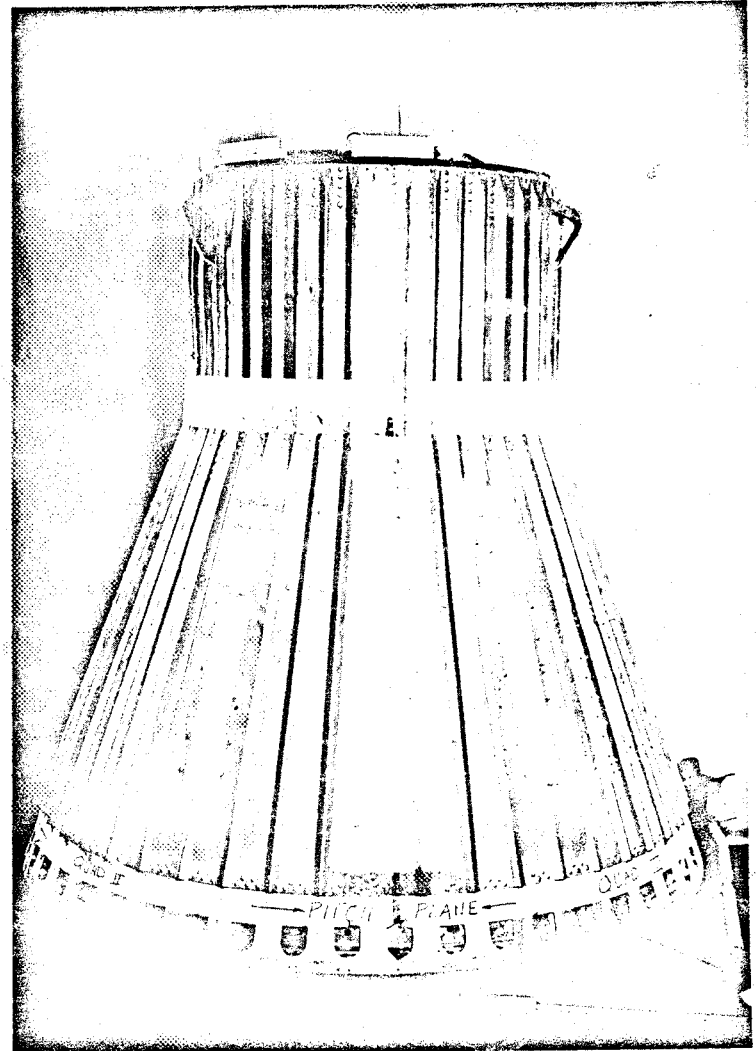
~~CONFIDENTIAL~~

~~CONFIDENTIAL~~



NASA  
B-59-524

(a) Quad I and IV.

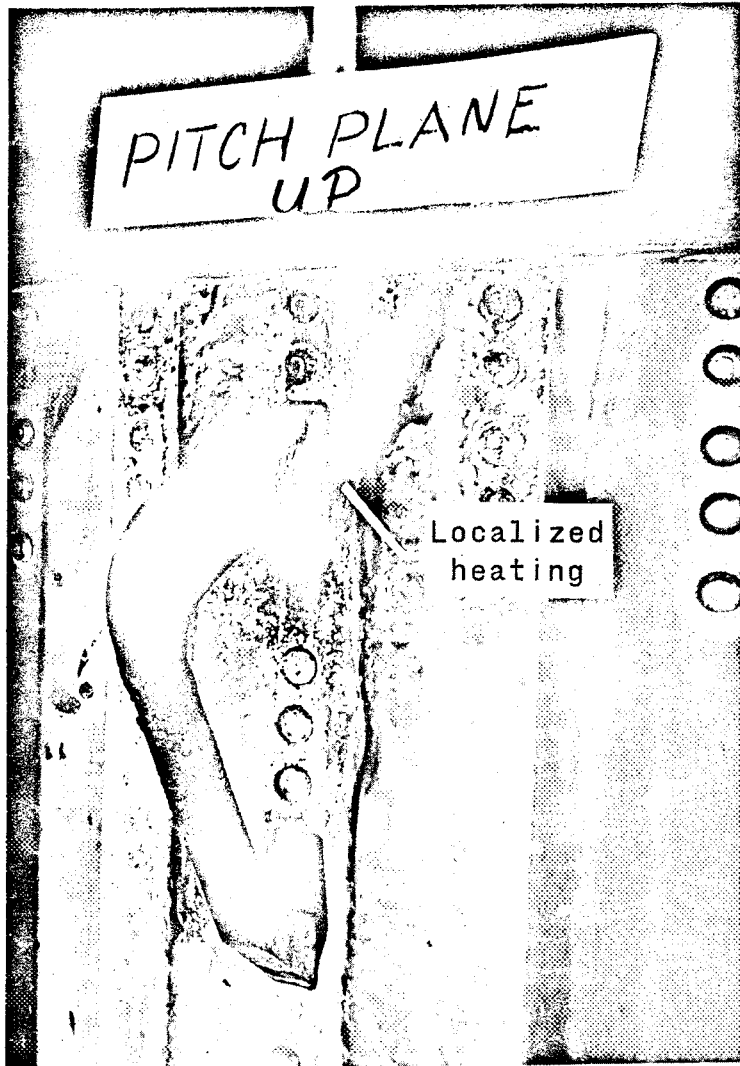


NASA  
R-49-525

(b) Quad II and III.

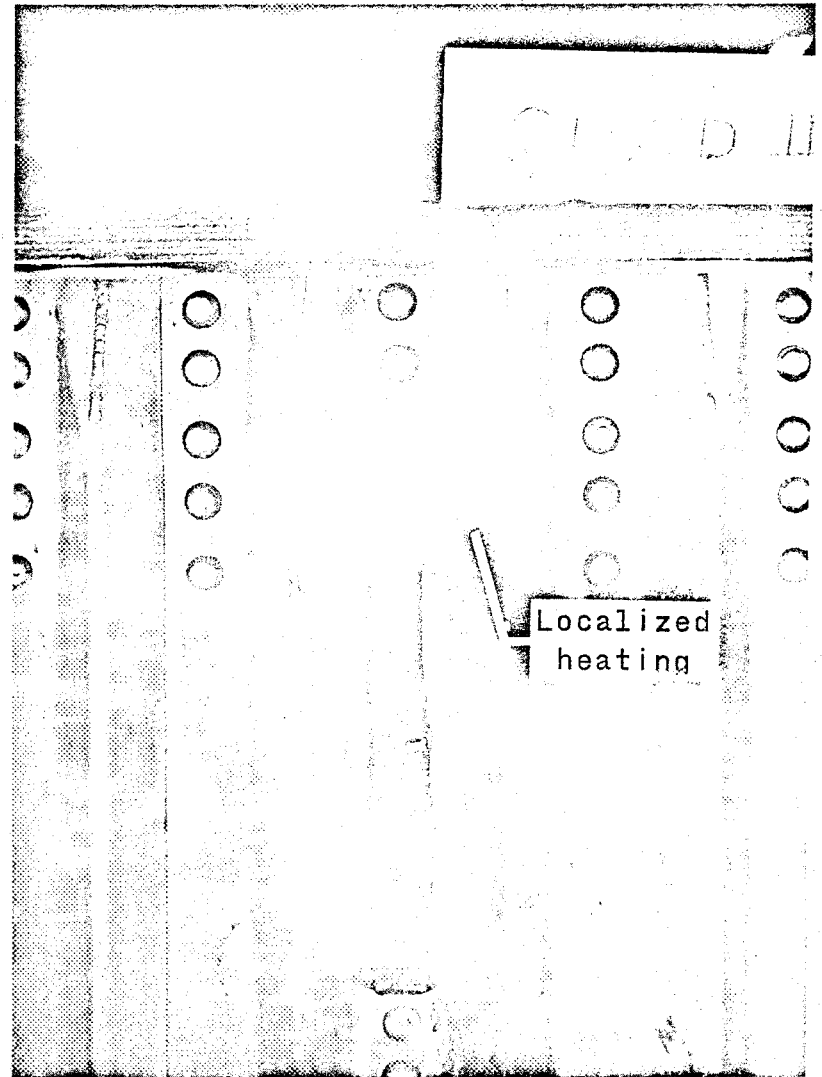
Figure 33.- Recovered afterbody.

~~CONFIDENTIAL~~



NASA  
B-59-528

(a) Hook located in pitch plane.

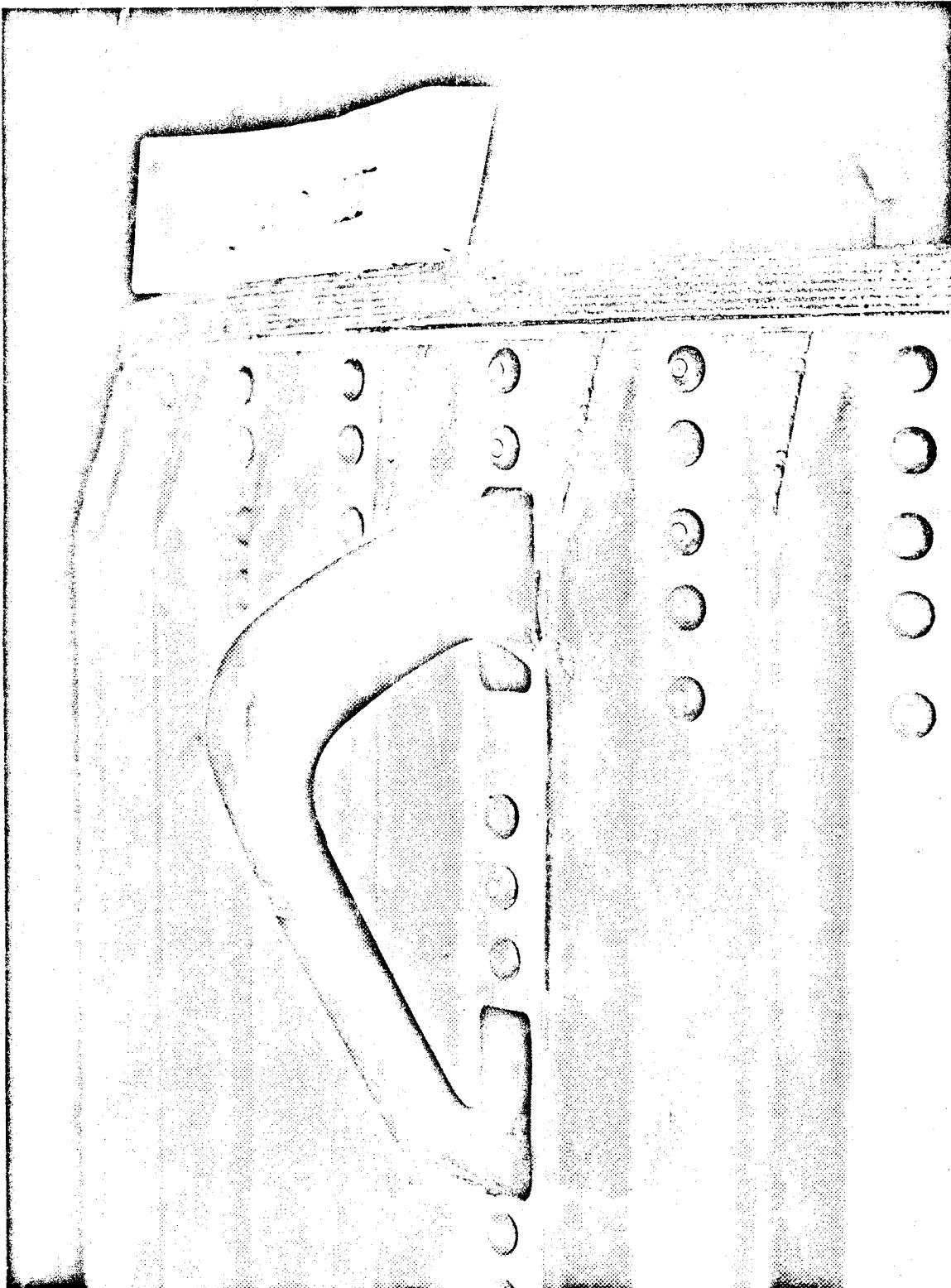


NASA  
B-59-528

~~CONFIDENTIAL~~

(b) Hook located in Quad II.

Figure 34.- Close-up of localized heating near recovery hooks.



NASA  
E-59-531

Figure 35.- Recovery hook in Quad III.

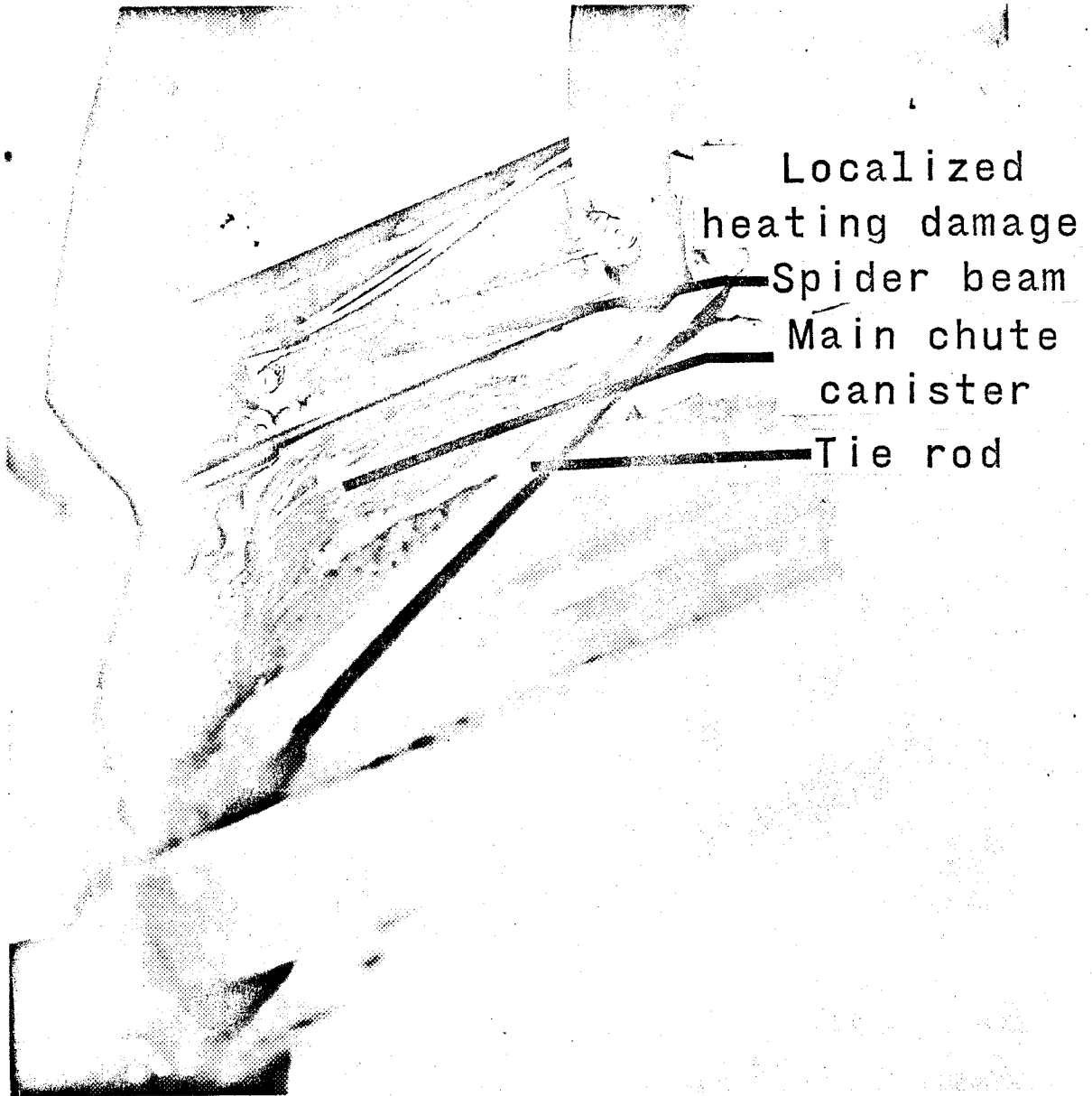
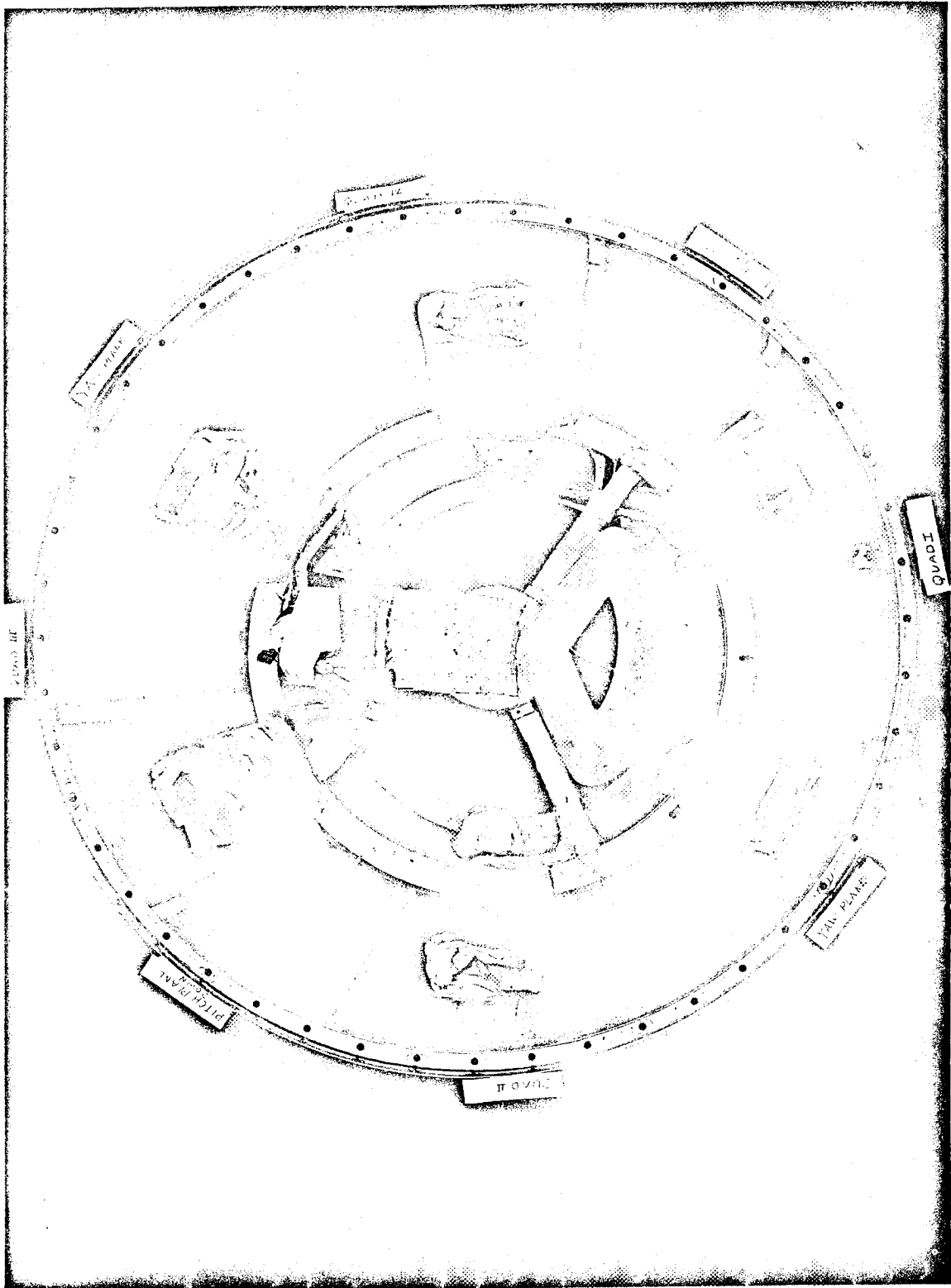


Figure 36.- View of internal damage near recovery hook (Quad II).



NASA  
B-59-551

Figure 37 .- Recovered afterbody interior.

~~CONFIDENTIAL~~

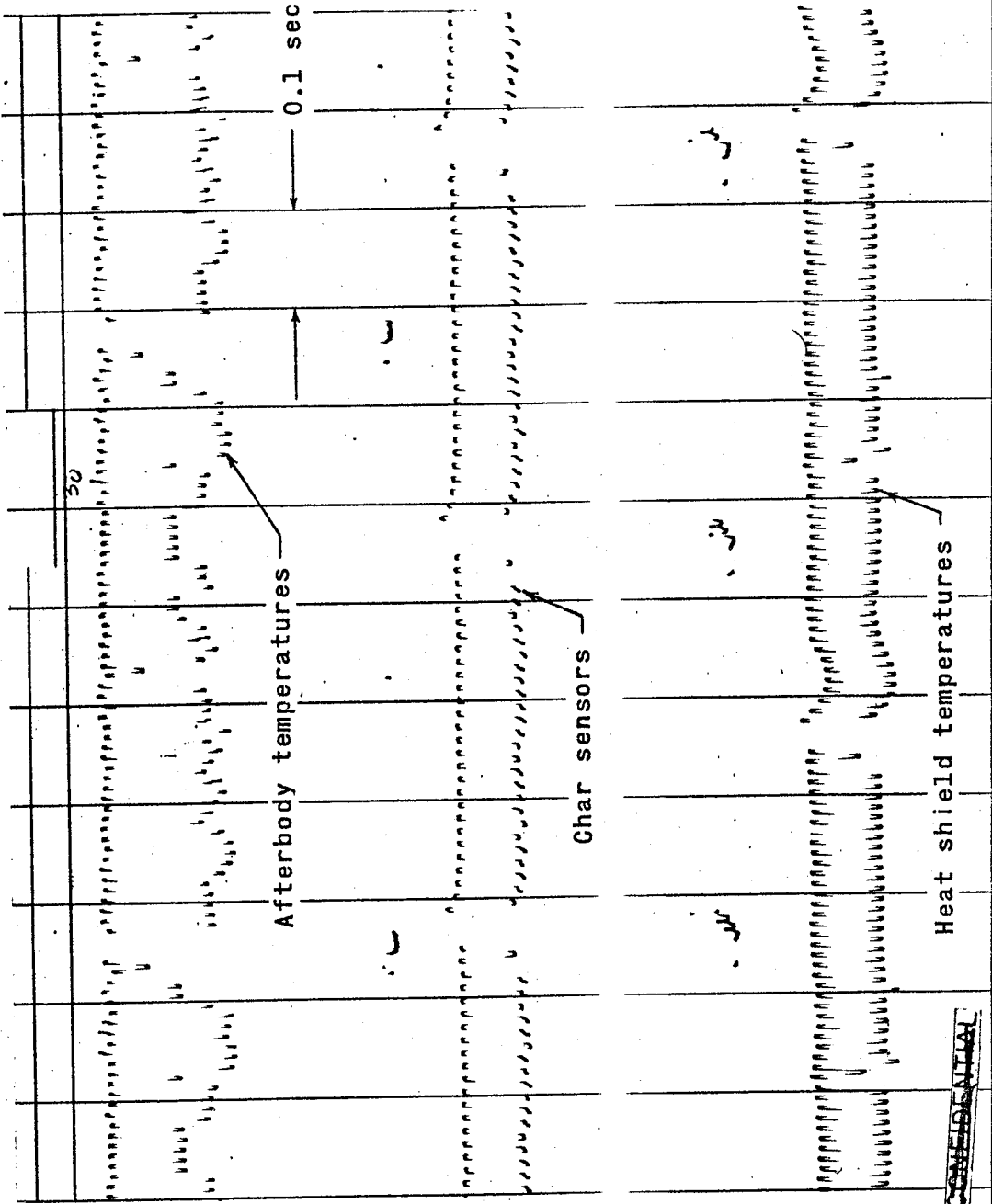
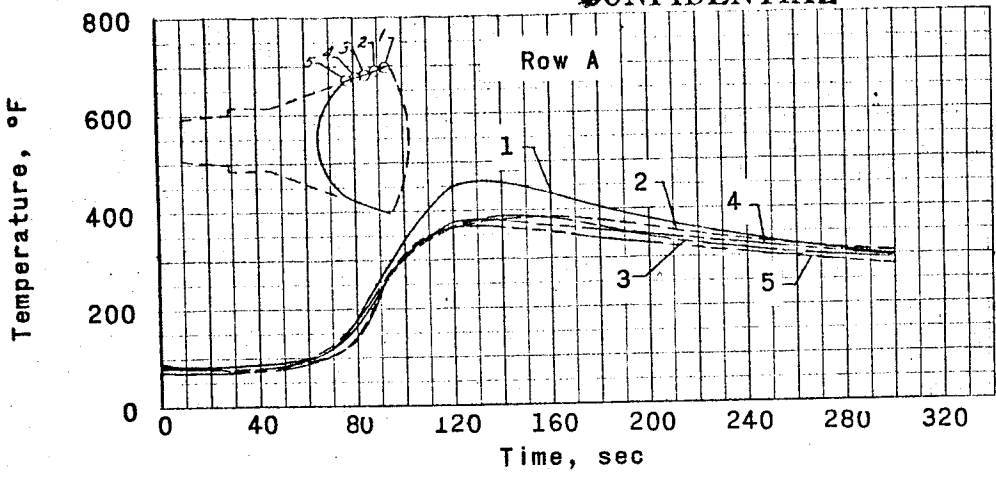
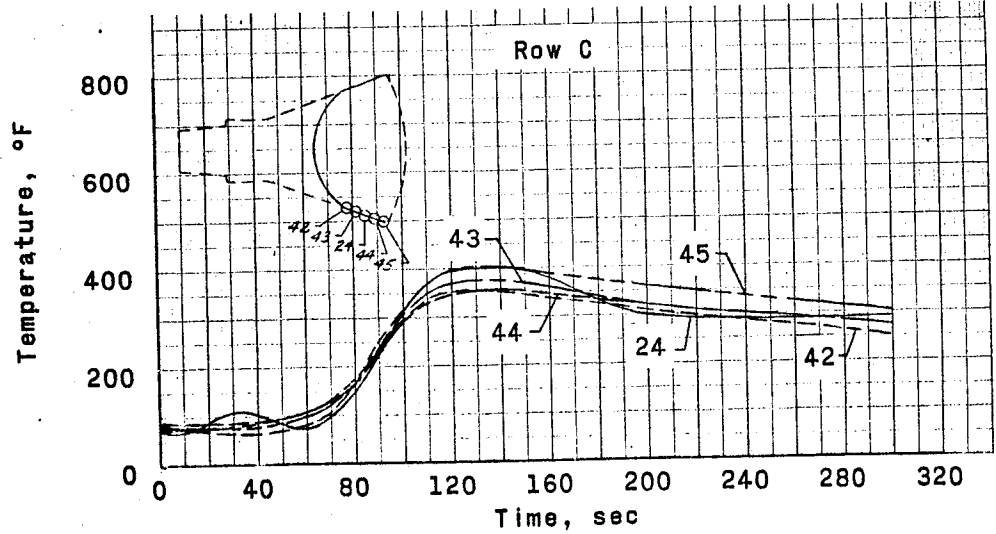
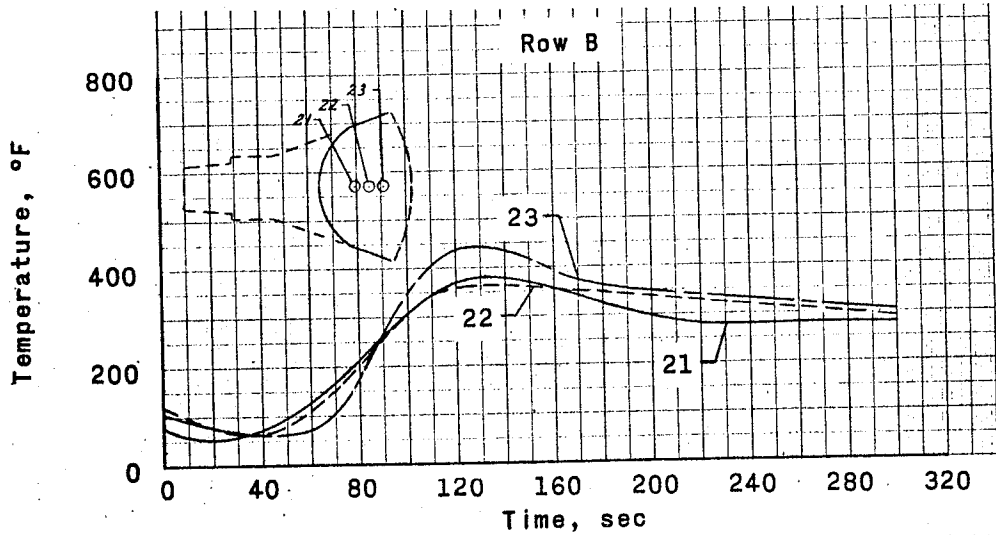


Figure 38.- Sample telemeter record.

~~CONFIDENTIAL~~



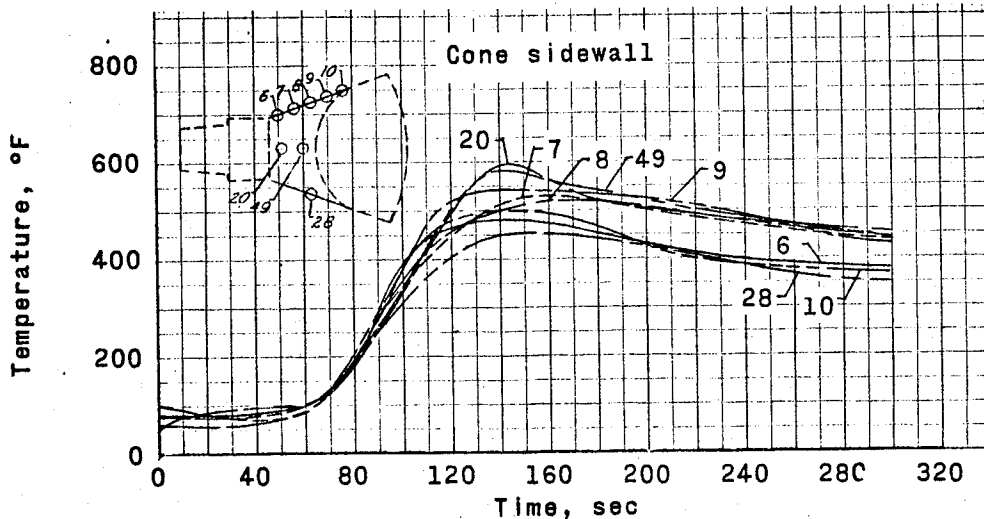
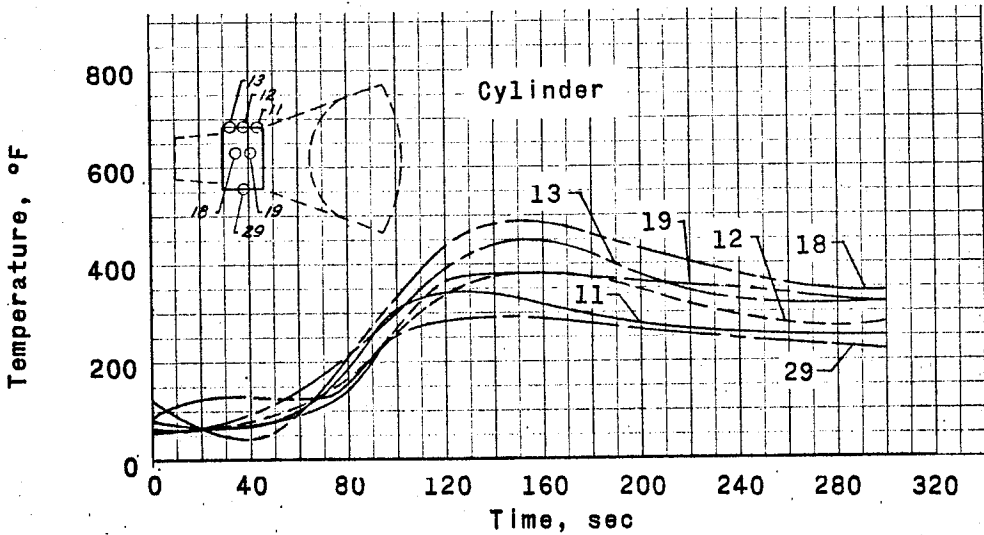
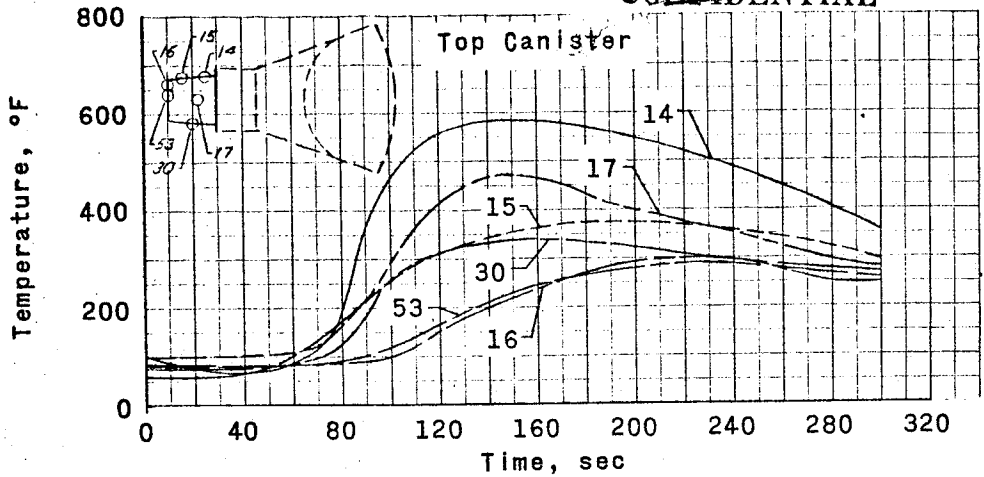
KEUPEL-KESSER CO. N. Y.



(a) Pressure vessel sidewalls.

Figure 39.- Exit heating on afterbody. ~~CONFIDENTIAL~~

~~CONFIDENTIAL~~

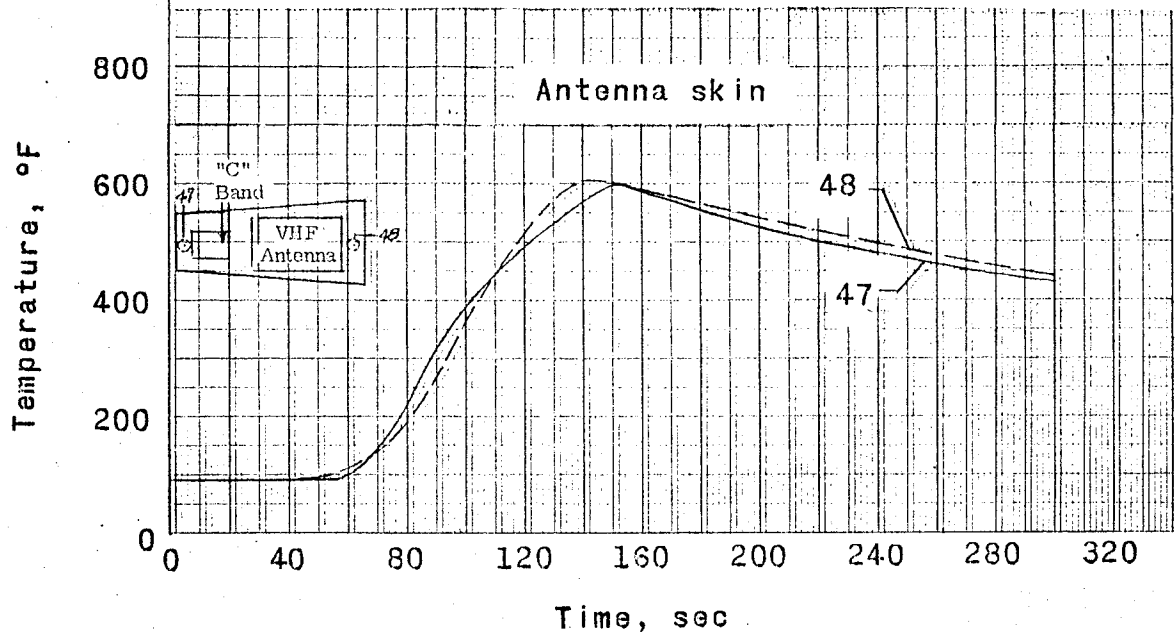


(b) Top canister, cylinder, and cone sidewall.

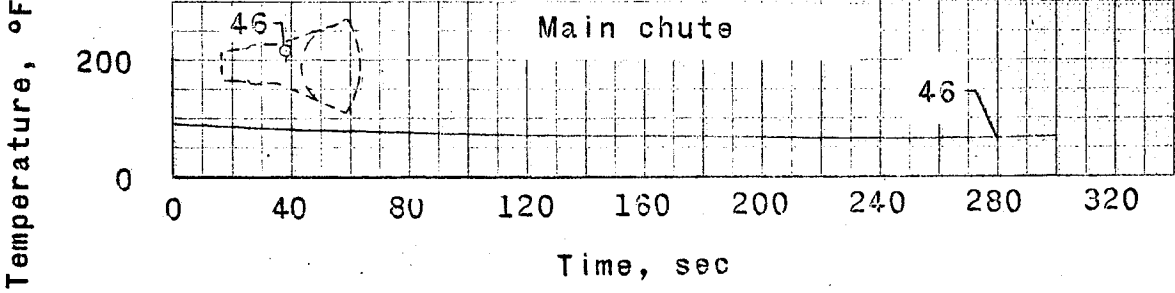
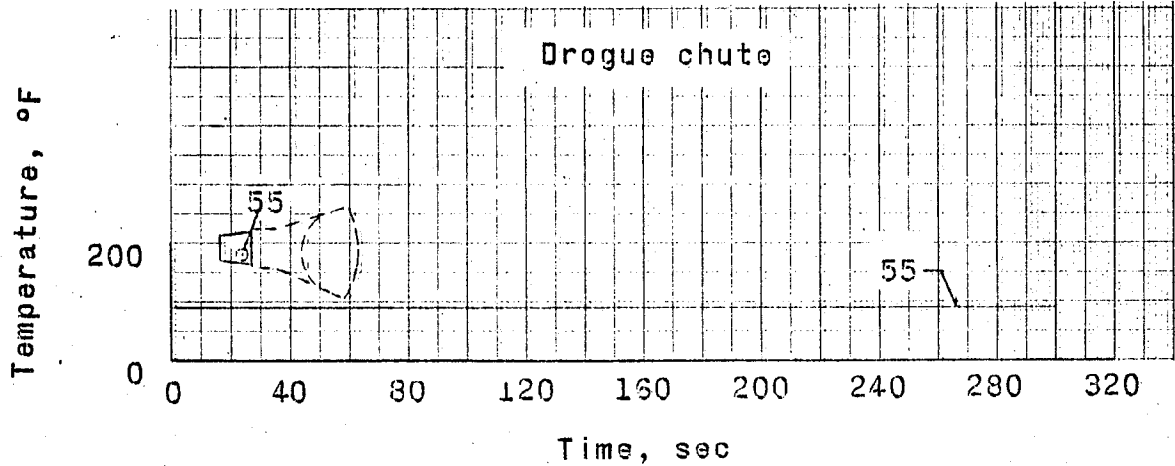
Figure 39.- Continued.

~~CONFIDENTIAL~~

~~CONFIDENTIAL~~



NEUFEL BESSER



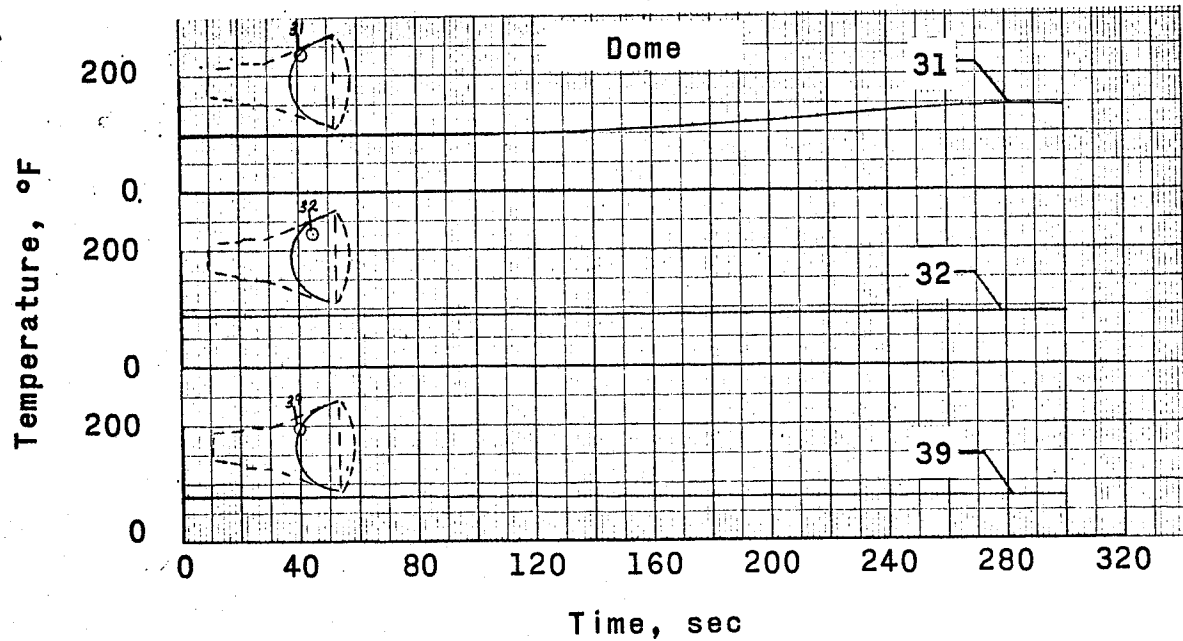
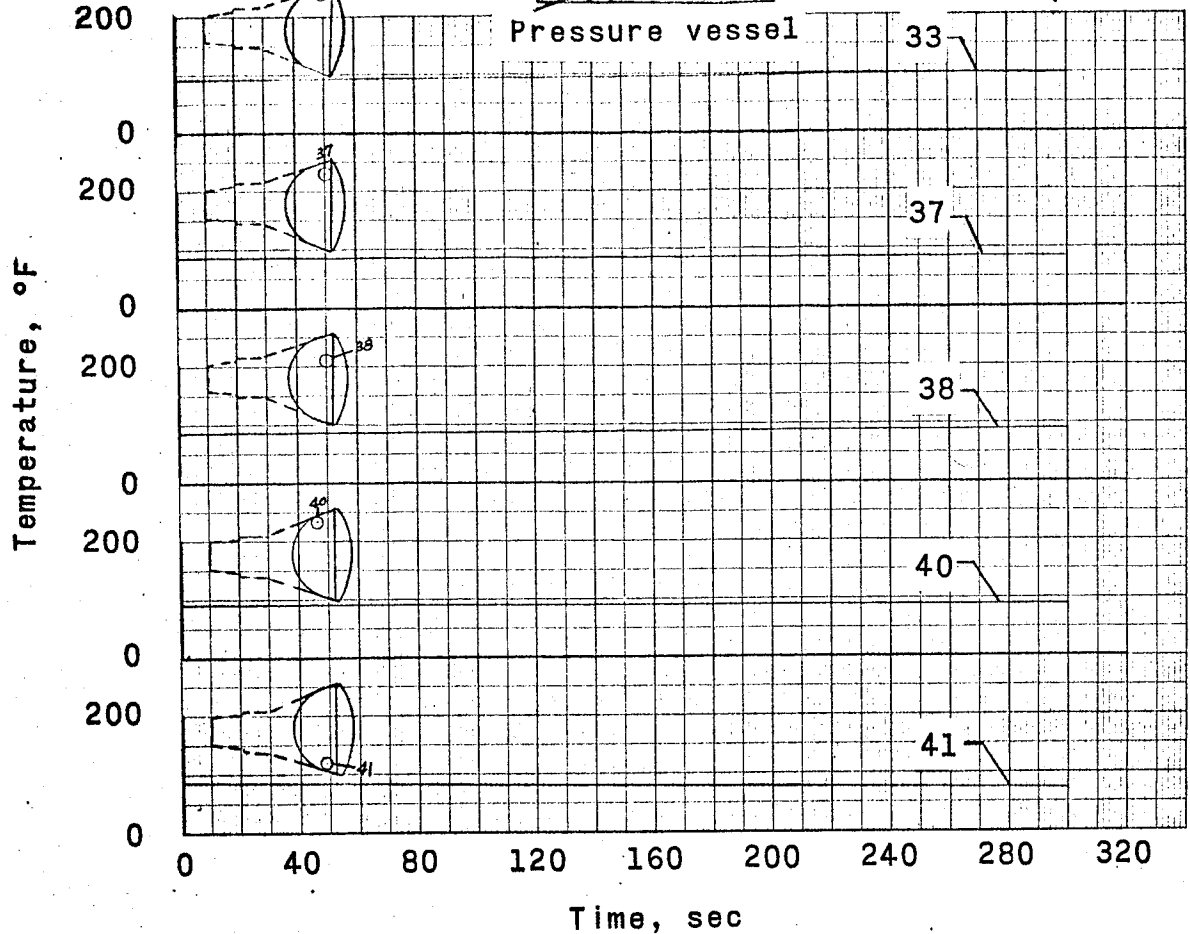
(c) Antenna skin, drogue chute and main chute.  
Figure 39.- Continued.

~~CONFIDENTIAL~~

~~CONFIDENTIAL~~

Expt

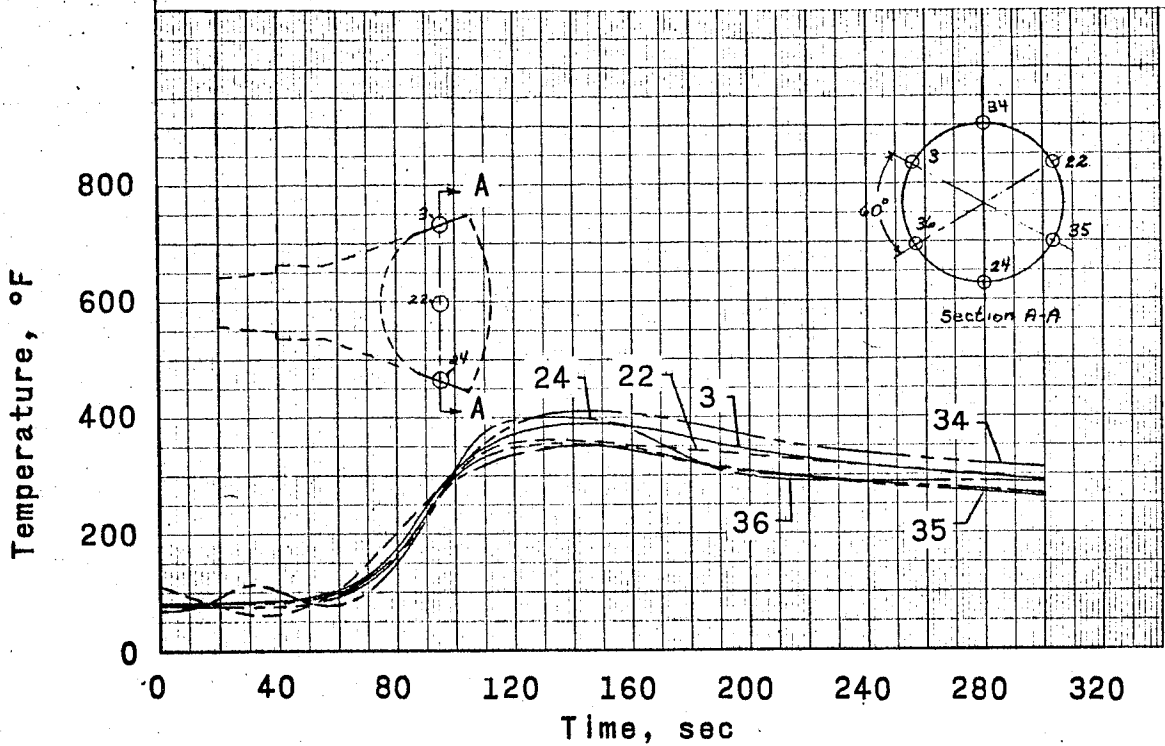
KEUFFEL & ESSER CO. N. Y.



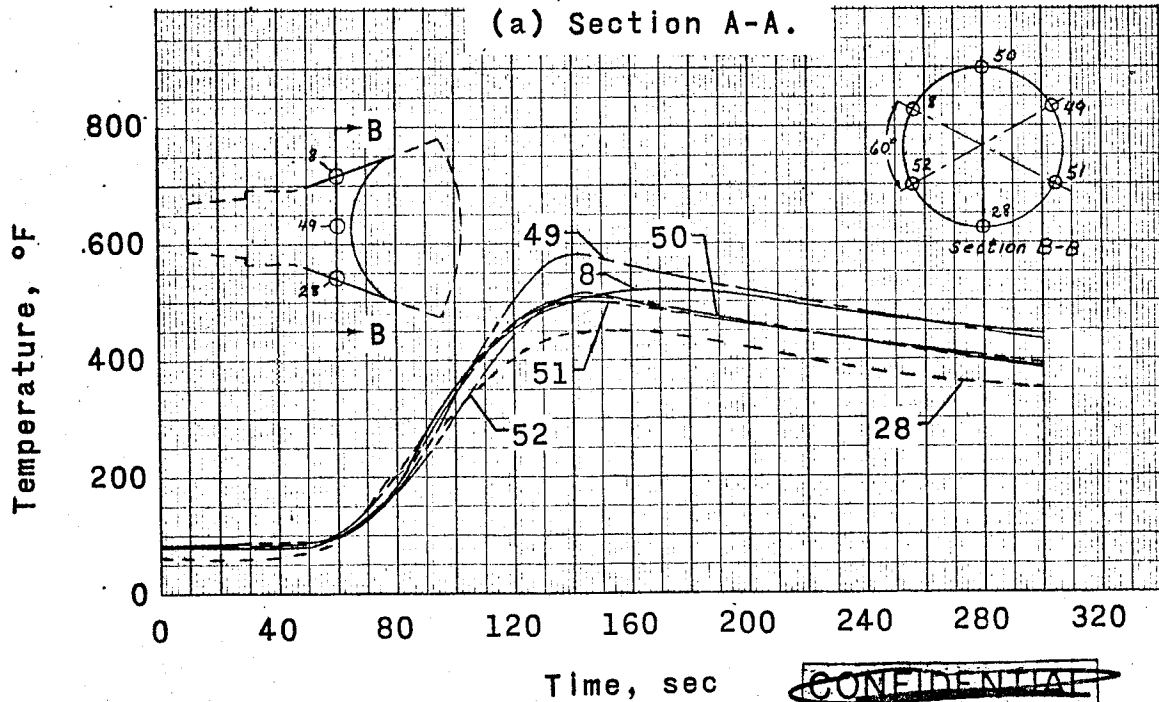
(d) Internal temperatures (Pressure vessel and Dome).  
Figure 39.- Concluded.

~~CONFIDENTIAL~~

~~CONFIDENTIAL~~



(a) Section A-A.



(b) Section B-B.

~~CONFIDENTIAL~~

Figure 40.- Exit heating for Sections A-A and B-B.

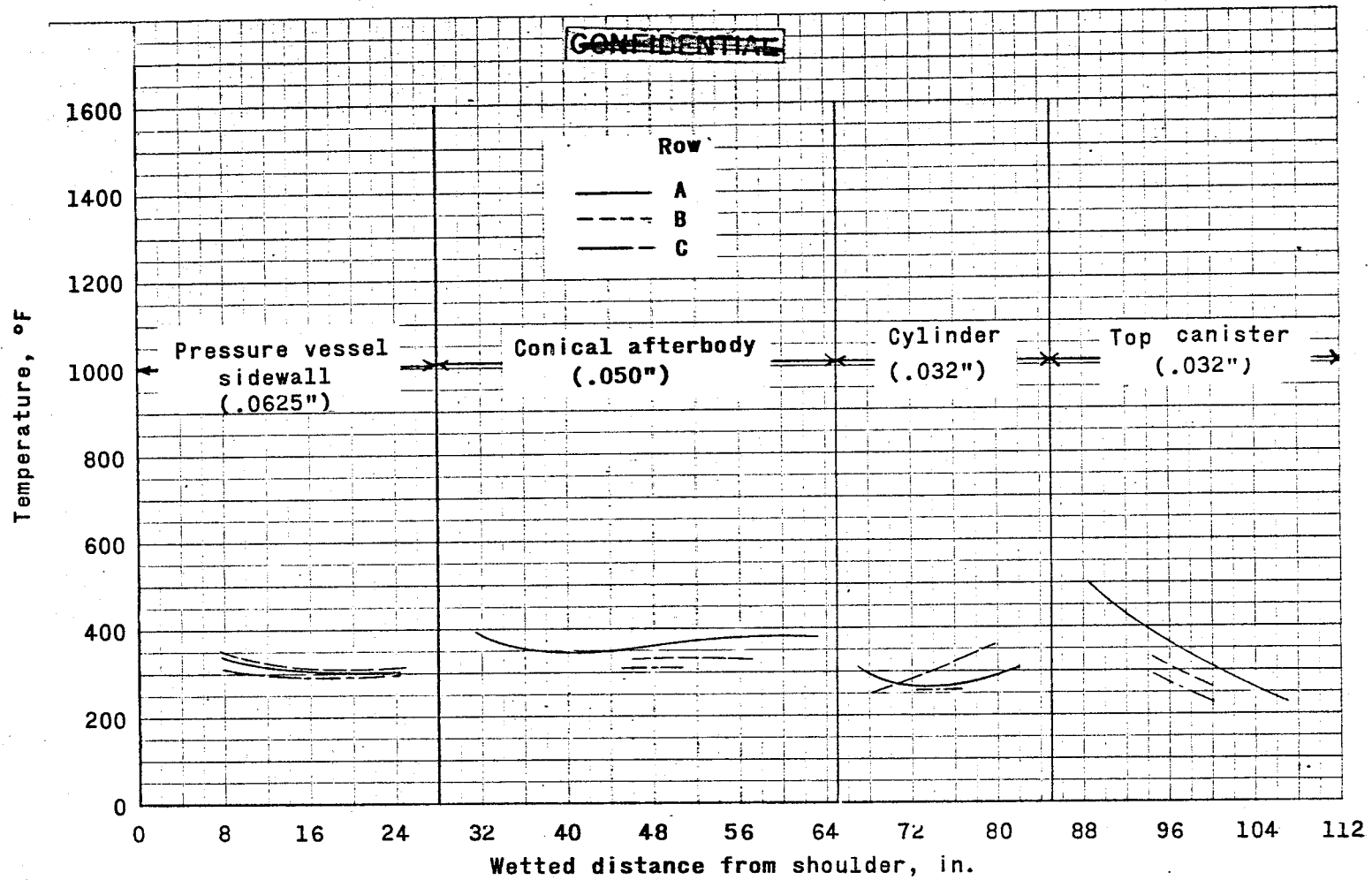
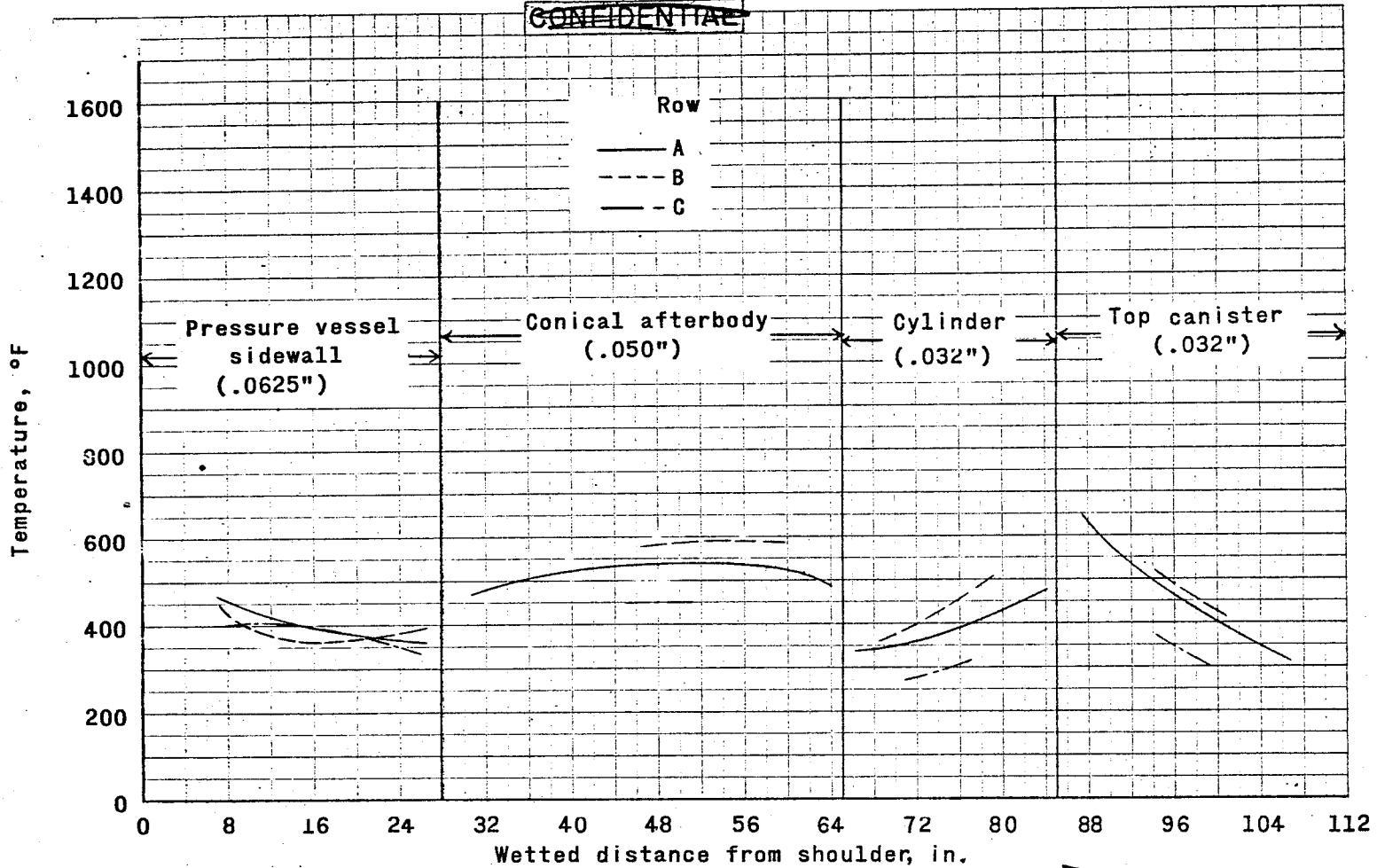


Figure 41.- Temperature distribution along afterbody during exit.

~~CONFIDENTIAL~~

~~CONFIDENTIAL~~



(b) Time = 140 sec.

~~CONFIDENTIAL~~

Figure 41.- Continued.

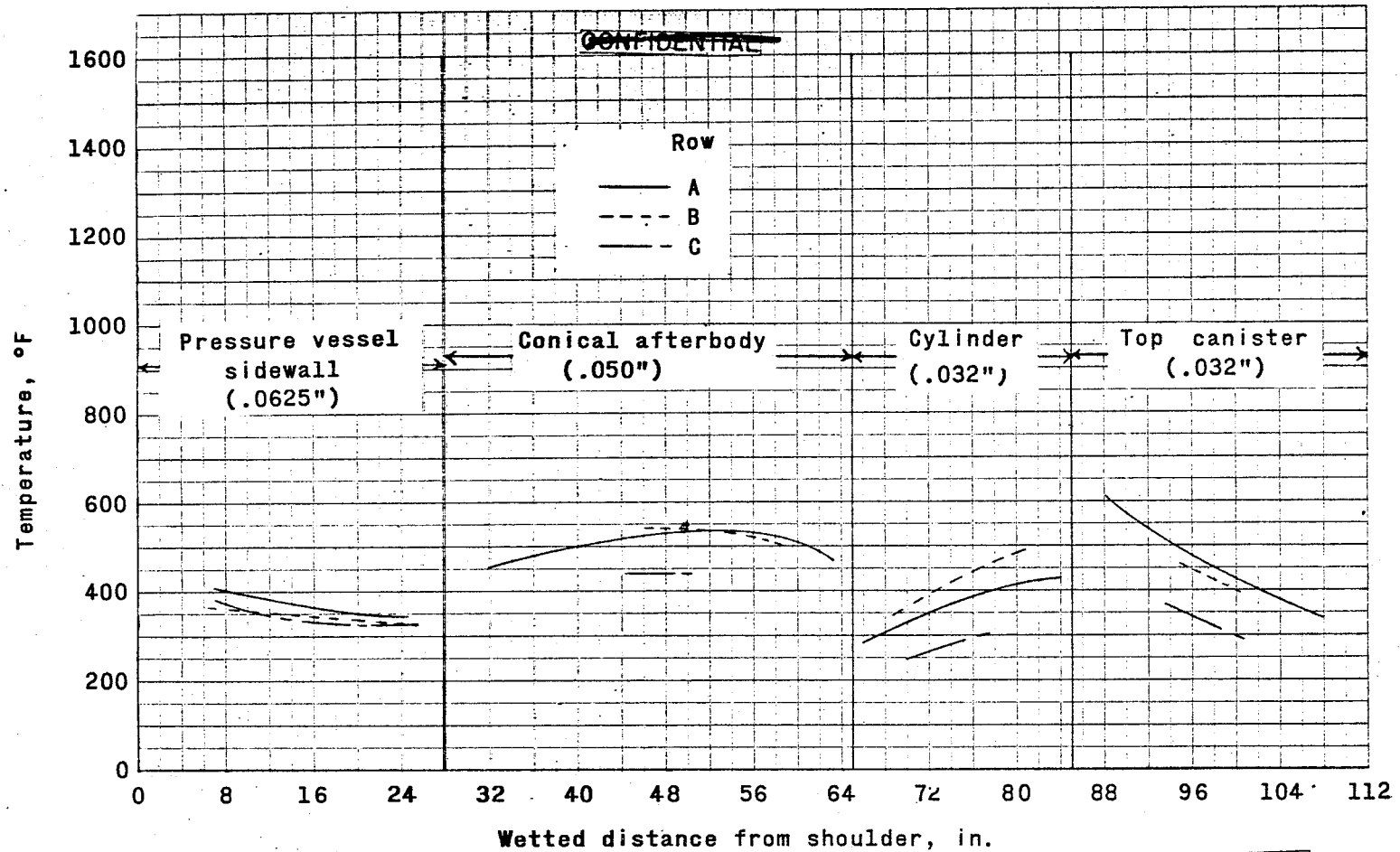
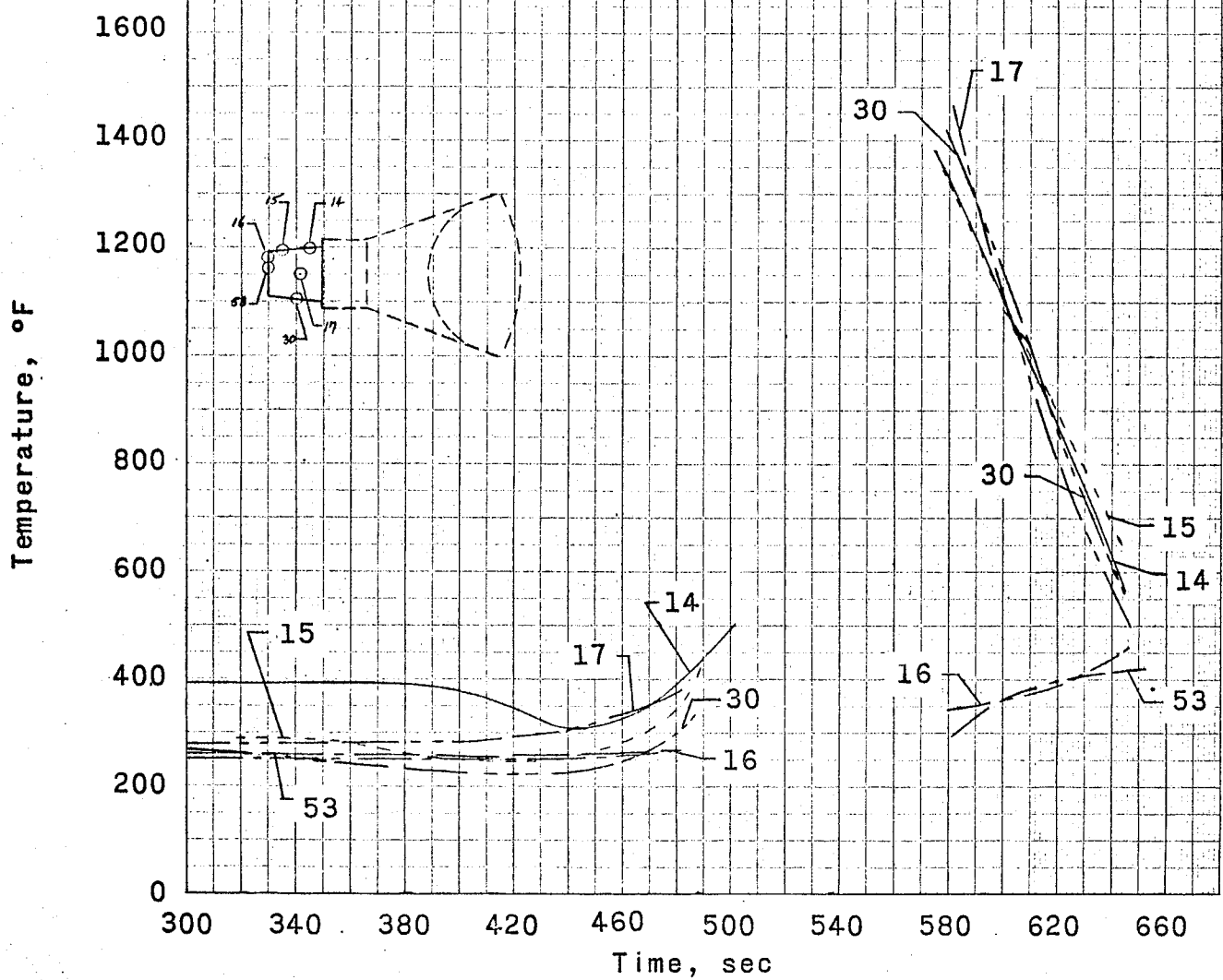


Figure 41.- Concluded.

(c) Time = 180 sec.

~~CONFIDENTIAL~~

~~CONFIDENTIAL~~



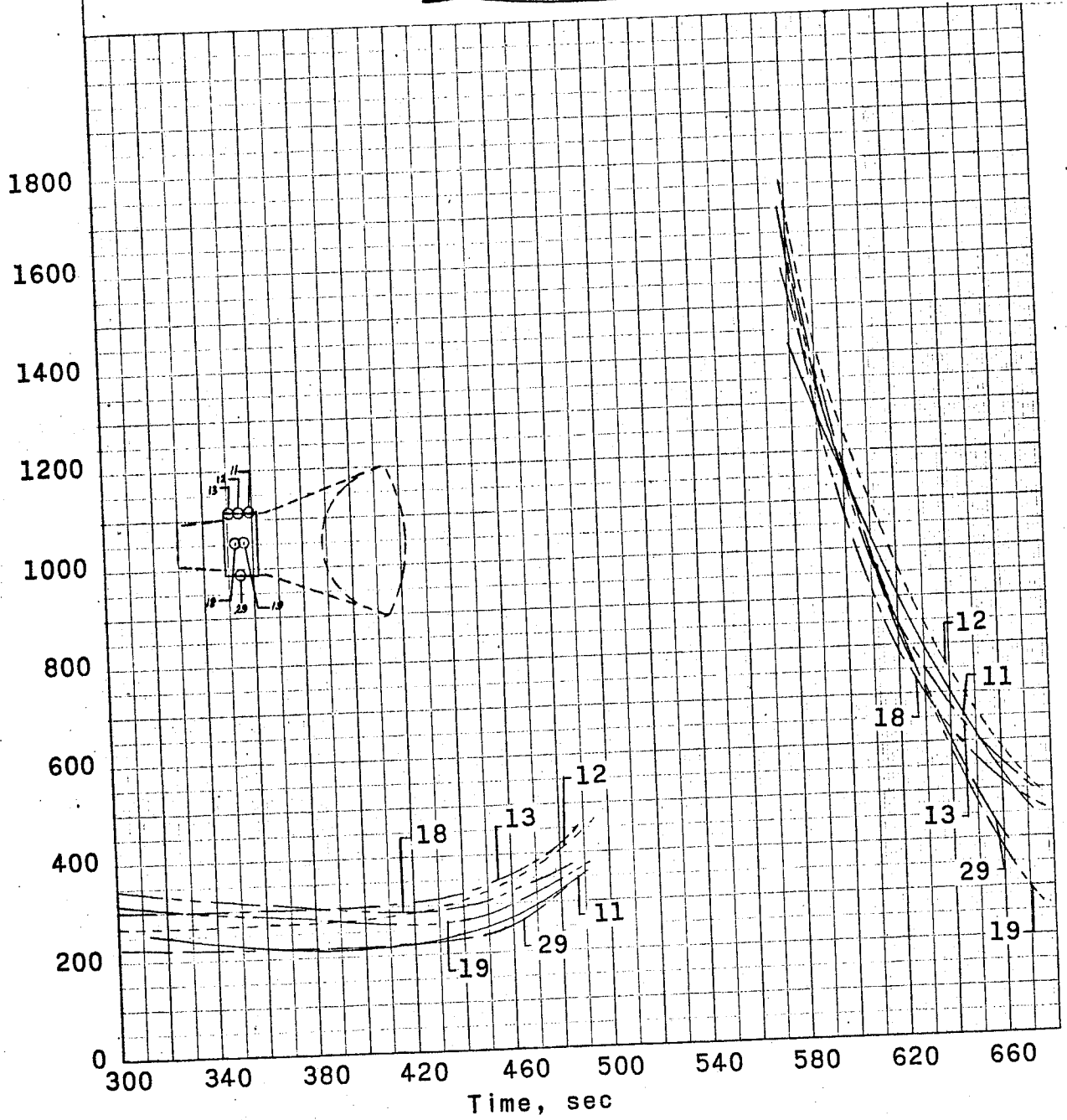
(a) Top Canister.

Figure 42.- Afterbody temperatures during reentry heating.

~~CONFIDENTIAL~~

~~CONFIDENTIAL~~

Temperature, °F

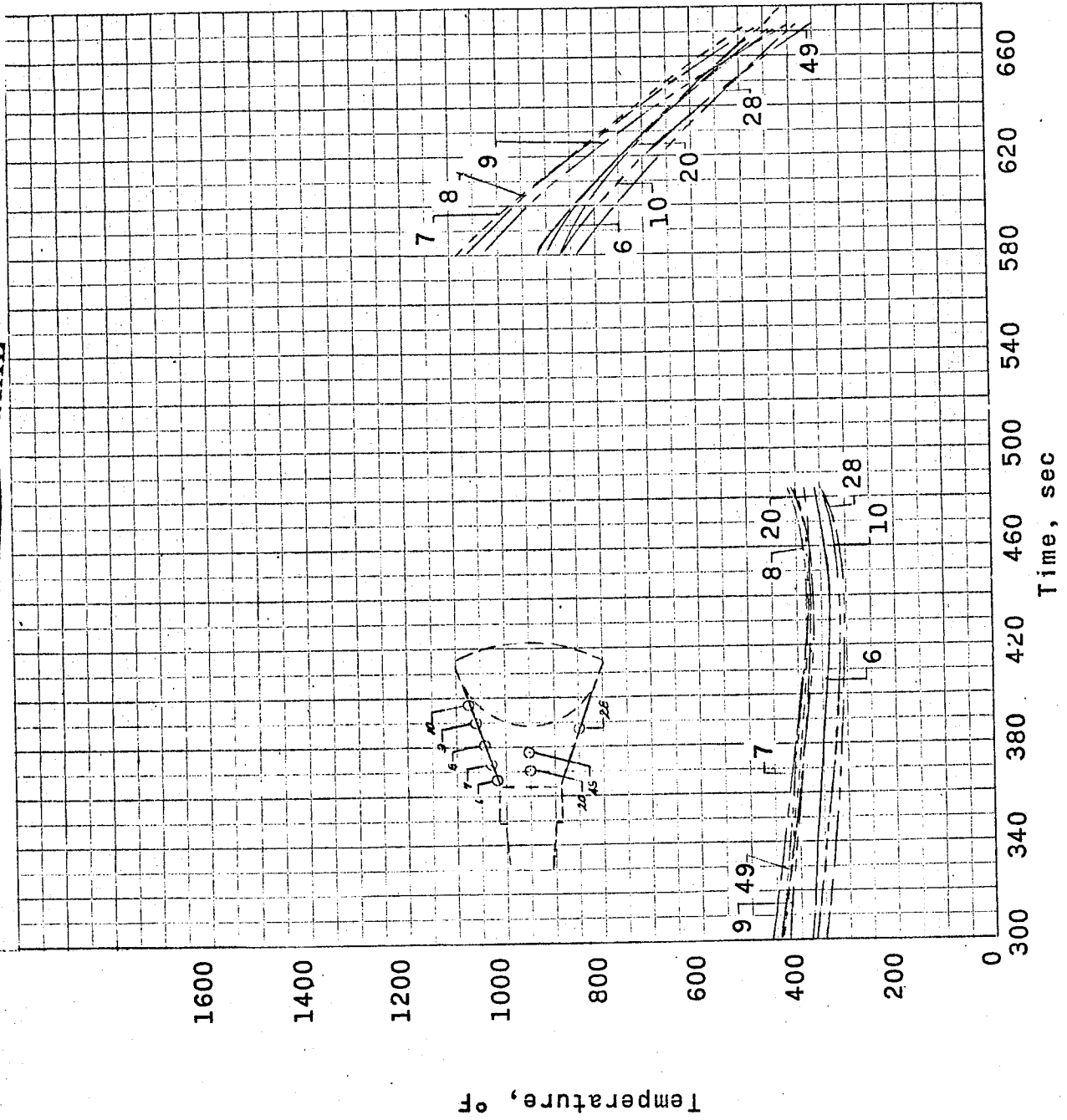


(b) Cylinder.

Figure 42.- Continued.

~~CONFIDENTIAL~~

~~CONFIDENTIAL~~

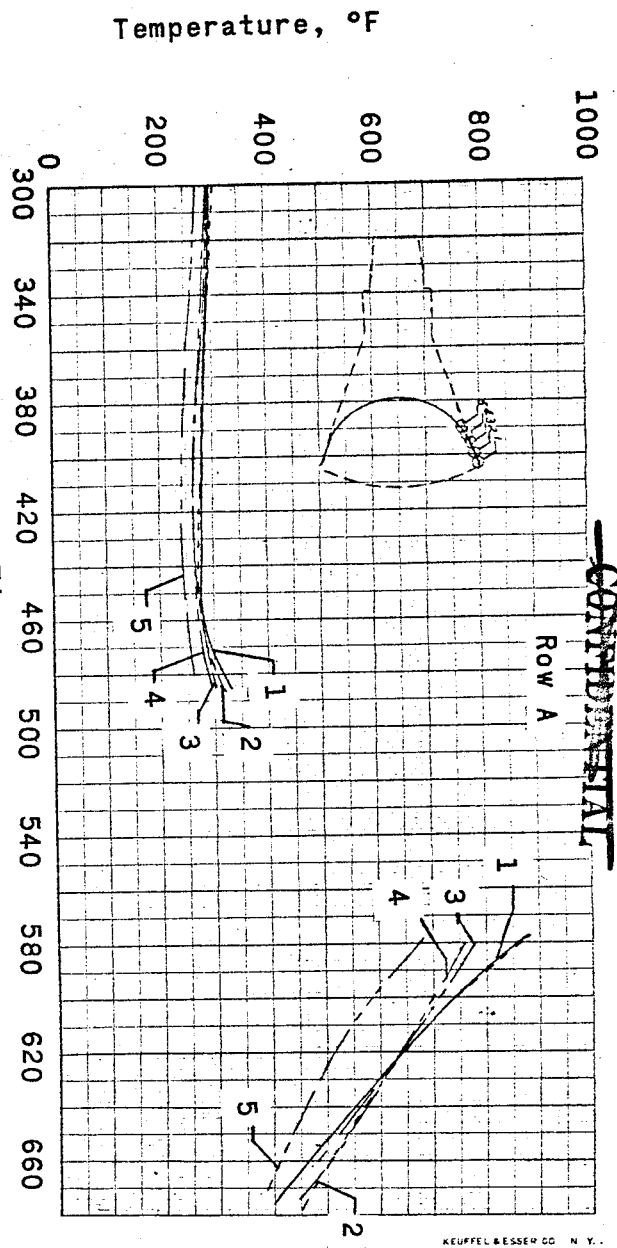


(c) Cone sidewall.

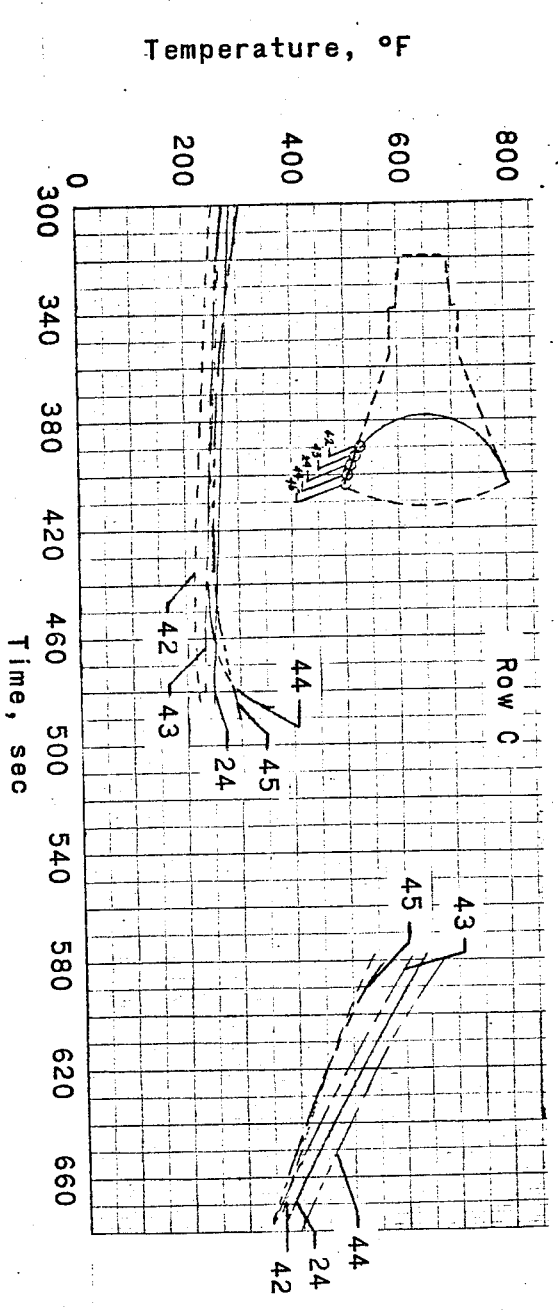
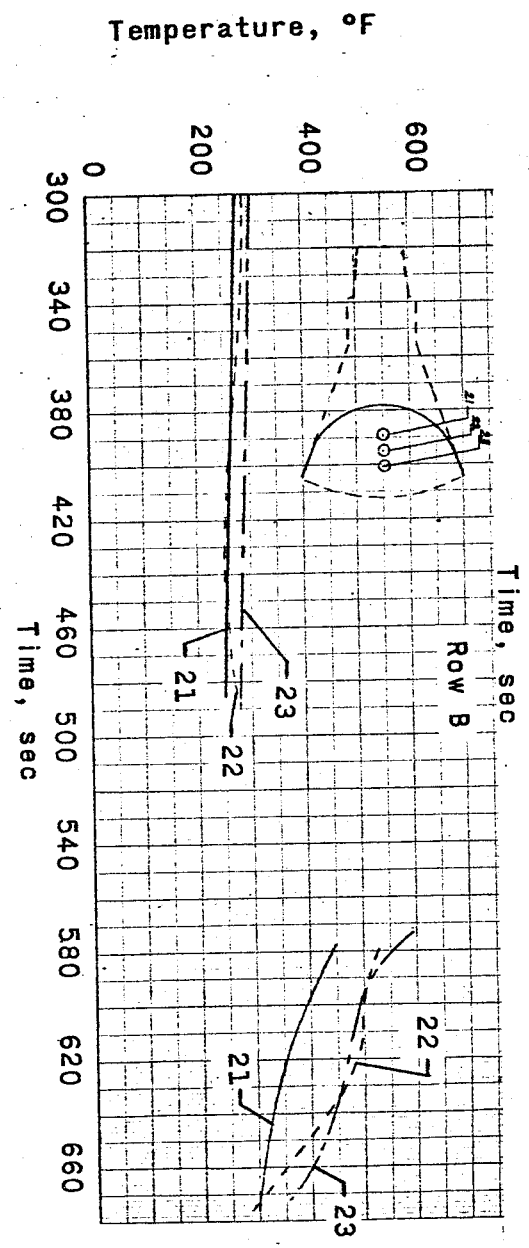
Figure 42.- Continued.

~~CONFIDENTIAL~~

~~CONFIDENTIAL~~



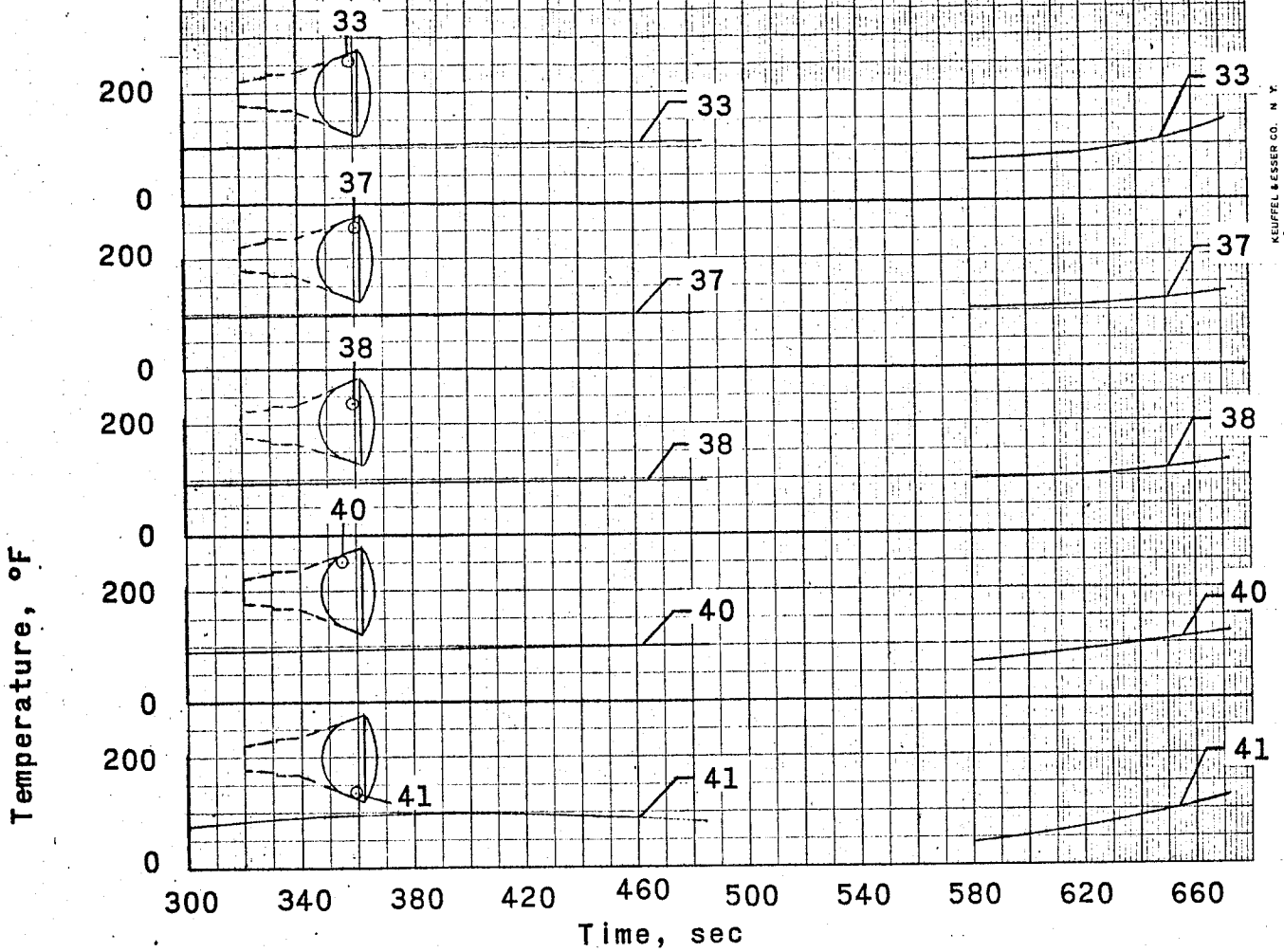
KEUFFEL & BESSER CO. N. Y.



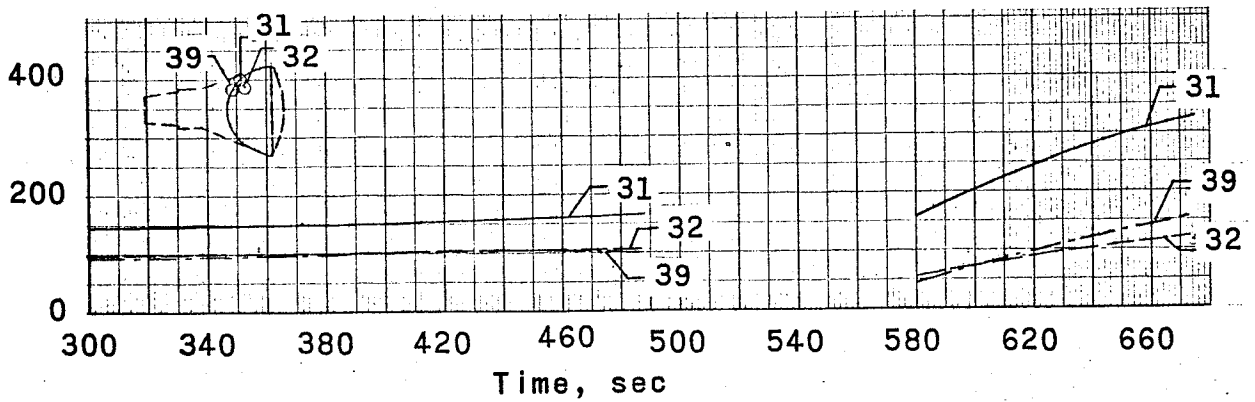
(d) Pressure vessel sidewalls.  
Figure 42. - Continued.

~~CONFIDENTIAL~~

~~CONFIDENTIAL~~



KEUFFEL & ESSER CO. N. Y.

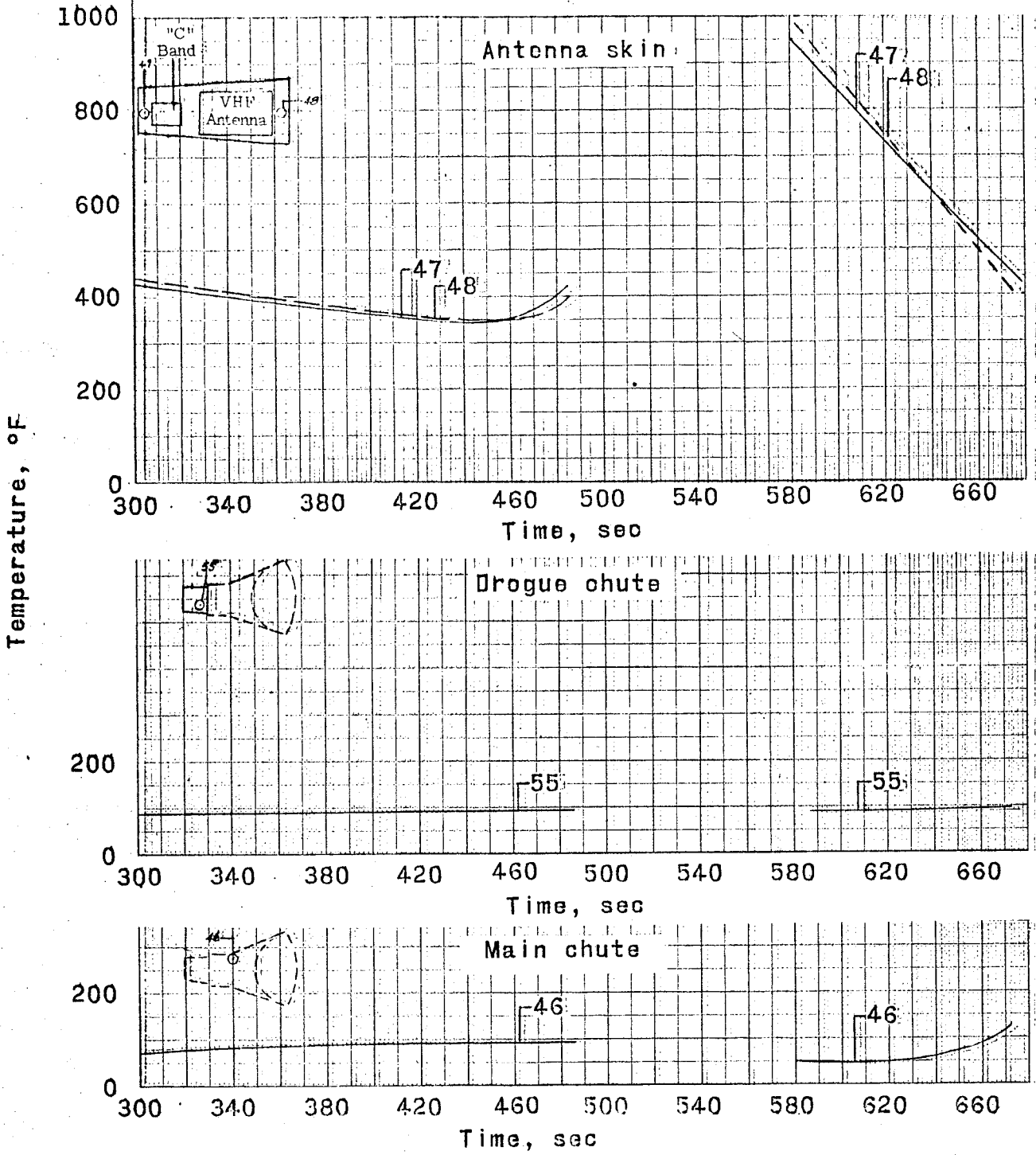


(e) Pressure vessel internal temperatures.

Figure 42.- Continued.

~~CONFIDENTIAL~~

~~CONFIDENTIAL~~

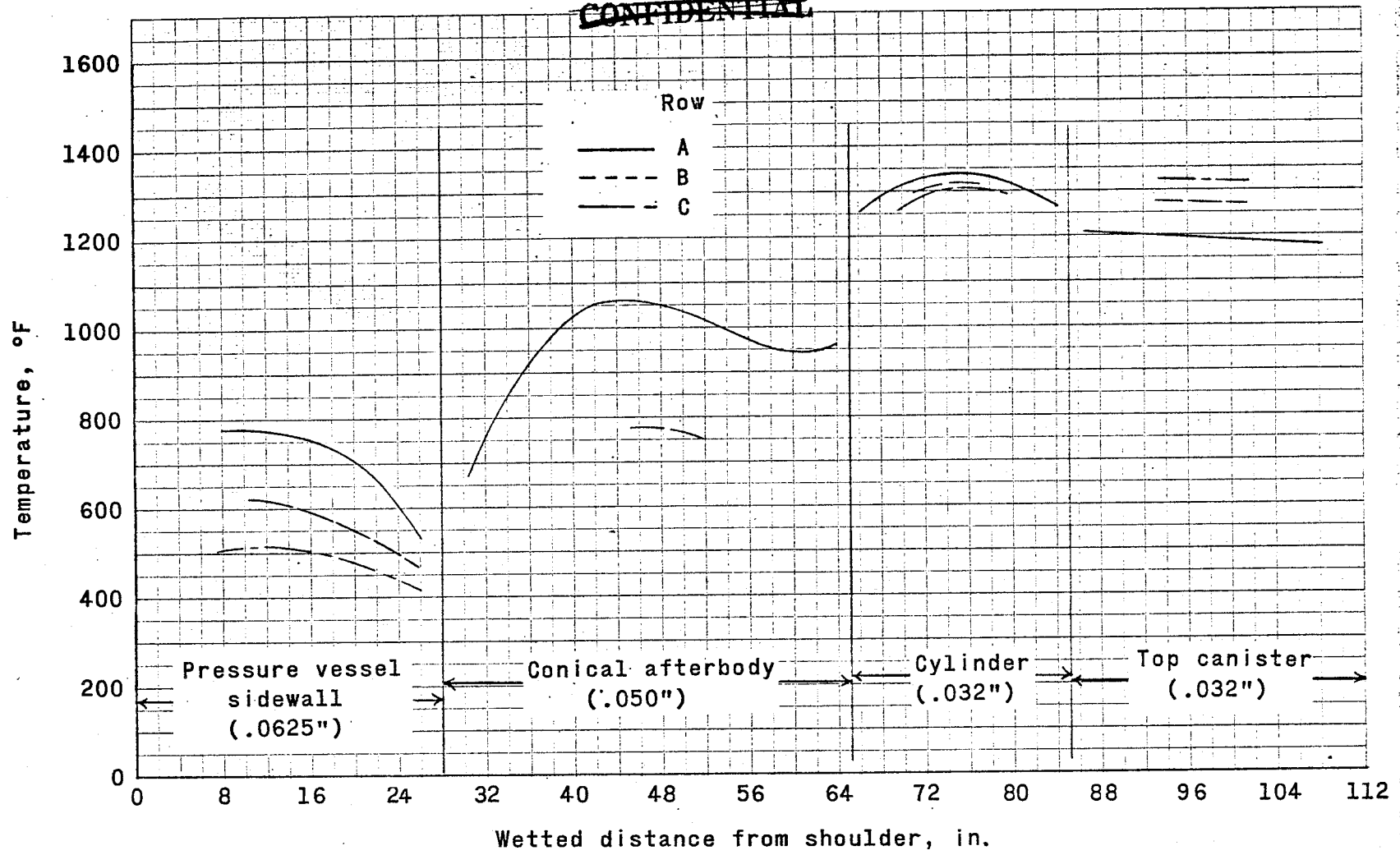


(f) Antenna skin, drogue chute and main chute.

Figure 42.- Concluded.

~~CONFIDENTIAL~~

~~CONFIDENTIAL~~

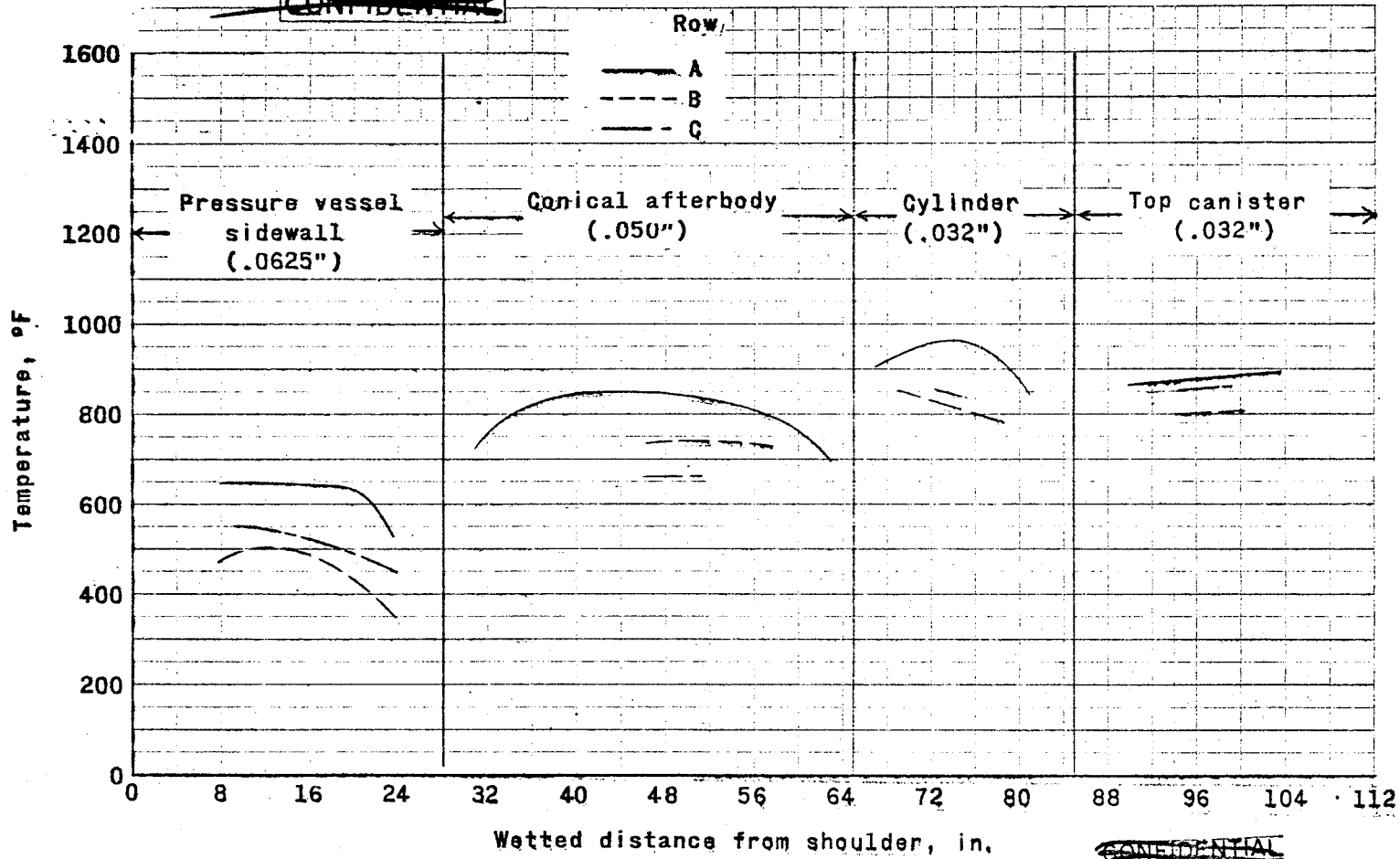


(a) Time = 592 sec.

~~CONFIDENTIAL~~

Figure 43.- Temperature distribution along afterbody after peak heating.

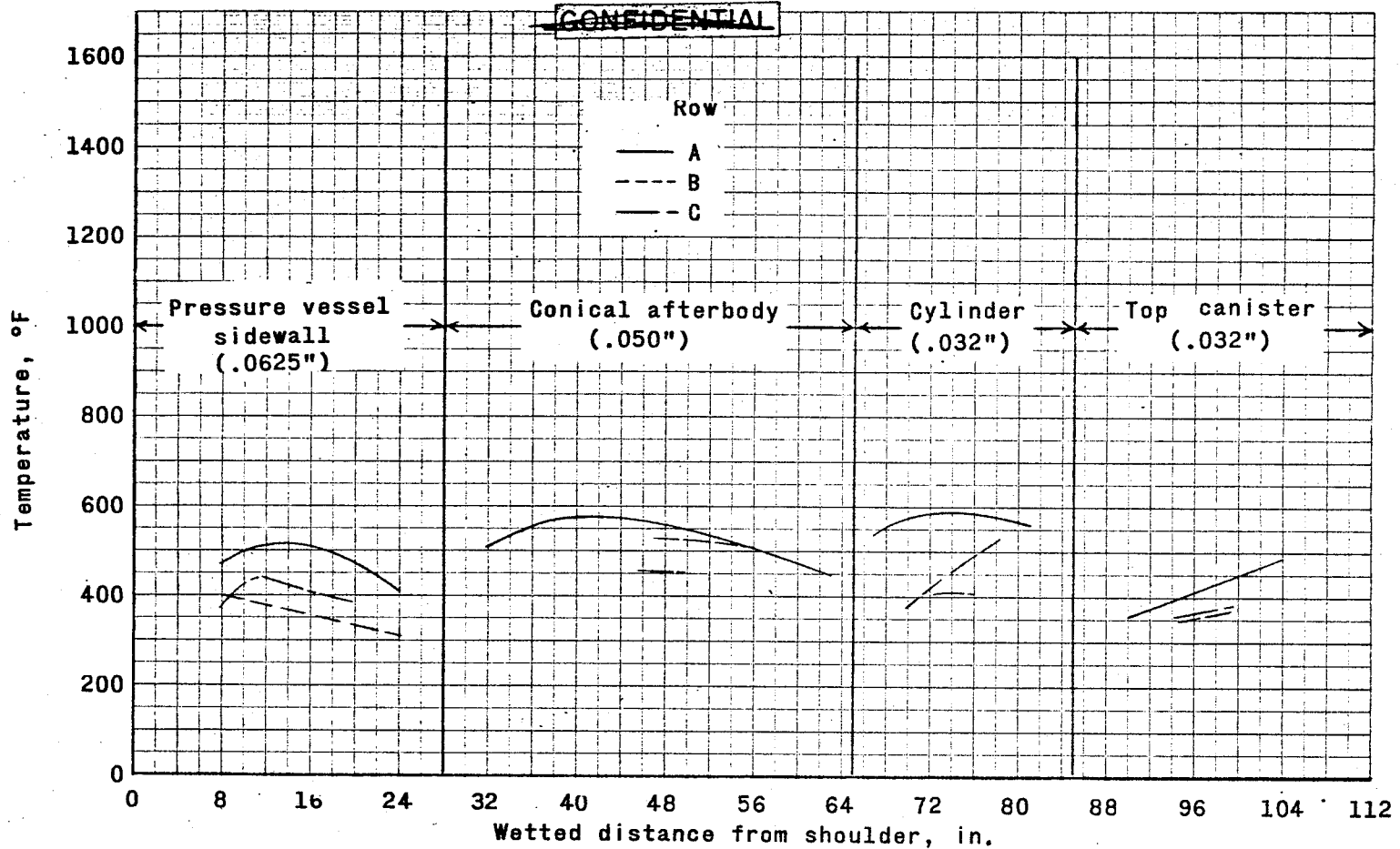
~~CONFIDENTIAL~~



(b) Time = 620 sec.

~~CONFIDENTIAL~~

Figure 43.- Continued.



(c) Time = 660 sec.

~~CONFIDENTIAL~~

Figure 43.- Concluded.

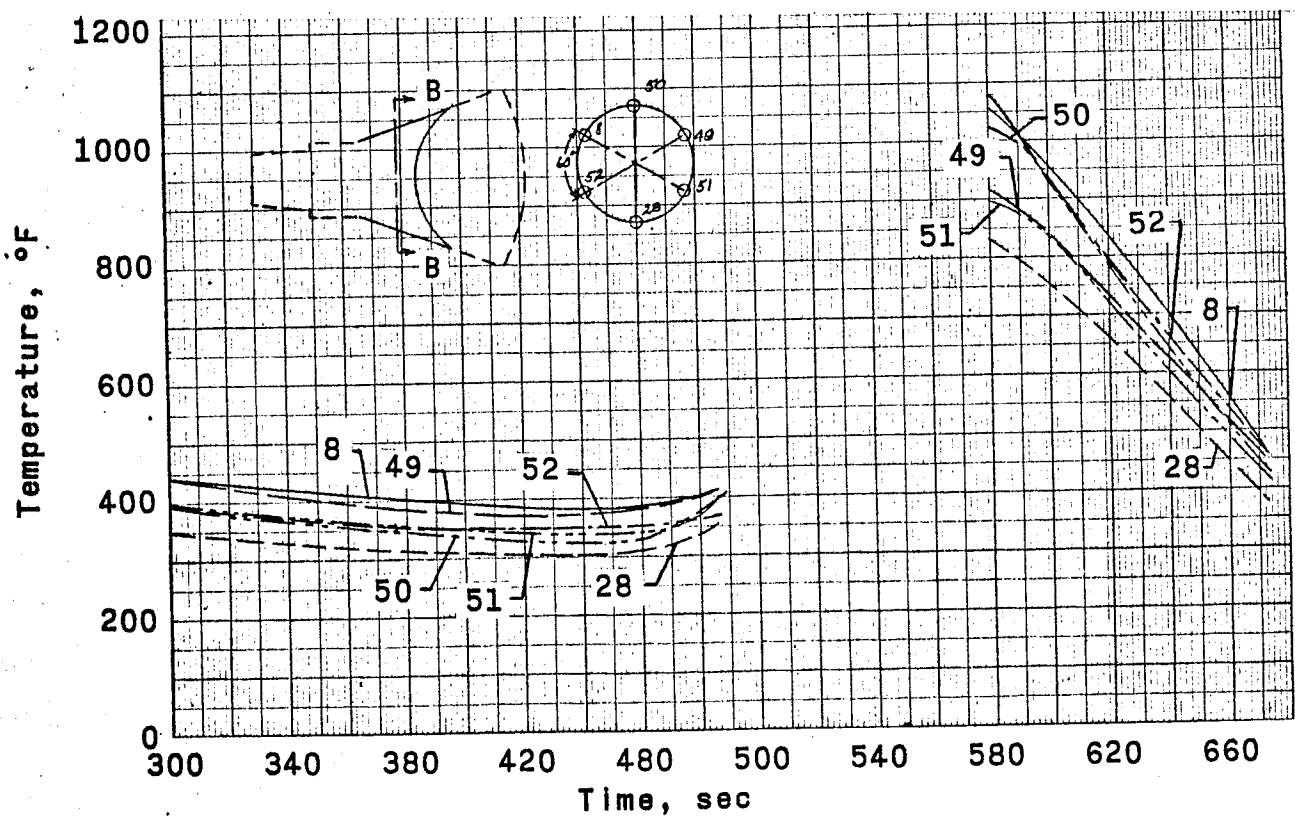
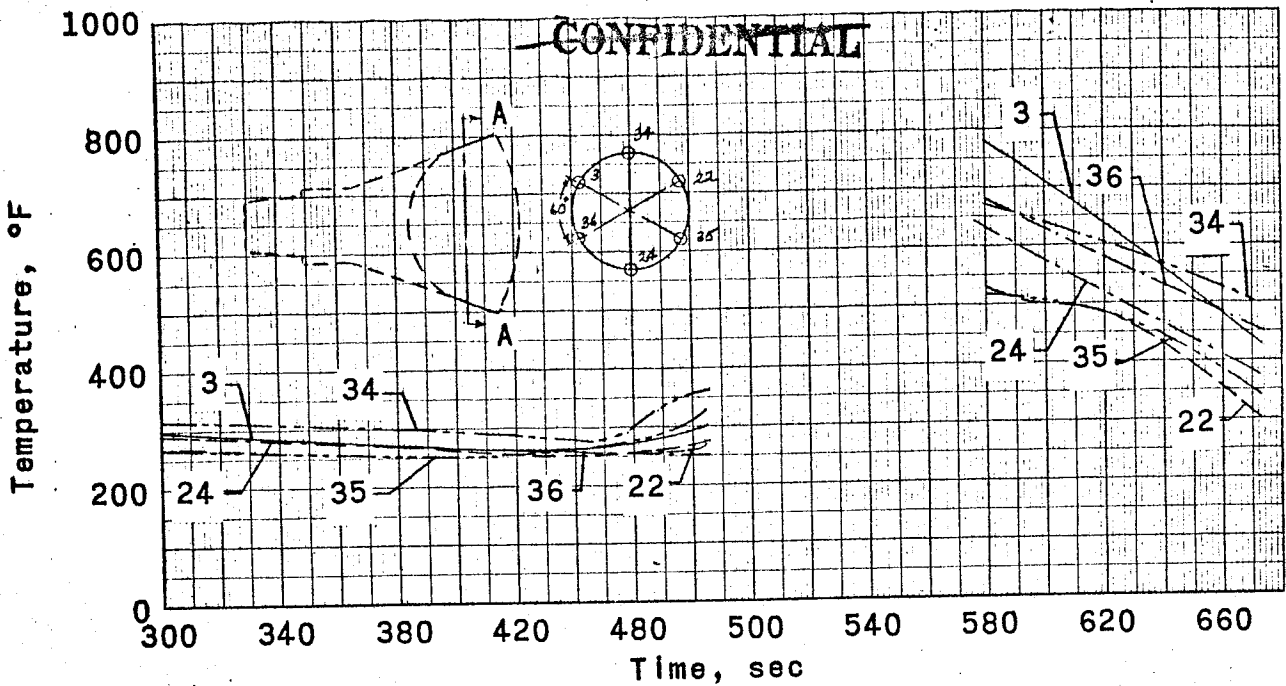
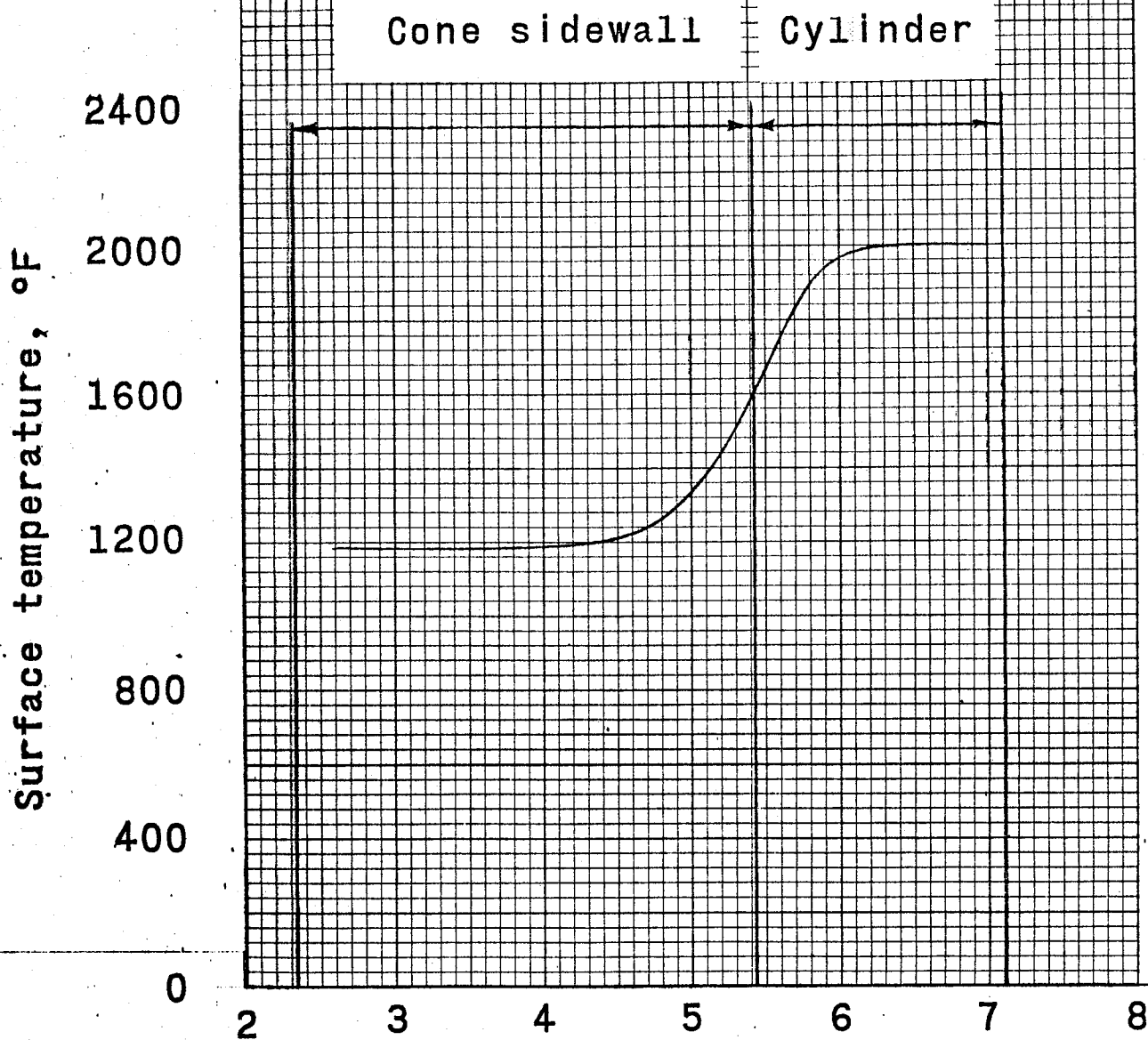


Figure 44.- Temperature at Section A-A and B-B during reentry heating.

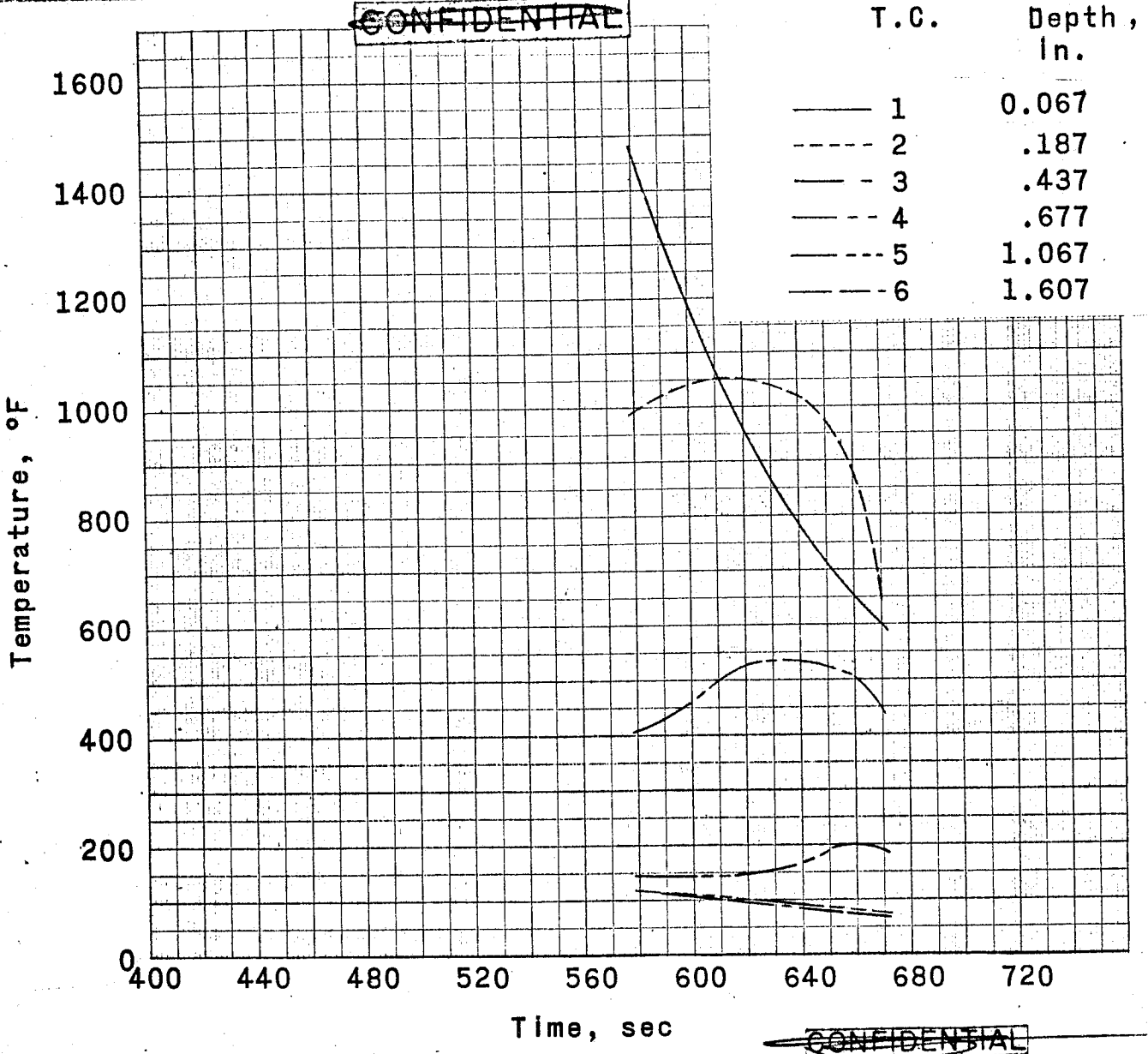
~~CONFIDENTIAL~~



Distance along afterbody measured from capsule shoulder, ft

Figure 45 .- Probable maximum temperature reached on afterbody as indicated by thermocolor paint. ~~CONFIDENTIAL~~

~~CONFIDENTIAL~~

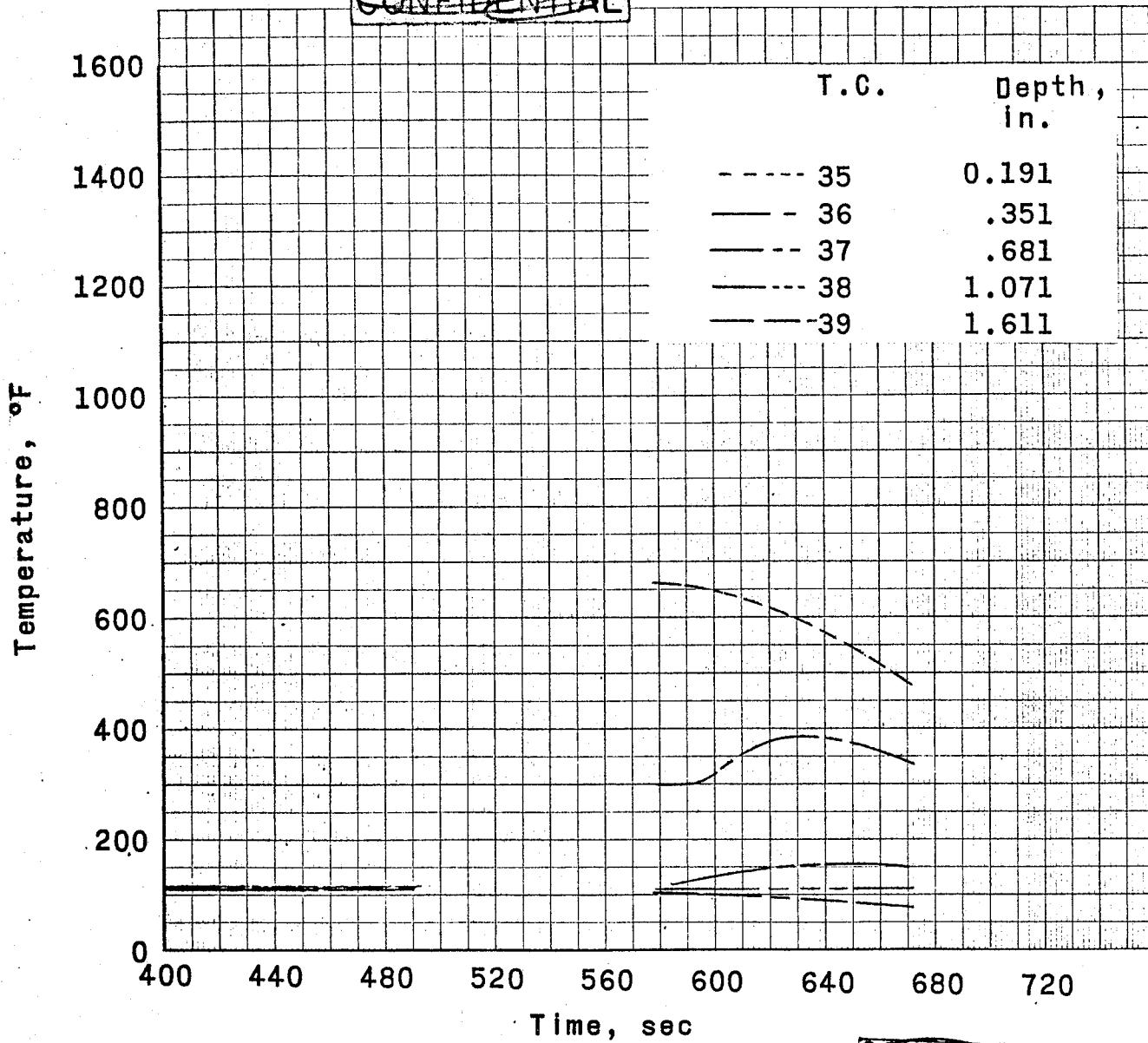


~~CONFIDENTIAL~~

(a) Sensor number 1.

Figure 46.- Temperature time history in heat shield.

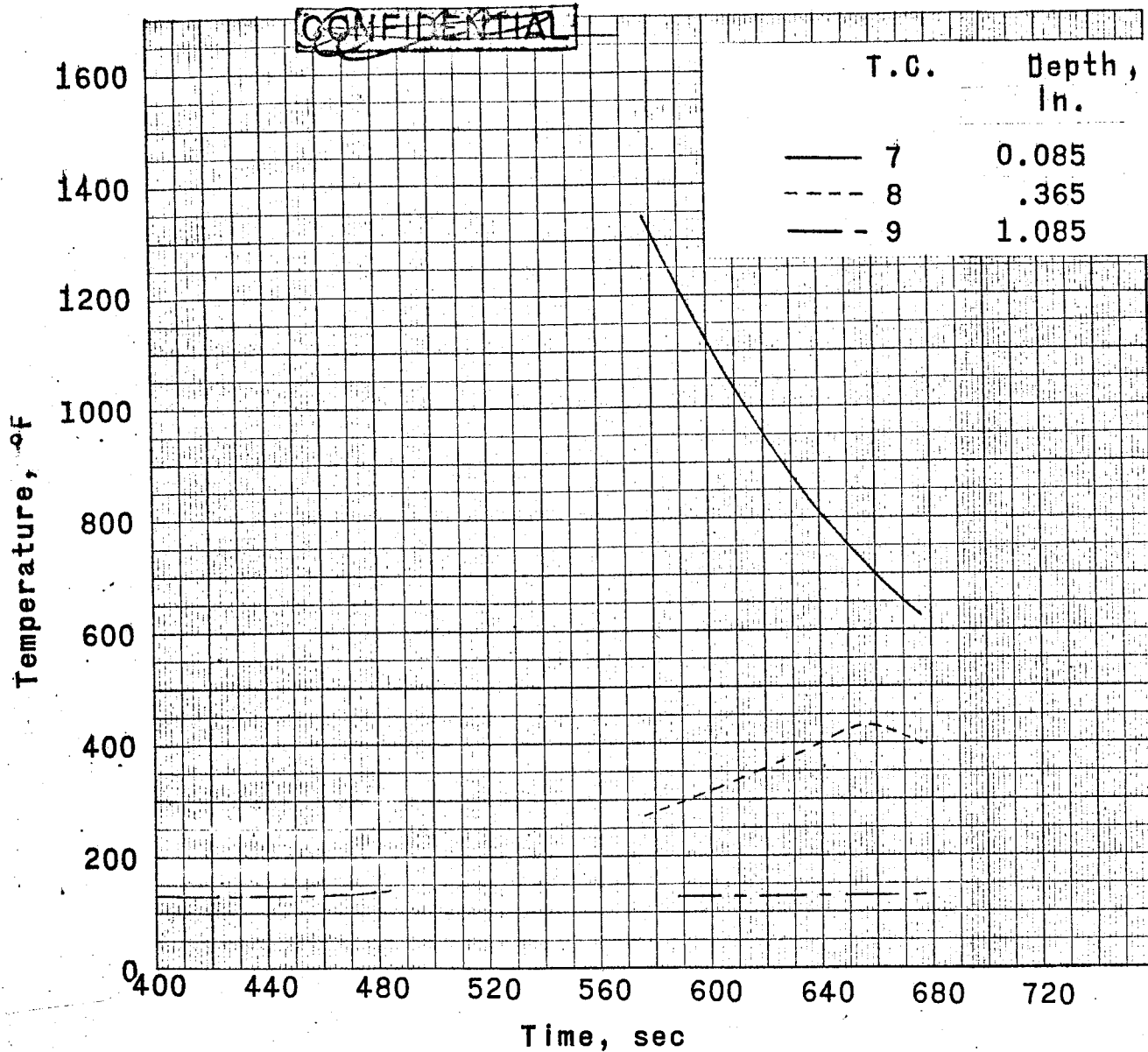
~~CONFIDENTIAL~~



(b) Sensor number 2.

~~CONFIDENTIAL~~

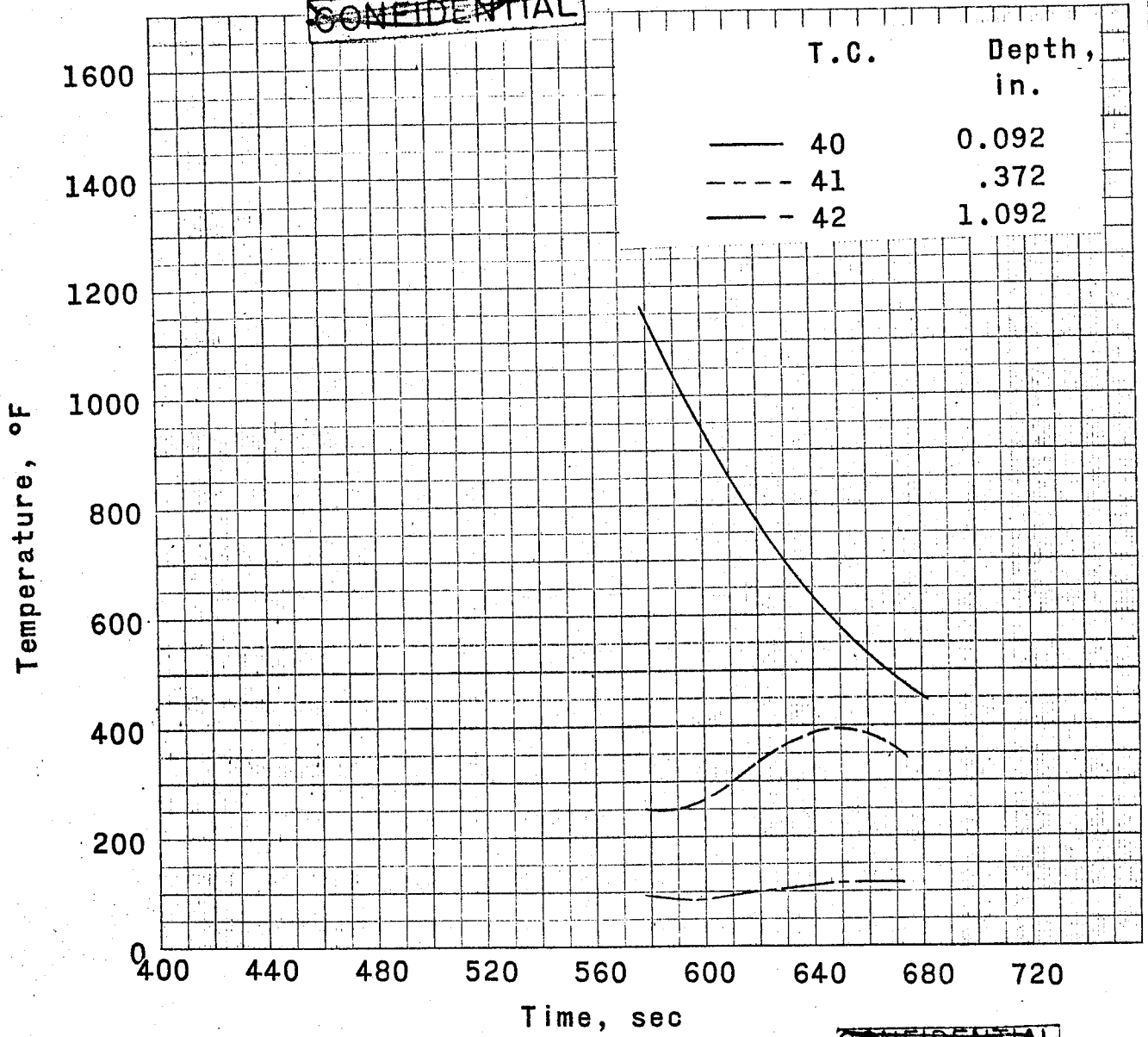
Figure 46.- Continued.



(c) Sensor number 3. ~~CONFIDENTIAL~~

Figure 46.- Continued.

~~CONFIDENTIAL~~

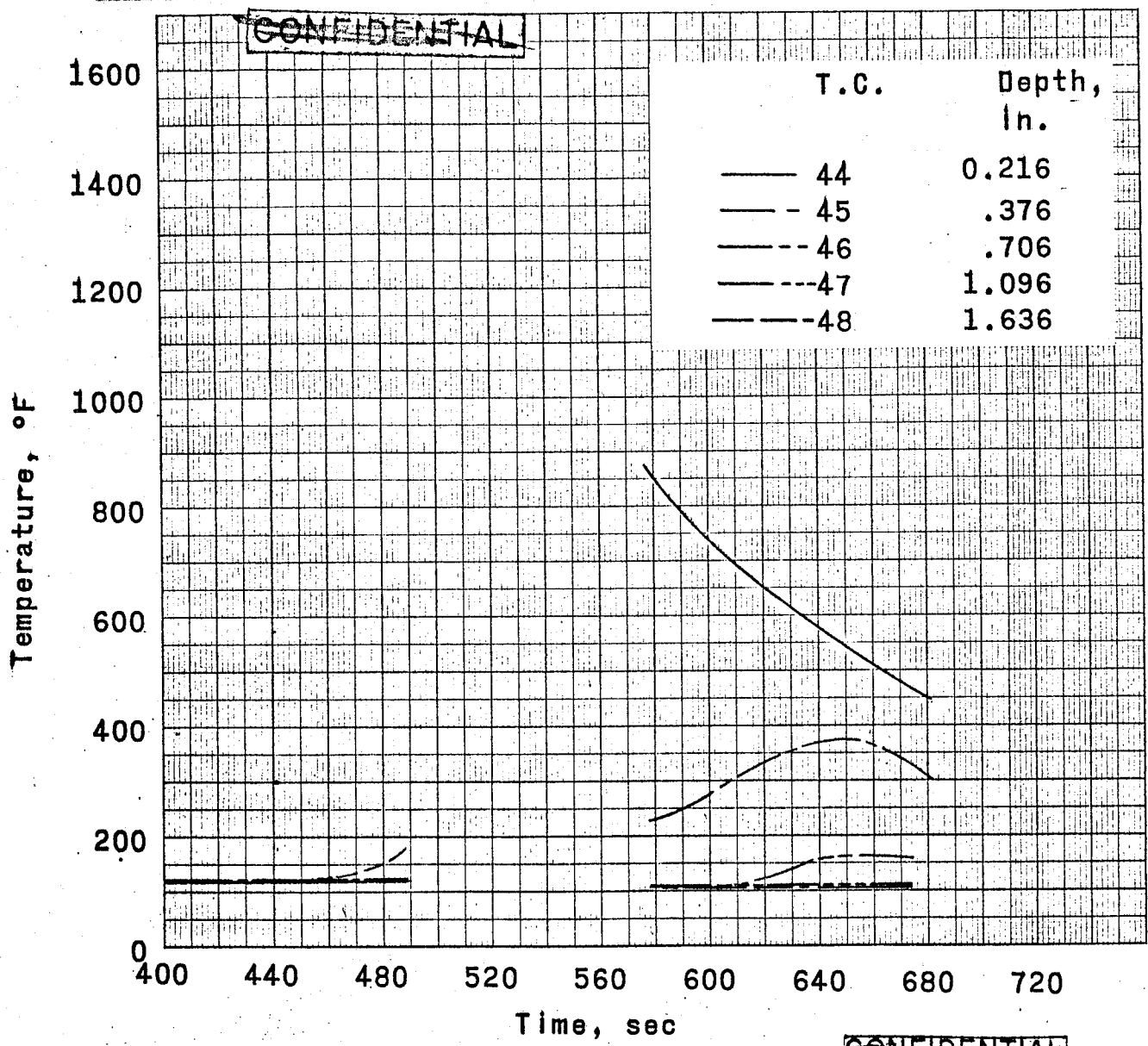


(d) Sensor number 4.

~~CONFIDENTIAL~~

Figure 46.- Continued.

~~CONFIDENTIAL~~

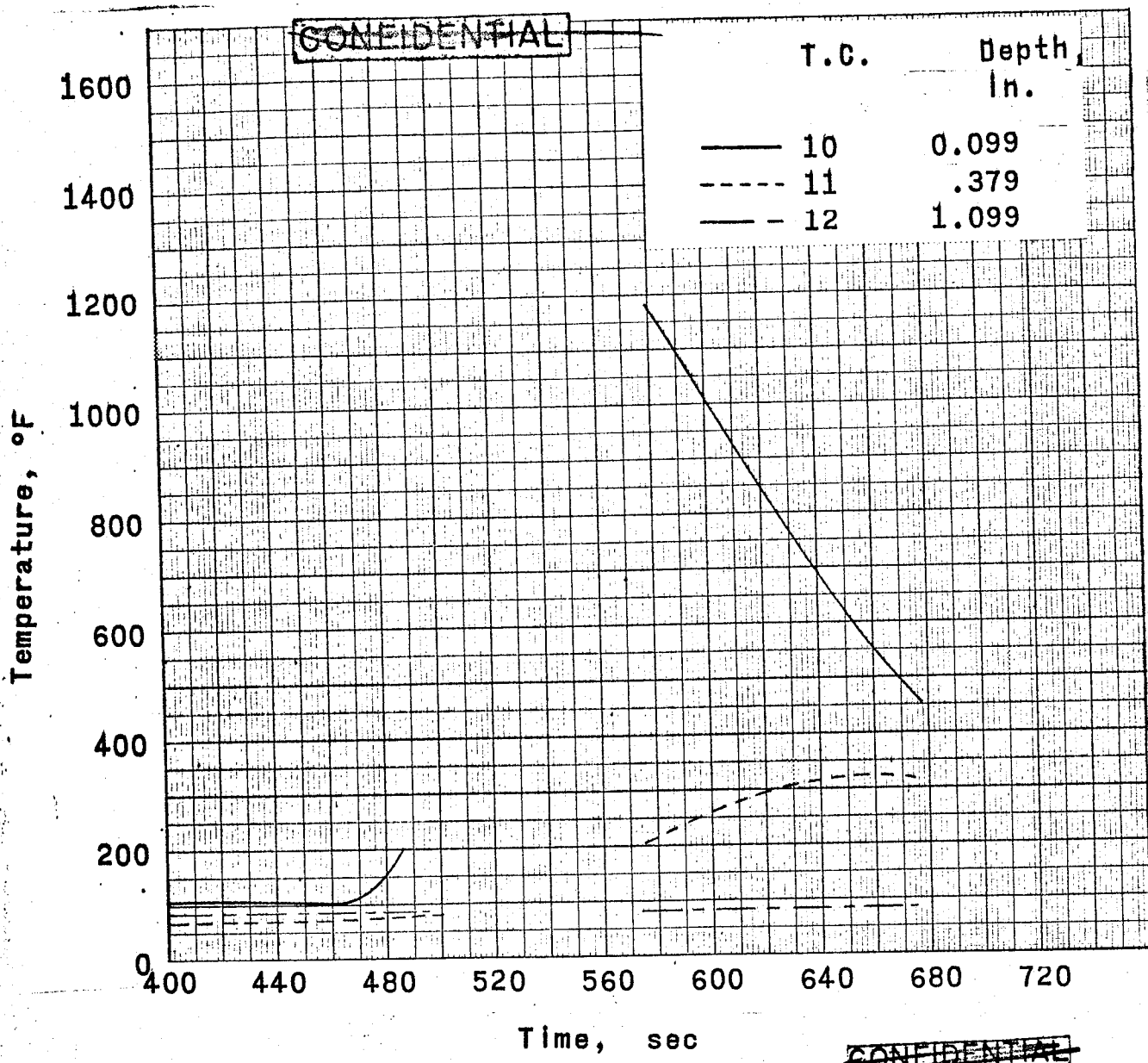


(e) Sensor number 5.

~~CONFIDENTIAL~~

Figure 46.- Continued.

~~CONFIDENTIAL~~

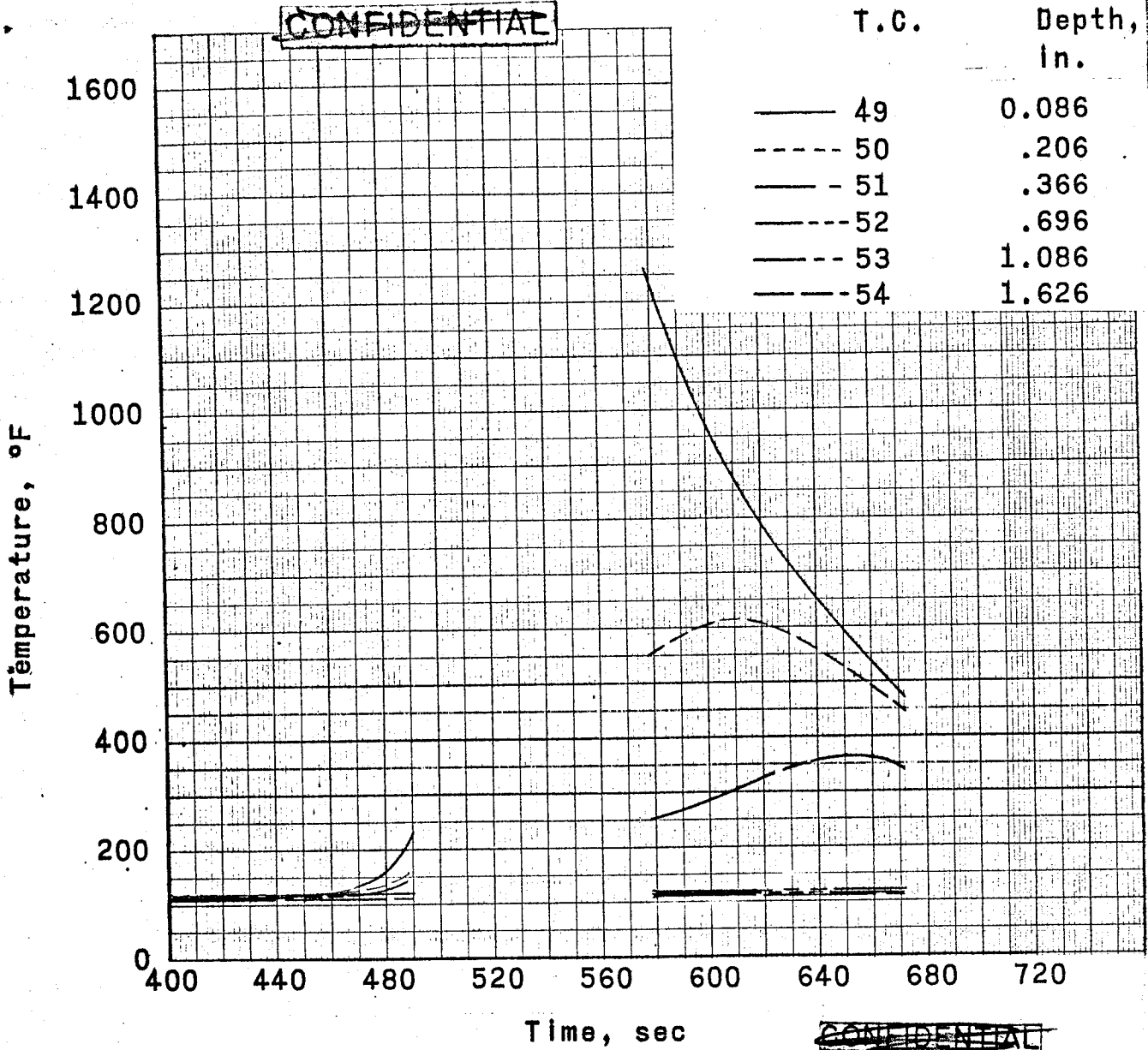


~~CONFIDENTIAL~~

(f) Sensor number 6.

Figure 46.- Continued.

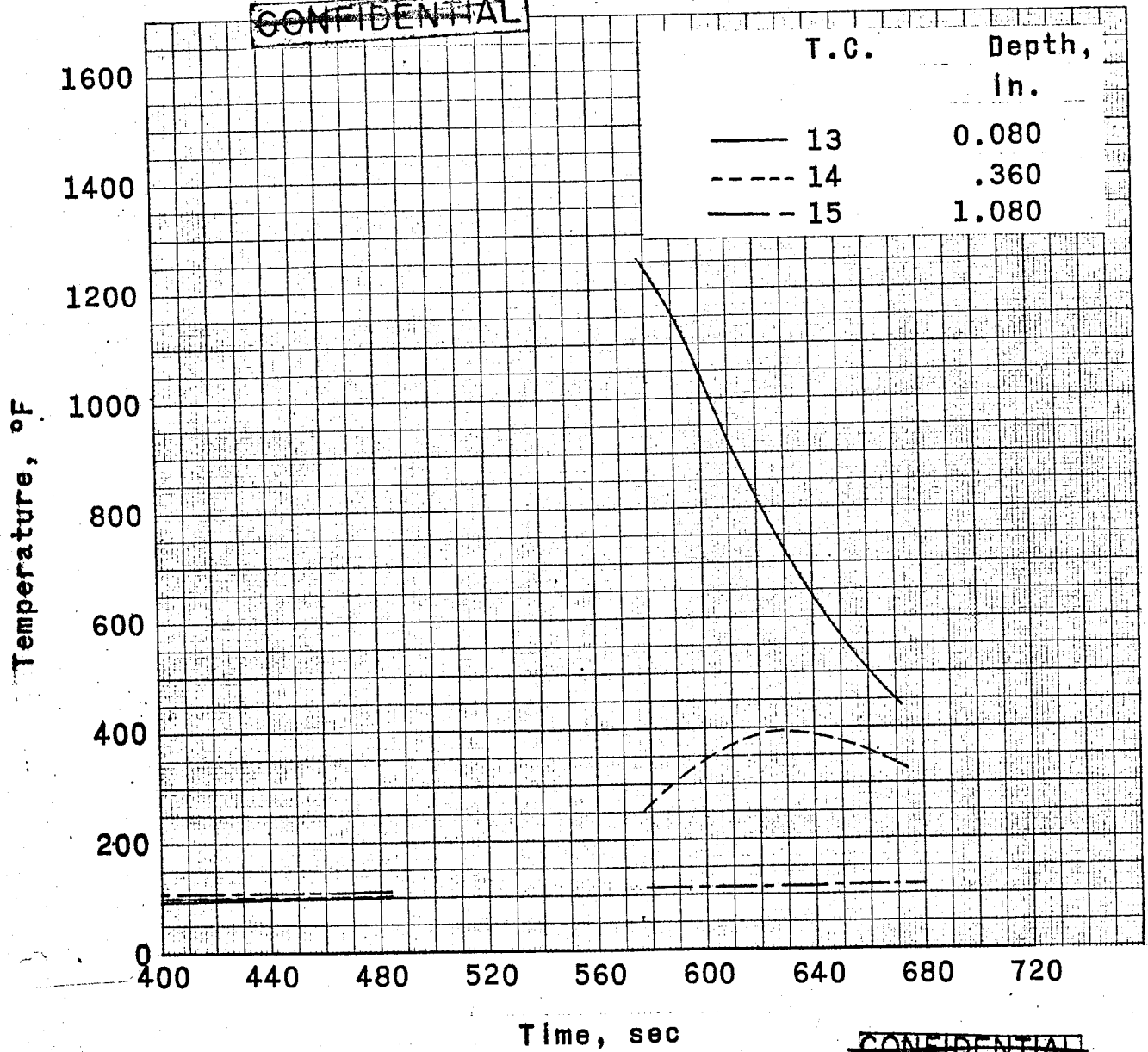
~~CONFIDENTIAL~~



(g) Sensor number 7.

Figure 46.- Continued.

~~CONFIDENTIAL~~

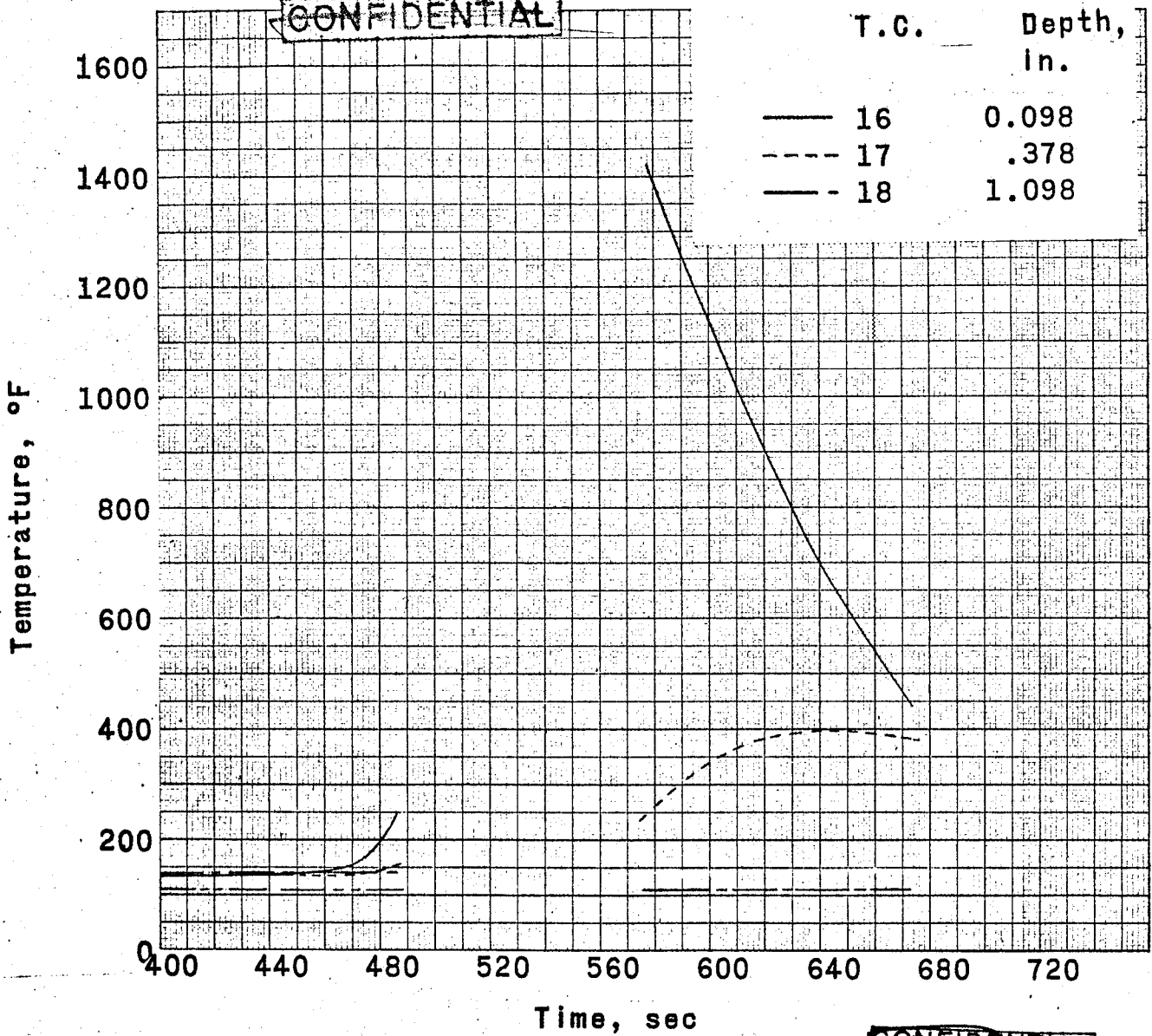


(h) Sensor number 8.

~~CONFIDENTIAL~~

Figure 46.- Continued.

~~CONFIDENTIAL~~



T.C.	Depth, in.
16	0.098
17	.378
18	1.098

~~CONFIDENTIAL~~

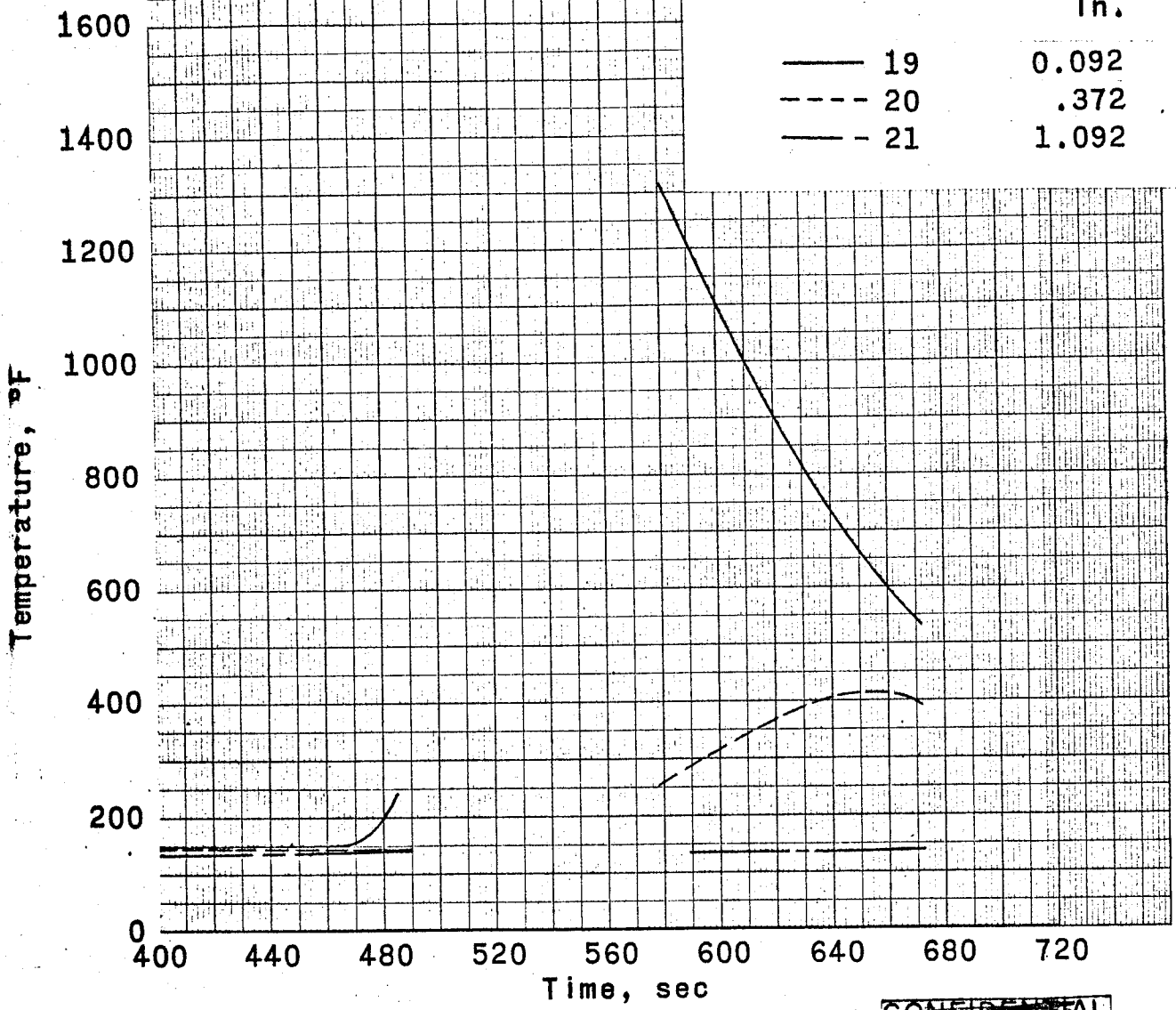
(i) Sensor number 9.

Figure 46.- Continued.

~~CONFIDENTIAL~~

T.C.

Depth,  
In.



— 19  
- - - 20  
- · - 21

0.092  
.372  
1.092

Temperature, °F

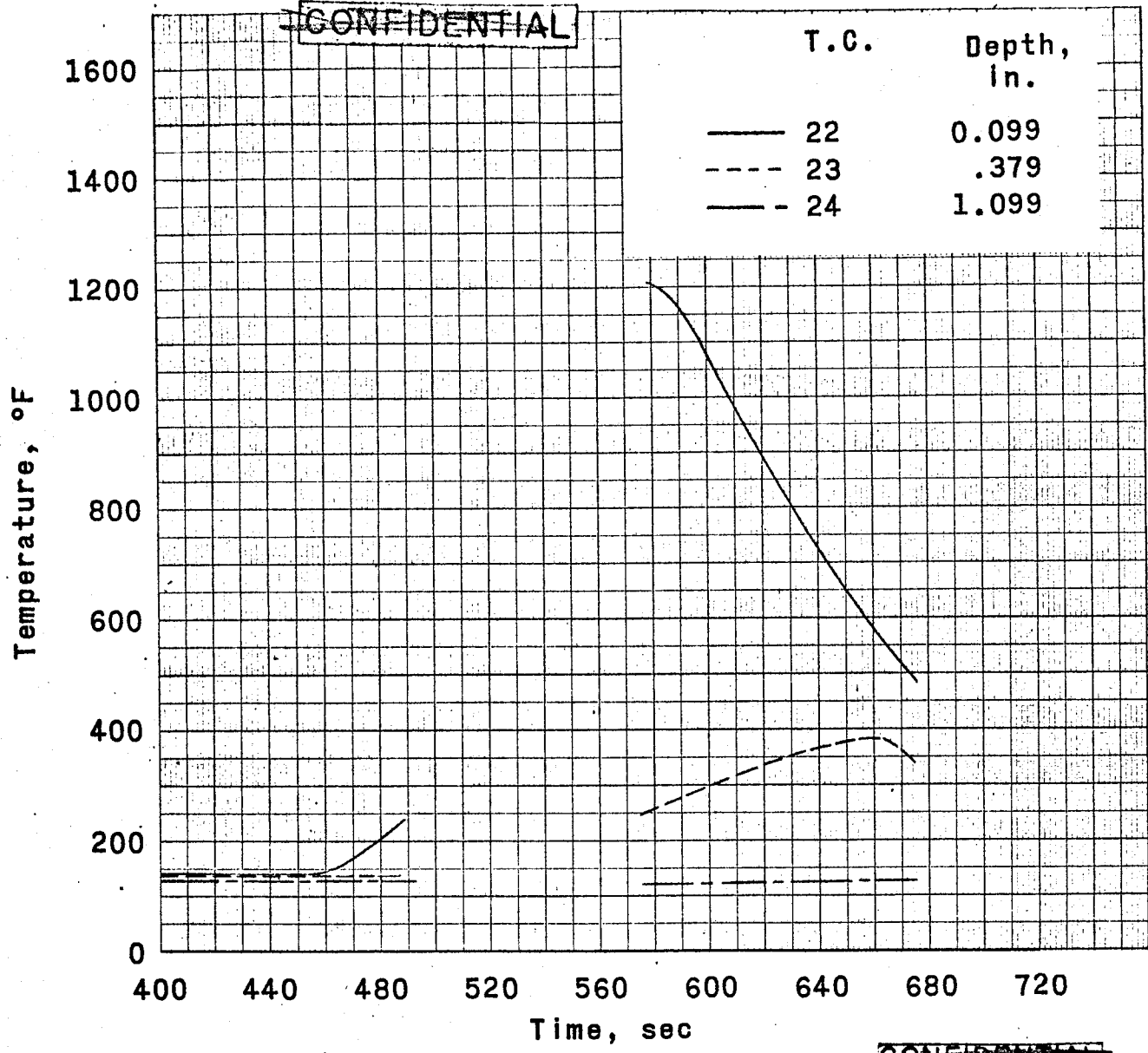
Time, sec

(j) Sensor number 10.

~~CONFIDENTIAL~~

Figure 46.- Continued.

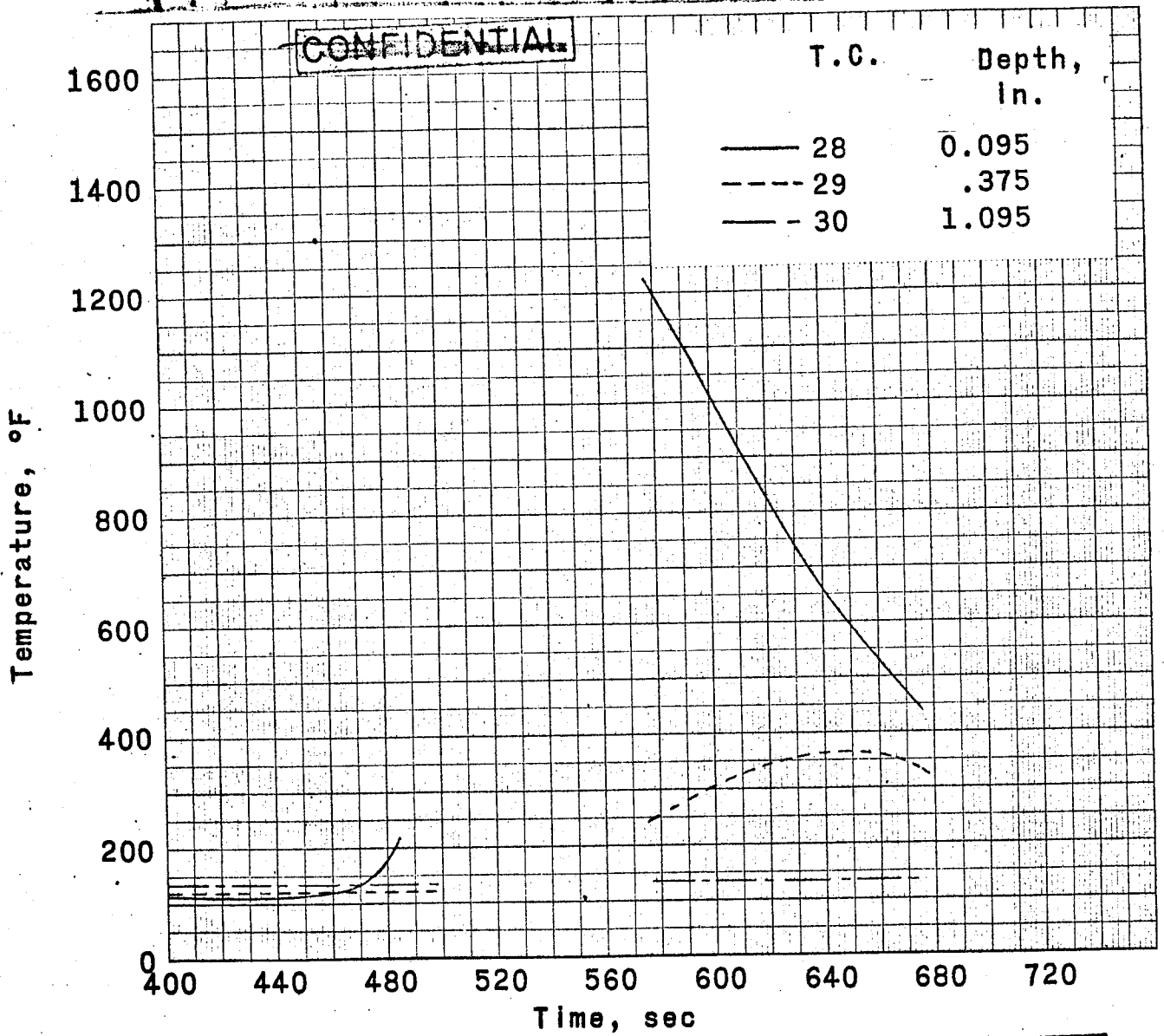
~~CONFIDENTIAL~~



(k) Sensor number 11.

~~CONFIDENTIAL~~

Figure 46.- Continued.

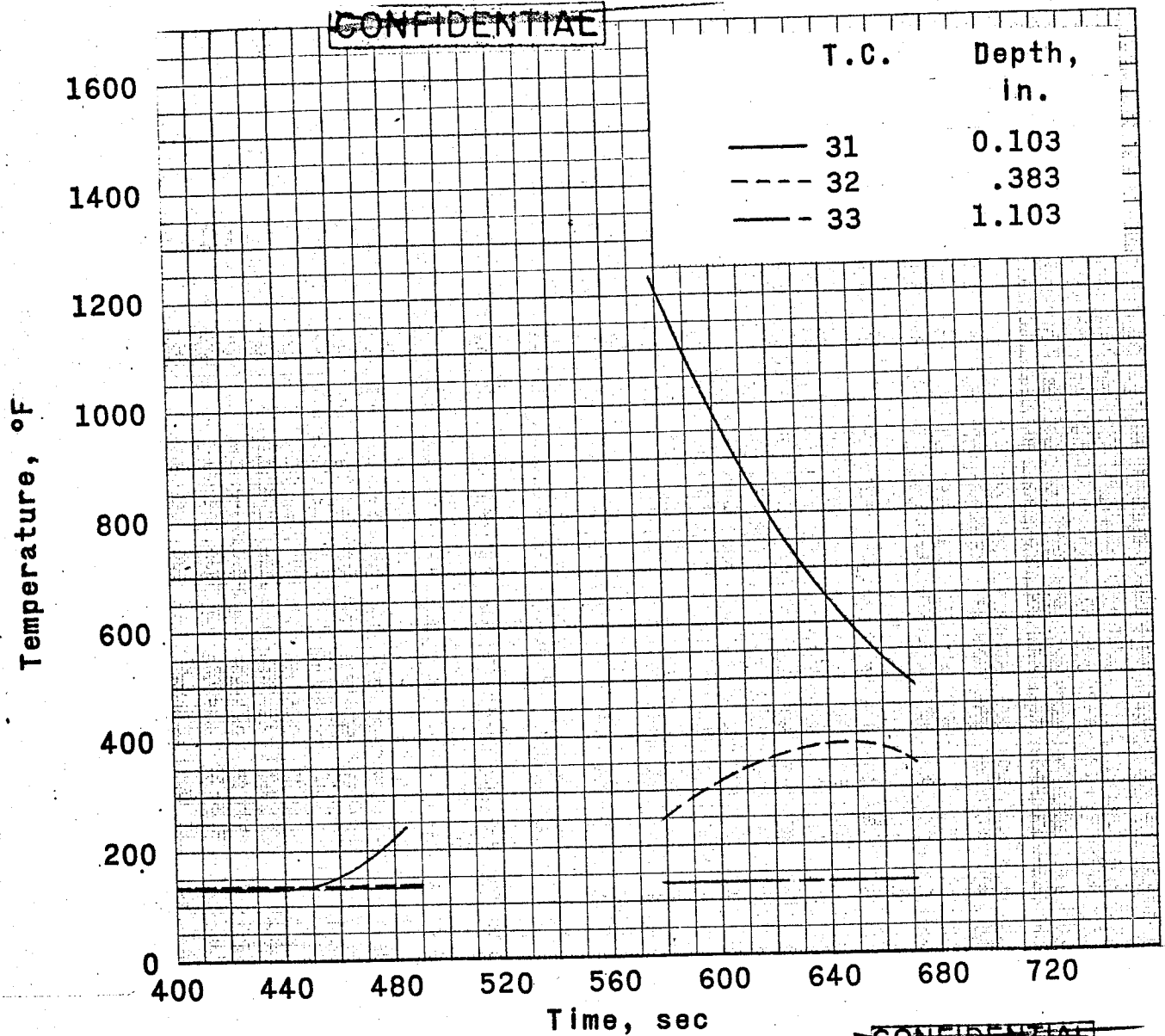


(1) Sensor number 12.

**CONFIDENTIAL**

Figure 46.- Continued.

~~CONFIDENTIAL~~

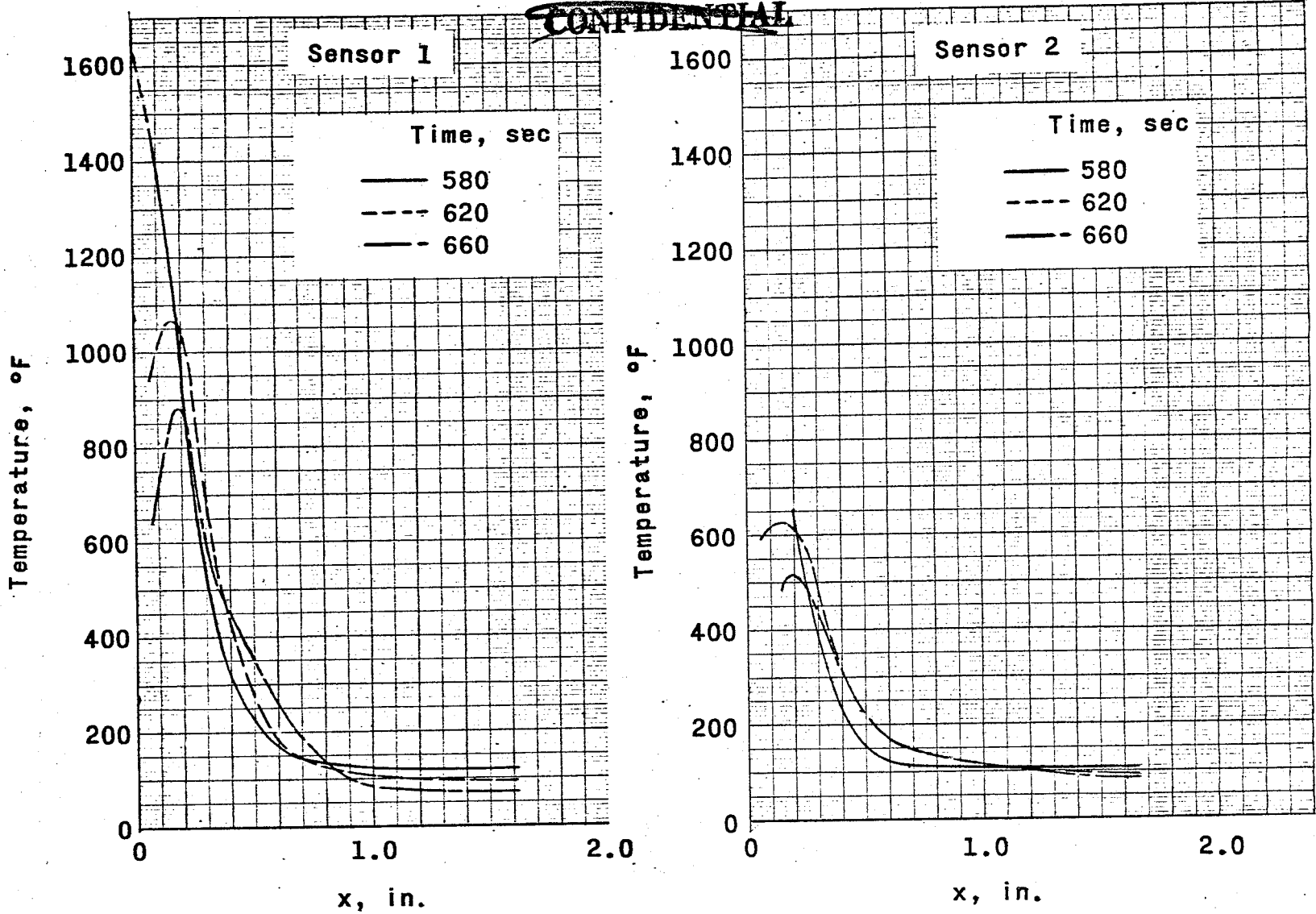


~~CONFIDENTIAL~~

(m) Sensor number 13.

Figure 46.- Concluded.

~~CONFIDENTIAL~~

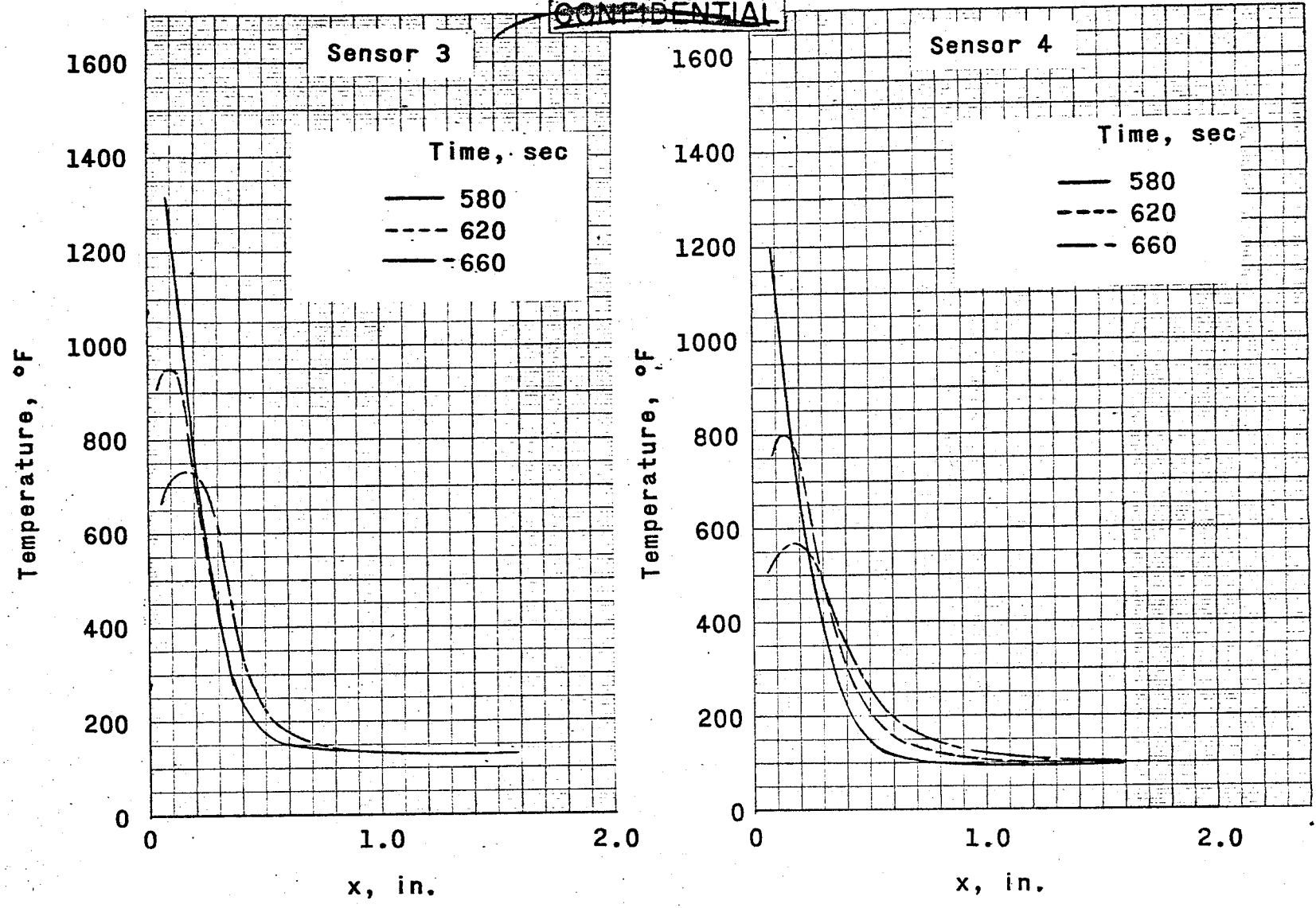


(a) Sensor 1 and 2.

Figure 47.- Temperature distribution in heat shield at sensor locations for times of 580, 620 and 660 seconds.

~~CONFIDENTIAL~~

~~CONFIDENTIAL~~

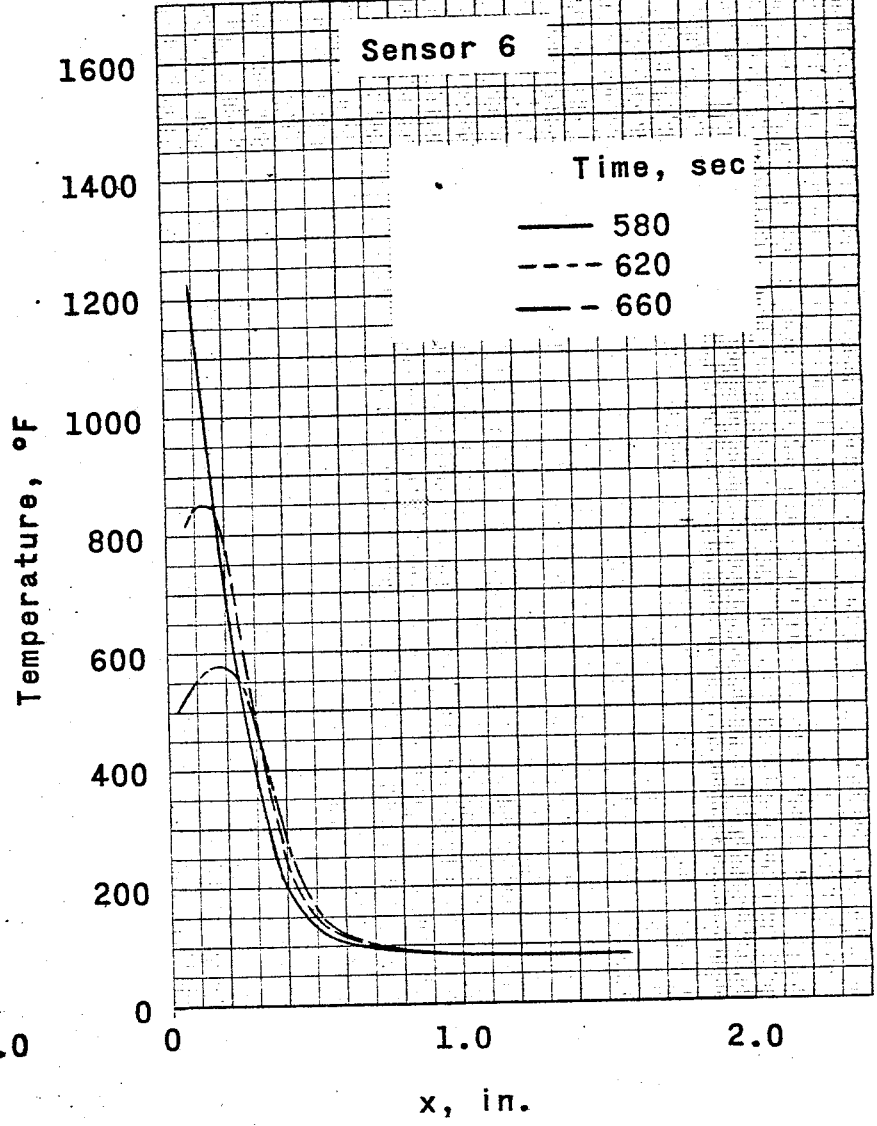
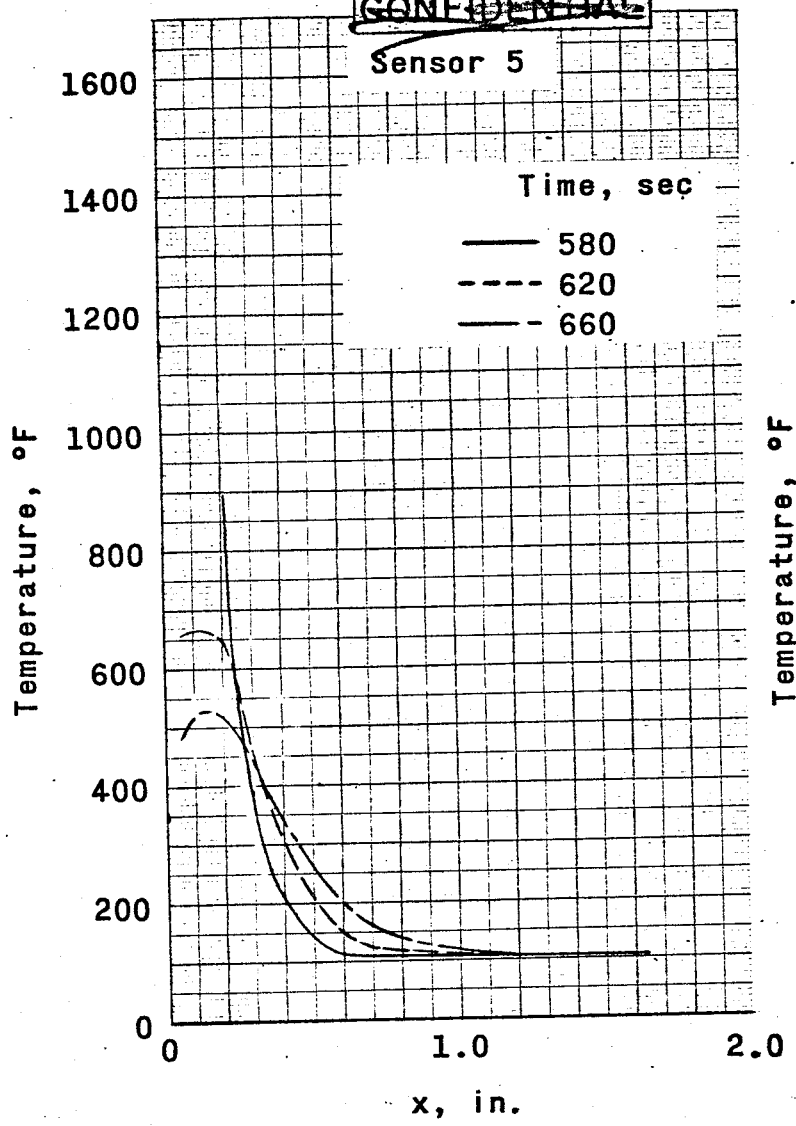


(b) Sensor 3 and 4.

~~CONFIDENTIAL~~

Figure 47.- Continued.

~~CONFIDENTIAL~~

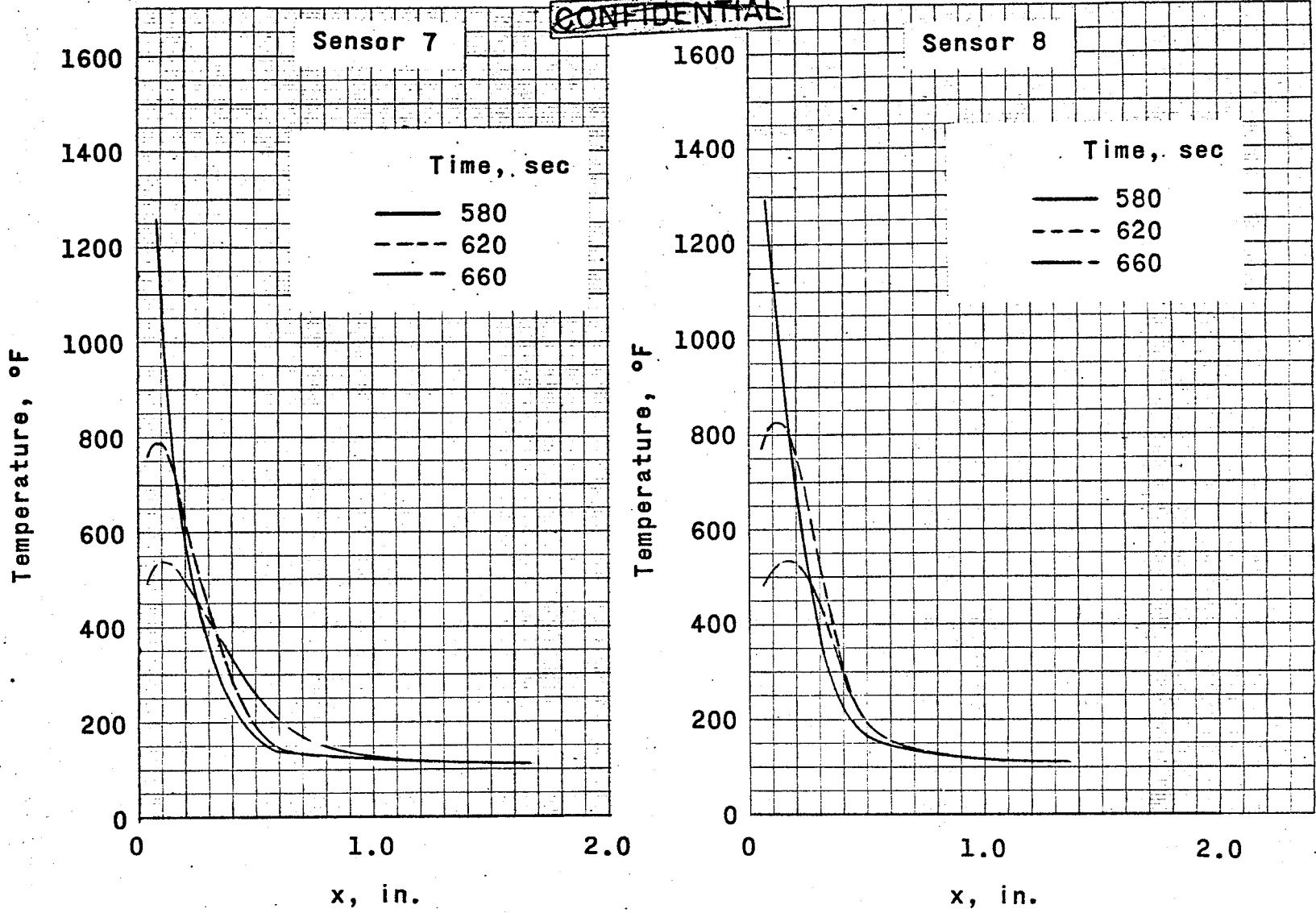


(c) Sensor 5 and 6.

~~CONFIDENTIAL~~

Figure 47.- Continued.

**CONFIDENTIAL**

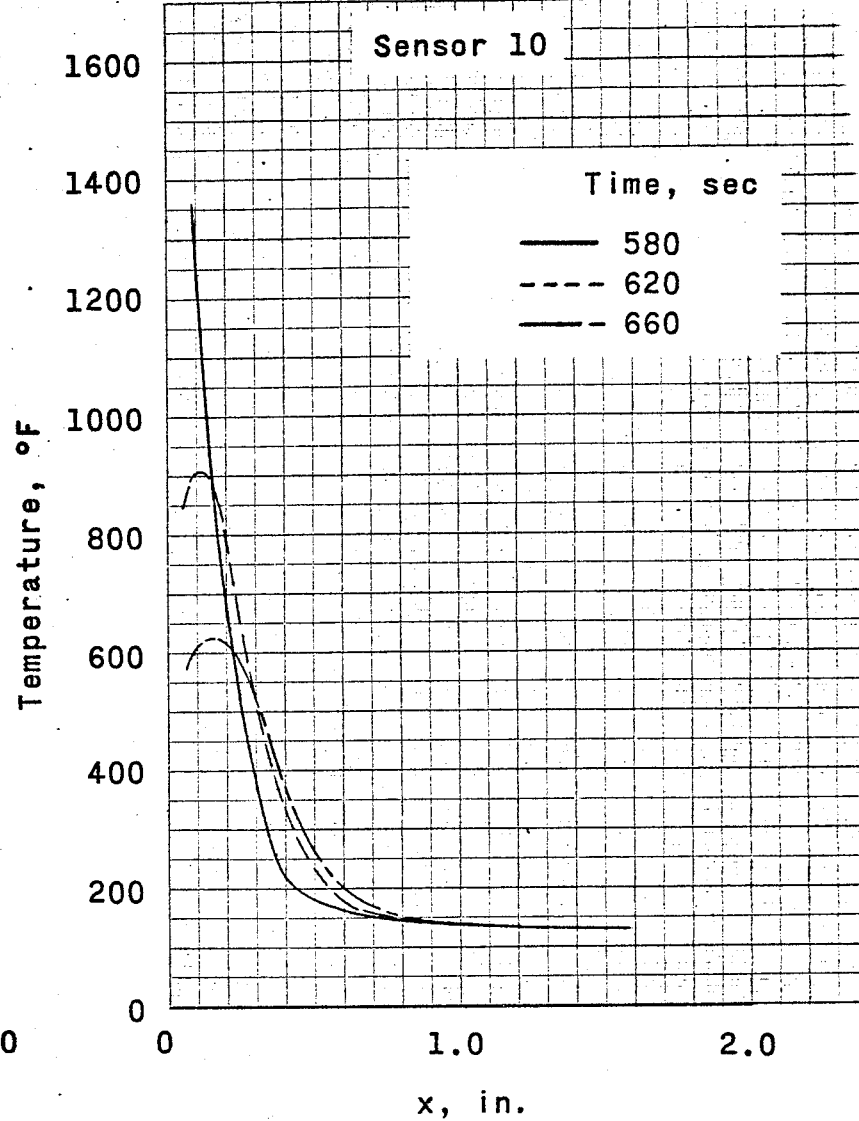
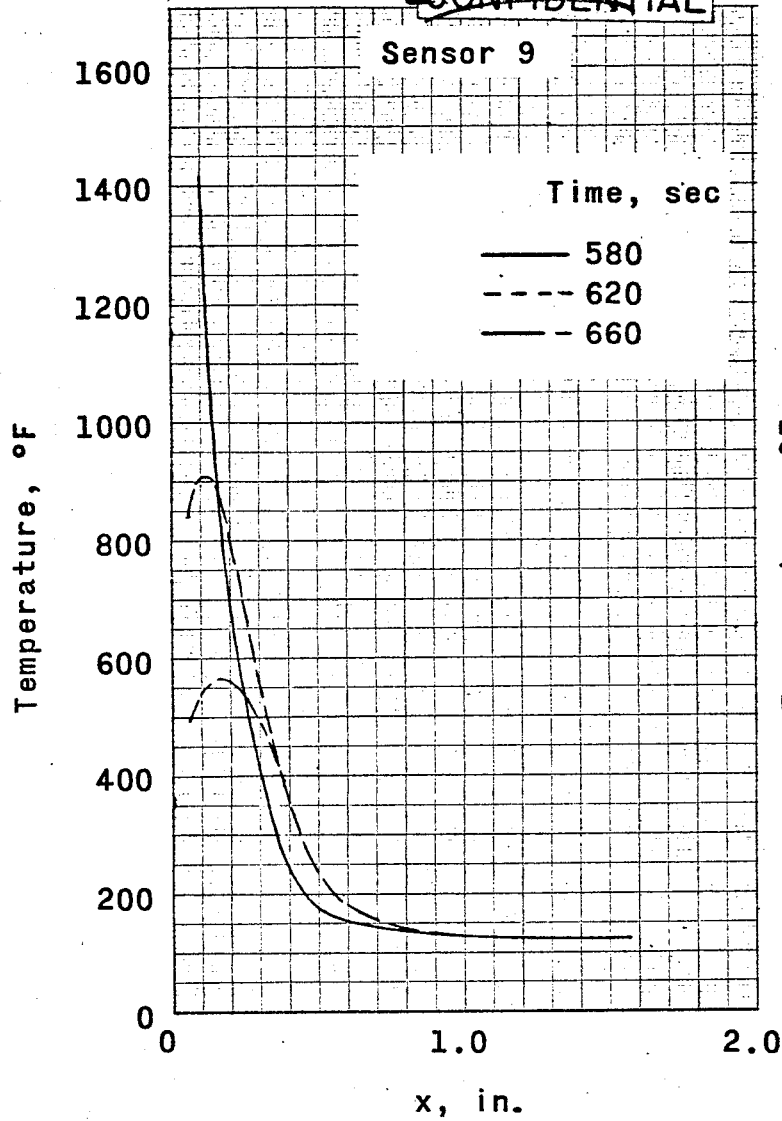


(d) Sensor 7 and 8.

**CONFIDENTIAL**

Figure 47.- Continued.

~~CONFIDENTIAL~~

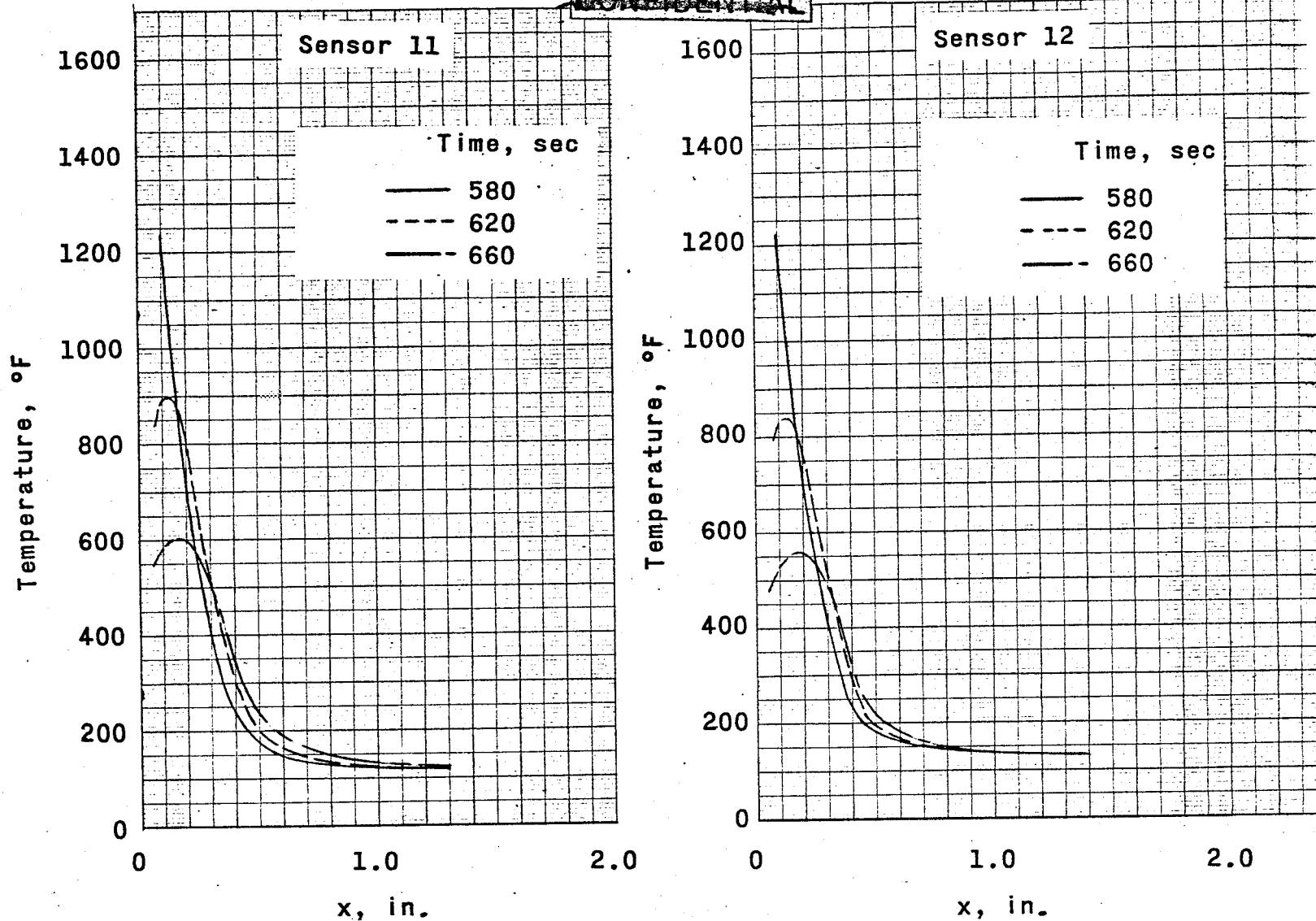


(e) Sensor 9 and 10.

~~CONFIDENTIAL~~

Figure 47.- Continued.

~~CONFIDENTIAL~~

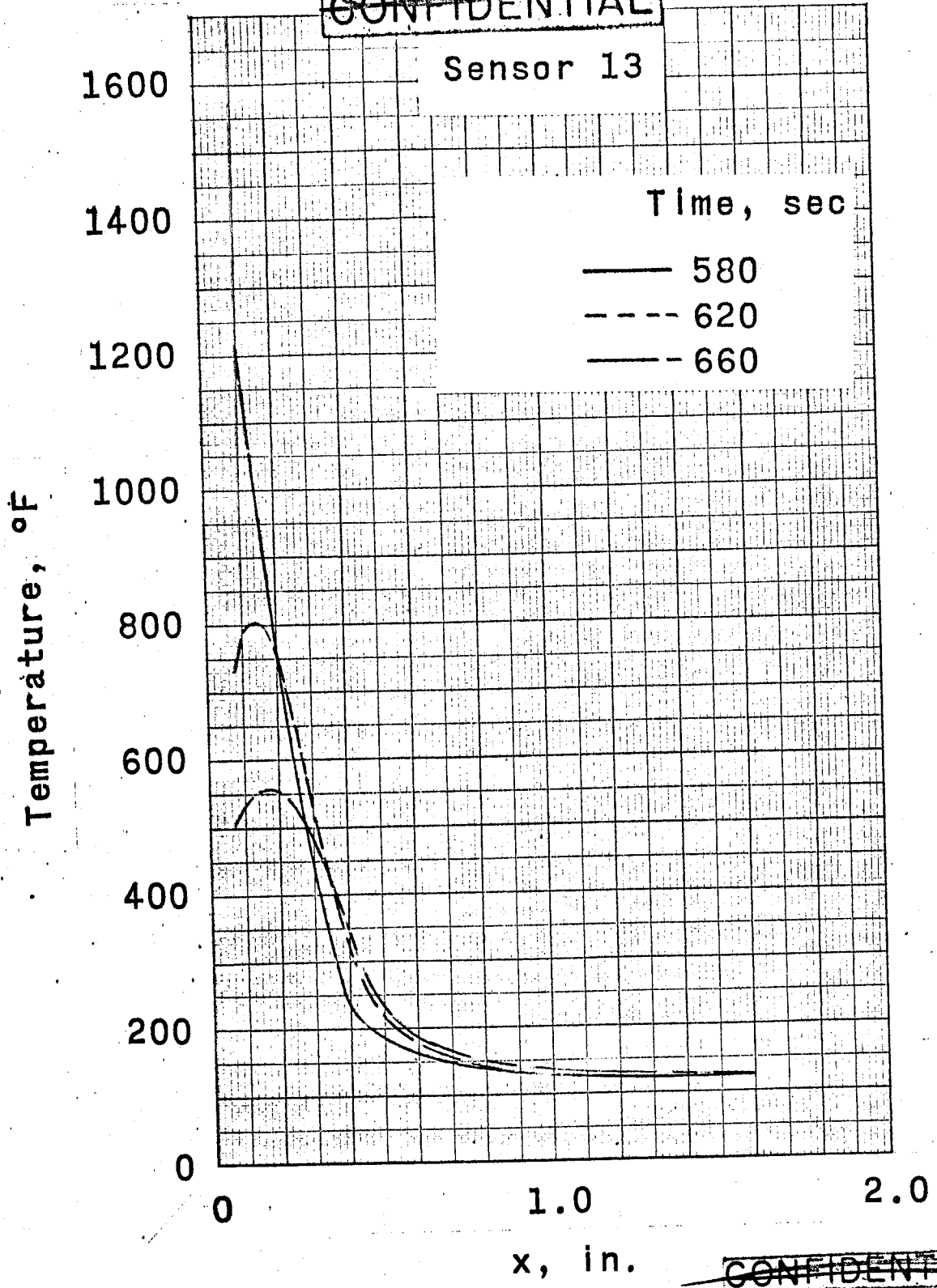


(f) Sensor 11 and 12.

~~CONFIDENTIAL~~

Figure 47.- Continued.

~~CONFIDENTIAL~~



(g) Sensor 13.

~~CONFIDENTIAL~~

Figure 47.- Concluded.

~~CONFIDENTIAL~~

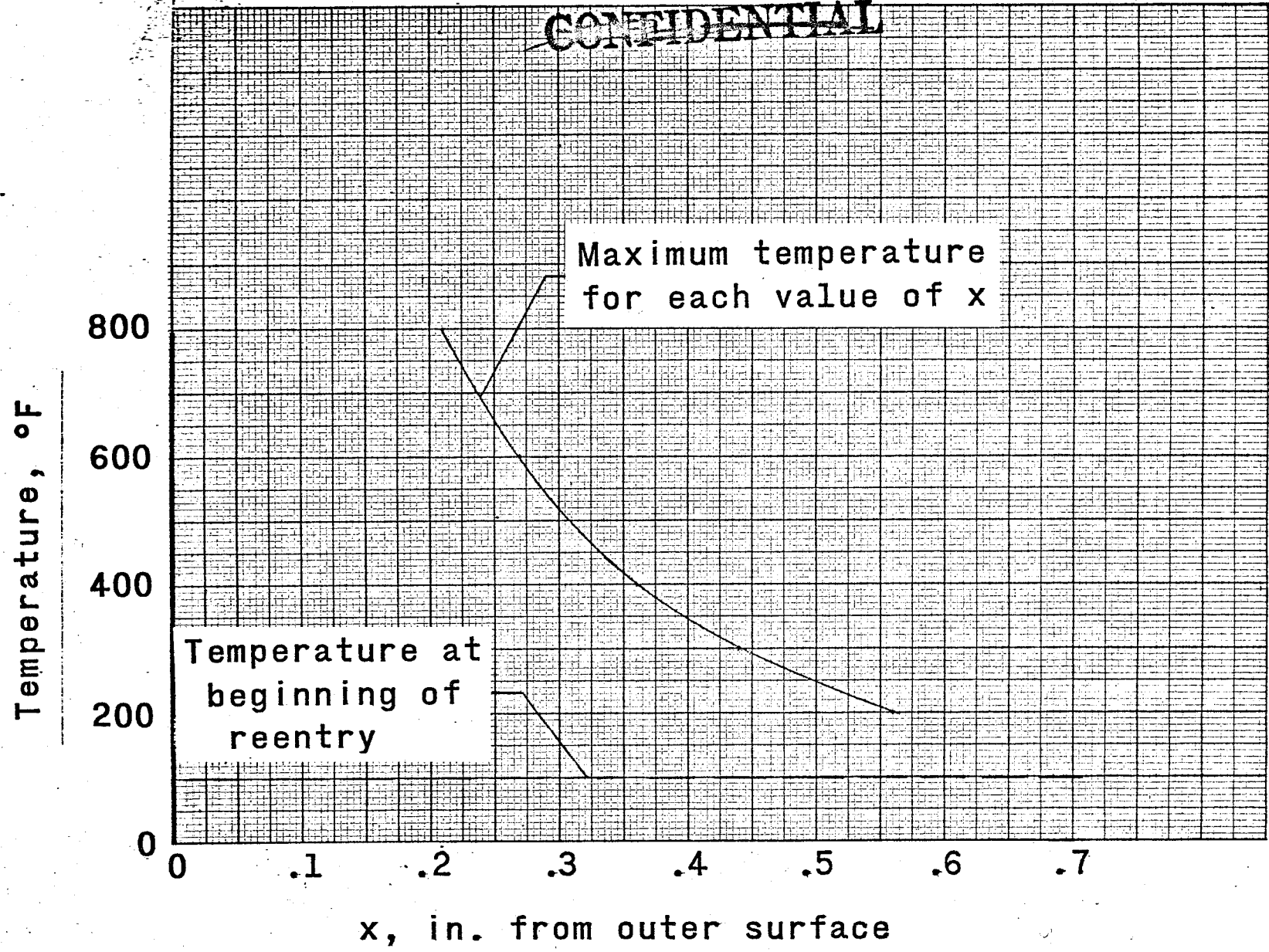
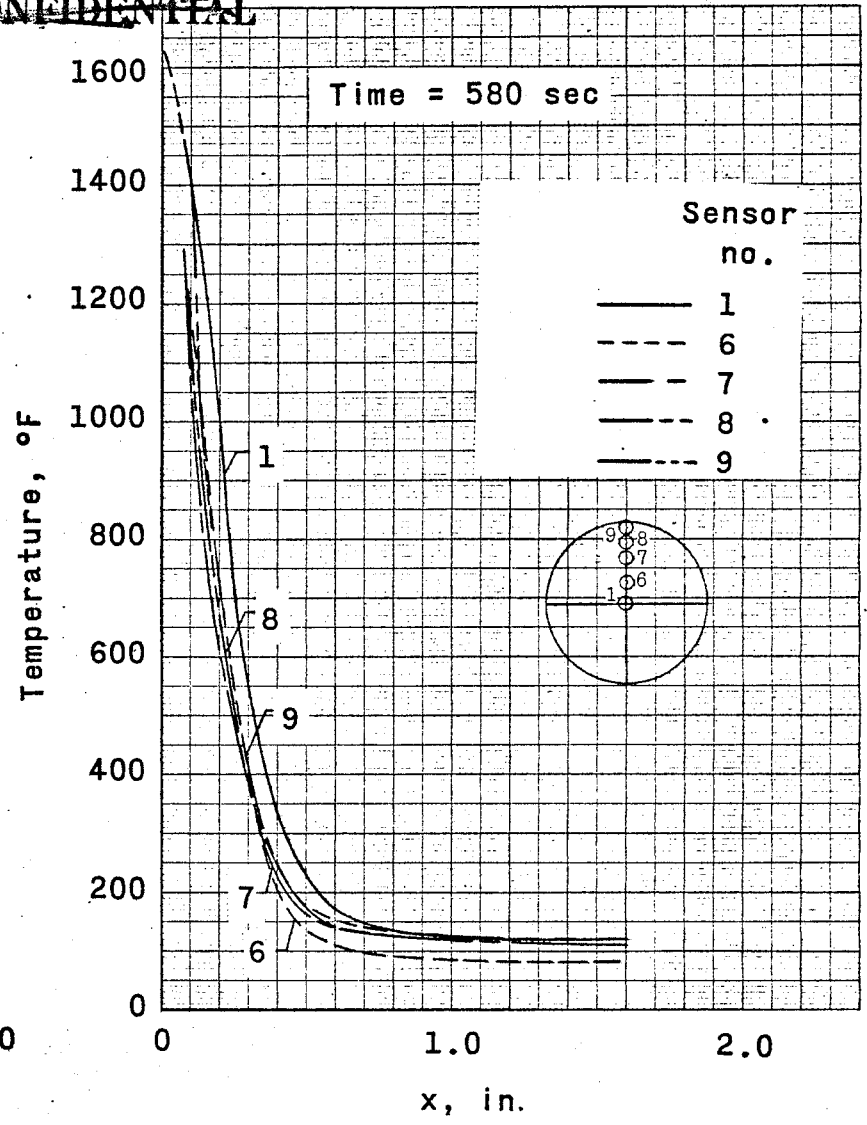
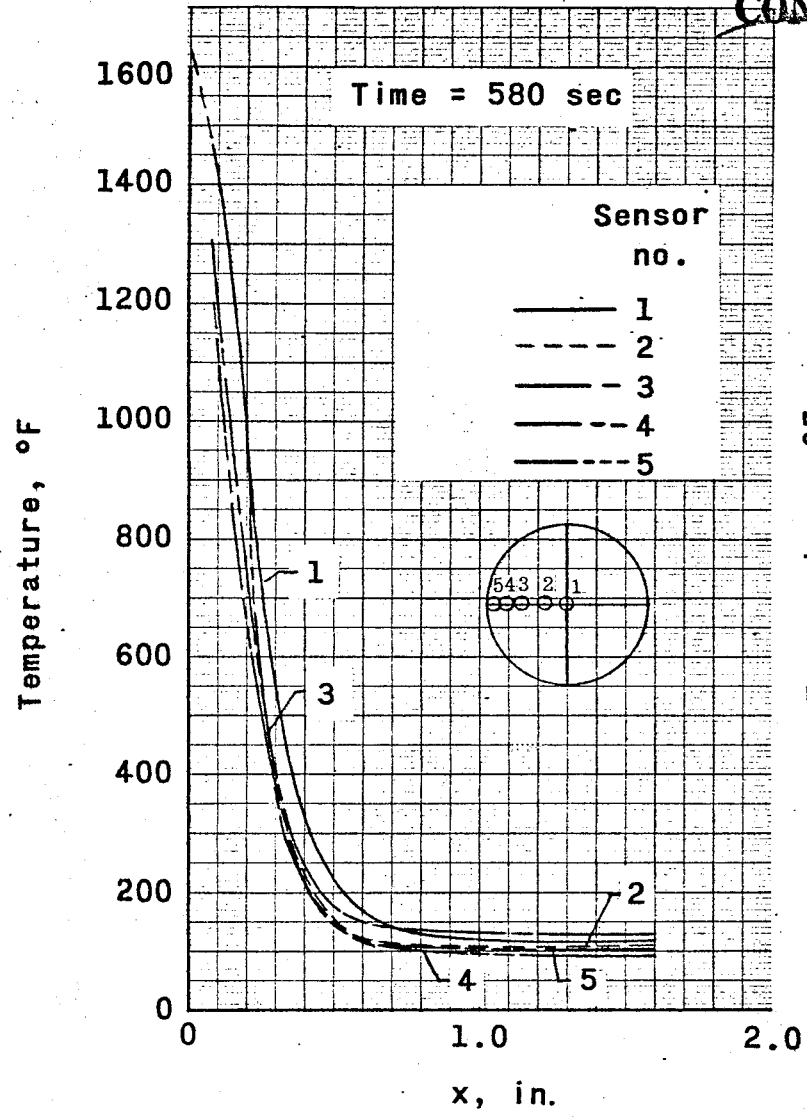


Figure 48.- Depth of temperature penetration in heat shield.

~~CONFIDENTIAL~~

~~CONFIDENTIAL~~

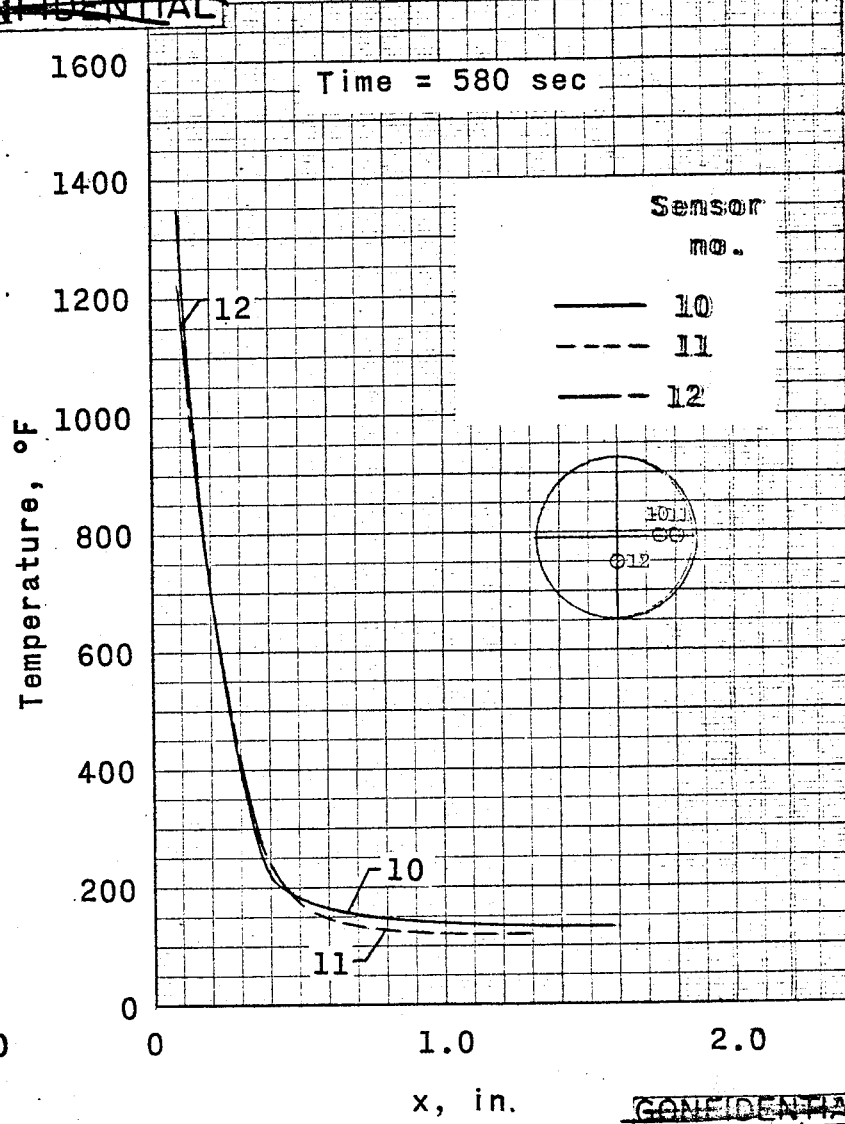
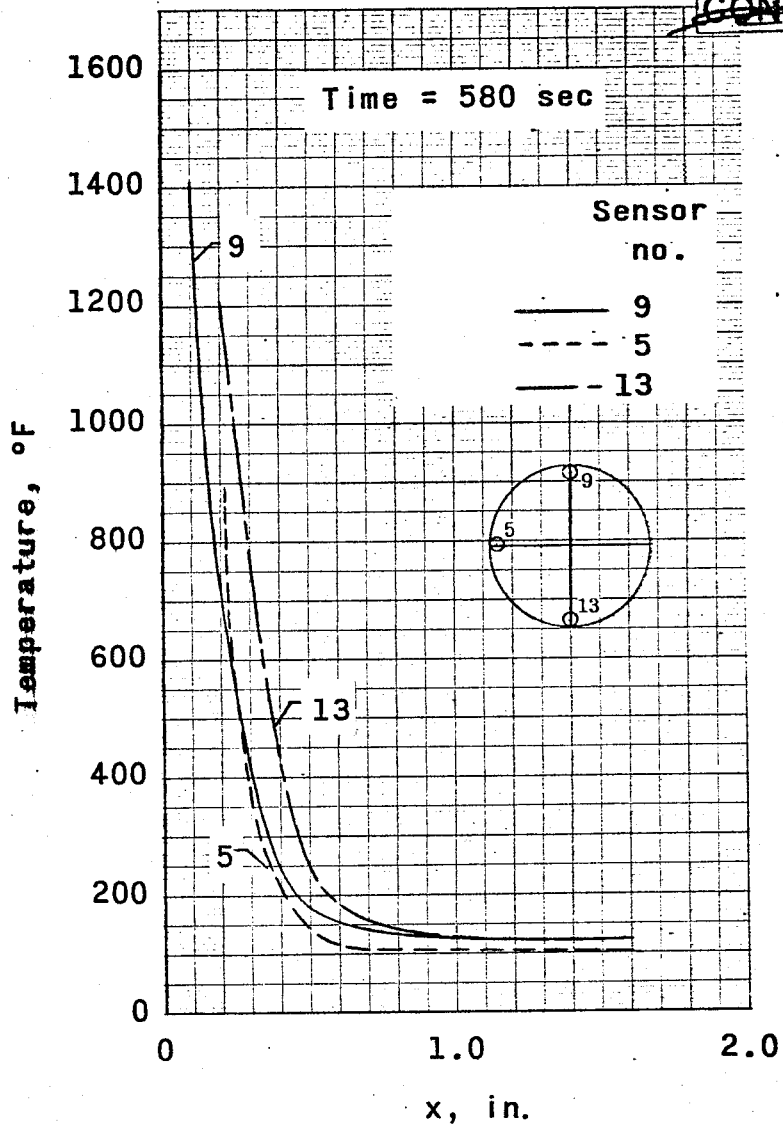


(a) Time 580 sec (Sensor 1 thru 9).

Figure 49.- Comparison of temperature distribution thru heat shield at selected time intervals.

~~CONFIDENTIAL~~

~~CONFIDENTIAL~~

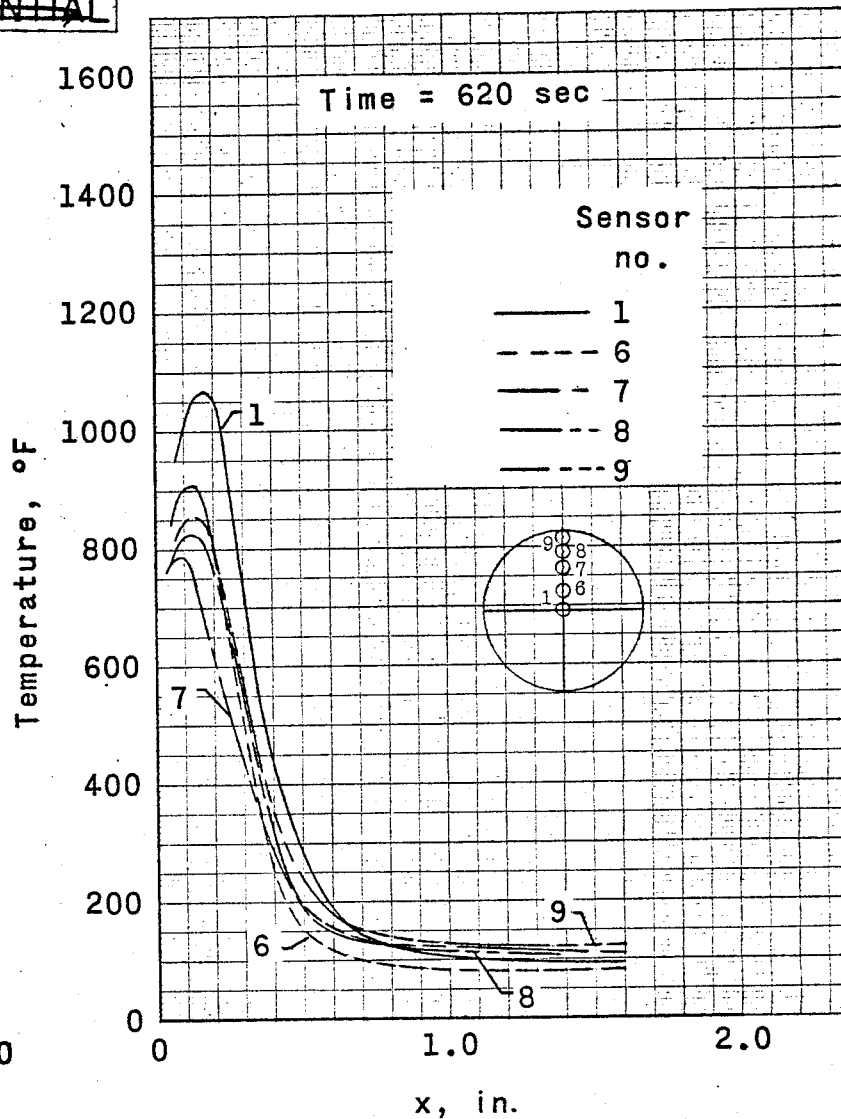
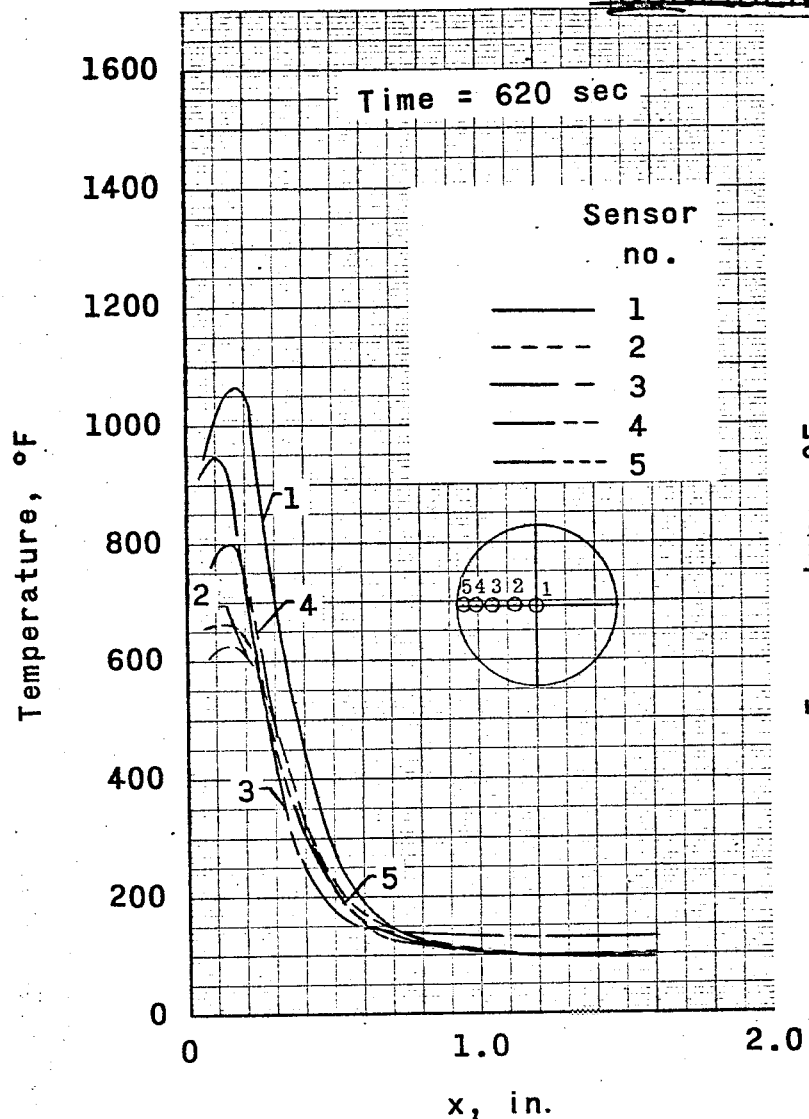


~~CONFIDENTIAL~~

(b) Time 580 sec (Sensor 5, 9, 13, 10, 11 and 12).

Figure 49 .- Continued.

~~CONFIDENTIAL~~

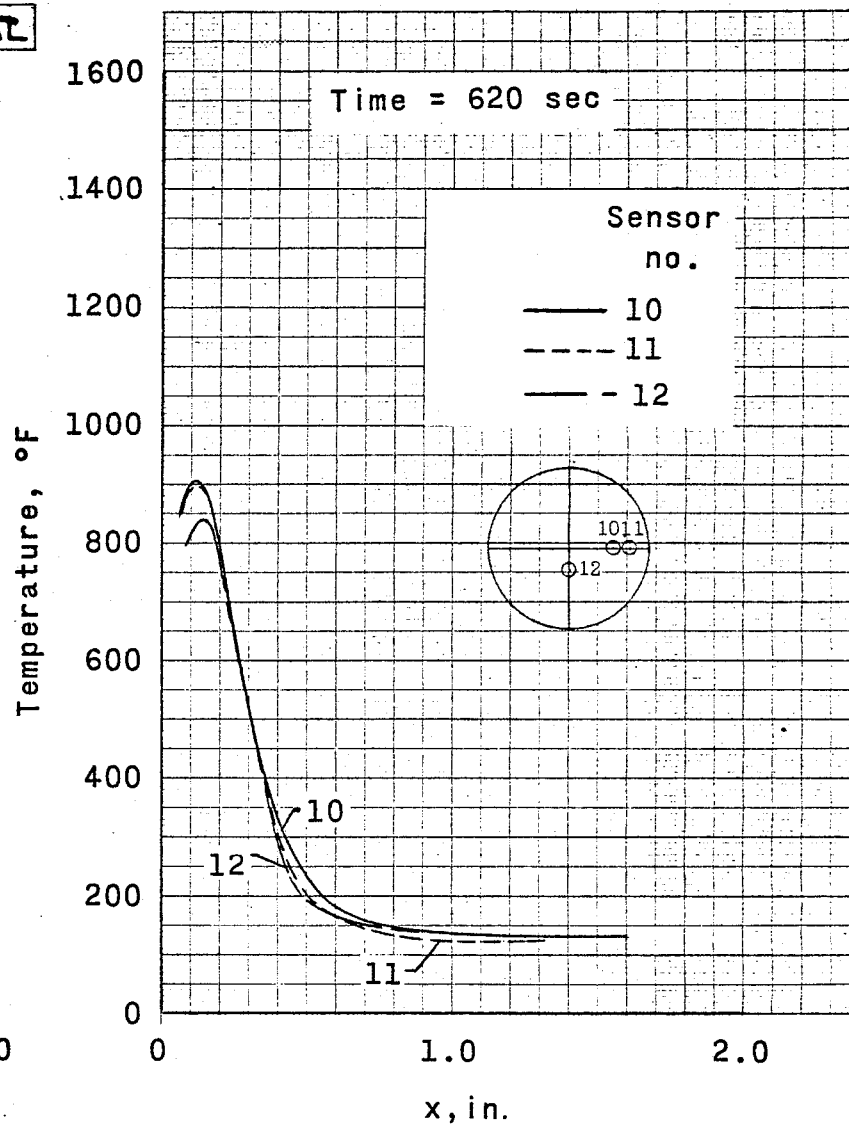
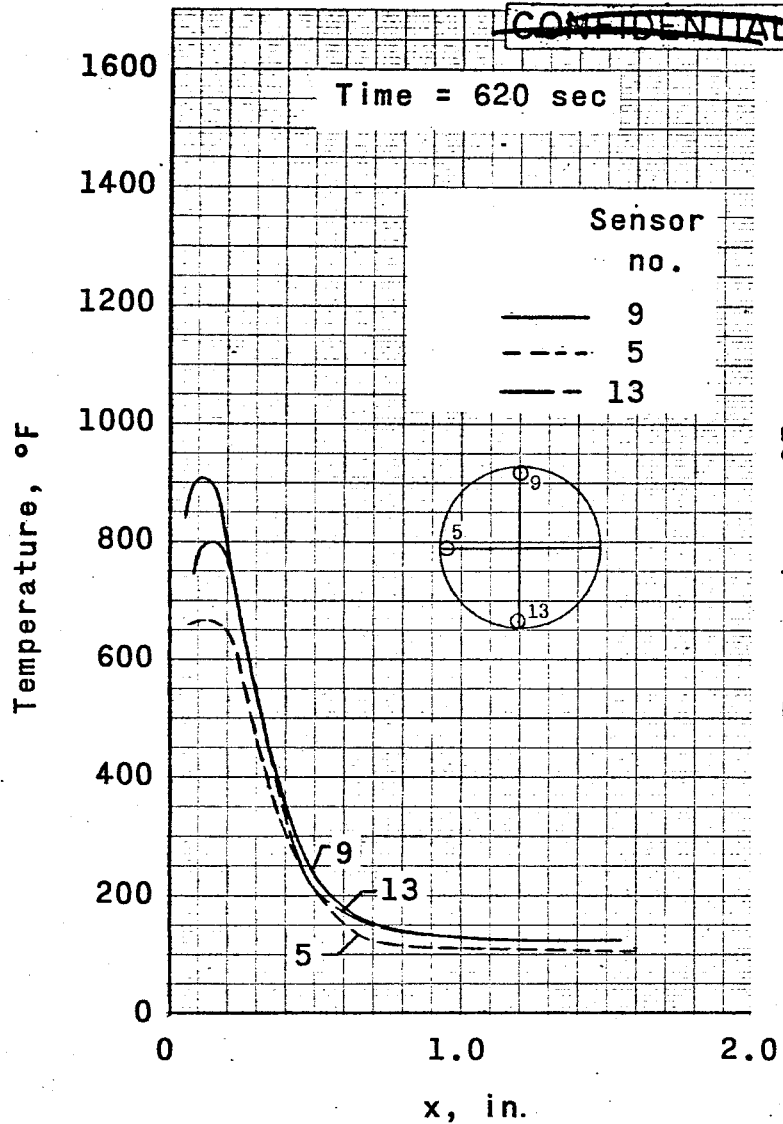


(c) Time 620 sec (Sensor 1 thru 9).

~~CONFIDENTIAL~~

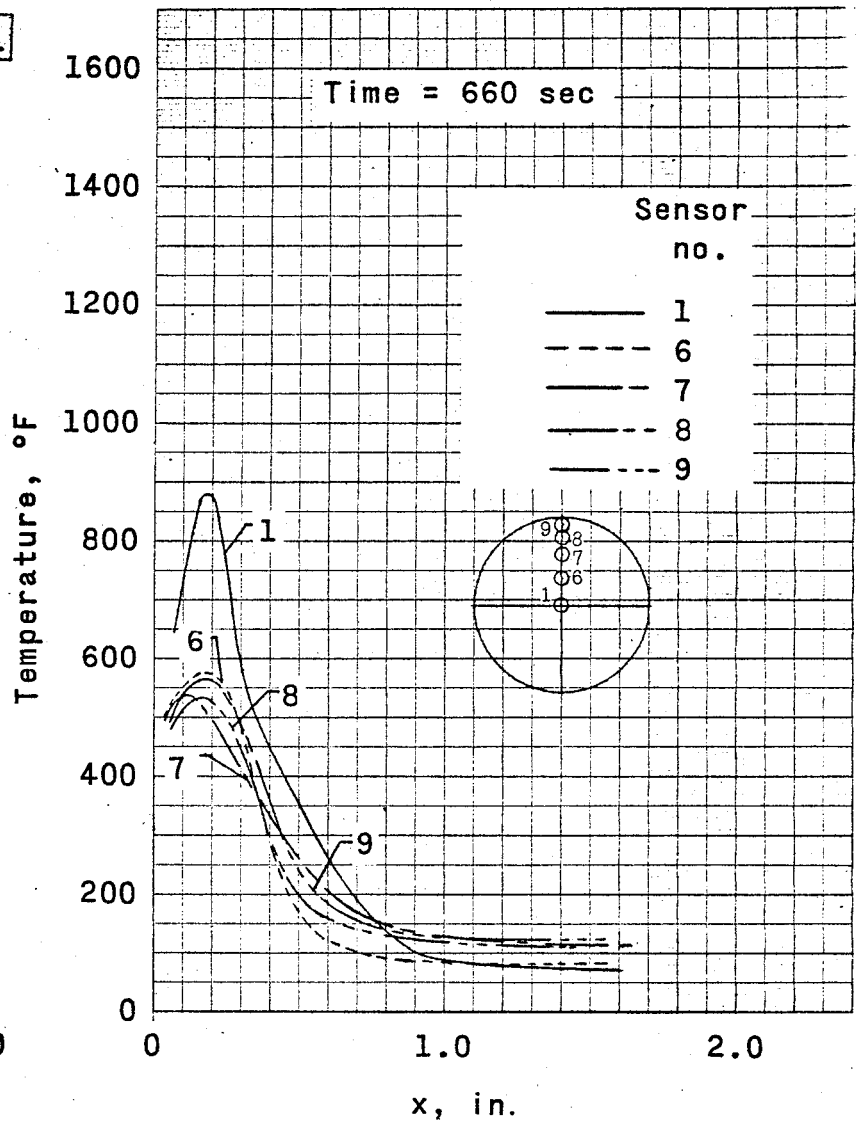
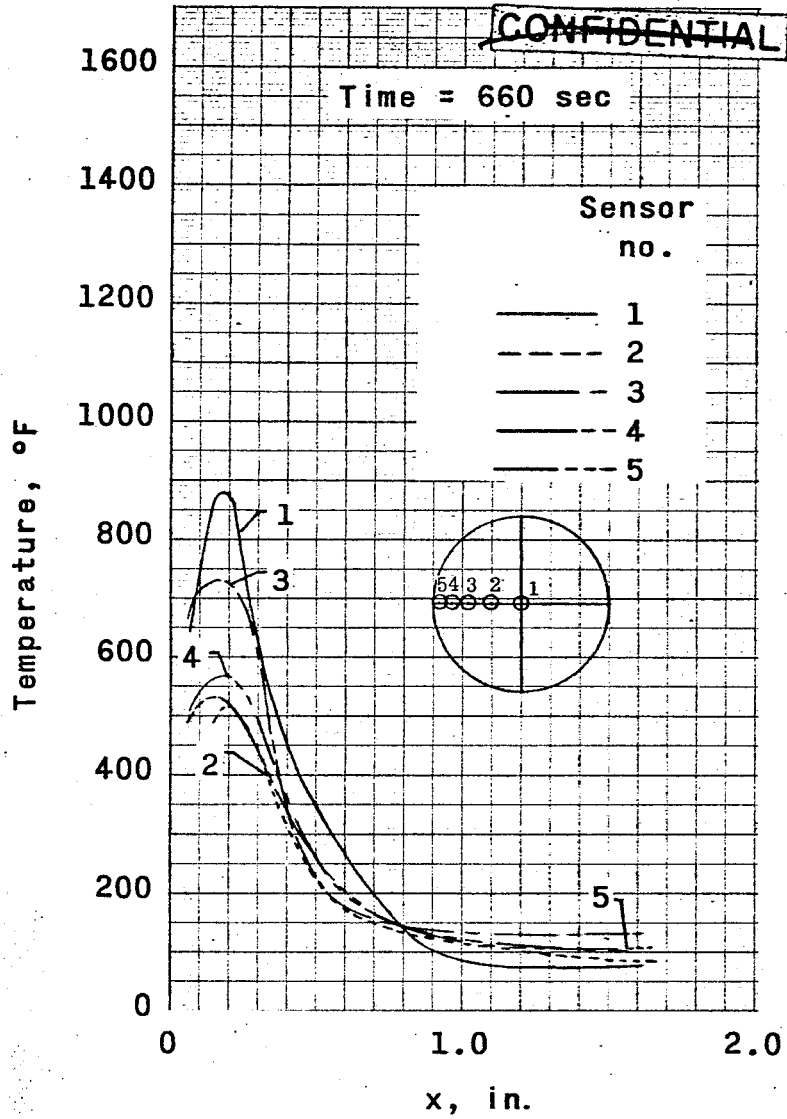
Figure 49 .- Continued.

~~CONFIDENTIAL~~



(d) Time 620 sec (Sensor 5, 9, 13, 10, 11 and 12). ~~CONFIDENTIAL~~

Figure 49.- Continued.

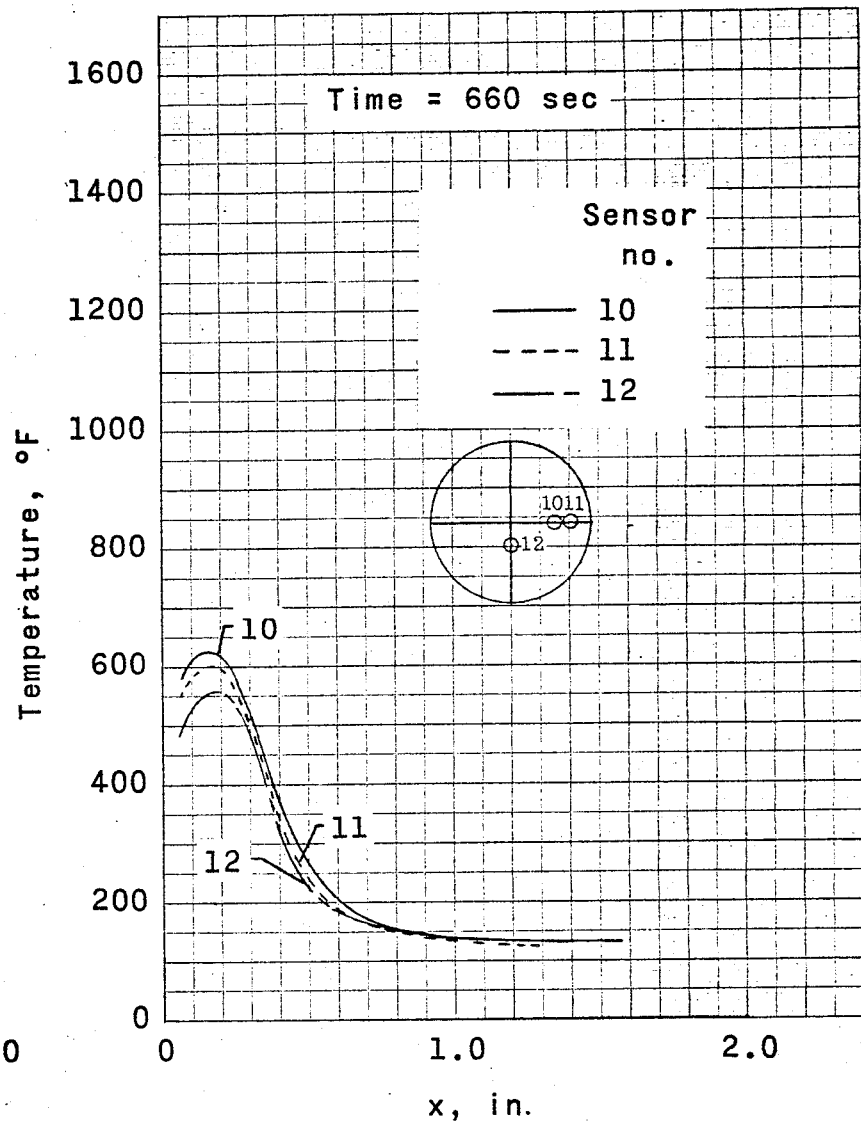
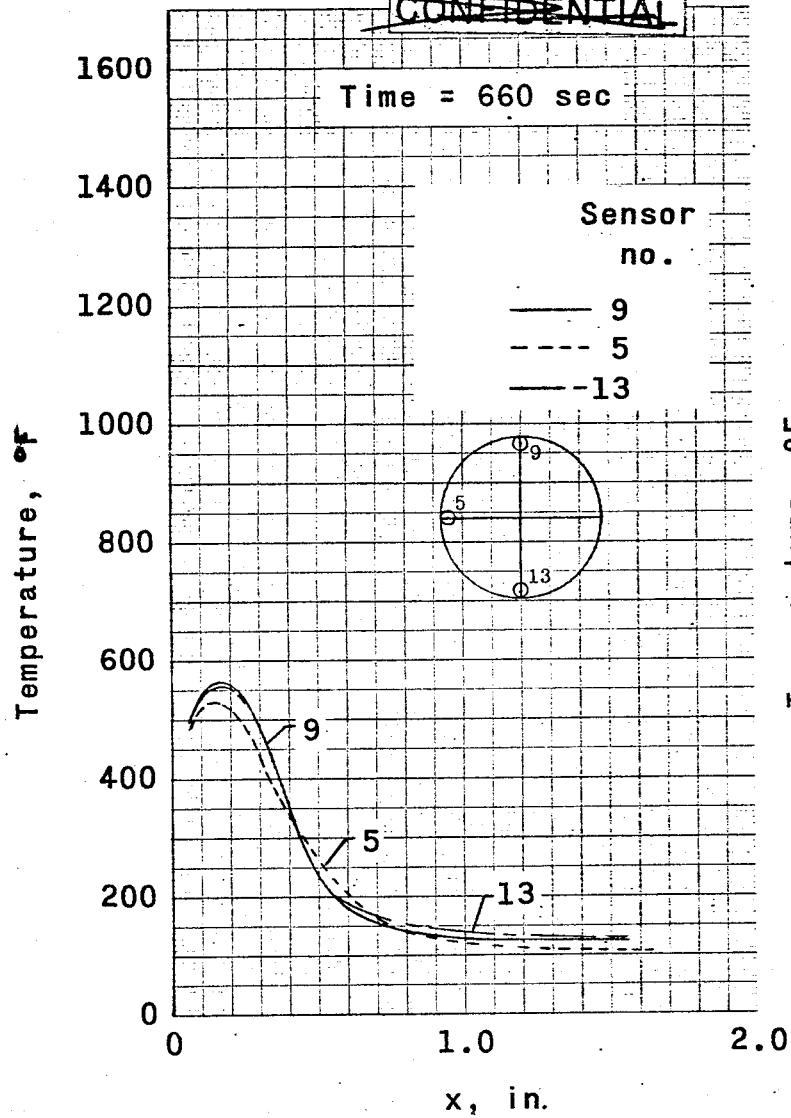


(e) Time 660 sec (Sensor 1 thru 9).

Figure 49 .- Continued.

**CONFIDENTIAL**

~~CONFIDENTIAL~~



(f) Time 660 sec (Sensor 5, 9, 13, 10, 11 and 12).

~~CONFIDENTIAL~~

Figure 49.- Concluded.

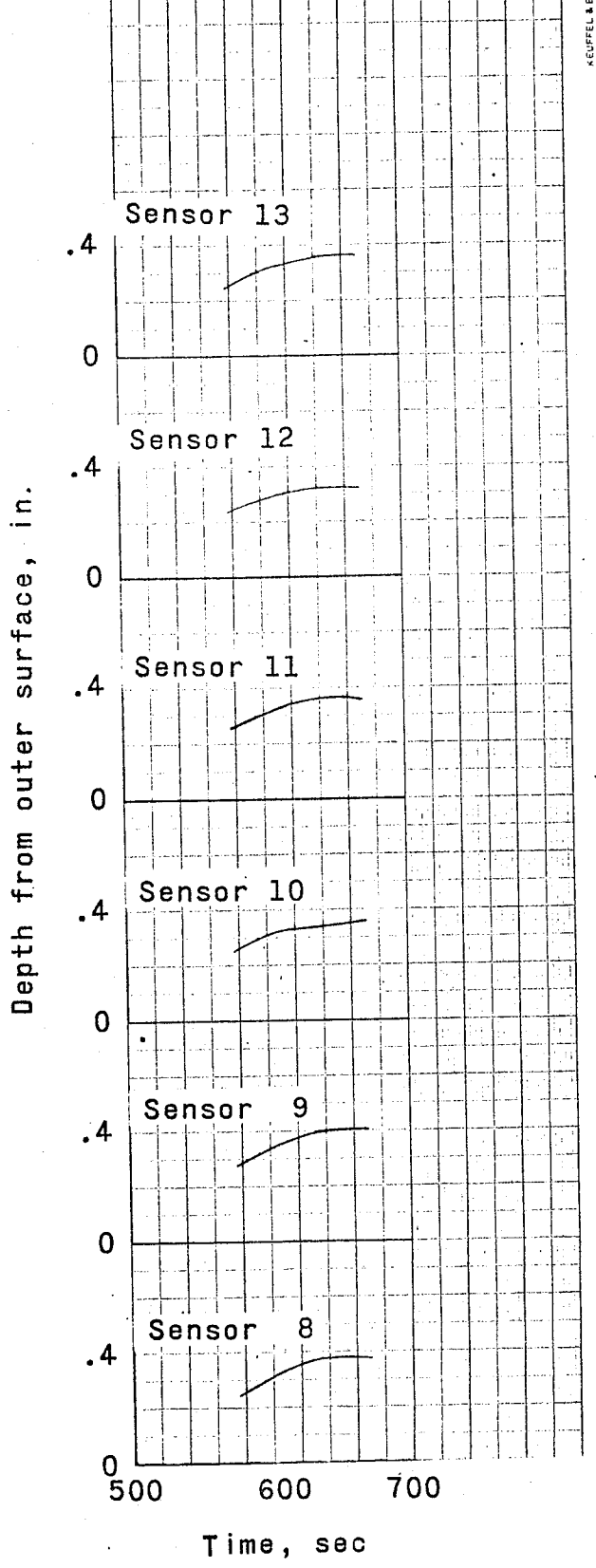
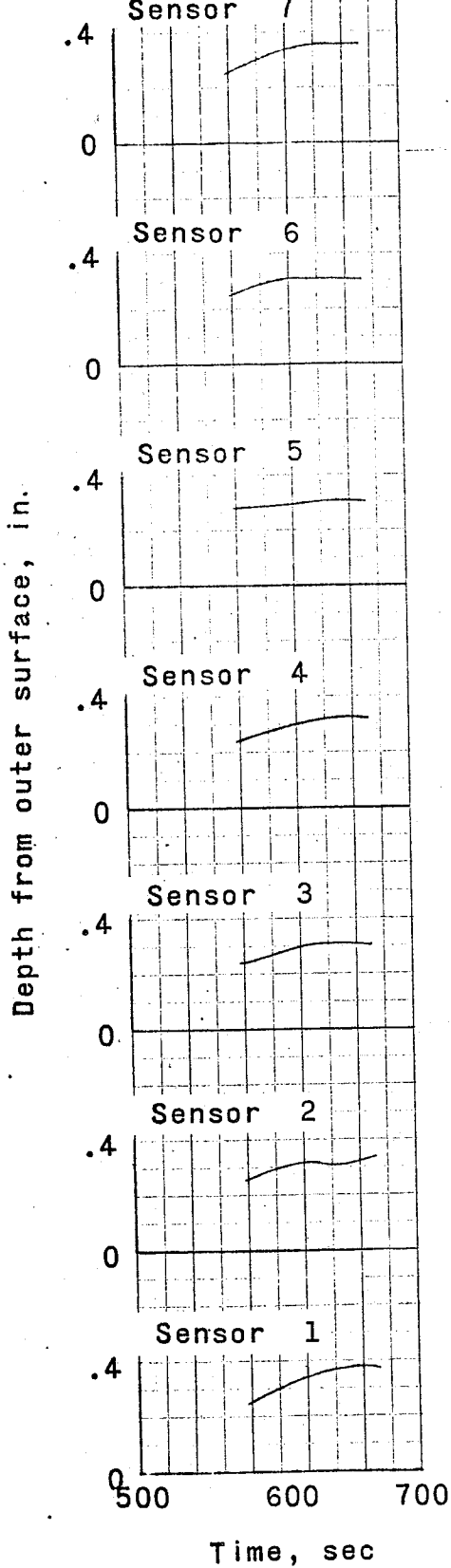
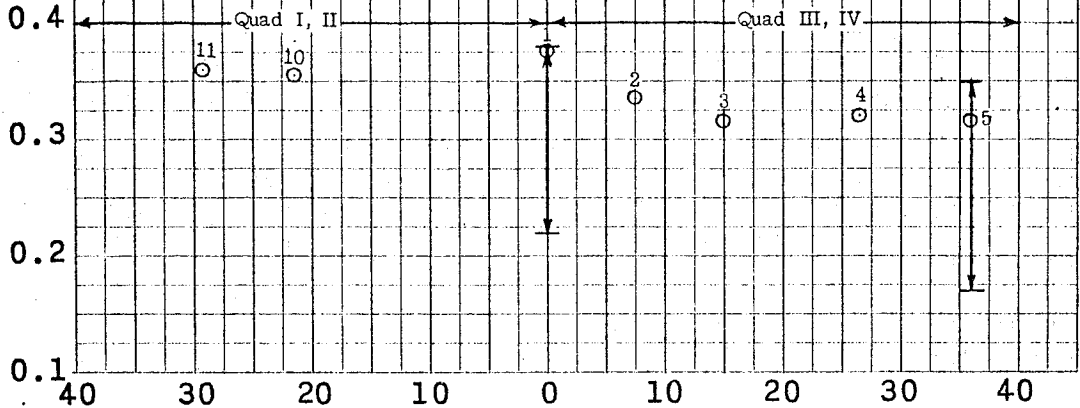


Figure 50.- Time history of apparent thermal penetration of heat shield as obtained from sensors. ~~CONFIDENTIAL~~

~~CONFIDENTIAL~~

KEUFFEL & ESSER CO. N. Y.

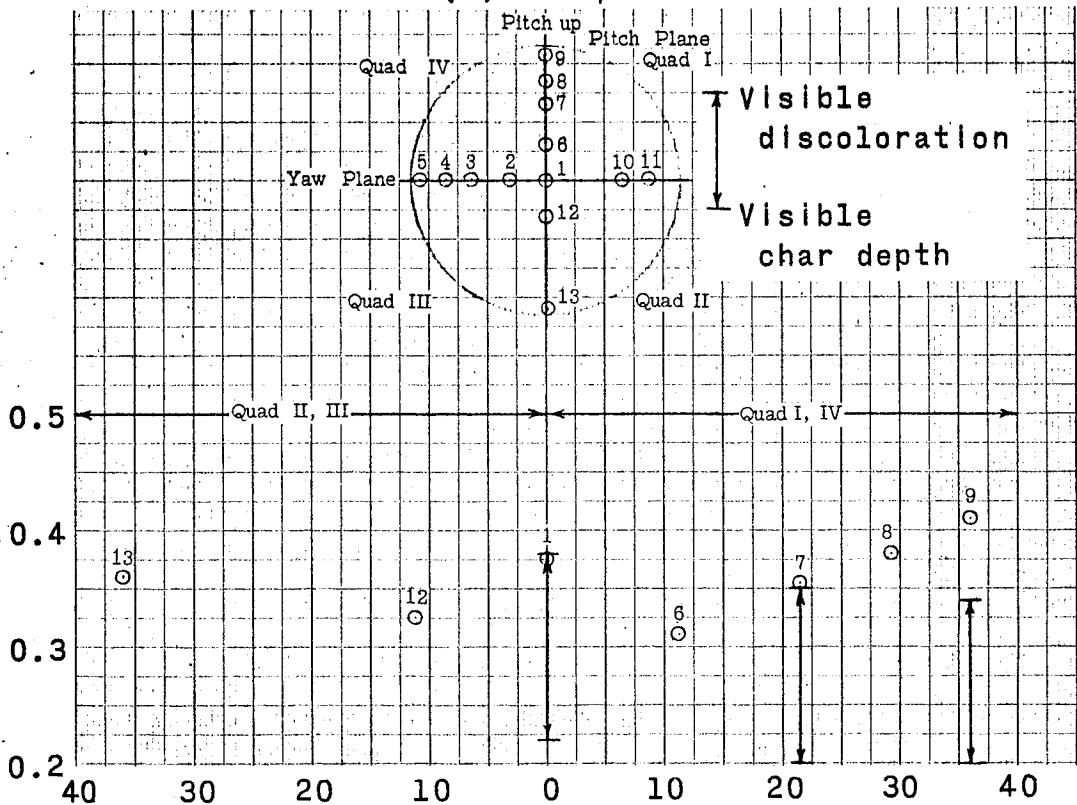
Maximum sensor readings, in.



Radial distance from geometric center of shield, in.

(a) Yaw plane.

Maximum sensor readings, in.



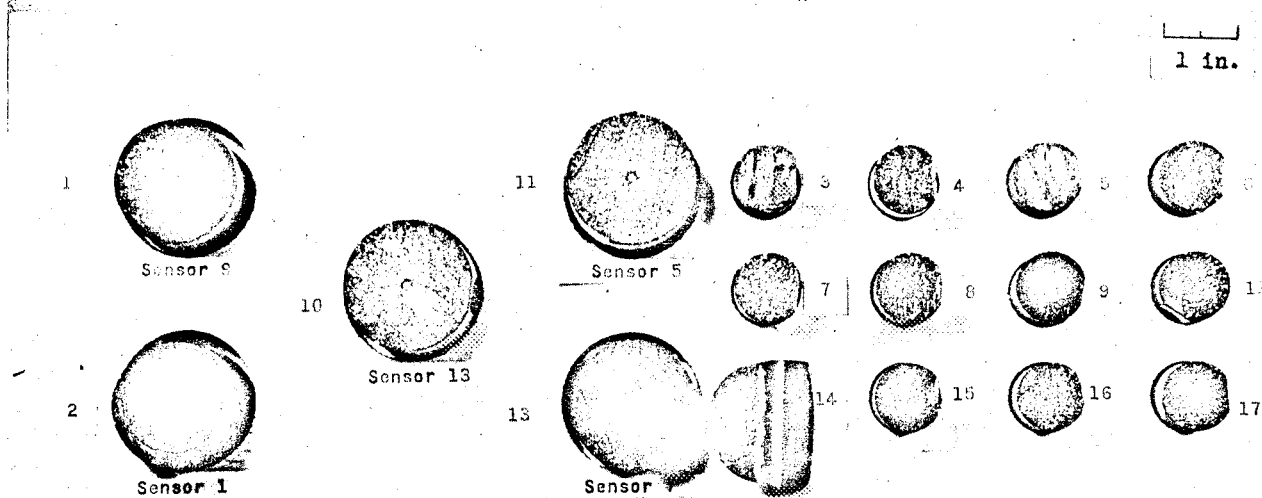
Radial distance from geometric center of shield, in.

(b) Pitch plane.

~~CONFIDENTIAL~~

Figure 51.- Comparison of sensor data and measured char and material discoloration.

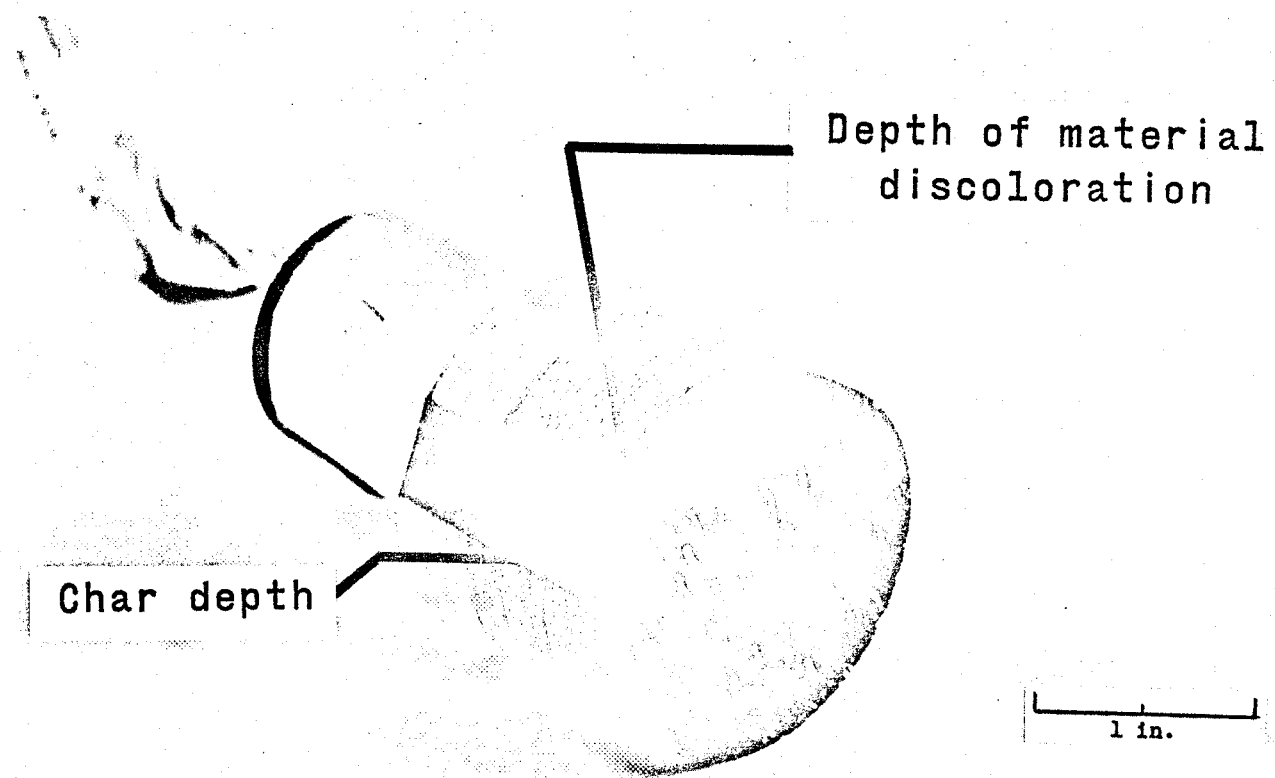
~~CONFIDENTIAL~~



~~CONFIDENTIAL~~

Figure 52.- Core samples obtained from recovered heat shield.

~~CONFIDENTIAL~~



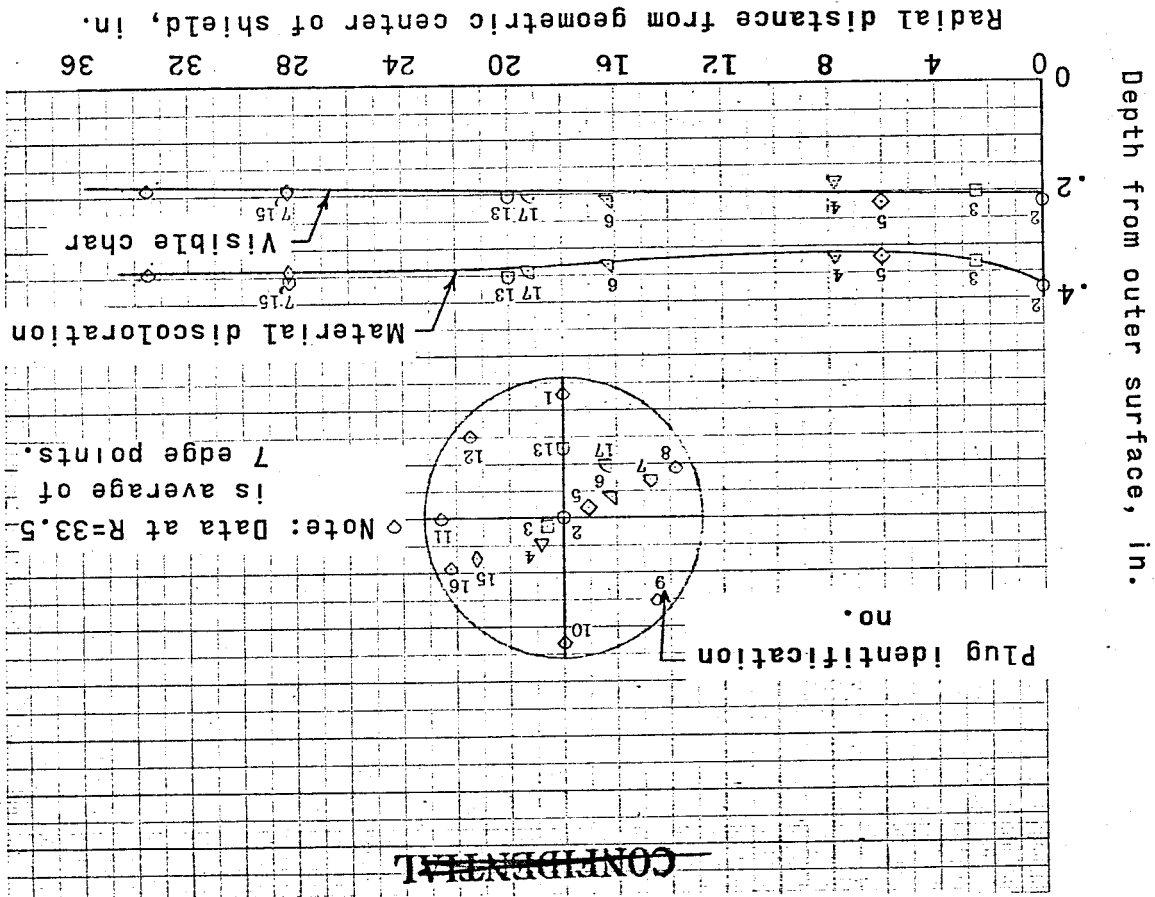
~~CONFIDENTIAL~~

Figure 53.- Typical core sample (Plug no. 10).

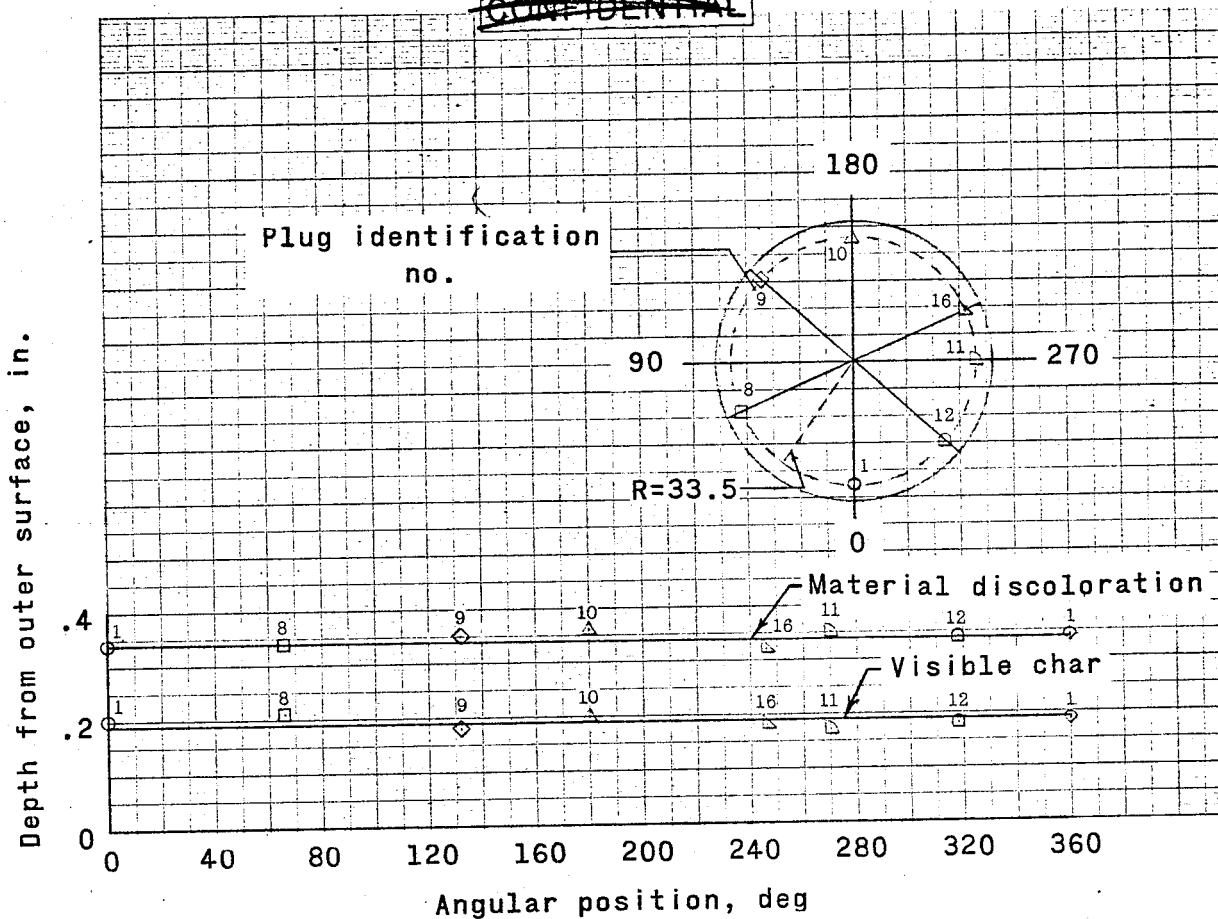
~~CONFIDENTIAL~~

Figure 54. - Char and discoloration measurements on Big Joe heat shield.

(a) Radial distribution.



~~CONFIDENTIAL~~



(b) Edge effect.

~~CONFIDENTIAL~~

Figure 54.- Concluded.

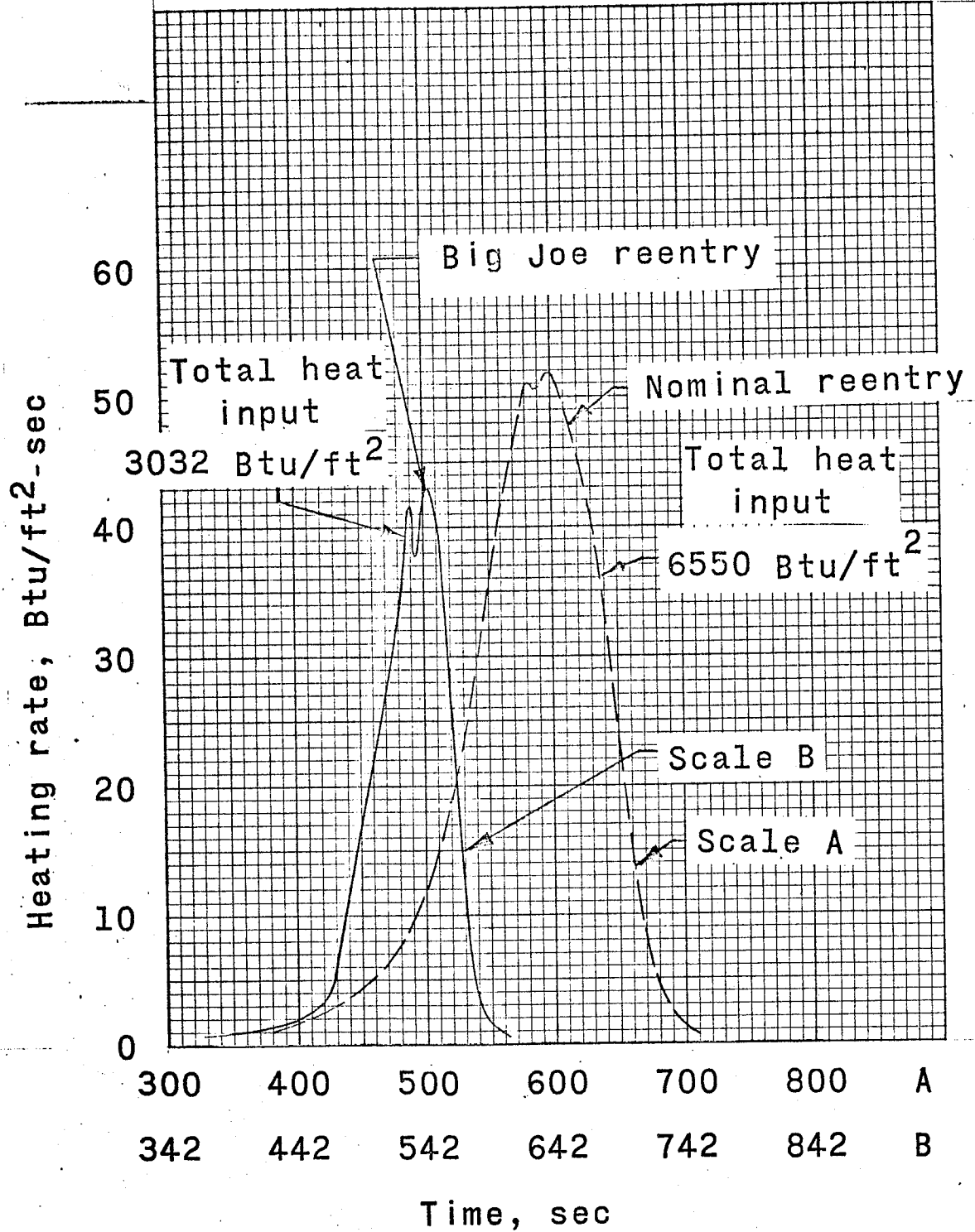


Figure 55.- Comparison of Big Joe and nominal stagnation point heating rates.

~~CONFIDENTIAL~~

~~CONFIDENTIAL~~

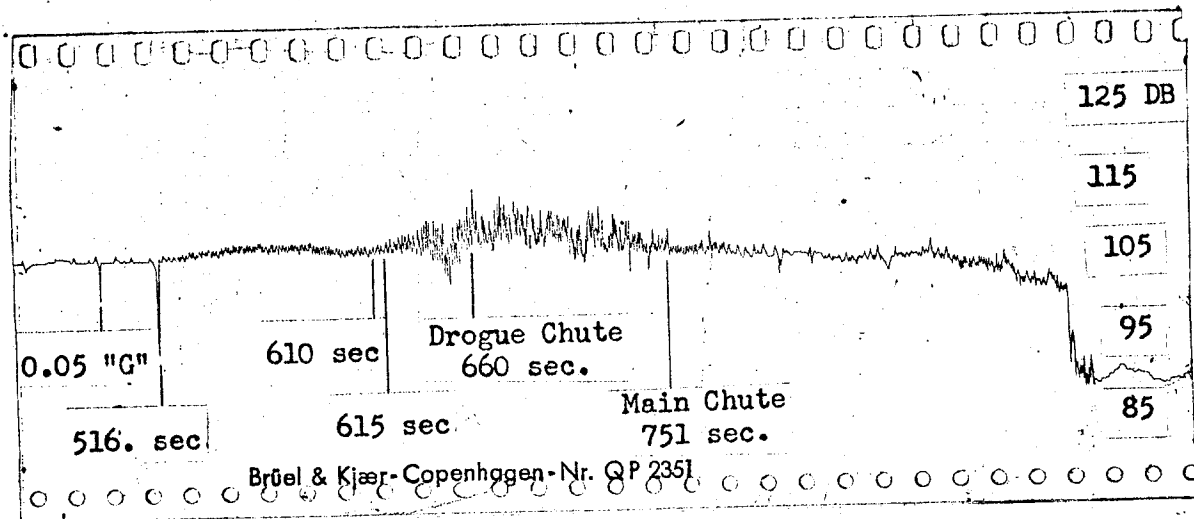
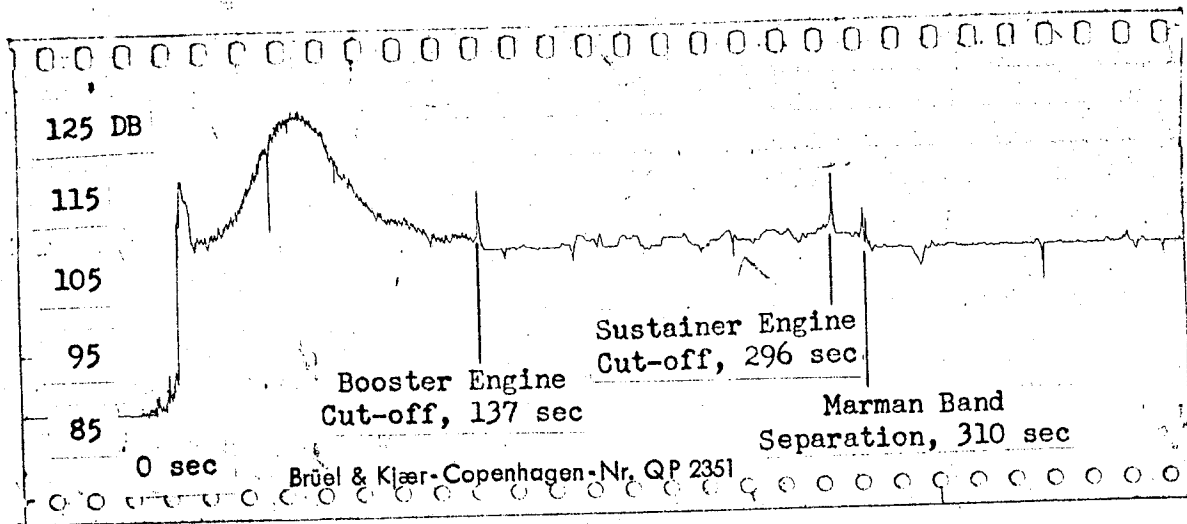
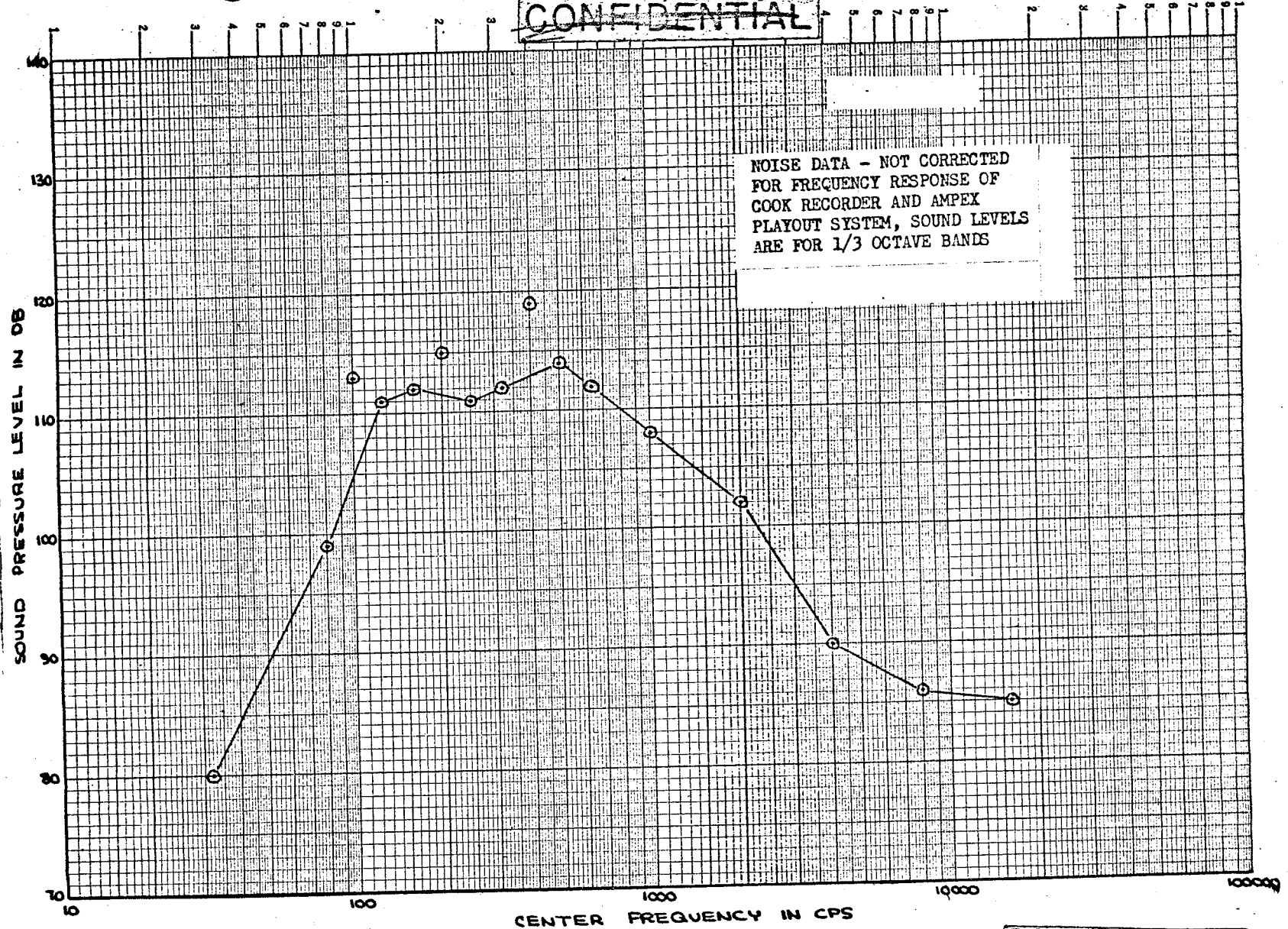


Figure 56.- Acoustic analyzer record.

~~CONFIDENTIAL~~

~~CONFIDENTIAL~~



~~CONFIDENTIAL~~